

RHYOLITIC EXPLOSIVE ERUPTIONS OF THE CENTRAL
SNAKE RIVER PLAIN, IDAHO: INVESTIGATIONS OF THE
LOWER CASSIA MOUNTAINS SUCCESSION AND
SURROUNDING AREAS

Thesis submitted for the degree of Doctor of Philosophy at the
University of Leicester

By

Benjamin Stephen Ellis MRes (Lancaster)

Department of Geology

University of Leicester

January 2009

**RHYOLITIC EXPLOSIVE ERUPTIONS OF THE CENTRAL SNAKE RIVER
PLAIN, IDAHO: INVESTIGATIONS OF THE LOWER CASSIA MOUNTAINS
SUCCESSION AND SURROUNDING AREAS**

Benjamin Stephen Ellis

The Snake River Plain of north-western U.S.A. was the site of voluminous, bimodal, hotspot volcanism in the Miocene. Between c. 12.7-6 Ma silicic volcanism produced an association of deposits so different to typical Plinian and ignimbrite deposits elsewhere it has been termed Snake River (SR)-type. The Cassia Mountains of southern Idaho contain SR-type ignimbrites produced from complex and dynamic magmatic plumbing systems involving multiple magma chambers which gave rise to multiple compositional populations of clinopyroxene that mixed during eruption and were deposited together. The Cassia Mountain ignimbrites become progressively more mafic up-succession in terms of whole rock, glass, feldspar and clinopyroxene compositions, reflecting decreasing time available for fractional crystallisation, as supported by geochronology. Two Cassia Mountain ignimbrites are among three newly discovered ‘super-eruptions’ defined on the basis of phenocryst, glass and whole rock compositions; magnetic polarity; $^{40}\text{Ar}/^{39}\text{Ar}$ geochronology; oxygen isotopes; and field data. Erupted volumes range between 640 and 1200 km³, amongst the largest recorded. Intercalated within the Cassia Mountain succession is a newly discovered deposit representing the first recorded explosive, rhyolitic phreatomagmatic eruption from the central Snake River Plain. The fine-grained, non-welded deposit has similar whole rock, glass, oxygen isotope and magmatic temperature characteristics to the surrounding welded ignimbrites, so the unusual deposit facies are interpreted as representing interaction of rising rhyolitic magma with near-surface water. During SR-type volcanism, lavas and ignimbrites of similar chemistry were erupted within a short time. Water contents of melt inclusions were low in both ignimbrites and lavas, consistent with the anhydrous mineralogy and high inferred magmatic temperature. Volatile contents of the magmas (as recorded by the melt inclusions) did not control eruptive style. The intense rheomorphism which characterises SR-type ignimbrites appears to be due to high emplacement temperatures rather than enhanced halogen contents.

Acknowledgements

I would like to thank my supervisors Mike Branney and Tiffany Barry for conceiving the project and their support and suggestions throughout which have improved the final version immeasurably. The project would not have been possible without the energy, enthusiasm and friendship of Bill Bonnicksen and Martha Godchaux. Norry, Mike McCurry, Rich Brown, Jake Lowenstern and Pete Kokelaar (as ever) have been generous with their time in making suggestions to improve the thesis.

Fieldwork in Idaho was made significantly more enjoyable due to my fortune in meeting the Hursch family of Rock Creek and Walker and Barbara Tollman.

Analytically speaking, the following people have helped make this thesis possible; Rob Wilson (for a fantastic job maintaining the microprobe), Dan Barfod and Darren Mark at SUERC, Richard Hinton and John Craven at the Edinburgh Ion microprobe. Andy Myers deserves great thanks for his last week computer magic.

Whilst in Leicester I've been lucky enough to overlap with a number of people who have both educated and entertained me. Simon 'the Jow' Jowitt for geochemical know-how and trips to the Marquis (as was), Dan Smith for his humour and moaning, Pablo for ideas and friendship, Dave Baines for chairing Cheese Club, and Xiaoya for looking after Dana while I was in the field.

While I have the opportunity, I'd like to thank Dave Cornwell, Alex Page (siphoning and cricket), David Jones (medieval warfare), Rob Kelly (for the bruised shins), Jamesor (the claw and G-unit), Graham Andrews (inspiration), Rippers (bad attitude!), Marc Reichow (argon advice and cake), Becky (travel organisation) and Vince (technology) for making the last four years more enjoyable. The rest of the PhD gang, Pete, Andy, Steve G and others also deserve some kind of mention. That was it.

Most importantly I would like to thank my parents, Sue and Paul and my sister Jo, for their unfailing support. I can't put into words how much your constant encouragement has been appreciated. It is true that you choose your friends and not your family, but I would have chosen you guys.

The final mention must go to Dana for her love and support over the last four years.

Dakujem pekne moj maly medved!

Table of contents

ABSTRACT	1
CHAPTER 1 - INTRODUCTION	2
Methodology	2
Aims and objectives	3
Regional geology	3
The Columbia River basalts	5
The Snake River Plain	6
The Oregon High Lava Plains	8
Overall model	9
Snake River Plain rhyolites	10
Eruptive centres	11
Snake River-type volcanism	12
<i>Volumes</i>	16
<i>Interaction with water</i>	18
Other styles of volcanism	19
Global occurrence of Snake River-type volcanism	21
This work	22
CHAPTER 2 – GEOCHEMICAL EVOLUTION OF THE TWIN FALLS ERUPTIVE CENTRE AND COMPARISON WITH THE BRUNEAU-JARBIDGE ERUPTIVE CENTRE	25
Abstract	25
Introduction	26
Snake River-type volcanism	26
Geological background	28
Unit descriptions	33
The Ibex Peak Member	33
<i>Interpretation</i>	33
The Magpie Basin Member	33
<i>Interpretation</i>	33
The Big Bluff Member	34
<i>Interpretation</i>	34
Unit ‘TT1’	36
The Steer Basin Member	36
<i>Interpretation</i>	36
Niles Gulch Member	38
<i>Interpretation</i>	38
Antelope Springs Member	38
<i>Interpretation</i>	40
Deadeye Member	40
<i>Interpretation</i>	40
Wooden Shoe Butte Member	42
<i>Interpretation</i>	44
McMullen Creek Member	44
Eruption sources	45
Geochemical techniques	45
Whole rock chemistry	45
Electron microprobe analysis	46
<i>Methodology</i>	46
Results	48
Whole rock chemistry	48
Glass chemistry	52

Mineral chemistry	56
<i>Pyroxene</i>	56
<i>Feldspars</i>	62
Geothermometry	62
Neodymium isotopes	68
Discussion	70
Cause of pyroxene modal compositions	70
<i>Incorporation of partially melted material</i>	70
<i>Wall rock assimilation</i>	73
<i>Oxygen fugacity conditions</i>	74
<i>Glomerocryst compositions</i>	74
<i>A stratified magma chamber</i>	75
<i>Multiple magma chambers</i>	76
Trend towards more mafic compositions	77
<i>Changing amount of crustal melting over time</i>	77
<i>Melting of a progressively more mafic source</i>	78
<i>Duration of residence in the magma reservoir</i>	78
Comparison with the Bruneau-Jarbidge eruptive centre	79
<i>Clinopyroxenes</i>	80
<i>Feldspars</i>	80
<i>Glass</i>	82
Bruneau Jarbidge model	83
Twin Falls eruptive centre model	85
Conclusions	87
CHAPTER 3 – ERUPTIVE VOLUMES OF SNAKE RIVER-TYPE IGNIMBRITES	88
Abstract	88
Introduction	88
Yellowstone hotspot track volumes	90
Regional stratigraphy	90
Bruneau-Jarbidge	91
Grasmere Escarpment	93
Browns Bench	93
Rogerson Graben	96
Cassia Mountains	96
West Bennett Mountain	99
East Bennett Mountain	99
Rationale for study	102
Zoning in ignimbrites	102
Analytical techniques	103
Argon dating methodology	104
<i>Preparation</i>	104
<i>Analysis</i>	104
<i>Comparison of ⁴⁰Ar/³⁹Ar ages</i>	105
Oxygen isotopes	105
<i>Methodology</i>	105
Results	106
⁴⁰ Ar/ ³⁹ Ar	106
Proposed correlation 1: Buckhorn Ignimbrite, Cougar Point Tuff 7 and Browns Bench 3	110
<i>Physical description</i>	110
<i>Glass and phenocryst characteristics</i>	113
⁴⁰ Ar/ ³⁹ Ar ages	113
Oxygen isotopes	116
<i>Interpretation</i>	117
Proposed correlation 2: Browns Bench 5, Upper Grasmere Escarpment Ignimbrite, Windy Gap and Cougar Point Tuff 11	117
<i>Physical description</i>	117

<i>Glass and phenocryst characteristics</i>	119
⁴⁰ Ar/ ³⁹ Ar ages	122
Oxygen isotopes	122
Interpretation	122
Proposed correlation 3: Big Bluff Member, Jackpot 1-6, Browns Bench 7 and Frenchman Springs Rhyolite	123
Physical description	123
Glass and phenocryst characteristics	127
⁴⁰ Ar/ ³⁹ Ar ages	129
Oxygen isotopes	129
Interpretation	129
Proposed correlation 4: Steer Basin Member, Jackpot 7 and Browns Bench 8	131
Physical description	131
Glass and phenocryst characteristics	134
⁴⁰ Ar/ ³⁹ Ar ages	136
Oxygen isotopes	136
Interpretation	136
Discussion	139
Eruptive volumes	139
<i>Cougar Point Tuff 11</i>	139
<i>The Big Bluff Tuff</i>	140
<i>The Steer Basin Tuff</i>	140
Volume or magnitude?	141
The Yellowstone hotspot track	141
Eruption frequency	144
Other possible correlations	145
<i>Big Bluff Tuff and Cougar Point Tuff 13</i>	145
<i>Steer Basin Tuff, Cougar Point Tuff 15 and Tuff of Knob</i>	146
<i>Tuff of Wooden Shoe Butte and Tuff of Thorn Creek</i>	149
Eruptive centres	149
Conclusions	151
CHAPTER 4 – THE DEADEYE MEMBER: A RHYOLITIC PHREATOMAGMATIC ERUPTION FROM THE YELLOWSTONE HOTSPOT	152
Abstract	152
Geological Background	153
‘Snake River-type’ volcanism	153
Aims	155
The Cassia Formation	155
The Deadeye Member	157
Lithofacies of the Deadeye Member	157
Clast-supported pumice bedded lapilli (bpL) facies	157
Description	157
Interpretation	159
Parallel-bedded coarse to fine ash (//bT) lithofacies	159
Description	159
Interpretation	160
Clast-supported pumice bedded lapilli with ash pods and parallel-bedded coarse to fine ash with ash pods (bpL pod and bT pod)	160
Description	160
Interpretation	160
Parallel-laminated fine to medium ash (//sT) facies	162
Description	162
Interpretation	162
Massive lapilli-tuff (mLT)	162
Description	162
Interpretation	164
Diffuse cross-stratified lapilli-tuff (dxsLT)	164

<i>Description</i>	164
<i>Interpretation</i>	165
Ash aggregate-bearing diffuse cross-stratified lapilli-tuff (dxsLT acc)	166
<i>Description</i>	166
<i>Interpretation</i>	167
Scoured, fine sand and silt lithofacies (ScS)	169
<i>Description</i>	169
<i>Interpretation</i>	169
Bedded sand of irregular thickness (bS)	169
<i>Description</i>	169
<i>Interpretation</i>	170
Lithofacies associations	173
Fallout deposit association	173
Pyroclastic density current association	175
Reworked association	177
Source of the Deadeye Member	177
Volume of the Deadeye Member	180
Geochemistry	181
Whole rock chemistry results	181
Multiple glass populations	183
White pumice population	183
<i>Description</i>	183
<i>Interpretation</i>	183
Black pumice population	184
<i>Description</i>	184
<i>Interpretation</i>	184
Macroscopic shard population	186
<i>Description</i>	186
<i>Interpretation</i>	186
Non-vesicular black glass population	187
<i>Description</i>	187
<i>Interpretation</i>	188
Overview of the Deadeye Member	192
Discussion	193
A phreatomagmatic origin?	195
Silicic phreatomagmatism	196
<i>Surtseyan</i>	196
<i>Taalian</i>	197
<i>Phreatoplinian</i>	197
Eruptive style of the Deadeye Member	202
Other phreatomagmatic units in the Snake River Plain	203
<i>Unnamed unit in Big Cottonwood Canyon</i>	203
<i>Jackpot 6 Member</i>	203
<i>Wooden Shoe Butte Member</i>	206
<i>Rabbit Springs Member</i>	206
<i>Cougar Point Tuff 15</i>	206
Conclusions	207
CHAPTER 5 – PRE-ERUPTIVE VOLATILE CONTENTS AND ERUPTIVE BEHAVIOUR OF SNAKE RIVER-TYPE IGNIMBRITES AND LAVAS	208
Abstract	208
Introduction	209
Rationale	209
Previous studies	210
<i>Lava versus ignimbrite discrimination criteria</i>	210
<i>Melt inclusions</i>	211
Criteria for unit selection	214
Analytical techniques	219
Whole rock chemistry	219

Electron microprobe	220
Ion microprobe	220
<i>Backgrounds</i>	221
<i>Analytical errors</i>	221
<i>Accuracy</i>	222
Experiment 1	222
Field description	222
<i>Cougar Point Tuff XII</i>	222
<i>Black Rock Escarpment Lava</i>	224
Electron microprobe	224
<i>Inclusions</i>	224
<i>Groundmass</i>	224
Experiment 2	227
Field description	227
<i>Balanced Rock Lava</i>	227
<i>Castleford Crossing Ignimbrite</i>	227
Electron microprobe	229
<i>Inclusions</i>	229
<i>Groundmass</i>	229
Experiment 3	230
Field description	230
<i>Sand Springs Ignimbrite</i>	230
<i>Shoshone Falls Rhyolite Lava</i>	230
Electron microprobe	232
<i>Inclusions</i>	232
<i>Groundmass</i>	232
Ionprobe results	232
H ₂ O	232
<i>Experiment 1</i>	232
<i>Experiment 2</i>	234
<i>Experiment 3</i>	234
<i>Leaked inclusions</i>	234
<i>Rehydration of the groundmass</i>	236
<i>Summary</i>	236
Fluorine	236
<i>Experiment 1</i>	236
<i>Experiment 2</i>	238
<i>Experiment 3</i>	238
<i>Summary</i>	238
Chlorine	238
<i>Experiment 1</i>	239
<i>Experiment 2</i>	239
<i>Experiment 3</i>	239
<i>Summary</i>	242
<i>A note regarding F and Cl results</i>	242
CO ₂	242
Discussion	246
Snake River-type rhyolites	246
<i>The Gawler volcanic province</i>	246
<i>Trans Pecos Texas</i>	246
<i>Etendeka-Paraná</i>	247
<i>Middle Proterozoic Keewenawan volcanics, Minnesota</i>	247
<i>Eritrea</i>	249
<i>Pantelleria</i>	249
‘Typical’ rhyolites	249
Eruptive style	251
<i>CO₂ content</i>	251
<i>Variation in ascent rate</i>	252
<i>Degassing</i>	252
Magma chamber conditions	253

Source of the volatiles	256
Rheomorphism	257
<i>Solid and bubble content</i>	257
<i>Water content</i>	258
<i>Halogens</i>	258
<i>Temperature</i>	260
Conclusions	262
CHAPTER 6 – CONCLUSIONS AND FURTHER WORK	263
Ignimbrite stratigraphy and geochemistry of the Cassia Mountains	263
New correlations and eruption volume calculations	264
A Snake River-type phreatomagmatic explosive eruption	265
Pre-eruptive volatile contents of Snake River-type magmas	266
Future work	267
References	270
Appendix A Sample location	290
Appendix B Electron microprobe	291
Appendix C Ion microprobe and Secondary Ion Mass Spectroscopy	294
Appendix D X-ray fluorescence spectroscopy	296

Chapter 1: Introduction

This study investigates the deposits of a newly defined category of volcanism documented from the central Snake River Plain of southern Idaho and northern Nevada, termed Snake River (SR)-type volcanism (Branney et al. 2008). SR-type eruptions have not been witnessed and the styles of eruption are poorly understood and must be reconstructed from evidence within the geological record.

Methodology

This work results from 8 months' fieldwork in southern Idaho with ideas tested both in the field and by a variety of analytical methods. In the field area intensely welded rhyolitic tuffs are exposed as steep, cliff-forming units separated by poorly exposed slope-forming non-welded units. Although significant thicknesses (tens of metres) of individual welded tuff units may be exposed, their bases including any fallout deposits are commonly obscured under bench talus. Because of the lack of exposure, no isopach maps exist for the fallout deposits from any eruption in the central Snake River Plain and so the sources of the rhyolitic eruptions are not known. The very limited exposure of fallout deposits has also hindered correlation of deposits (fallout and ignimbrite) between massifs that surround the Snake River Plain. The non-welded deposits of the province have received little attention and have commonly been referred to as sediments. The present project aims to analyse these scarce exposures of non-welded material, to explore what they reveal about correlation and eruption styles.

Previous work in the central Snake River Plain has involved mainly reconnaissance-scale mapping (Wood and Gardner 1984; Williams et al. 1990; Mytton et al. 1990; Oakley and Link 2006) with phenocryst and geochemical studies of local successions (Honjo and Leeman 1987; Honjo et al. 1992; Wright et al. 2002; Andrews et al. 2008). Most work has

been done on the Cougar Point Tuff succession with these 9 ignimbrites well-characterised physically (Bonnichsen and Citron 1982), chemically (Cathey and Nash 2004) isotopically (Boroughs et al. 2005) and in terms of geochronology (Bonnichsen et al. 2008). Elsewhere in the central Snake River Plain, a lack of detailed geochemical data has prevented the correlation of any individual eruption units between the adjacent massifs.

Aims and objectives

The aim of this study is to improve the understanding of the processes and deposits of SR-type volcanism, by focussing on aspects of the styles and scales of the explosive eruptions. The project concentrates on the Cassia Mountains of southern Idaho because they expose some non-welded units, are part of the type area of SR-type volcanism (Branney et al. 2008) and are relatively accessible. Characterising the volcanic stratigraphy of the Cassia Mountains will improve understanding of the inferred Twin Falls eruptive centre from where they derive (Pierce and Morgan 1992) and help develop methods of correlating individual eruption units between massifs. Correlating units between the massifs is an essential first step towards resolving the volumes of individual eruptions.

Regional geology

The Snake River Plain of southern Idaho and northern Nevada in the western United States of America is a region of conspicuously low topographic relief that cuts across the basin-and-range topography of western North America. It spans 600 km from Yellowstone in the east to northern Nevada in the west and is approximately 100 km north-south (Fig. 1.1). The 16.6 Ma and younger volcanic rocks in the north western U.S.A., including the Columbia River basalts and the Snake River Plain-Yellowstone silicic rocks represent a volcanic province that began with the eruption of the Columbia River flood basalts and associated rhyolites in northern Nevada before the production of the basalt and rhyolite in the Snake River Plain-Yellowstone system.

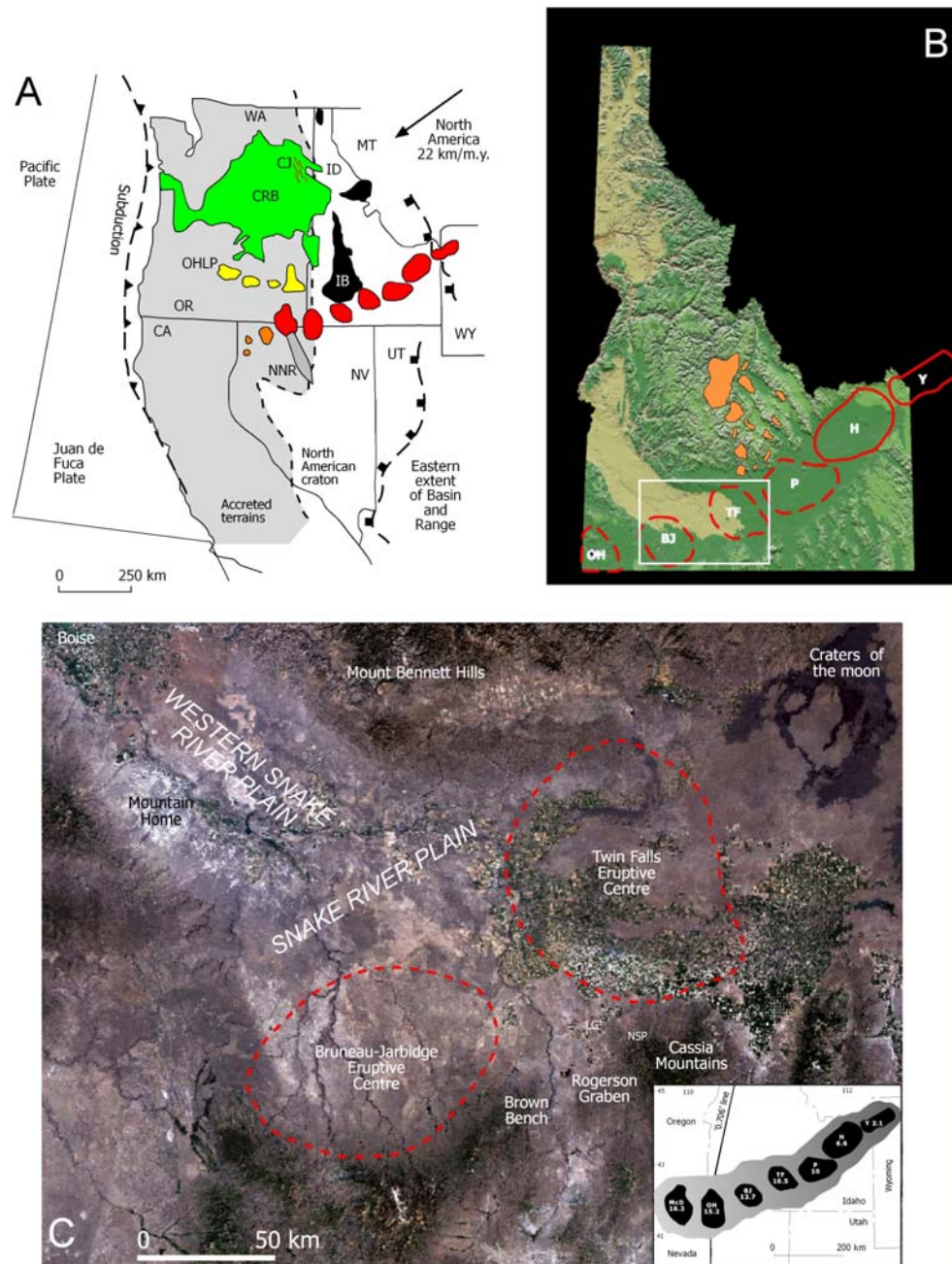


Figure 1.1 A. Location map showing the eruptive centres along the Snake River Plain (red) adapted from Nash et al. (2006) showing the Idaho batholith (black) the Columbia River basalts (green) and the Oregon High Lava Plains (yellow). Grey filled area represents the accreted terrains and the white area represents the North American craton, separated by the $^{87}\text{Sr}/^{86}\text{Sr}$ 0.706 line in Mesozoic plutonic rocks. CJ represents the Chief Joseph dike swarm considered to be the source of the CRB and NNR is the northern Nevada rift. B. DEM image of Idaho showing the prominent topographic feature of the Snake River Plain. Locations of the proposed eruptive centres in red (Armstrong et al. 1975; Pierce and Morgan 1992) and the location of the Challis volcanic deposits in orange. The type area for SR-type volcanism is shown in white C. Composite satellite image of the central Snake River Plain showing the two main eruptive centres thought to be responsible for Snake River-type volcanism. Inset shows the eruptive centres with ages of onset of activity at each eruptive centre in Ma: McD - McDermitt, OH - Owyhee Humboldt, BJ - Bruneau Jarbidge TF - Twin Falls, P - Picabo, H - Heise, Y - Yellowstone. NSP is Nat Soo Pah, LG is Lily Grade, locations mentioned in the text.

The Snake River Plain volcanism was preceded in Idaho by an Eocene episode of volcanism, referred to as Challis volcanism which produced a series of calderas in central Idaho (Fig. 1.1 B). This earlier episode is thought to have resulted from the shallow subduction of the Farallon plate under the North American plate (e.g. Lipman et al. 1971; 1972). The Challis volcanics comprise intermediate to evolved rocks, emplaced in three phases: initial effusions of andesitic to dacitic lavas, followed by a period of explosive dacitic to rhyolitic volcanism with a final stage of intrusive activity (Sanford 2005). In addition, plutons were emplaced along the western margin of the Wyoming craton, with the Idaho batholith present in the central Snake River Plain (Fig. 1.1 A). A terrain boundary separates the craton in the east and the accreted terrains to the west and is marked by the line of 0.706 $^{87}\text{Sr}/^{86}\text{Sr}$ ratios in plutonic rocks (e.g. Leeman et al. 1985; Nash et al. 2006). Cretaceous transpression created the anomalously sharp (< 10 km) terrain boundary, which steepened the initially shallow (as seen in the Sierra Nevada) Sr isotope gradient (Giorgis et al. 2005). The location of the terrain boundary is supported by work on Pb, Nd and Hf isotopes from hotspot tephra samples which shows co-variance in these isotopic systems with abrupt shifts across the cratonic boundary at around 15 Ma (Bennett and De Paolo 1987; Nash et al. 2006).

The Columbia River flood basalts

The >230,000 km³ Columbia River basalts were emplaced over 10.5 million years from 16.6-6 Ma (Camp et al. 2003; Hooper et al. 2007) with the majority (c. 98 % of the volume) emplaced within the first two million years 16.6-14.5 Ma (Swanson et al. 1979; Hooper et al. 2002; Hooper et al. 2007). The basalts lie mostly within Washington and Oregon states, with volumetrically minor deposits in Idaho (Fig 1.1 A). Individual lavas were erupted from the Chief Joseph dike swarm on the Idaho-Oregon border (Fig. 1.1 A) from where they may be traced into the Pasco basin on the basis of their homogeneous and characteristic chemistry (Hooper et al. 2007).

Mechanisms to explain the flood basalt volcanism have been suggested including mantle flow around a residuum body of melt which forms earlier, and buoyantly rises then adheres to the base of the North American plate, although why the original residuum forms is not clear (Humphreys et al. 2000) and exploitation of lithospheric structure (Christiansen and Lageson 2003). However, the high productivity and the restricted geographic range of the volcanism are most commonly attributed to a mantle plume (e.g. Draper 1991; Pierce and Morgan 1992; Takahashi et al. 1998; Camp and Ross 2004; Hooper et al. 2007). Helium isotopes also support a plume origin for the Columbia River Basalts. The $^3\text{He}/^4\text{He}$ ratio in MORB is commonly around eight times the present atmospheric ratio and the ratio in mantle plumes is generally considerably higher than this (e.g. Breddam et al. 2000); the Innaha Basalt of the CRFB has a ratio of ~ 11.5 times atmospheric consistent with a plume origin (Dodson et al. 1997).

The Snake River Plain

The volcanic products of the central Snake River Plain are compositionally bimodal, dominated by basalt and rhyolite. The rhyolitic volcanism from the Snake River Plain was broadly time-transgressive, younging towards Yellowstone in the east (Armstrong et al. 1975; Pierce and Morgan 1992); although the Arbon Valley Tuff (Kellogg et al. 1984) and the Magic Reservoir eruptive centre (Honjo and Leeman 1987) are exceptions to this trend (they are not of SR-type). The oldest silicic volcanism associated with the hotspot is a matter of debate, silicic deposits are known from the McDermitt eruptive centre around 16.5 Ma (Henry et al. 2006) and some deposits of the High Rock caldera in northern Nevada may predate this with an estimated age of 16.6 Ma (Perkins and Nash 2002), however the oldest unit with a measured date from the High Rock caldera is the Tuff of Craine Creek which has a K-Ar age of 16.1 ± 0.5 Ma (Noble et al. 1970) which would make it approximately time-equivalent to the McDermitt centre. Further west of McDermitt some new calderas have been located (Coble and Mahood 2008) but no geochronological data are available to constrain the ages of these deposits (Fig. 1.2 A).

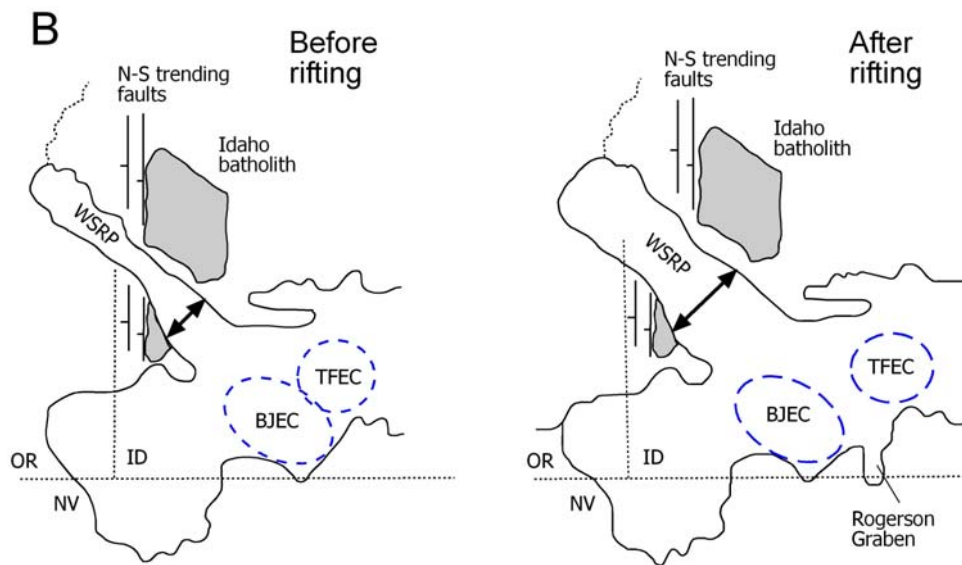
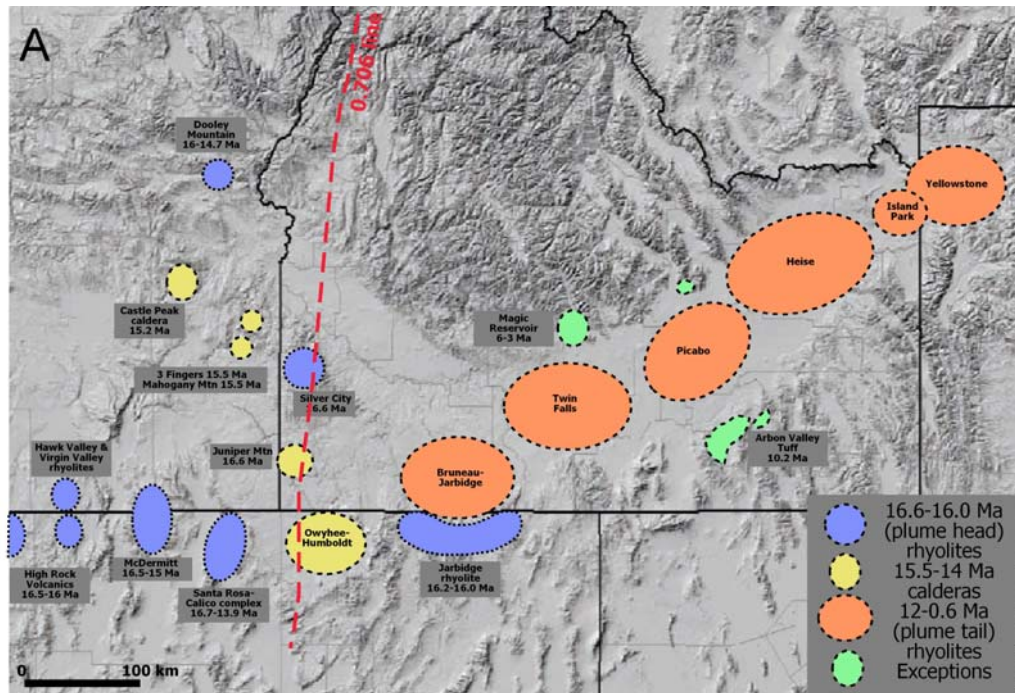


Figure 1.2 A. Map showing the locations of widely distributed silicic volcanism in the vicinity of the Idaho, Oregon, Nevada border around 16 Ma, after Shervais and Hanan (2008). To the east, the Magic Reservoir eruptive centre and Arbon Valley Tuff are shown which are exceptions to the age progression of silicic volcanism along the central Snake River Plain. **B.** Diagram from Bonnichsen and Godchaux (2004) illustrating how the effect of the rifting to produce the western Snake River Plain Graben may have caused an apparent increase in the distance between the Bruneau-Jarbidge and Twin Falls eruptive centres.

At any location along the Snake River Plain, the eruption of rhyolite (as both lavas and ignimbrites) was followed by the eruption of basaltic lavas and phreatomagmatic tuffs. The basalts, erupted from small vents both within the plain and at its margins, do not show the same systematic time-transgressive behaviour (Bonnichsen and Godchaux 2002). The nature of the volcanism along the Snake River Plain has been interpreted as from a mantle plume (e.g. Pierce and Morgan 1992; Cathey and Nash 2004) supported by recent geophysical work at the Yellowstone volcanic field, which has detected the presence of a plume beneath Yellowstone (Yuan and Decker 2005; Waite et al. 2006). This plume plunges at $\sim 65^\circ$ to the north beneath the Rocky Mountains (Yuan and Decker 2005; Waite et al. 2006; Shervais and Hanan 2008).

The Oregon High Lava Plains

The Oregon High Lava Plains province is also bimodal basaltic-rhyolitic, shown on Figure 1.1. It youngs westwards, the opposite direction to that of the Snake River Plain (Walker 1974; Jordan et al. 2004). It may be the product of enhanced extension at the northern margin of the Basin and Range province (Christiansen et al. 2002), but structural extension is thought to be only 1%, which is thought to be insufficient to drive a magmatic system by decompression (Jordan et al. 2004). An alternative is that the volcanism was a response to the entrainment of the plume head with subduction-induced counter-flow (Draper 1991). This model would also produce an age propagation of the basalts but this is not seen. The most recent model for the formation of the Oregon High Lava Plains involves the head of the plume flattening against the lithosphere with some of the material flowing west to the cratonic margin, producing the trend of the Oregon High Lava Plains province (Jordan et al. 2004).

Overall model

If the Columbia River Flood Basalts, the Snake River Plain and the Oregon High Lava Plains are related, a model must be capable of explaining all these occurrences. One such model involves a plume rising near the cratonic margin, which subsequently moved laterally until it reached a crustal weakness which allowed it to reach the surface. In this area, the most prominent crustal weakness is the margin between the accreted terrains to the west and cratonic North America to the east (Jordan et al. 2004). The impact of the plume head at the base of the lithosphere may have caused the eruption of the Columbia River basalts. The Oregon High Lava Plains may represent secondary flow from the hotspot enhanced by a subducting plate giving the trend towards the west with time. A plume tail then remained stationary and caused the time-transgressive silicic and basaltic volcanism seen along the Snake River Plain. Shervais and Hanan (2008) suggest that flattening of the plume head occurred beneath an anisotropic lithosphere. To the north of the site of impact of the plume, the lithosphere of the accreted terrains is thin which caused the plume head to pass beneath it. The thickness of the cratonic lithosphere is not constant with the divergence of the $^{87}\text{Sr}/^{86}\text{Sr}$ 0.706 and 0.704 lines (recorded in the earlier intrusions) inferred to represent the extending of the lithosphere prior to volcanism. This lithospheric structure may have forced some of the plume head northwest (under the accreted terrains) and some southeast (under thinned craton) producing the geographically dispersed volcanism around 16 Ma (Shervais and Hanan 2008; Fig. 1.2). In this scenario the part of the plume forced south under the extended craton causes the reorientation of the plume tail to its current orientation. This model also proposes that the first volcanism produced by the plume tail is that from the Bruneau-Jarbidge eruptive centre of northern Nevada at ~ 12.7 Ma on the basis that volcanism previously attributed to the hotspot is geographically widespread and does not fit well with reconstructed plate motions of North America (Shervais and Hanan 2008). However the model of a 'plume tail' does not explain the 'flare-up' in silicic volcanism from 11.7-10.2 Ma (Bonnichsen et al. 2008).

Snake River Plain Rhyolites

The rhyolitic lavas and ignimbrites which dominate the Snake River Plain are the product of rising basaltic magma melting the crust (Leeman 1982; Bonnicksen et al. 2008 and references therein). They have similarities to A-type granites in terms of inferred magmatic temperatures and elevated high field strength elements (Bonnicksen 1982; Cathey and Nash 2004). Abundant basalt is required to cause fusion of the crust (e.g. Annen and Sparks 2002; Leeman et al. 2008), estimated as twice the volume of rhyolite (Bonnicksen et al. 2008).

Under the eastern Snake River Plain, geophysical (Peng and Humphreys 1998) and geochemical evidence (Shervais et al. 2006) has indicated the presence of a mid-crustal sill, c. 10 km thick and c. 90 km wide. Shervais et al. (2006) found cyclical geochemical variations in basalts consistent with models of layered intrusive complexes. The presence of a 10 km thick sill at a depth of c. 12 km supports modelling of the amount of basalt required to create the erupted volumes of rhyolite (Bonnicksen et al. 2008) and helps to explain the low topographic relief of the Snake River Plain, caused by basaltic intrusions loading the crust and causing it to sag (Anders and Sleep 1992; Humphreys et al. 2000). The chemistry of the rhyolite produced across the Snake River Plain is a function of the type of crust that was melted. In the west, where the crust is accreted oceanic terrain, peralkaline magmas were formed (McDermitt centre; Henry et al. 2006; Nash et al. 2006). Further east, the magmas are more metaluminous in character caused by the transition to North American craton which is being melted. An alternate suggestion is that rare 'post-hotspot' rhyolites in the eastern Snake River Plain were formed by extreme fractionation of basalt (McCurry et al. 2008) although no rocks of intermediate composition have been reported.

Eruptive centres

The sources of the rhyolitic ignimbrites exposed along the margins of the Snake River Plain are not exposed. It is thought that they are located within the plain and have been covered by basalt (Williams et al. 1990; McCurry et al. 1996). The term ‘eruptive centre’ was used for the region in which the Cougar Point Tuff succession is exposed in the Bruneau and Jarbidge canyons with the caveat that it referred to a geographic location from which the Cougar Point Tuff units were erupted, rather than any single caldera (Bonnichsen 1982). The area of the Bruneau-Jarbidge eruptive centre is $\sim 4,100 \text{ km}^2$ inferred from aeromagnetic anomalies and delimited by a series of faults on the south and west and with the northern and eastern boundaries (Bonnichsen 1982). Lineations suggest that rheomorphic flow in ignimbrites was either to or from this region post deposition and following cessation of the explosive activity, several rhyolite lavas are confined within this area. Some features of the Bruneau-Jarbidge eruptive centre are however inconsistent with an eruptive centre, for example no lithic breccias have been reported in the ignimbrites. These are common in proximal areas as a product of caldera collapse during the climactic phase of eruption e.g. Mt. Mazama (Druitt and Bacon 1986), Campi Flegrei (Rosi et al. 1996) and Santorini (Druitt and Sparks 1982). Mesobreccias and megabreccias which also typify caldera successions (e.g. Troll et al. 2004; Kokelaar et al. 2007) have also yet to be reported from the central Snake River Plain. The thickness of the ignimbrites is not typical of intracaldera facies, the maximum thickness of a single unit is the 100 m thick Cougar Point Tuff VII (Bonnichsen and Citron, 1982) whereas intracaldera facies from elsewhere are reported to be 300-1,000 m thick (Steven and Lipman 1976; Schermer and Busby 1994; Morgan and McIntosh 2005). Furthermore, no proximal Plinian fall deposits or caldera lake sediments have been reported which are common from other intra-caldera sequences (e.g. English Lake District, Kokelaar et al. 2007; Katmai, Fierstein and Hildreth 1992).

A number of discrete spaced eruptive centres have been proposed along the Snake River Plain (Fig. 1.1) from the McDermitt centre at c. 16 Ma through to the Yellowstone plateau

(Pierce and Morgan 1992) in the east. However, the concept of discrete eruptive centres has been challenged by several authors: Bonnicksen and Godchaux (2002) suggest that the distance between the inferred Bruneau-Jarbridge and Twin Falls eruptive centres may have been increased during opening (rifting) of the western Snake River Plain graben (Fig 1.2 B). During the period 10.4-9.5 Ma there were rhyolitic eruptions spanning 200 km along the plain, inconsistent with the idea of discrete spaced eruptive centres (Bonnicksen et al. 2008). Branney et al. (2008) also suggested that the calderas produced during the explosive eruptions may be overlapping and shingled along the plain as is apparent around the Yellowstone volcanic field.

Snake River-type volcanism

Snake River (SR)-type volcanism is a recently defined category of volcanism. It was proposed because it differs markedly from the better-known rhyolitic activity which typically gives rise to Plinian fall deposits, non-welded ignimbrites and rhyolitic domes (Table 1.1). The type area for SR-type volcanism is the central Snake River Plain which encompasses the massifs bordering the Bruneau-Jarbridge and Twin Falls eruptive centres (c. 13-8 Ma; Fig. 1.1 B). SR-type volcanism is defined by an association of eighteen facies, some of which are apparently unique to the Snake River Plain while others have been reported from other volcanic provinces although not to the same degree, or with the same association. Snake River-type ignimbrites are commonly intensely welded (Fig. 1.3 A, B), often lava-like (*sensu* Branney and Kokelaar 1992) and highly rheomorphic (e.g. Andrews et al. 2008) despite metaluminous chemistry (Bonnicksen and Citron 1982; Cathey and Nash 2004; Bonnicksen et al. 2008). The ignimbrites and lavas of the central Snake River Plain are inferred to have had high magmatic temperatures, commonly > 900 °C (e.g. Honjo et al. 1992; Cathey and Nash 2004; Andrews et al. 2008) whereas typical rhyolites have magmatic temperatures of 700-900°C (e.g. Hildreth 1979; Coombs and Gardner 2001; Wilson et al. 2006). Commonly fallout deposits beneath SR-type ignimbrites are fused due to heat conducted downwards reflecting high emplacement temperatures.

Feature	Snake River-type volcanism (Branney et al. 2008)	Conventional silicic volcanism (e.g. Branney and Kokelaar 2002)
Large volume eruptions	Characteristic	Absent or present
Fallout deposits of pumice lapilli	Rare	Common
Associated voluminous basalt	Characteristic	In some, not characteristic
Rhyolitic domes / spines / coulees	Characteristic	Common
Laminated thin-bedded ashfall deposits	Rare	Phreatomagmatic or distal
Fused ashfall layers	Characteristic	Rare / localised
Rheomorphic ignimbrites	Abundant, widespread	Rare (unless strongly peralkaline)
Lava-like facies in ignimbrites	Characteristic, widespread	Absent to rare / localised
Vesiculated, scoriaceous tops to ignimbrites	Common	Absent (present in some strongly peralkaline ignimbrites)
Pumice lapilli and blocks in ignimbrites	Absent to rare	Characteristic
Co-ignimbrite lag breccias	Absent to rare	Common
Grade of ignimbrites	High to extremely high	Mostly low to moderate
Crystal breakage in ignimbrites	Limited	Characteristic (rare in strongly peralkaline ignimbrites)
Pumice lenses, concentration zones, lithic coarse-tail grading	Absent to rare	Characteristic
Ignimbrite sorting	Poor to well-sorted	Mostly very poorly sorted
Elutriation pipes in ignimbrite	Rare, occur locally	Common
Cusped shards	Megascopic and microscopic	Microscopic
Spherical globule-like pyroclasts	Present	Absent, common in some strongly peralkaline ignimbrites
Inferred rhyolite viscosities	Low	High
Ash pellets and accretionary lapilli	Characteristic	Common
Abundant glassy chips in ignimbrites and ashfall deposits	Common	Not typical
High magmatic temperature of rhyolite	Characteristic	Not characteristic
Low f_{H_2O} rhyolite magmas	Characteristic	Variable
Evidence for surface water	Widespread, abundant	Variable

Table 1.1 Comparison of the characteristics of SR-type volcanism (Branney et al. 2008) and conventional silicic volcanism as seen elsewhere, as summarised by Branney and Kokelaar 2002)

The rhyolites have an anhydrous mineralogy (e.g. Honjo et al. 1992) dominated by quartz, plagioclase, sanidine, pigeonite, augite, fayalite, ilmenite, titanomagnetite and accessory

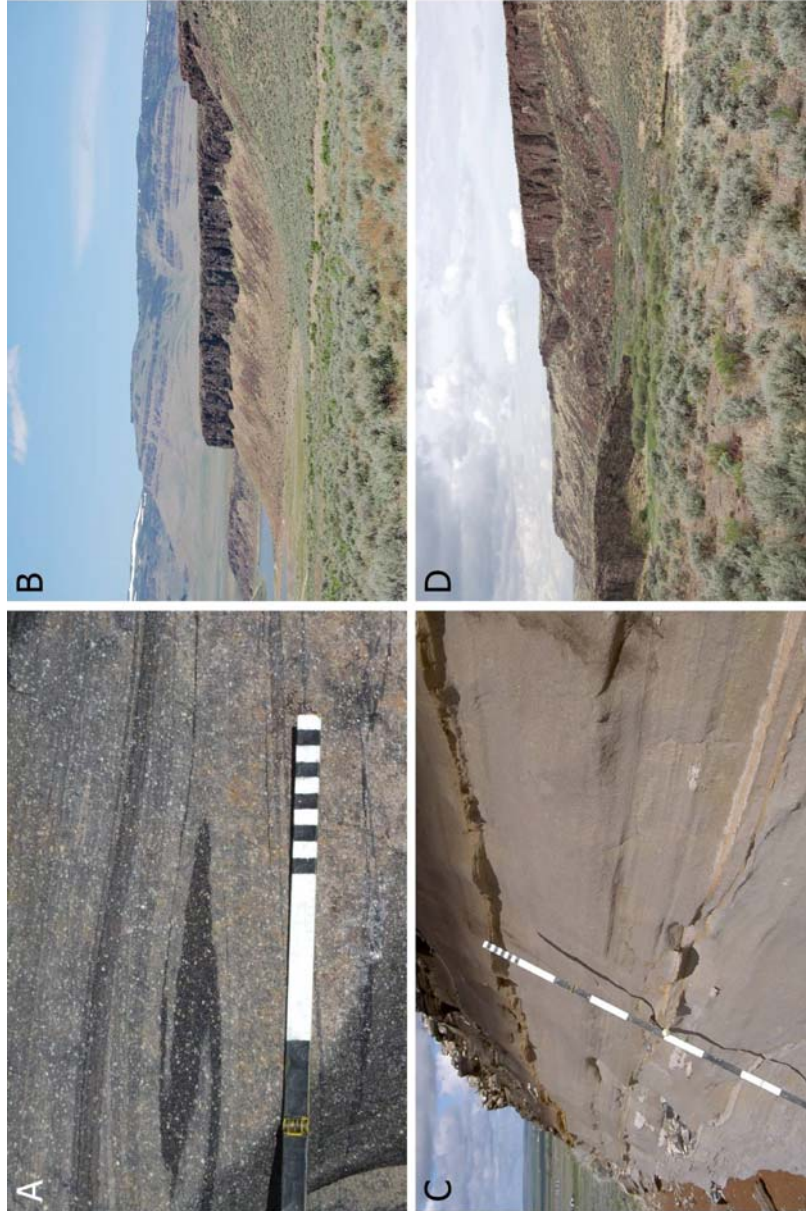


Figure 1.3 Aspects of Snake River-type volcanism; **A.** Flow banding in a rhyolitic unit of equivocal origin from the Mount Bennett Hills (Fig. 3.1). **B.** Grey's Landing ignimbrite in foreground (c. 30 m thick) in the Rogerson Graben with welded ignimbrites of the Browns Bench escarpment in background (Fig. 3.1) **C.** Fallout ash deposits under thin rhyolitic ignimbrite, Nat Soo Pah hot springs (Fig. 1.1) **D.** Large volume rhyolitic lava (the Indian Batt lava) from the Bruneau-Jarbridge eruptive centre (Fig. 1.1).

zircon and apatite which, when allied to the high magmatic temperatures suggests low magmatic water contents.

SR-type ignimbrites are well-sorted ($\sigma\phi$ 0.8 -1.5) compared to typical ignimbrites ($\sigma\phi$ 2-5) as defined by Walker (1971). This well-sorted nature is a function of the lack of pumice or lithic lapilli in the ignimbrites; commonly less than 5% of the material in these ignimbrites is lapilli-sized or larger. The lack of pumice lapilli is not confined to the ignimbrites; the underlying fallout deposits are commonly layers of parallel-bedded medium ash (Bonnichsen and Citron 1982; Branney et al. 2008; Fig 1.3 C) with individual shards having thick bi and tri-cusate remnant bubble walls. This contrasts with the framework supported, angular lapilli of microvesicular pumice which typify the fallout deposits in many rhyolitic provinces (e.g. Bond and Sparks 1976; Hildreth 1979; Fierstein and Wilson 2005).

Snake River-type rhyolites are also associated with a strong depletion in $\delta^{18}\text{O}$, with both ignimbrites and lavas producing values ranging between -1.3 and 3.8 ‰, significantly lower than the 7–10 ‰ $\delta^{18}\text{O}$ of typical rhyolites (Boroughs et al. 2005). One possibility to account for the depletion of $\delta^{18}\text{O}$ is assimilation of hydrothermally altered crust such as Idaho batholith with the amount of assimilant required dependent upon its isotopic characteristics (Boroughs et al. 2005). Further east, outside of the type area of SR-type volcanism, rhyolites from the Heise volcanic field have been reported with a variable depletion in $\delta^{18}\text{O}$. Three ignimbrites of normal $\delta^{18}\text{O}$ were erupted and followed by the Kilgore Tuff and post-Kilgore lavas which have low $\delta^{18}\text{O}$ (Bindeman et al. 2007). The ignimbrites from Yellowstone have slightly low to normal $\delta^{18}\text{O}$ (Bindeman and Valley 2000). At the Heise and Yellowstone centres, Bindeman et al. (2007) have suggested that the depletion of $\delta^{18}\text{O}$ can be linked to the progressive evolution of a volcanic centre, with the deposits of larger volume ignimbrites having higher $\delta^{18}\text{O}$. How this relationship may

be applied to the central Snake River Plain is unclear as currently no isotopically normal rhyolite from the central Snake River Plain has been reported.

Volumes

The erupted volumes of the younger eruptive centres (Yellowstone and Heise) are reasonably well constrained. The Yellowstone volcanic field has a cumulative erupted volume slightly larger than 3,800 km³ (Christiansen 1984; 2001) whereas the Heise Group has a total volume ~ 4,050 km³ (Morgan and McIntosh 2005). The volume of the older eruptive centres is even less well constrained. Estimates for the amount of rhyolite in the central Snake River Plain vary widely, estimated at 7,000 km³ (Bonnichsen et al. 2008) whereas the volume of just the Cougar Point Tuff succession has been estimated as 10,000 km³ (Perkins and Nash 2002).

Volumes of individual ignimbrites within the Snake River Plain are equally poorly constrained, as a result of poor characterisation of the individual units in terms of geochemistry, stratigraphy and the lack of geological maps for much of the region. The largest estimates come from those in the Cougar Point Tuff whereby individual events are estimated at 1,000 km³ (Bonnichsen et al. 2008) and up to 500 km³ (Boroughs et al. 2005). Recently Leeman et al. (2008) estimate volumes of between 100 and 1,800 km³ for the individual eruption units although no justification (e.g. distribution maps) is given for the volumes assigned to each unit. Between the larger ignimbrites are some smaller units, such as those seen near the top of the Rogerson Graben stratigraphy, with individual volumes ~ 10 km³ (e.g. Sand Springs Ignimbrite of Andrews et al. 2008). These estimates have to be considered as having large errors, for example the volumes of individual Cougar Point Tuff ignimbrites were previously estimated to an order of magnitude (Boroughs et al. 2005).

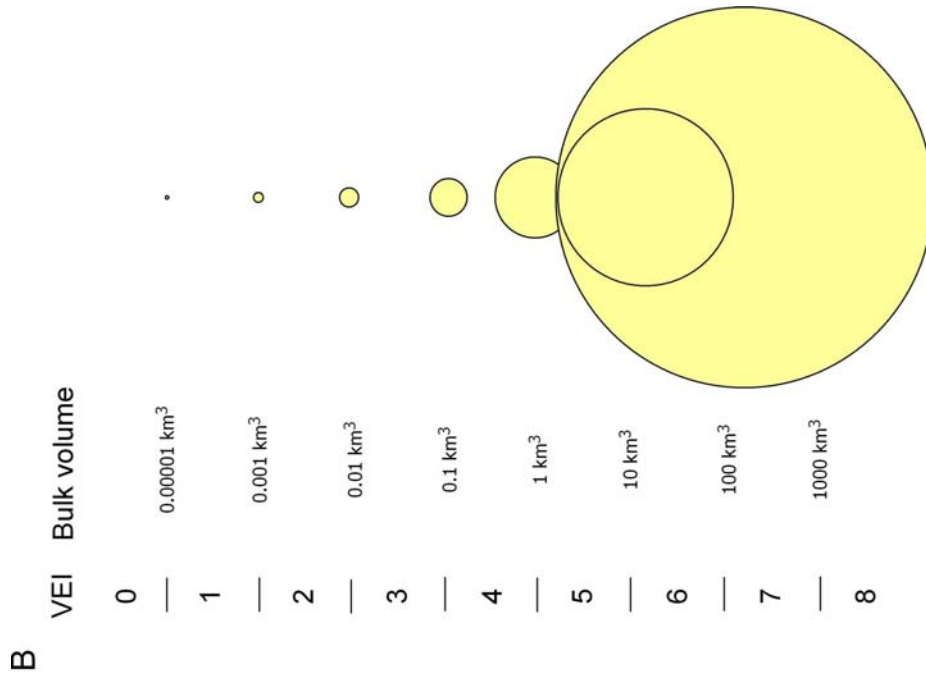


Figure 1.4 A. Eruption volumes of some of the large eruptions from the Yellowstone hotspot, compared to other well known eruptions (e.g. Mazama) and those from historical times (e.g. Mount St. Helens) based on Smith and Siegel (2000) **B.** Semi-quantitative VEI scale of Newhall and Self (1982), based on erupted volume and observed features of the eruption.

Current estimates of eruption volumes for individual central Snake River Plain ignimbrites are amongst the largest known. Mason et al. (2004) classify ignimbrites by way of erupted mass rather than volume, which allows comparison between non-welded deposits and intensely welded deposits on an equal basis. Using this classification, eruptions from outside the type area of SR-type volcanism e.g. the Huckleberry Ridge Tuff from Yellowstone and the Kilgore Tuff from Heise were within the top 25 largest eruptions known. If the volumes of Leeman et al. (2008) are correct, Cougar Point Tuff units 11 and 13 would be of similar magnitude. The largest eruptions of historical times, those of Tambora and Krakatau are compared in Figure 1.4 with the Huckleberry Ridge Tuff and the Kilgore Tuff. Whilst compiling the volumes of big eruptions, Mason et al. (2004) suggested there may be more ‘super-eruptions’ (those with volumes $> 300 \text{ km}^3$ DRE and 750 km^3 of ash; Sparks et al. (2005) within the CSRP.

In addition to the ignimbrite volumes, SR-type volcanism is characterised by large volume rhyolitic lavas (Bonnichsen and Kauffman 1987; Branney et al. 2008) with volumes reaching 200 km^3 (Bonnichsen 1982; Fig 1.3 D). These lavas are many times larger than the (5 km^3) small domes and couleés that typify rhyolitic eruptive centres elsewhere (e.g. Fink and Bridges 1995).

Interaction with water

Evidence is emerging that some of the volcanic deposits in central Idaho show evidence of having been emplaced into wet, fluvio-lacustrine environments. The most widespread evidence comes in the form of basaltic pillow lavas and ‘water-affected basalt’ (Godchaux and Bonnichsen 2002). Pillow lavas are common in western Idaho at an altitude of > 800 metres, reflecting the presence of Lake Idaho during the Miocene. The lake was hosted in the Western Snake River Plain graben and was of similar size to the present-day great lakes of North America (Bonnichsen and Godchaux 2002). During the Miocene the extent of the lake is supposed to have waxed and waned with the eastern and southern margins of the

lake not currently established. The western and northern margins of this lake are well constrained with evidence from rhyolitic lavas suddenly becoming brecciated upon entering water (e.g. Jump Creek Rhyolite) or having strong development of opal, restricted to beneath 2900 feet (~ 800 m). The Wilson Creek Rhyolite has an age of 11.41 ± 0.08 Ma (Godchaux and Bonnichsen 2002) helping to constrain the timing of Lake Idaho, which is estimated to have been present from 12 to 2 Ma in the western Snake River Plain graben (Bonnichsen and Godchaux 2002). In the massifs to the south of the Snake River Plain, there is abundant evidence for interaction of pyroclastic material and water. Some rhyolite units are silicified reflecting post-depositional alteration (e.g. Browns Bench Unit 1; Bonnichsen et al. 2008), whilst other units have peperitic bases reflecting emplacement on a wet substrate (e.g. Tuff of Wooden Shoe Butte; Fig. 1.5 D; Branney et al. 2008).

Volcaniclastic sediments have been reported from the Bruneau-Jarbridge eruptive centre (Bonnichsen 1982), the Rogerson Graben (Andrews et al. 2008) and the Cassia Mountains (Williams et al. 1990; Perkins et al. 1995). These may contain ripples (e.g. Fig. 1.5 A) and scour surfaces (e.g. Tuff of Wooden Shoe Butte) as well as massive facies.

Ash aggregates, often used to infer activity involving water, are common with numerous units in the central Snake River Plain containing accretionary lapilli (e.g. Jackpot 6 of Andrews et al. 2008) or rimmed pellets (e.g. the Tuff of Wooden Shoe Butte, Tuff of Magpie Basin).

Other styles of volcanism

SR-type volcanism is defined with respect to the deposits surrounding the inferred Twin Falls and Bruneau-Jarbridge eruptive centres, in that succession, all deposits are of SR-type. Outside the type area of SR-type volcanism deposits may or may not show some characteristics of SR-type volcanism.

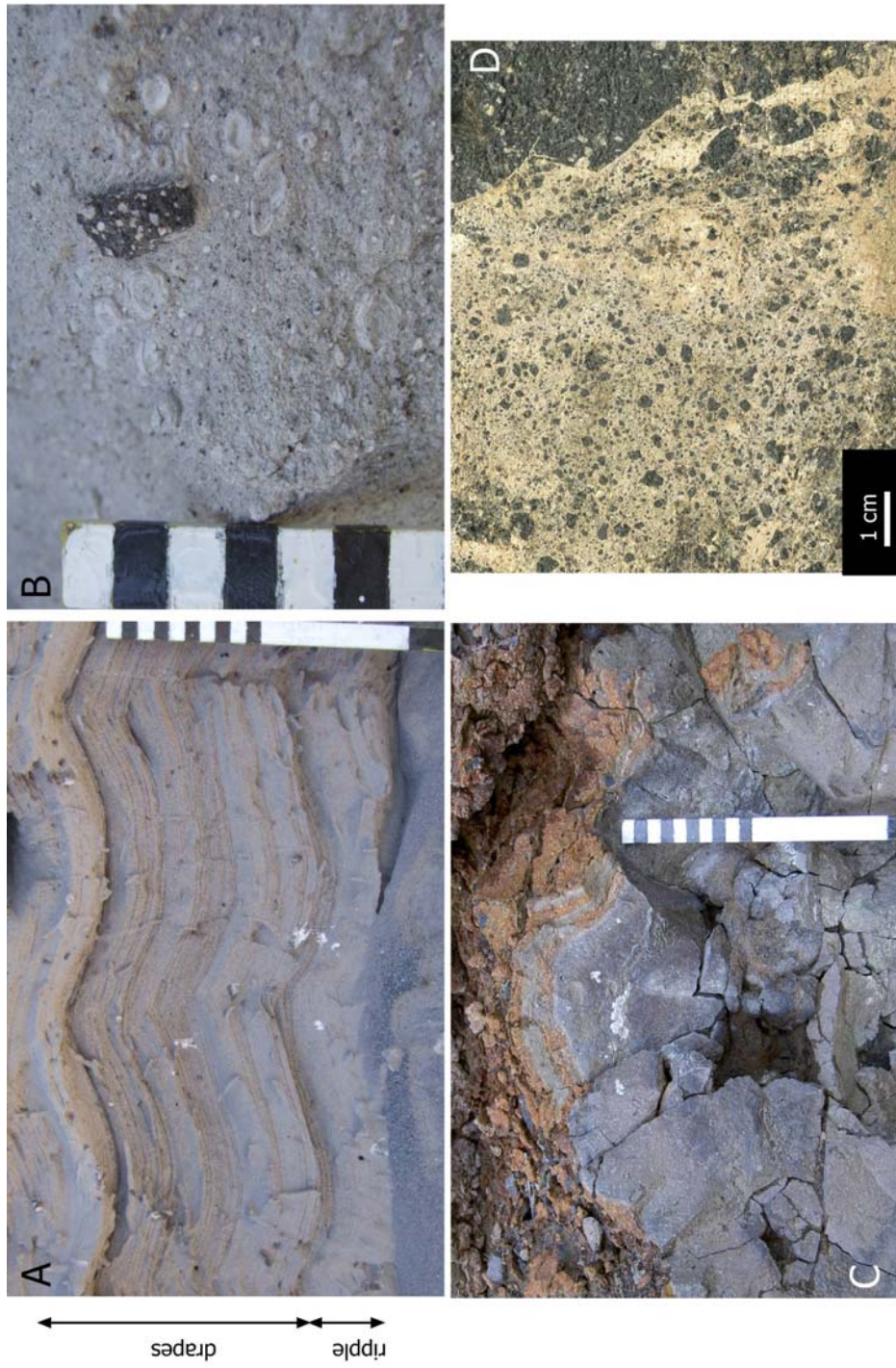


Figure 1.5 Examples of water:magma interaction in the Snake River Plain. **A.** Draped ripples in basaltic phreatomagmatic tuff near Hagerman. **B.** Un-named rhyolitic phreatomagmatic tuff in Big Cottonwood Canyon (Fig. 4.1) with accretionary lapilli and glassy non-vesiculated clasts. **C.** Basaltic pillow lava at Lily Grade formed by basalt flow entering Lake Idaho. **D.** Peperite at the base of the Wooden Shoe Butte Member, Rock Creek canyon (Fig. 4.1).

The Magic Reservoir eruptive centre (MREC) exhibits deposits that are not of SR-type (Leeman 1982; Honjo and Leeman 1987); it is excluded from the ‘type area’ of SR-type volcanism because its younger age (c. 3 Ma) places it out of age progression (Leeman 2004; Fig. 1.2 A) and it is located off axis to the north of the plain. The MREC contains non to weakly welded ignimbrites (e.g. the Young Tuff of Magic Reservoir) with abundant pumice clasts in their non-welded facies. Where the ignimbrites are weakly welded the MREC ignimbrites show a well-developed eutaxitic texture which has not been reported from SR-type ignimbrites. Fallout deposits from the MREC are clast supported, well-sorted, framework supported angular pumice lapilli. The Magic Reservoir eruptive centre also contains numerous small volume ($\leq 1 \text{ km}^3$) rhyolitic lava domes.

The 10.2 Ma Arbon Valley Tuff (Kellogg et al. 1994) is one of the few units thought to have been erupted from the Picabo eruptive centre (Fig. 1.1 B; Fig. 1.2 A). This unit is distinctly different to the time-equivalent ignimbrites erupted from the Bruneau-Jarbridge and Twin Falls eruptive centres further west. The Arbon Valley Tuff is dominantly non-welded, pumice and lithic-bearing, moderate to poorly-sorted and containing framework-supported pumice-lapilli fallout deposits. The ignimbrite contains many features characteristic of ignimbrites produced from normal explosive rhyolitic volcanism e.g. presence of non-rhyolitic lithics, imbrications of pumice clasts and elutriation pipes, all of which are rare to absent in Snake River-type ignimbrites. The Arbon Valley Tuff also has a distinctive isotopic signature compared to the SR-type ignimbrites further west, it has ϵNd of -20 compared to ϵNd of c. -7 for SR-type rhyolites and ϵHf of -22 compared to ϵHf of c. -5 for SR-type rhyolites (Nash et al. 2006).

Global occurrence of SR-type volcanism

Understanding SR-type volcanism is of importance as it represents a devastating style of volcanic activity which has seemingly occurred numerous times through Earth history.

Given that Snake River-type volcanism has been defined on the basis of an association of facies (Branney et al. 2008), the ‘degree’ of Snake River-type behaviour may vary. The locations of volcanic provinces worldwide with aspects of Snake River-type behaviour are shown in Figure 1.6. The deposits in Etendeka are of very similar style with large volume, intensely welded rhyolites, produced from magmas of inferred high magmatic temperatures and estimated low water contents (e.g. Ewart et al. 1998). The rhyolites of the mid-continental rift in Keweenaw are also of Snake River-type with some intensely welded, lava-like ignimbrites of high inferred temperatures intercalated with reworked volcanoclastic deposits (e.g. Green 1989; Green and Fitz 1993). In the English Lake District, SR-type deposits are present in intra-caldera deposits with intensely welded lava-like ignimbrites (e.g. Branney et al. 1992), fine-grained ashfall deposits and ash aggregates (e.g. Branney 1991) but other aspects differ such as the presence of fiammé and pumice in some of the ignimbrites, small-volume lava domes and coulees, and a calc-alkaline chemistry which are not characteristic of SR-type volcanism.

This work

This thesis is organised as follows:

Chapter 2 investigates the geochemical evolution of the Twin Falls eruptive centre and compares the petrology of the erupted products to those of the preceding Bruneau-Jarbidge eruptive centre.

Chapter 3 combines field, geochemical and geochronological data to correlate units described in Chapter 2 with others from adjacent massifs along the southern margin of the Snake River Plain. In addition to the correlations based on the units of Chapter 2, further correlations are tested based on the regional stratigraphic framework proposed by Bonnicksen et al. (2008).

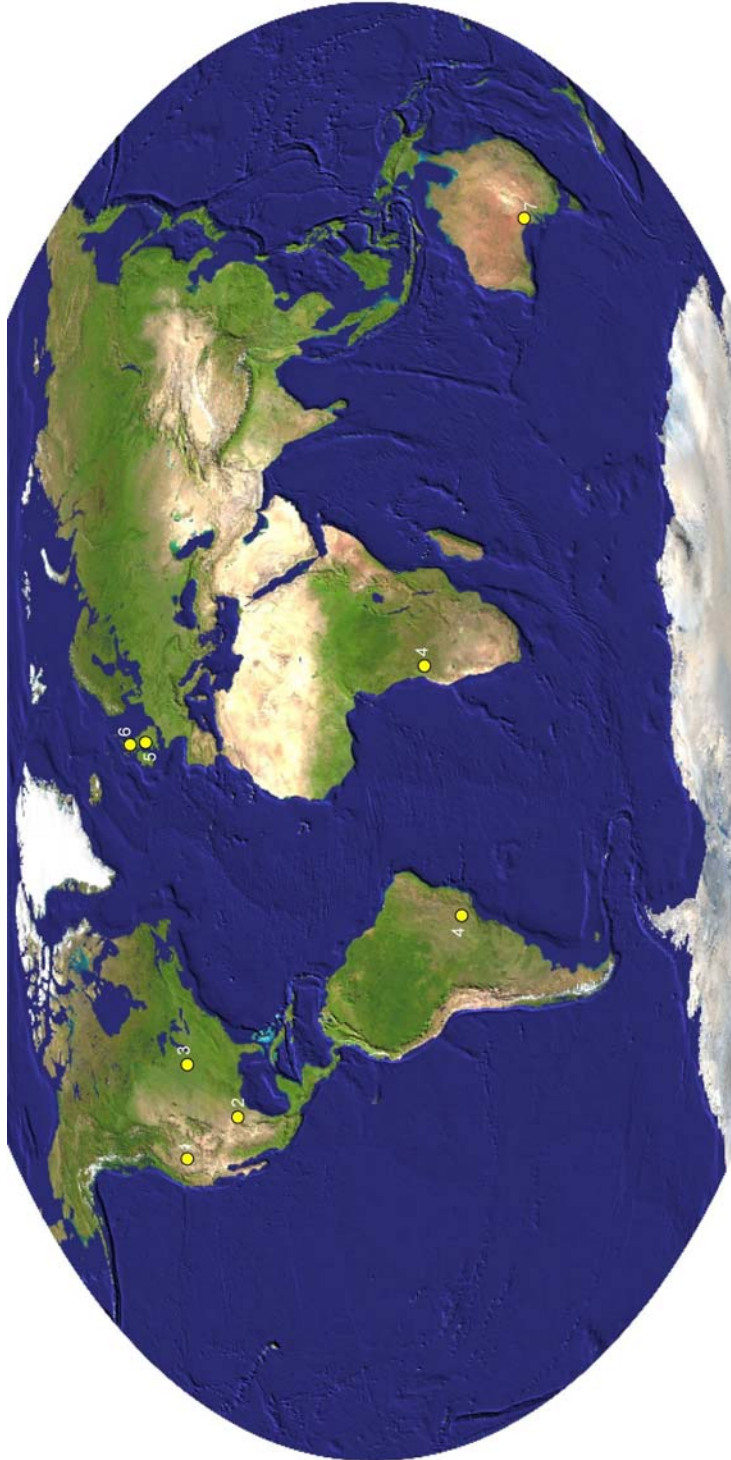


Figure 1.6 Locations of volcanism with some Snake River-type characteristics worldwide (Branney et al. 2008):

1. The Yellowstone hotspot track: outside the type area of SR-type volcanism some units show aspects of SR-type behaviour e.g. rheomorphic and locally lava-like Kilgore Tuff (Morgan and McIntosh 2005) 2. Trans Pecos, Texas: intensely welded, lava-like ignimbrites of high (>900 °C) magmatic temperature (Henry et al. 1990). 3. Keweenaw, Minnesota: High temperature rhyolites, up to 250 m thick which are intensely rheomorphic (Fitz and Green 1993) interbedded with fluvio-lacustrine deposits.
4. Etendeka-Parana: Voluminous rhyolites, individually > 100 m thick (Milner et al. 1992; Jerram 2002) of high magmatic temperatures, >1000 °C (Ewart et al. 1998)
5. Scafell caldera, English Lake District: Lava-like ignimbrites, widespread bedded ashfall deposits (Branney et al. 1992) 6. Glencoe caldera: Thick, lava-like rheomorphic ignimbrites with upper autobreccias, interbedded with fluvio-lacustrine deposits and phreatomagmatic deposits (Kokelaar and Moore 2006). 7. Yardea dacite, south Australia: Large volume, high magmatic temperature dacitic units (Creaser and White 1991).

Chapter 4 investigates the eruptive mechanism of a non-welded ignimbrite intercalated within the succession described in Chapter 2 to consider the effect of water in the formation of the fine-grained non-welded ignimbrite and the implications for the eruptive centre.

Chapter 5 utilises data obtained from melt inclusions to determine the degree to which the pre-eruptive volatile content may have controlled the eruptive style of that magma. It also explores the relative roles of halogens and emplacement temperatures upon the rheomorphic behaviour of Snake River-type ignimbrites.

Chapter 6 synthesises the work and suggests some possible avenues for future study.

Chapter 2: Geochemical evolution of the Twin Falls eruptive centre and comparison with the Bruneau-Jarbridge eruptive centre

Abstract

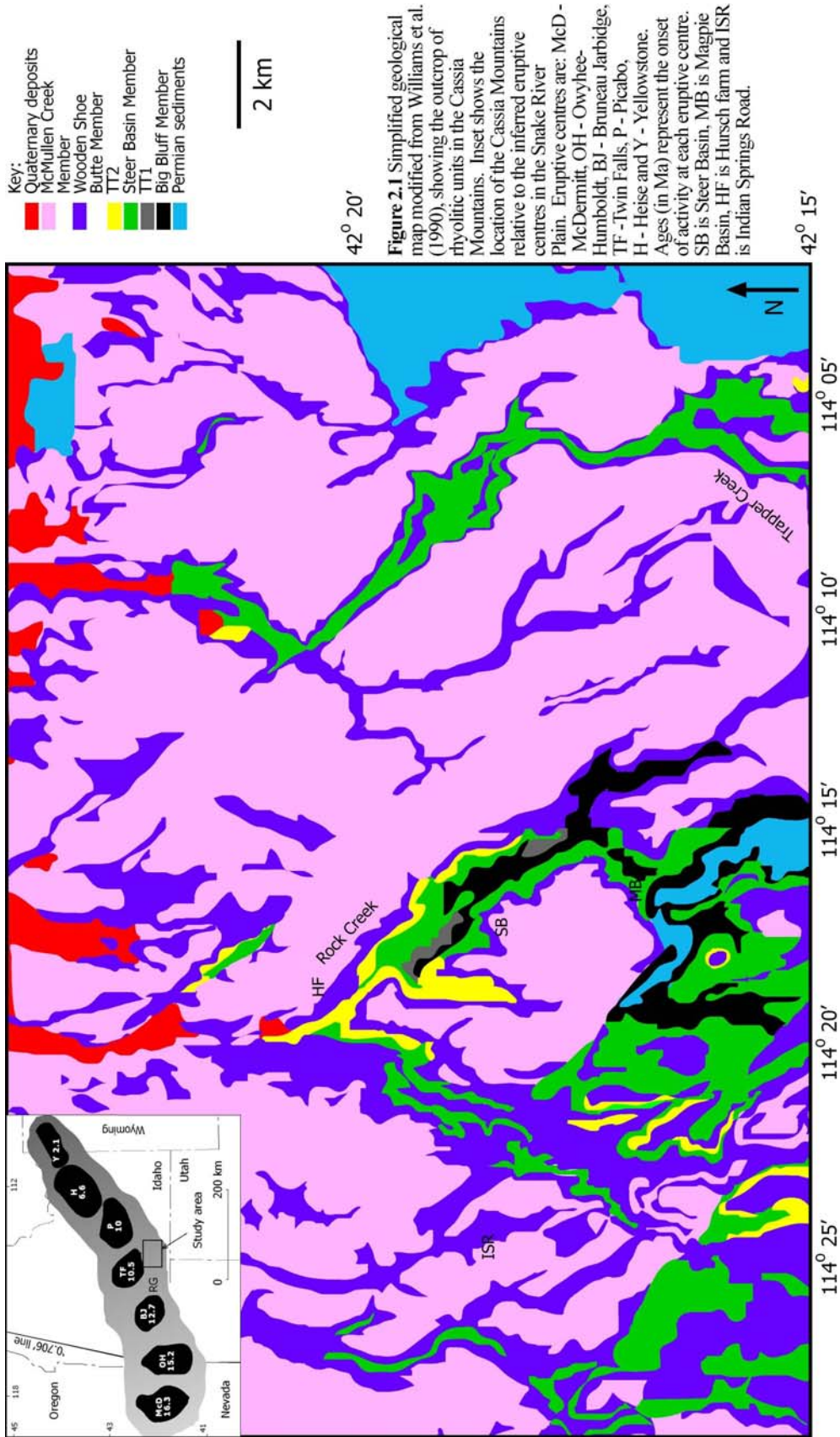
A succession of rhyolitic ignimbrites in the Cassia Mountains of southern Idaho record the ~11.3-8.6 Ma eruptive behaviour of the Yellowstone hotspot. They are thought to be derived from the proposed Twin Falls eruptive centre, buried beneath younger basalts of the central Snake River Plain. Most are intensely welded and separated by slope-forming non-welded volcanoclastic deposits including ashfall layers, sediments and one non-welded ignimbrite. The volumes of individual eruption units range from tens to hundreds of cubic kilometres. High (900 ± 50 °C) magmatic temperatures are inferred from a variety of geothermometers and are consistent with anhydrous phenocryst assemblages. The ignimbrites show remarkable chemical heterogeneity on a phenocryst scale with multiple compositional modes of both pigeonite and augite, present within a single ignimbrite. Crystal aggregates of clinopyroxene, feldspar and iron oxides record only a single mode of pigeonite and a single mode of augite. This is thought to reflect a magmatic system in which a single parental magma generated a number of smaller magma chambers, which then under slightly different conditions fractionated slightly differently to produce the different clinopyroxene compositions. The silicic volcanic succession shows a temporal trend towards more mafic compositions in whole rock, feldspar, clinopyroxene and glass compositions. The uppermost unit, the McMullen Creek Member, represents a marked change in this trend with a return to more evolved compositions than the preceding units. The McMullen Creek Member is also distinct in terms of neodymium isotopes indicating a larger crustal component. The Cassia Mountain ignimbrites are interpreted as being produced from a complex magmatic system in which multiple batches of magma became physically separated prior to eruption and then mixed during the eruptions. This model contrasts with the preceding Bruneau-Jarbridge eruptive centre, which has been inferred to represent a large-volume, long-lived, thermo-chemically zoned magma system.

Introduction

The Cassia Mountains are located on the southern margin of the Snake River Plain in southern Idaho, USA. The Snake River Plain represents the trace of the Miocene Yellowstone hotspot, thought to have initiated around 17 Ma with the impact of a mantle plume at the base of the continental lithosphere near the Idaho-Oregon border (Draper 1991; Camp and Ross 2004). Silicic volcanism associated with the hotspot is broadly time transgressive, younging northeast towards Yellowstone (Pierce and Morgan 1992). The sources of the silicic eruptions are thought to have been spaced ‘eruptive centres’ (Bonnichsen 1982; Pierce and Morgan 1992; McCurry et al. 1996) between McDermitt in the west ~16 Ma (Henry et al. 2006) to Yellowstone in the east ~2 Ma (Christiansen 2001; Fig. 2.1). Bonnichsen (1982) proposed that the Bruneau-Jarbidge region of northern Nevada represents a buried ‘eruptive centre’ with the caveat that it was possible that the sources of these eruptions were overlapping calderas rather than a discrete caldera volcano. A succession of outflow ignimbrite sheets are exposed in the hills bordering the Snake River Plain. The sources of these ignimbrites have been obscured by later basalt lavas (Williams et al. 1990; Shervais et al. 2006). The Twin Falls eruptive centre (Fig. 2.1) proposed by Pierce and Morgan (1992) is located north of the Cassia Mountains, and has been considered to be the source of some of the ignimbrites within the Cassia Mountains (McCurry et al. 1996). This chapter characterises the stratigraphy of the ignimbrites and provides geochemical data to provide constraints on the possible Twin Falls eruptive centre and its magmatic system.

Snake River-type volcanism

The Cassia Mountains lie within the type area of Snake River or ‘SR’-type volcanism (Branney et al. 2008), which includes the Bruneau-Jarbidge eruptive centre in the west and the Twin Falls eruptive centre in the east. Snake River-type volcanism is defined by a distinctive association of volcanic facies. Some of the facies occur at other volcanic provinces but to a lesser extent or degree, while others appear to be unique to Snake River-type volcanism. The SR-type association includes large volume (VEI 6-8) ignimbrites that are intensely welded. They are unusually well-sorted compared to ignimbrites elsewhere and typically contain few if any lapilli. Pumice lapilli are rare within SR-type ignimbrites and fall deposits, which are commonly parallel



bedded fine to coarse ash rather than typical Plinian pumice fall layers. SR-type volcanism contains abundant evidence of interaction with water, including basaltic pillow deltas, peperitic bases to ignimbrites, volcanoclastic sediments, 'water-affected basalt' (Bonnichsen and Godchaux 2002) and ash aggregates. Many of the features of SR-type volcanism are well displayed within the Cassia Mountain succession, which forms the basis of this chapter.

Geological Background

The Cassia Mountains (Fig. 2.2) are one of a series of massifs flanking the central Snake River Plain (CSRP); others include the fault-bounded Browns Bench massif to the west and the Mount Bennett Hills on the north side of the Plain (see Chapter 3). All these massifs are composed of rhyolitic ignimbrites with subordinate ashfall layers and lavas. Typical exposures are found in deep canyons. The intensely welded units form cliffs separated by gentle slopes that record non-welded ignimbrites and ashfall layers, reworked volcanoclastic deposits and palaeosols. The ages of the rhyolitic rocks are not well constrained, although more geochronological data has recently become available (Link and Oakley 2006; Bonnichsen et al. 2008 and Chapter 3). Ages of some of the volcanic units in the Cassia Mountains have been published, however there is some disagreement about the correct age of the individual units. The Big Bluff Member (Fig. 2.3) was dated by $^{40}\text{Ar}/^{39}\text{Ar}$ and found to be 10.83 ± 0.03 Ma using crystal separates from a distal correlative ashfall collected at Trapper Creek (Perkins et al. 1995). However, this age was later revised to 10.93 ± 0.03 Ma by Perkins et al. (1998) and is revised to 11.01 using the Renne et al. (1998) Fish Canyon Tuff age. The Steer Basin Member (Fig. 2.3) was estimated to be 10.50 ± 0.2 Ma based on interpolation between known units (Perkins and Nash 2002). Cathey and Nash (2004) show that the interpolation method of Perkins and Nash (2002) is robust as indicated within the Cougar Point Tuff succession where it is based on a stratigraphy with good geochronological control. The Wooden Shoe Butte Member was dated as 8.6 ± 0.2 Ma by $^{40}\text{Ar}/^{39}\text{Ar}$ age based on a welded unit in the Trapper Creek area (Fig. 2.1), some 30 kilometres east of Rock Creek (Perkins et al. 1995), but a more recent date of 10.20 ± 0.03 (Perkins et al. 1998; again recalculated to Renne et al. 1998) is preferred as the Wooden Shoe Butte Member likely represents the 'unknown tuff' of Trapper Creek (Perkins et al. 1995) which was dated by

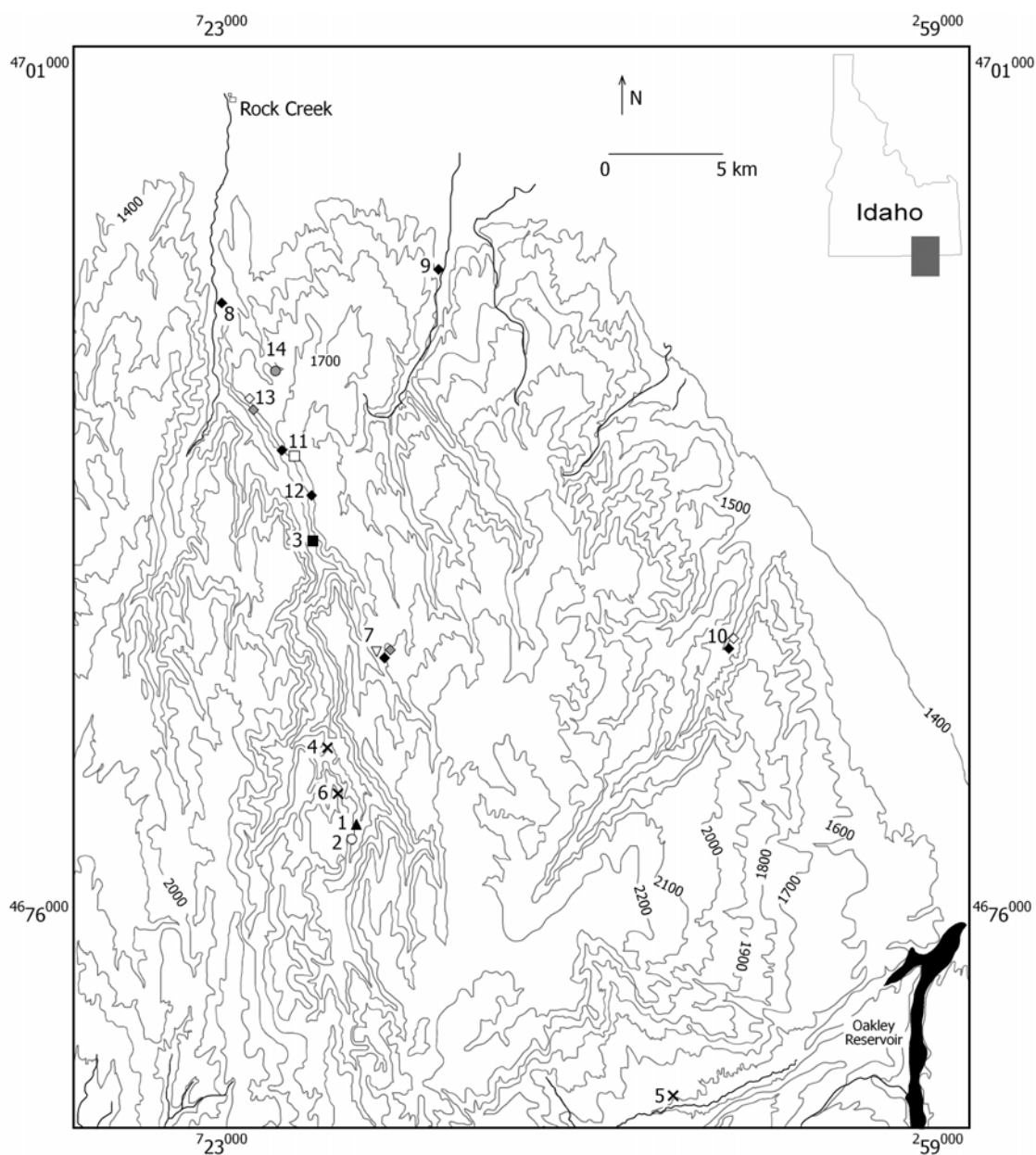


Fig. 2.2 Locations of samples for geochemical analyses and additional information for the generalised logs of the unit. Numbers next to the samples are referred to the sample names below:

- 1. Magpie, MAGFA2; 2. TBB; 3. BVSF;
- 4. PJI; 5. TCPU7, TCPU8; 6. PJFC11;
- 7. HARWS1, 2, 5, BV, UV; 8. TWSBBV
- 9. WSBV3 DRY; 10. TWSBBV BCC2, TWSBMV BCC2; 11. TWSB CAS2;
- 12. TWSBBV CAS1, SBV; 13. WSBMV2, WSBV1; 14. MCMJO

- McMullen Creek Member basal vitrophyre
- ◆ Wooden Shoe Butte Member upper vitrophyre
- ◇ Wooden Shoe Butte Member medial vitrophyre
- ◆ Wooden Shoe Butte Member basal vitrophyre
- ▽ Wooden Shoe Butte Member fallout
- × Deadeye Member
- Steer Basin Member upper vitrophyre
- Steer Basin Member basal vitrophyre
- Big Bluff Member upper vitrophyre
- Big Bluff Member basal vitrophyre
- ▲ Magpie Basin Member

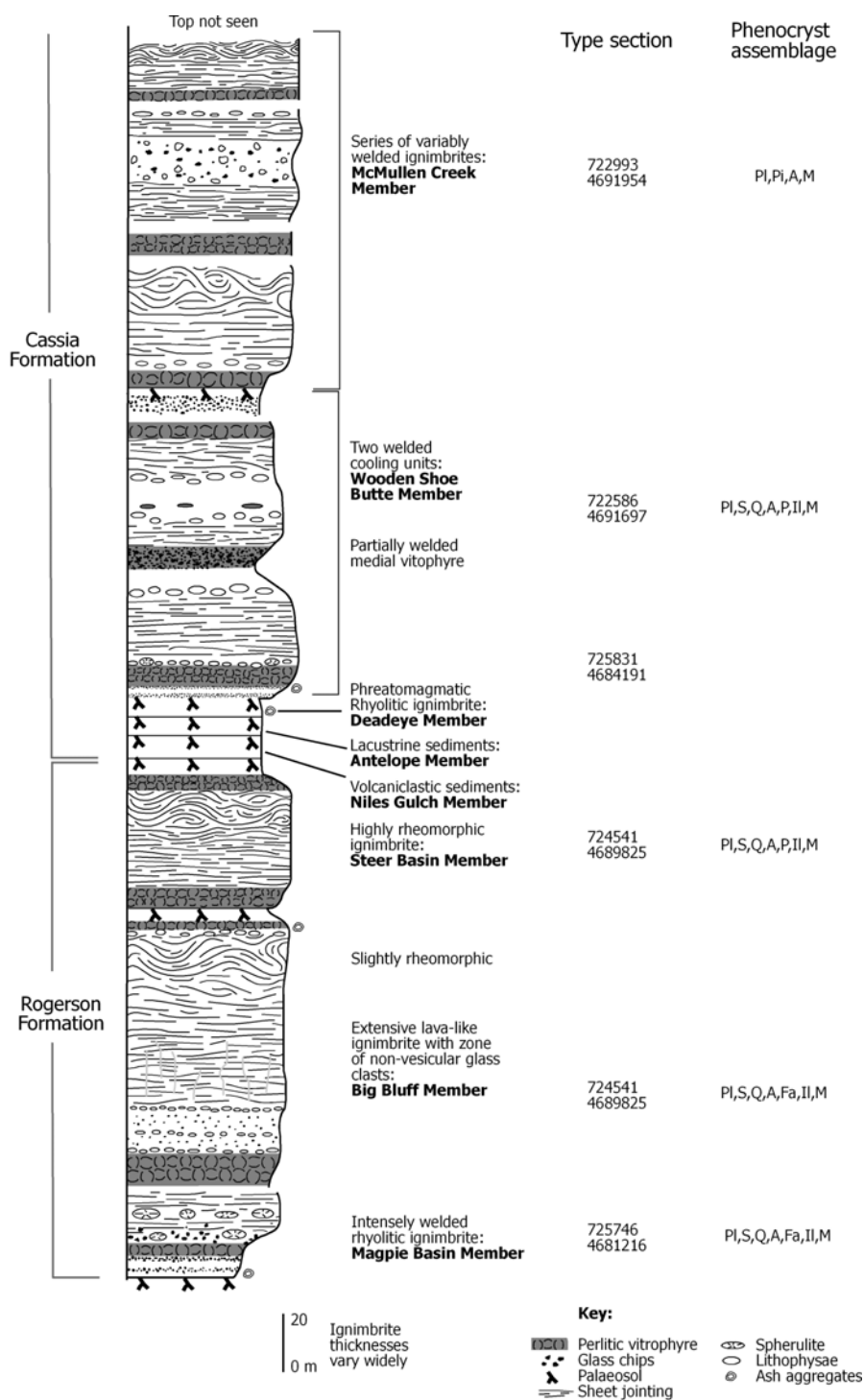


Figure 2.3 Generalised vertical section of the Cassia Mountains, showing the dominance of intensely welded ignimbrites in the succession. The type locality for the major units is provided. Phenocryst assemblage is given with the abbreviations: Pl - plagioclase, S - sanidine, Q - quartz, A - augite, P - pigeonite, Fa - fayalite, Il - ilmenite, M - magnetite. Accessory zircon and apatite are found throughout the stratigraphy

$^{40}\text{Ar}/^{39}\text{Ar}$ as 10.02 ± 0.03 Ma. The overlying McMullen Creek Member (Fig. 2.3) from the Trapper Creek section is reported as 8.94 ± 0.07 Ma (Nash et al. 2006), consistent with the age of the Wooden Shoe Butte Member being 10.13 Ma as reported by Perkins et al. (1998).

The lowermost units in the Cassia Mountains (from the Ibex Peak to the Steer Basin Member; Fig. 2.3, 2.4, 2.5, 2.6) are considered to be part of the Rogerson Formation (Andrews et al. 2008; see Chapter 3). The Rogerson Formation is named after the Rogerson Graben area 40 km to the west of the Cassia Mountains. The Cassia Mountains were mapped by Mytton et al. (1990) and Williams et al. (1990, 1991). Two of the units at the base of the Rock Creek section, the Big Bluff and Steer Basin members (Fig. 2.3) are thought to be the equivalents of the Jackpot Member 1-6 and Jackpot Member 7 in the Rogerson Graben (Andrews et al. 2008; Chapter 3). Since the mapping work, studies have mostly focussed on the geochemistry and petrology of individual units (Watkins et al. 1996; Parker et al. 1996). Lineation data have been mapped and tentatively indicate that the Big Bluff Member came from the east, whereas other ignimbrites have sources to the north of the Cassia Mountains (McCurry et al. 1996; Fig 2.1). The units above the Steer Basin Member are termed the Cassia Formation, based on their outcrop in the Cassia Mountains.

This study investigates how the magmatic system that produced these units evolved through time, as recorded by the rhyolitic stratigraphy of the Cassia Mountains. The stratigraphy in this paper is based on that in Rock Creek (Fig. 2.2) with supporting evidence from Trapper Creek, and the intervening canyons.

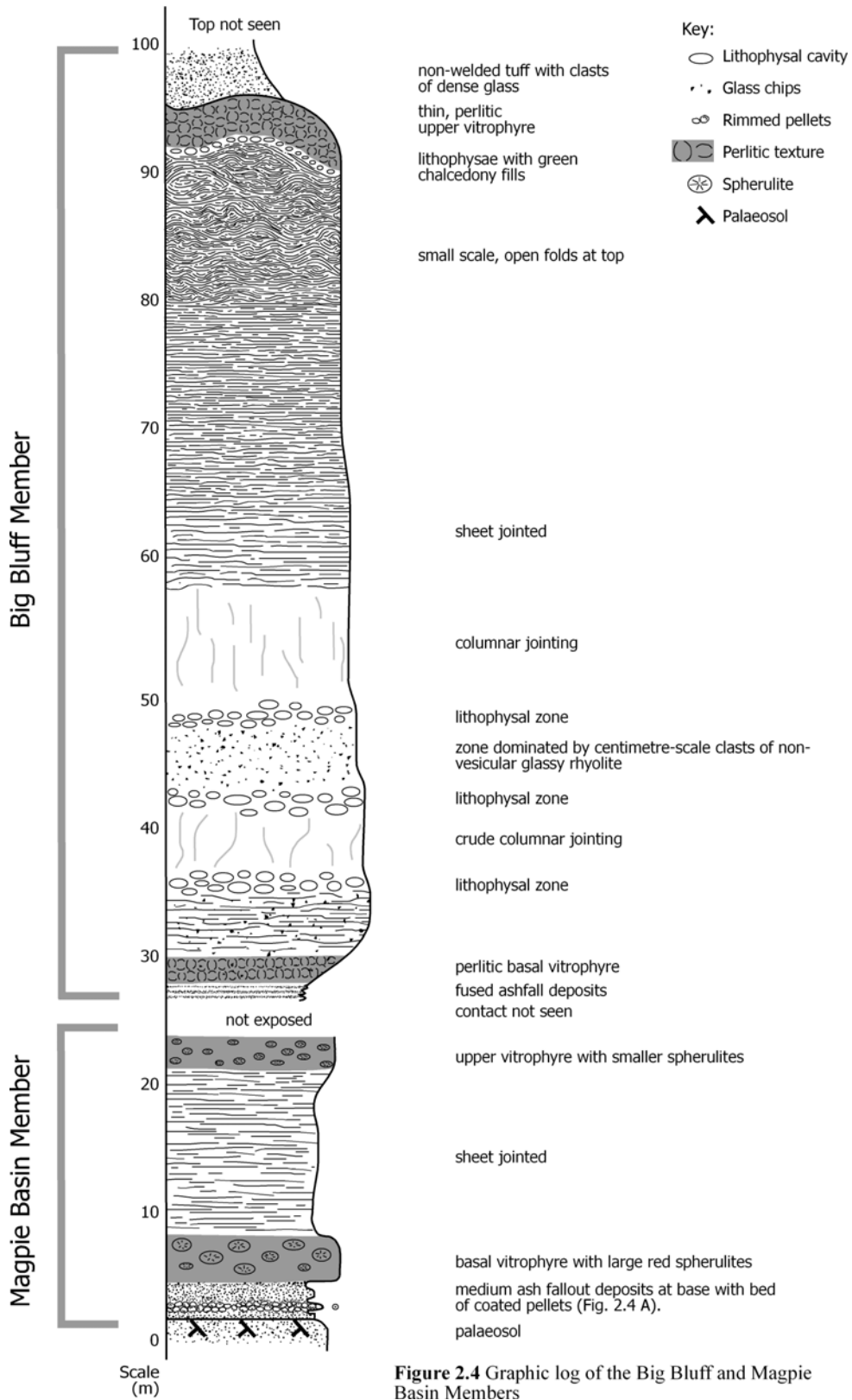


Figure 2.4 Graphic log of the Big Bluff and Magpie Basin Members

Unit descriptions

The Ibex Peak Member

The Ibex Peak Member is poorly exposed in the Rock Creek area. It reaches 10 m thickness and unconformably overlies Permian limestone (Williams et al. 1990). To the east, in Trapper Creek the Ibex Peak Member thickens dramatically to > 50 m. In Trapper Creek, the Ibex Peak Member contains silicified deposits and abundant diatomite.

Interpretation: the Ibex Peak Member is mostly volcaniclastic sediment. The greater thickness of the formation in the eastern Cassia Mountains (e.g. Trapper Creek) suggests that this eastern area was a local depocentre for sediments, possibly a fault-bound basin formed by Miocene extension (Hildebrand and Newman 1985).

Magpie Basin Member

The base of the Magpie Basin Member rests on a well developed palaeosol containing calcified rootlets. Above this, a metre-thick parallel-bedded, well-sorted ash, exposed in a single erosional gully (Fig. 2.5 A), contains a bed of coated pellets. The pellets are up to a centimetre in diameter and composed of a core of medium ash surrounded by a single layer of white fine ash. Above the bedded ash is a 10-20 m thick sheet of intensely welded rhyolitic tuff with thick (3 m) upper and lower vitrophyres and a sheet-jointed, lithoidal centre (Fig. 2.4). The vitrophyres host abundant red spherulites that are characteristic of the Magpie Basin Member and angular fragments of non-vesicular glass < 3 cm in diameter.

Interpretation: The presence of the laterally continuous parallel bedding and coated pellets and the good sorting are characteristic of deposition by fallout. The absence of a basal breccia and limited thickness of the overlying welded rhyolite suggests that it is an ignimbrite rather than a lava. Rhyolitic lavas in the Snake River Plain have basal autobreccias and are generally > 30 m in thickness (e.g. Bonnicksen and Kaufman 1987; Branney et al. 2008). The presence of abundant small clasts of black glass within the interior of the unit further supports the

interpretation as an intensely welded ignimbrite. The bedded ash and coated pellets are interpreted to represent a series of discrete fallout events preceding the emplacement of the ignimbrite.

Big Bluff Member

The lowest exposure of the Big Bluff Member is composed of ≤ 2 m of parallel-bedded, well-sorted ash similar to that seen within the base of the Magpie Basin Member (Williams et al. 1990). Above this at the type section in Magpie Basin is at least 70 m of intensely welded rhyolitic tuff (Fig 2.3, Fig. 2.5 B) including a couple of metres thickness of crystal rich (c. 15%) black basal vitrophyre above which is sheet jointed rhyolite. Both the vitrophyre and the sheet jointed rhyolite contain small angular chips of dense black glass, commonly ~ 0.5 cm in size but reaching 3 cm. This zone is separated from the overlying columnar jointed zone by a lithophysal horizon. The columnar jointed zone reaches ten metres in thickness and its upper contact is marked by a second lithophysal horizon with some of the lithophysae reaching 5-10 cm in diameter. Above this is a lithoidal intensely welded zone with abundant glass chips topped by a third lithophysal horizon. Most of the thickness of the Big Bluff Member lies above this lithophysal horizon: the basal part is weakly columnar and the overlying part is massive and lithoidal (Fig. 2.4). The lithoidal zone becomes increasingly more sheet-jointed and slightly rheomorphic towards the top. Above the rheomorphic zone is a zone of spherulites, some containing green chalcedony fills. The upper vitrophyre of the Big Bluff Member is thin and has perlitic texture which underlies a non-welded massive tuff containing small (centimetre scale) chips of black glass and rare tubular pumice in a pink matrix. The top of this is not seen.

Interpretation: the Big Bluff Member is interpreted as an intensely welded rhyolitic ignimbrite. The lithophysal horizons mark the former presence of vitrophyres that have subsequently devitrified. The absence of a basal breccia, entirely pyroclastic nature of the deposit, presence of zones of glassy chips and very large volume, indicate that the Big Bluff Member above the basal ashfall layer is an ignimbrite. This interpretation is supported by the presence of the non-welded facies seen at the top of the Big Bluff Member (Fig. 2.4).

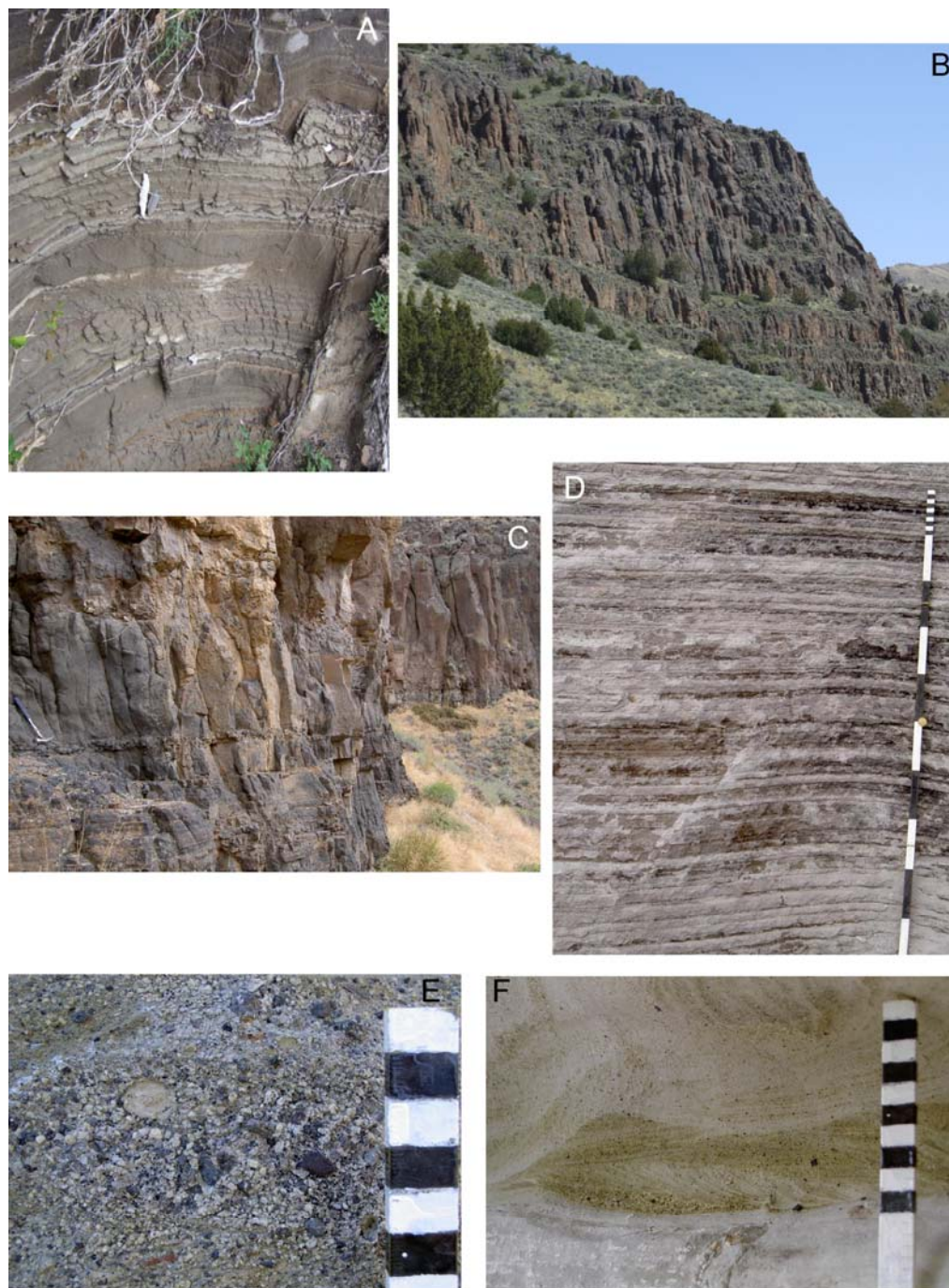


Figure 2.5 **A.** Slightly oblique view of the parallel-bedded ashfall deposits of the Magpie Basin Member at Magpie Basin which are dominated by medium to fine ash and contain a single bed of rimmed pellets. Field of view approximately 60 centimetres. **B.** Big Bluff Member showing the variation in weathering horizons, total thickness shown > 70 m. **C.** Basal vitrophyre of the Steer Basin Member in Rock Creek. **D.** Finely bedded couplets of sand and mud from the Antelope Springs Member. **E. and F.** Fluvial gravel from the top of the Antelope Springs Member in Rock Creek.

Unit 'TT1'

Previous accounts describe a '*white to grey, locally light green, thin to thick-bedded airfall tuff and silty to sandy thin-bedded water-laid tuff*' (Williams et al. 1990) above the Big Bluff Member and beneath the Steer Basin Member. Throughout the Cassia Mountain region this map unit is poorly exposed, commonly forming grassed slopes between the two cliff-forming rhyolites. It is not described further herein.

The Steer Basin Member

The lowest exposure of the Steer Basin Member is a highly distinctive layer of aphyric obsidian with large scale perlitic texture, at least a metre thick. Above this is a succession of vitrophyre layers with contrasting phenocryst abundances (Fig. 2.5 C). Overlying the parallel bedded ash facies is a 5 m thick section of massive vitrophyre which contains lenses of feldspar crystals. Above the vitrophyre, the lithoidal rhyolite is strongly sheet-jointed (cm scale) and contains small fiammé typically several centimetres long and up to a centimetre thick in the basal part. Similar features have been reported from the Jackpot 7 Member in the Rogerson Graben (Andrews et al. 2008). The upper half of the member is strongly deformed by medium scale open to tight rheomorphic folds (Fig. 2.6) picked out by flow banding and partly by sheet jointing. This flow folded section is the source of the 'talus apron' characteristic of the Steer Basin Member (Williams et al. 1990). The uppermost 5 m show flow banding extending up into the thin (50 cm), glassy upper vitrophyre that grades up into a non-welded tuff (Fig. 2.6) which shows evidence of incipient soil formation at the top.

Interpretation: The flow-banded Steer Basin Member is interpreted as a high grade, lava-like ignimbrite on the basis of widespread eutaxitic fabric in the lower parts and the absence of a basal autobreccia. The basal obsidian layer within the parallel bedded lower section may represent a distal, vent-derived ashfall deposit. The obsidian deposit appears exceptionally well-sorted and is entirely aphyric, an alternate possibility is that it represents a co-ignimbrite fallout deposit (which are commonly finer-grained) subsequently covered by the ignimbrite and fused. The bedding in the vitrophyre of phenocryst rich and poor layers is taken to represent an ashfall deposit

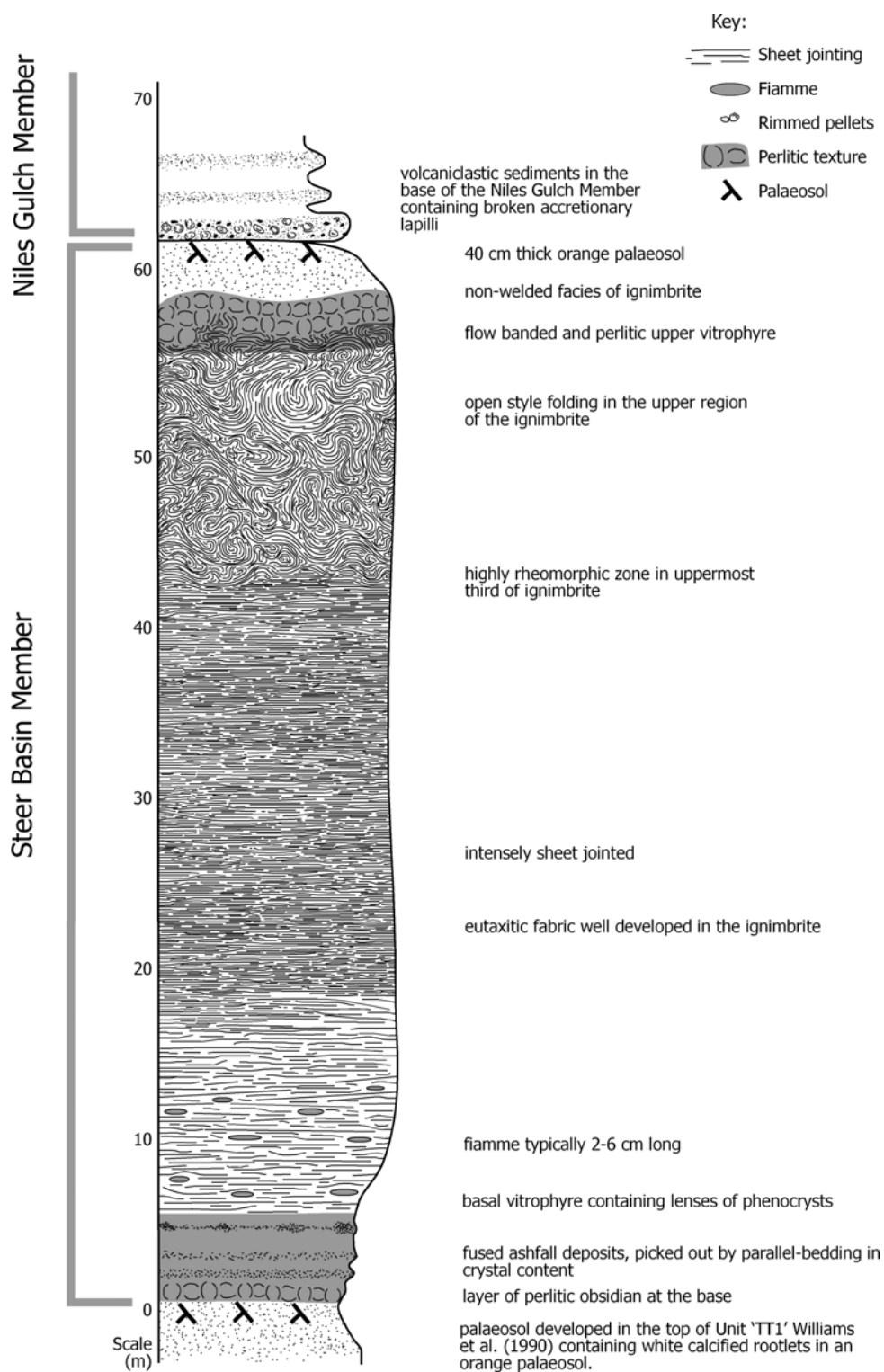


Figure 2.6 Graphic log of the Steer Basin Member, illustrating the highly rheomorphic upper part of the unit.

associated with the same eruption that produced the overlying ignimbrite. The upper flow folded region of the ignimbrite, a common feature of SR-type volcanism (Branney et al. 2008), but lack of an upper autobreccia implies that rheomorphism was predominantly syn-depositional and post-depositional rheomorphism was minimal. The gradational contact between the upper vitrophyre and the non-welded facies of Steer Basin Member ignimbrite is further evidence that this unit is not a lava.

Niles Gulch Member

The Niles Gulch Member lies on top of the palaeosol at the top of the Steer Basin Member (Fig. 2.7). At the base of the member are a series of thin beds of moderate to well-sorted gravel containing sub-rounded to rounded millimetre to centimetre-scale clasts, often exhibiting cross-stratification. Above this gravel is a 5 to 10 metre thickness of interbedded sand and mud showing irregular thickness variations. The top of the Niles Gulch member is another gravel overlain by a well-developed palaeosol.

Interpretation: the Niles Gulch Member is interpreted as representing a transgression and regression of the margin of a lake. The upper and basal gravels that are seen represent the rearrangement of small drainages in response to the change in lake level, whereas the variably thick, well bedded repetitions of sand and mud are interpreted as representing deposition from suspension in the centre of the lake during a hiatus in eruptive activity.

Antelope Member

The Antelope Member is up to 6 m thick at its type locality in Rock Creek. This member shows great variety between locations, typically it is dominated by normally graded couplets of sand and silt often interbedded with rippled sand (Fig 2.5 D). The lowest exposure of the Antelope Member represents a weakly developed palaeosol, overlain by massive sand which exhibits small-scale scours with fine mud drapes on top and lenses of coarse sand and gravel near the top. Within the centre of the Antelope Member, ripples are seen interbedded with the normally-graded

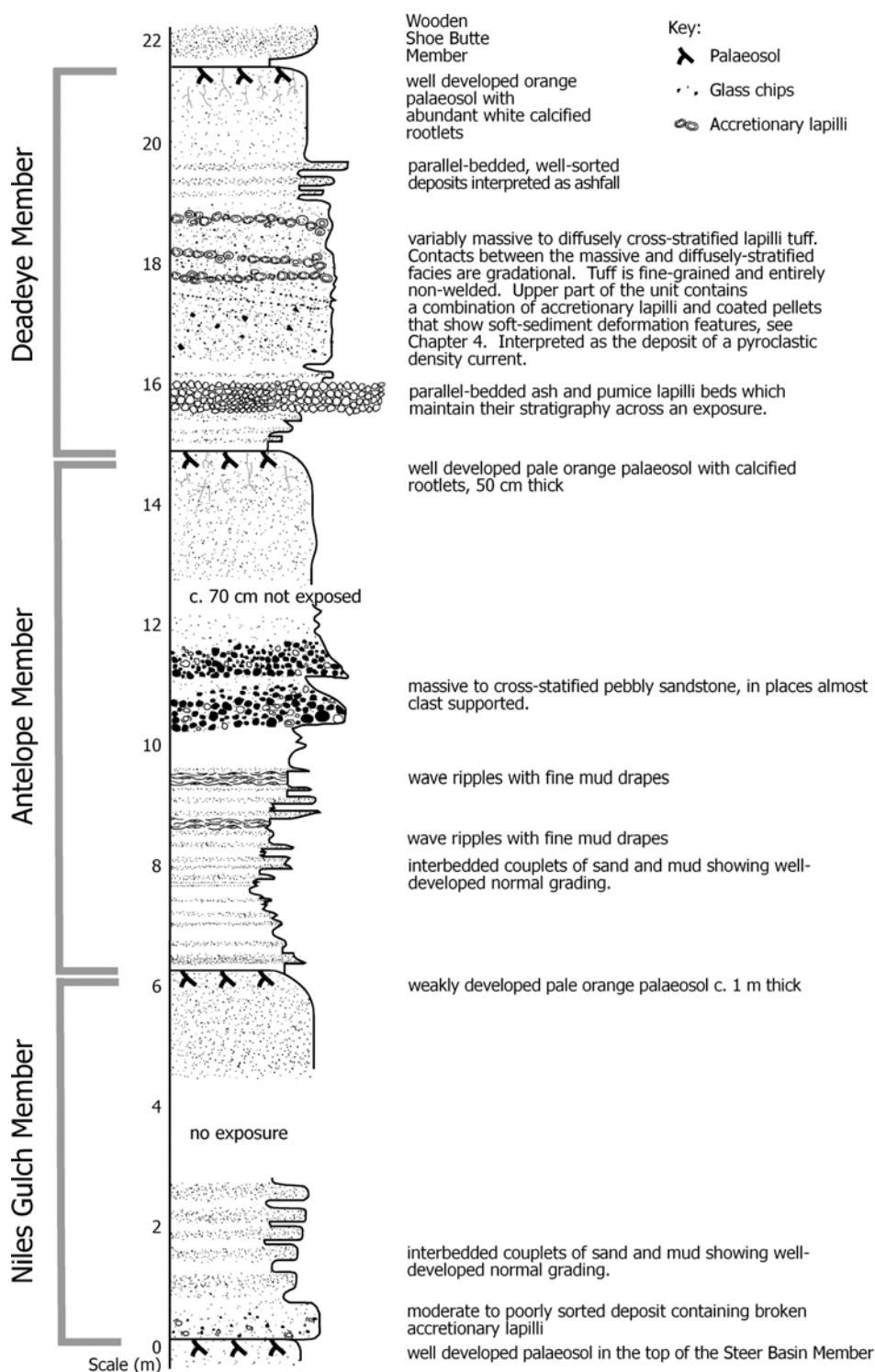


Figure 2.7 Generalised log of the Niles Gulch, Antelope and Deadeye Members from Rock Creek canyon (Fig. 2.1). The Niles Gulch and Antelope Members show considerable variation between exposures in contrast to the Deadeye Member which retains its stratigraphy. The Deadeye Member is described in detail in Chapter 4.

couplets of sand and silt. The upper reaches of the Antelope Member contain clast-supported gravels (Fig. 2.5 E) overlain by a massive sand grade unit which has been bioturbated and contains calcified rootlets, representing a palaeosol.

Interpretation: The Antelope Member is interpreted here as being a volcanoclastic lacustrine deposit. The two dominant lithofacies are interpreted as representing suspension settling (producing the normally graded couplets) and the presence of ripples strongly suggests that this member was deposited subaqueously. The interbedded nature of the two dominant facies suggests that the environment of deposition was fluctuating between still water and tidal dominated environments. The clast supported gravels and the presence of palaeosols suggest that the Antelope Member records a series of changing palaeoenvironments, passing from sub-aerial to lacustrine to fluvial back to sub-aerial.

Deadeye Member

The lowest deposits of the Deadeye Member are a series of centimetre-scale beds of parallel-bedded ash and pumice which together are 2 m thick (Fig. 2.7, Fig. 2.8A). Above this lies a 2.5 m thick deposit of massive tuff which on passing upwards exhibits diffuse cross-stratification and an abundance of accretionary lapilli which occur in diffuse cross-stratified layers. The accretionary lapilli are composed of cores of medium ash surrounded by concentric laminations of fine grained white ash. Some show evidence of soft-state deformation suggesting that they were moist upon emplacement. The accretionary lapilli (Fig. 2.8 B) are clast supported in places. Above this lie a series of well-bedded deposits which pass upwards into a thick (> 1m) orange palaeosol. The Deadeye member is discussed in greater detail in Chapter 4.

Interpretation: The Deadeye Member is interpreted here as a pyroclastic deposit, rather than a volcanoclastic sediment as mapped by Williams et al. (1990). This interpretation is based on the paucity of reworking features throughout the Member. The presence of coated pellets and accretionary lapilli in a diffuse cross-stratified tuff suggest it is a pyroclastic unit. The lowermost part of the Deadeye Member, dominated by the thin bedded fine to coarse ash facies is interpreted

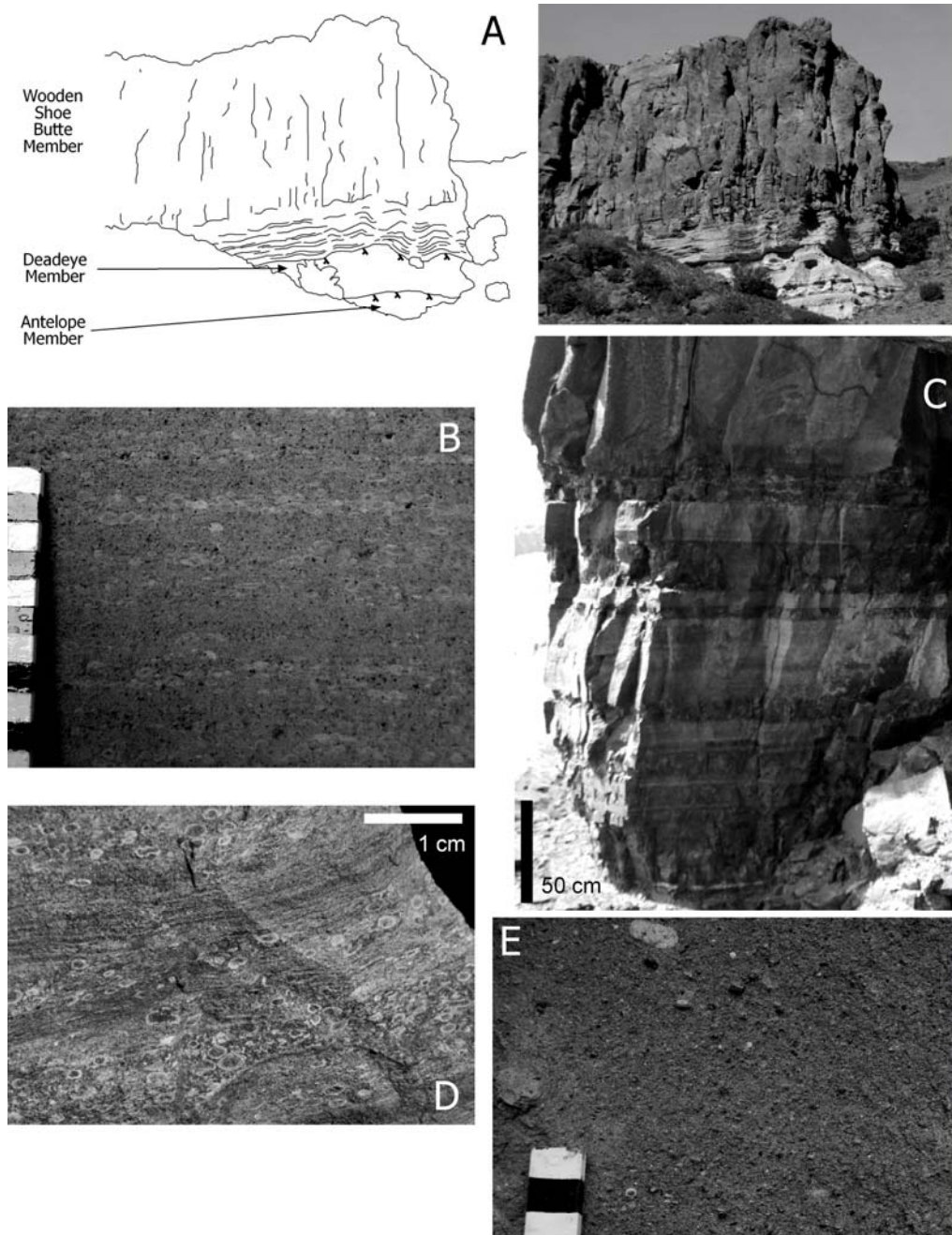


Figure 2.8 **A.** Sketch and photo of the contacts between the Wooden Shoe Butte Member (top) the Deadeye Member (centre) and the Antelope Member (base) at the Steer Basin campground in Rock Creek canyon (Fig. 2.1) **B.** Diffusely cross-stratified accretionary lapilli-bearing tuff in the Deadeye Member. **C.** The 3 m thick bedded ashfall deposit of the Wooden Shoe Butte Member, fused to glass by heat conducted downwards from the overlying ignimbrite at the Harrington Fork picnic ground. **D.** Fused coated pellets in the Wooden Shoe Butte pre-ignimbrite succession. **E.** Non-welded, well-sorted massive lapilli-tuff of Wooden Shoe Butte at Trapper Creek (Fig. 2.1), composed of shards, rare pellets and dense glass chips.

as a succession of fall deposits. They are overlain by a non-welded ignimbrite (pyroclastic nature, diffuse cross-stratification) overlain by further ashfall layers which record a return to fallout deposition. The Deadeye eruption is interpreted as having involved external water which enhanced the fragmentation of the erupting magma, resulting in the fine-grained ashfall and entirely non-welded ignimbrite (see Chapter 4).

Wooden Shoe Butte Member

The Wooden Shoe Butte Member (WSB) overlies the soil developed at the top of the Deadeye Member. In Rock Creek, the basal 3 m of the Wooden Shoe Butte Member are alternating rippled sand, parallel-bedded ash and diffusely cross-stratified ash containing pellets (Fig 2.8 D and E, Fig. 2.9). This becomes progressively more fused upwards. Above these deposits is a 70 m thick welded rhyolitic tuff containing various proportions of glassy fragments reaching 2 centimetres in diameter. Close to the Snake River Plain at the Hursch farm (HF Fig. 2.1) the basal contact of the rhyolite is distinctly peperitic with tongues of non-welded material injecting up into the welded tuff and small chips of the welded tuff are enclosed in the sediment surrounding the intrusion (Branney et al. 2008). The substrate is ashfall as seen beneath the Wooden Shoe Butte Member elsewhere, however close to the plain it is not fused, possibly due to the presence of water.

Above the basal vitrophyre a hackly zone with lithophysae passes upwards into a zone of dimple jointing (Bonnichsen 1982b) and to a thick sheet-jointed zone, 10 and 20 m thick topped by a lithophysal zone. In places above a bench a second vitrophyre is present in the WSB. The medial vitrophyre is partially welded and eutaxitic with abundant dense glassy clasts. The vitric chips extend upwards into the devitrified part of WSB. The upper portion of WSB may reach 25 m thick with a 2 m thick upper vitrophyre that caps an upper flow-folded zone.

At Trapper Creek (Fig. 2.1), the WSB has a different internal stratigraphy, with the lowermost part dominated by rippled and scoured sand interbedded with reworked fallout deposits. Above this is a non-welded ignimbrite (Fig. 2.8 E) with abundant dense glass clasts that grades upwards into a thin (c. 5 m) sheet of dense black glass containing abundant spherulites.

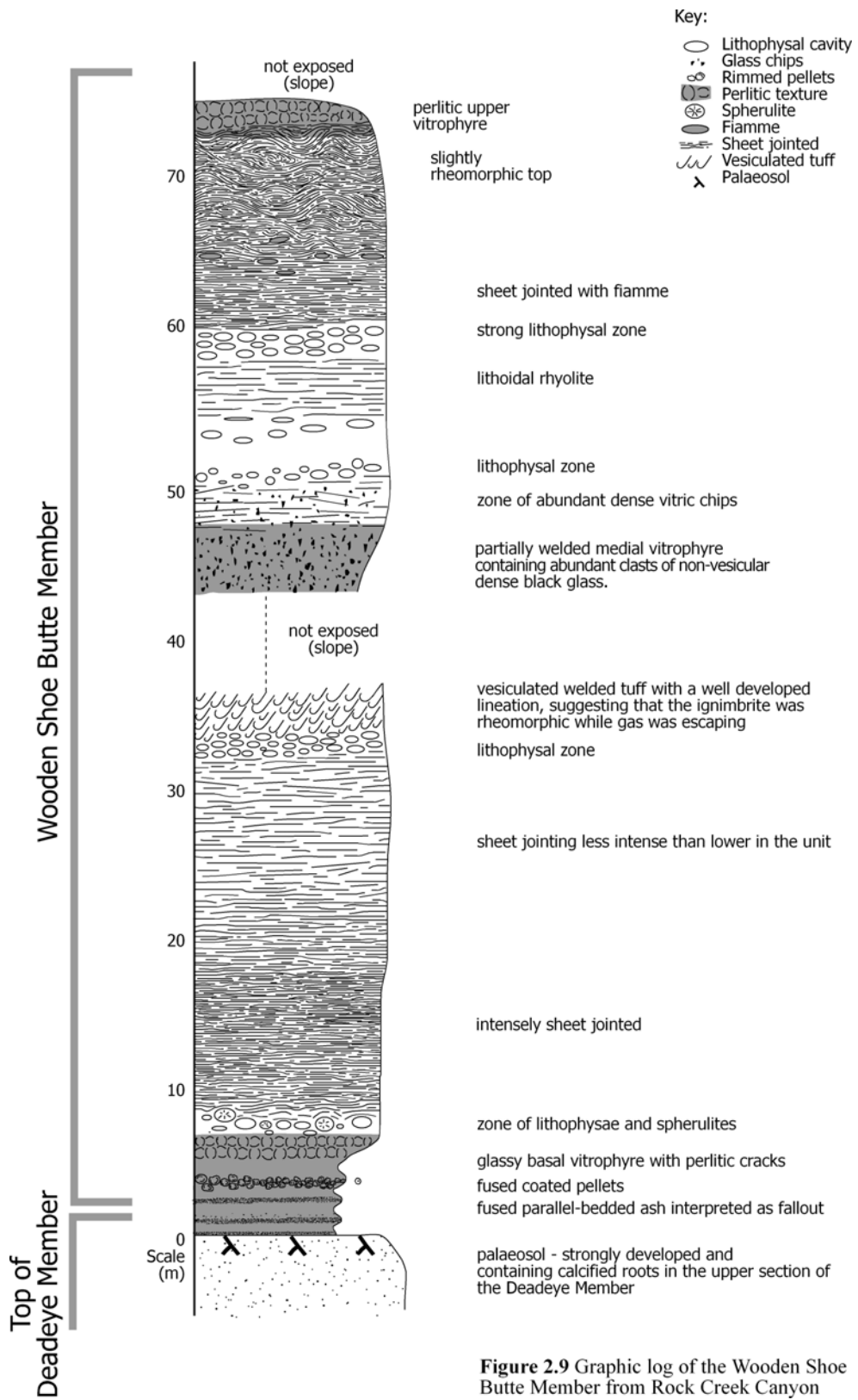


Figure 2.9 Graphic log of the Wooden Shoe Butte Member from Rock Creek Canyon

Interpretation: the WSB is interpreted to represent the product of an explosive eruption, emplaced onto a variable landscape. In Rock Creek, the pre-ignimbrite succession is dominated by parallel-bedded well-sorted tuff interpreted as resulting from sub-aerial fallout, whereas at Trapper Creek the pre-ignimbrite stratigraphy is dominated by lithofacies produced by reworking. The majority of the Member, the massive lapilli-tuff, is interpreted as an ignimbrite as shown by the gradational contact between non-welded and welded massive lapilli tuff seen at Trapper Creek (Fig. 2.8 E), the pyroclastic nature of both the welded and non-welded deposits and the presence of a basal fines-poor layer (a ground layer). The unusual thickness variations and pinching out of tuffs is consistent with a density current advancing over topography and the erosive base of the unit at Trapper Creek and the absence of any basal autobreccia further strengthen the interpretation. In Rock Creek, the uppermost parts of the bedded ash facies are progressively fused due to the conduction of heat downwards from the hot ignimbrite, reflecting the high temperature of emplacement of the ignimbrite. The presence of peperite at the Hursch farm (HF Fig. 2.1) is interpreted as being due to the 'wetness' of the substrate upon which the ignimbrite was emplaced.

McMullen Creek Member

The McMullen Creek Member is a series of thin, densely to incipiently welded ignimbrites that cap the Cassia Mountain Formation. Due to their thin and variable nature they cannot be traced significant distances (> 10 km) and there is disagreement over whether there are four units (Williams et al. 1990) or five (Wright et al. 2002). Reconnaissance work around Indian Springs Road during this study suggests there may be as many as seven. Given the uncertainty surrounding the McMullen Creek Member, only the stratigraphically lowest McMullen Creek unit in Rock Creek is considered. This unit overlies a weakly developed palaeosol and has a basal vitrophyre which passes up into sheet jointed rhyolite dominated by lithophysae at the contact between the vitrophyre and the lithoidal rhyolite. The upper reaches of the unit are rheomorphic.

Eruption sources

Sources of the Cassia Mountains ignimbrites are exposed. It has been proposed that they lie north of the Cassia Mountains within the Snake River Plain (McCurry et al. 1996; Andrews et al. 2008), and were subsequently covered by later basalt lavas. No other candidates for source areas (within sufficient close proximity) are exposed elsewhere. The thickness of fallout deposits in both the Wooden Shoe Butte and Deadeye members increase to the north (i.e. towards the Snake River Plain) suggesting that either the source of the eruption, or the dispersal axis of that eruption plume, was to the north. This is consistent with the source of the ignimbrites being within the Snake River Plain, although the location specifically within the inferred Twin Falls eruptive centre (Pierce and Morgan 1992) cannot be confirmed.

Geochemical Techniques

Whole rock chemistry

Bulk rock samples of welded and non-welded ignimbrites and ashfall deposits were prepared for X-ray fluorescence spectrometry and analysed on a Philips PW 1400 at the Geology Department at the University of Leicester. Bulk rock samples were analysed because they are considered to represent the juvenile content of the eruption as they have low (< 2%) lithic contents and the intensely welded nature of most of the rocks makes removing lithic material difficult. Samples were split by hand before being fly-pressed and then milled using a Retsch planetary mill for twenty minutes at 280 revolutions per minute using agate pots and balls. All samples were then dried in an oven at 110 °C. For analysis of major elements, samples were heated to 950 °C in a furnace to determine the loss on ignition (which ranged from 0.14 to 7.87%, averaging 2.66%). Once cooled, 0.6 g of powder was combined with 3 g of lithium metaborate flux and melted to form glass beads in 95% platinum, 5% gold crucibles. Trace element concentrations were determined from powder pellets made from 7 g of sample combined with Mowiol 88 adhesive fluid. The pellets were pressed using a hydraulic press with a pressure of ten tonnes per square inch.

Electron Microprobe Analysis

To investigate how glass and phenocryst compositions change throughout the Cassia Mountain stratigraphy they were analysed by electron microprobe.

Methodology:

All samples were analysed with a JEOL JXA-8600S electron microprobe at the Department of Geology of the University of Leicester, with various operating conditions used for the different constituents of the samples. For glass analysis, initial experiments showed that using typical operating conditions of 30 nanoamps probe current and a beam diameter of 10 microns resulted in excess volatilisation of sodium from the sample and corresponding increases in the detected proportions of other elements. The results of experiments showing the decrease in the amount of sodium detected with increasing time are shown in Figure 2.10.

The conditions used to collect glass data for this study involved two runs to collect data from each sample. The initial analysis for sodium, fluorine, chlorine and sulphur was made using a beam diameter of 30 microns and a probe current of 10 nanoamps. Counting time for each element was 80 seconds; 40 seconds for characteristic X-ray peak measurement and 20 seconds for each of positive and negative background. The second analysis involved analysing the remaining elements under conditions of 30 nanoamps probe current with a beam diameter of 10 microns from adjacent areas of glass that had not been previously been analysed. To integrate the data from the two analysis runs, the values of volatiles from the first run were combined with the values for the remaining elements from the second run. The remaining elements were each reduced by 1.5% relative, to negate the effect of volatilising sodium during the run. The value of 1.5% was taken as an average based on calibration experiments which showed that by the time that elements such as silicon and aluminium, comprising more than 80% of the glass typically, were analysed, their abundance had increased by roughly this amount (Figure 2.9). Unlike the glass samples, feldspar, pyroxene and iron oxide phenocrysts were analysed using a single run with a beam diameter of 10 μm and a probe current of 30 nA.

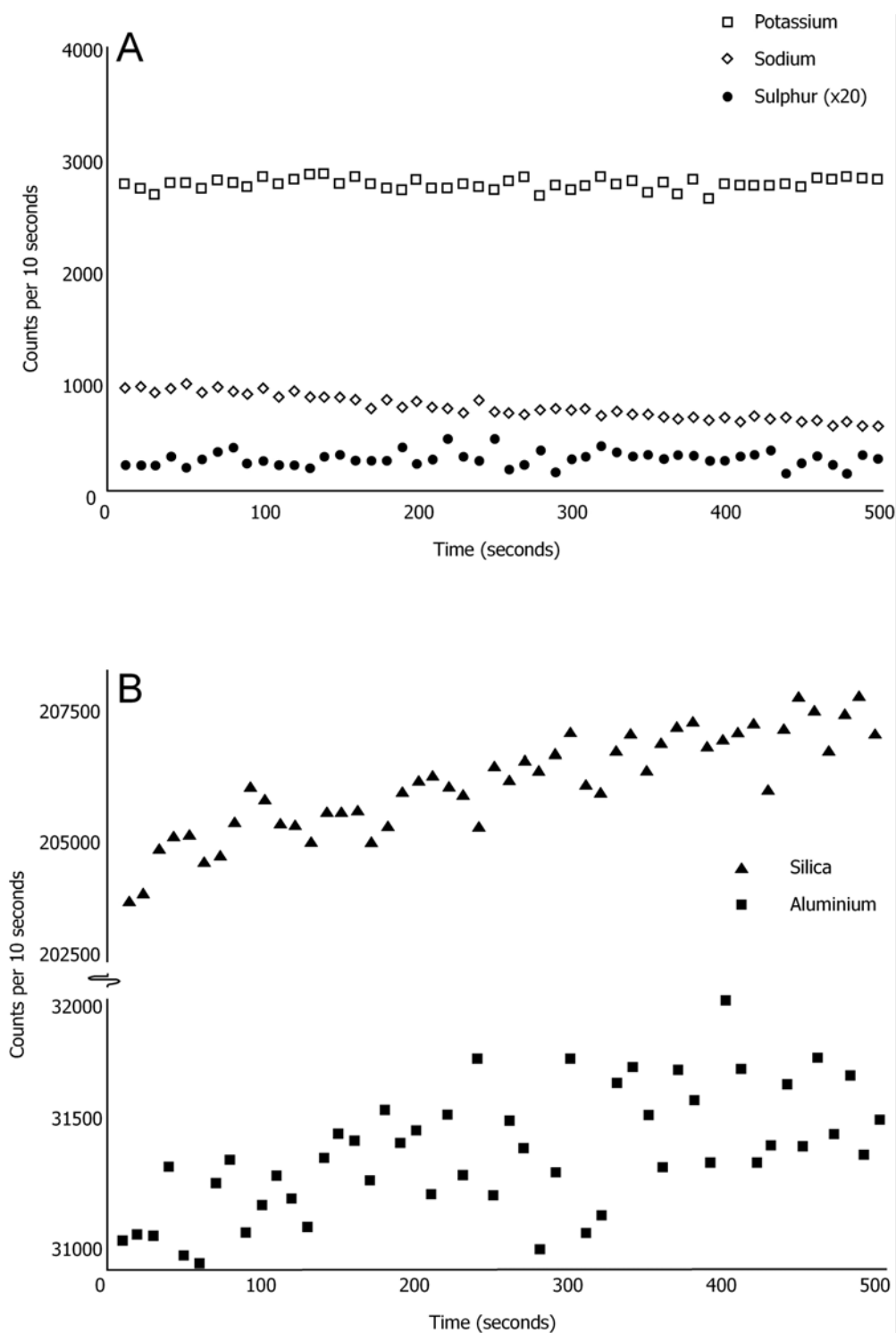


Figure 2.10 Counts of elements from Snake River rhyolitic glasses using conditions of a beam diameter of 10 microns and an operating current of 30 nanoamps. **A.** Graph showing the decrease in counts per second of sodium with increasing time, reflecting the volatilisation of sodium and to a lesser extent, sulphur. **B.** Graph showing the concurrent increase in counts of silica and aluminium due to the volatilisation of sodium.

When analysing quartz for thermometry, titanium contents were so low that long counting times were necessary to reduce backgrounds allowing the collection of meaningful data. For these analyses, probe current was increased to 100 nanoamps, and counting times were increased to 600 seconds for Si, Ti and Al, on peak and 300 seconds on both positive and negative background. The counts of 600 seconds on peak were measured as 6 x 100 seconds to prevent overflow on the ratemeter due to the high counts on Si.

Results

Whole Rock Chemistry

In common with the rhyolites in the rest of the CSR (Honjo et al. 1992; Cathey and Nash 2004), the ignimbrites in the Cassia Mountains (Cassia and Rogerson formations) are composed of metaluminous rhyolite (67.88 to 75.04 wt% SiO₂) with high levels of TiO₂ (0.26 to 0.86 wt%). All the ignimbrites analysed plot within the 'within plate granites' fields of Pearce et al. (1984) in terms of Rb/Y+Nb, Nb/Y, Si/Nb, Si/Rb and Si/Y. The totals of high field strength elements (Zr+Nb+Y+Ce) is around 800 ppm, within the 500-1000 range defined by Eby (1990) for anorogenic granites.

The high concentrations of TiO₂, MgO, Fe₂O₃ (total iron), high Fe₂O₃/MgO ratios and high inferred magmatic temperatures (see below) are in agreement with studies of other rhyolitic ignimbrites from the central part of the Snake River Plain such as the Cougar Point Tuffs (Bonnichsen and Citron, 1982; Cathey and Nash, 2004) and the Rogerson Formation of Andrews et al. (2008). The results of whole rock chemical analysis are given in Table 2.1 and Figures 2.11 and 2.12. Passing up succession, SiO₂ decreases and TiO₂, CaO, Fe₂O₃ and MgO increase, reflecting an upward trend towards less silicic compositions. Bonnichsen et al. (2008) suggest a province-wide trend of rhyolitic ignimbrites and lavas becoming more mafic up succession in the central Snake River Plain (Fig. 2.11). Whole rock data from the various massifs along the central Snake River Plain, show trends of increasing TiO₂ and decreasing SiO₂ with height. The Cassia Mountain units (of which only the McMullen Creek Member is included in the trends shown by Bonnichsen et al. 2008) follow the same trend as the rest of the central Snake River rhyolites

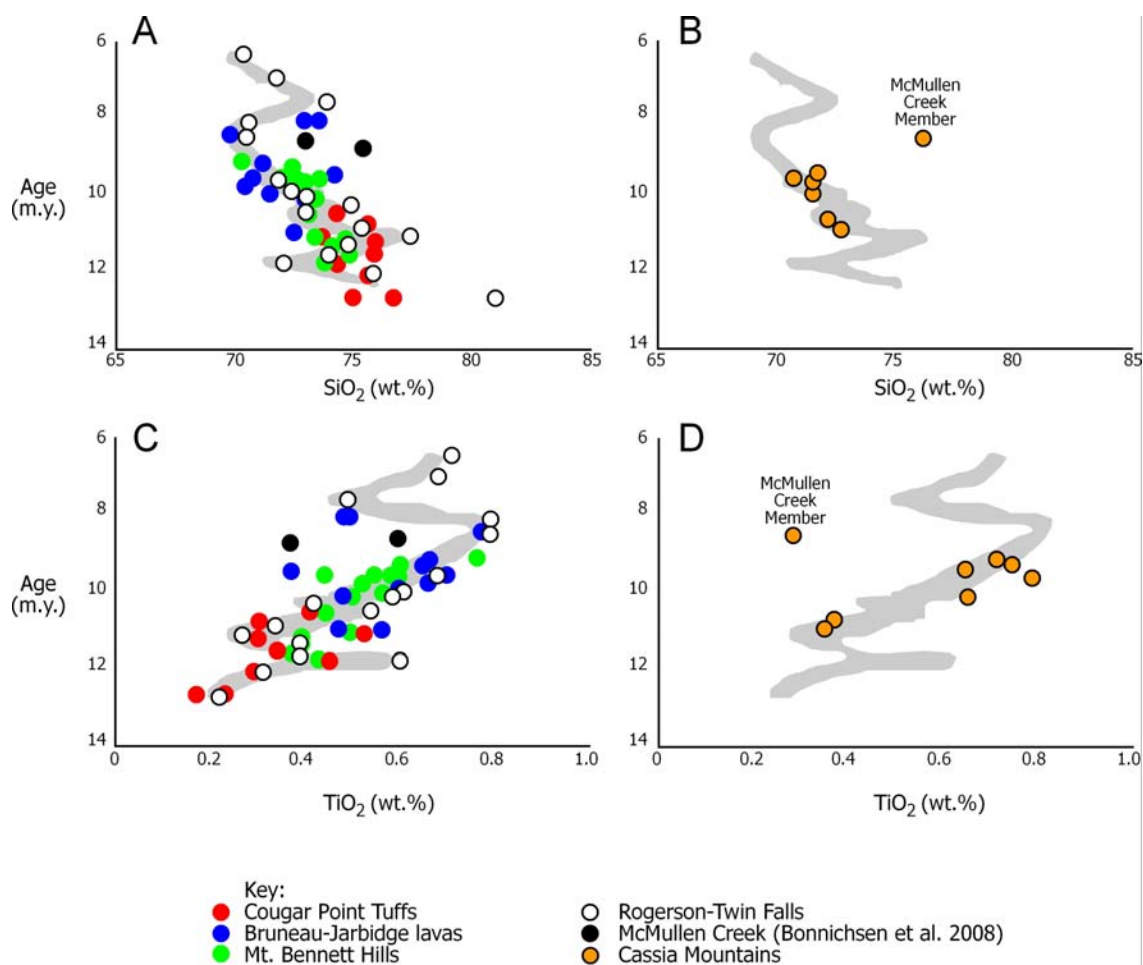


Figure 2.11 Trends in whole rock compositions of rhyolitic units in the central Snake River Plain through time after Bonnichsen et al. (2008). The orange circles in B. and D. are units in this study that were not incorporated in A. and C. (Bonnichsen et al. 2008). **A. and B.** SiO₂ versus ages of units from the central Snake River Plain. **C. and D.** TiO₂ versus age for the units of the central Snake River Plain. Bonnichsen et al. (2008) noted that the McMullen Creek Member had anomalous chemistry (black), confirmed by results in this chapter (orange). Trends shown in grey are those of Bonnichsen et al. (2008).

(Fig. 2.11). However, the McMullen Creek Member plots off the trend shown in Figure 2.11, with a sharp increase in SiO₂ and a decrease in the other major elements.

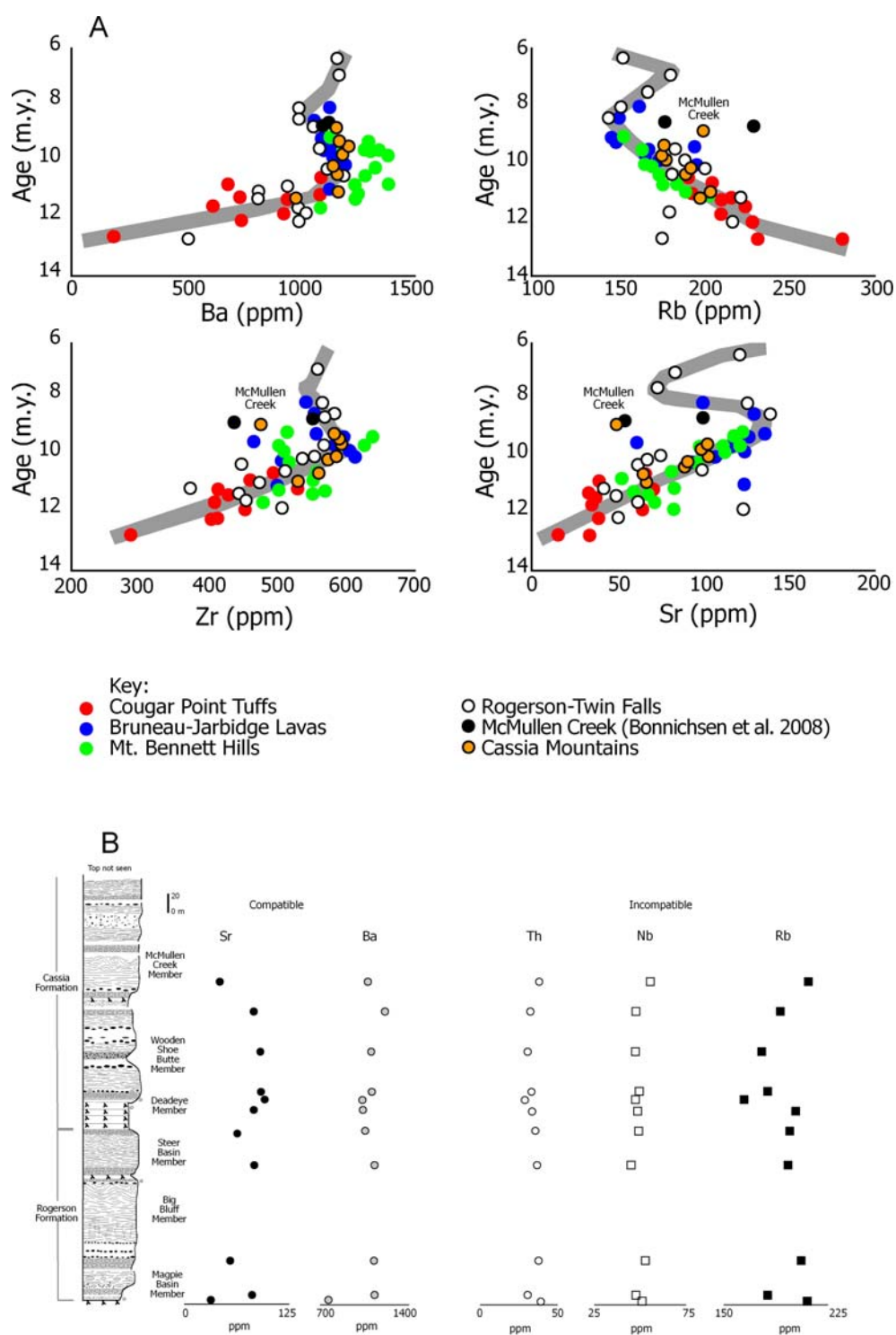


Figure 2.12 A. Trends in selected trace elements for the Cassia Mountains ignimbrites follow similar trends to those seen from the Snake River Plain as a whole with the McMullen Creek analysis in this work supporting the break in the trend seen in previous work (Bonnichsen et al. 2008). **B.** Selected trace elements showing little variation up succession. Trace elements determined by XRF.

Sample Name	Magpie Basin Member Basal vitrophyre	Big Bluff Member Basal vitrophyre	Steer Basin Member Basal vitrophyre	Steer Basin Member Upper vitrophyre	Deadeye Member Fall deposit	Wooden Shoe Butte Member Basal vitrophyre	Wooden Shoe Butte Member Medial vitrophyre	Wooden Shoe Butte Member Upper vitrophyre	McMullen Creek Member Basal vitrophyre
	TMB	TBB	BVSB	SBUV	PJFCAS11	TWSBBV	WSBMV2	WSBVU	McMLV
SiO ₂	72.96	71.99	70.60	71.04	68.03	71.18	69.35	71.41	75.04
TiO ₂	0.36	0.38	0.59	0.59	0.67	0.51	0.77	0.66	0.26
Al ₂ O ₃	12.03	11.76	12.09	12.28	12.79	12.03	12.52	12.35	11.69
Fe ₂ O ₃	2.66	3.10	3.89	3.64	4.98	3.53	4.42	3.72	2.30
MnO	0.03	0.05	0.06	0.07	0.05	0.05	0.05	0.04	0.04
MgO	0.00	0.14	0.40	0.52	0.35	0.39	0.49	0.30	0
CaO	0.78	1.17	1.85	1.42	1.63	1.97	1.92	1.47	0.76
Na ₂ O	2.34	3.14	2.57	2.49	1.18	2.79	2.64	2.37	3.22
K ₂ O	6.39	5.795	6.29	6.129	4.76	6.09	5.48	6.04	5.40
P ₂ O ₅	0.02	0.09	0.09	0.08	0.09	0.07	0.14	0.11	0.02
Total	100.19	99.74	100.26	100.54	100.43	100.65	99.64	100.63	98.82
L.O.I.	2.68	2.19	1.89	2.30	5.91	2.05	1.84	2.17	0.14
Nb	47	53	43	43	51	44	63	46	55
Zr	592	574	559	563	656	524	606	574	472
Sr	93	59	92	74	92	88	93	73	43
Y	68	81	67	67	63	66	61	58	72
Rb	179	200	192	189	237	194	175	185	204
Mo	3	3	4	3	3	3	4	4	3
U	7	6	6	8	7	7	7	7	5
Th	30	37	36	32	38	37	29	31	37
Pb	27	29	24	28	22	25	25	27	24
Cu	n.d.	n.d.	n.d.	n.d.	1.3	n.d.	7	n.d.	n.d.
Ga	21	22	21	20	21	20	18	18	19
Zn	58	79	62	61	72	54	59	46	48
La	82	88	76	78	90	78	78	79	81
Ce	158	169	145	158	164	145	154	151	162
Nd	46	71	61	43	77	62	62	44	68
Cs	n.d.	2	1	n.d.	5	5	n.d.	n.d.	6
Ba	1200	1189	1193	1152	1210	1088	1127	1066	1128
Co	1	6	6	1	9	6	7	1	6
Sc	7	6	6	5	7	4	7	5	5
V	10	5	16	10	22	11	24	14	5

Table 2.1 Representative bulk rock chemical analyses of the volcanic units from the Cassia Mountain succession

Trace elements show little variation with height, not only within a single unit, but throughout the Cassia succession as a whole (Fig. 2.12). Sr and Ba show some variation, which is attributed here to the proportion of feldspar within the sample because the samples with the lowest Sr and Ba are also those with the lowest proportion of feldspar; the fallout deposit of Magpie Basin which is predominantly of glass shards and the McMullen Creek Member which is crystal poor in comparison to other units in the stratigraphy.

Glass Chemistry

Glass from each eruption unit was analysed by electron microprobe. Samples were collected from both upper and basal vitrophyres of the ignimbrites and ash fallout where exposed. Analyses were made on individual glass shards ranging in size from 0.5 to 5 mm, or from intensely welded glass where welding precluded identification of individual shards. At least 50 glass spots were analysed for each sample. The averages for each eruption unit are presented in Table 2.2 and Figure 2.13.

Glass chemistry showed some variation within individual eruption units e.g. SiO₂ (74 to 78.5 wt.%) and TiO₂ (0.1 to 0.44 wt.%) (Figure 2.13). Values of Na₂O are commonly around 2 wt%, and K₂O range between ~ 5 and 7 wt.%. Fluorine is typically present at levels of 0.1%, S and Cl are present in smaller proportions. Ignimbrites in the Cassia Mountains exhibit a much wider range of FeO than fall deposits from the same eruption. The narrowest range of FeO values are in the Deadeye Member fall deposit (1.8 to 2.1 wt.%) and the widest range occurs in the Wooden Shoe Butte basal vitrophyre (0.7 to 3.7 wt.%). Within individual fall deposits, as analysed here, there is little evidence of multiple compositional modes with the exception of the Deadeye fall deposits.

Glass chemistry for units in the Cassia Mountain succession shows a trend of increasing TiO₂ and decreasing SiO₂ passing up succession (Fig. 2.13, 2.14), with glass compositions overlapping between adjacent units. Although the glass compositions overlap between units (Fig. 2.14) there is a distinct trend from the Big Bluff Member at the base of the stratigraphy to the Wooden Shoe

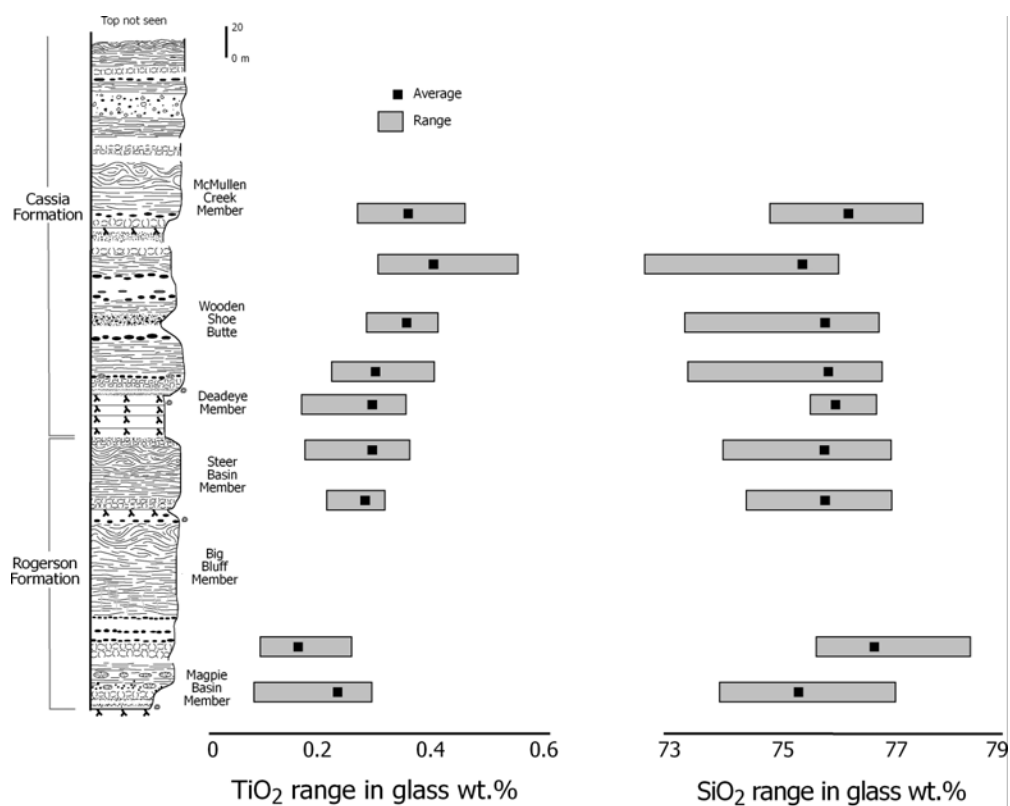


Figure 2.13 Ranges of TiO₂ and SiO₂ in the glass matrix and shards for each unit.

Butte Member near the top. As in the whole rock data (Fig. 2.11), the glass compositions shows a clear and abrupt change at the base of the McMullen Creek Member which has lower values of TiO₂, and higher values of SiO₂ than the trend for the rest of the succession would suggest for its stratigraphic position (Fig. 2.14).

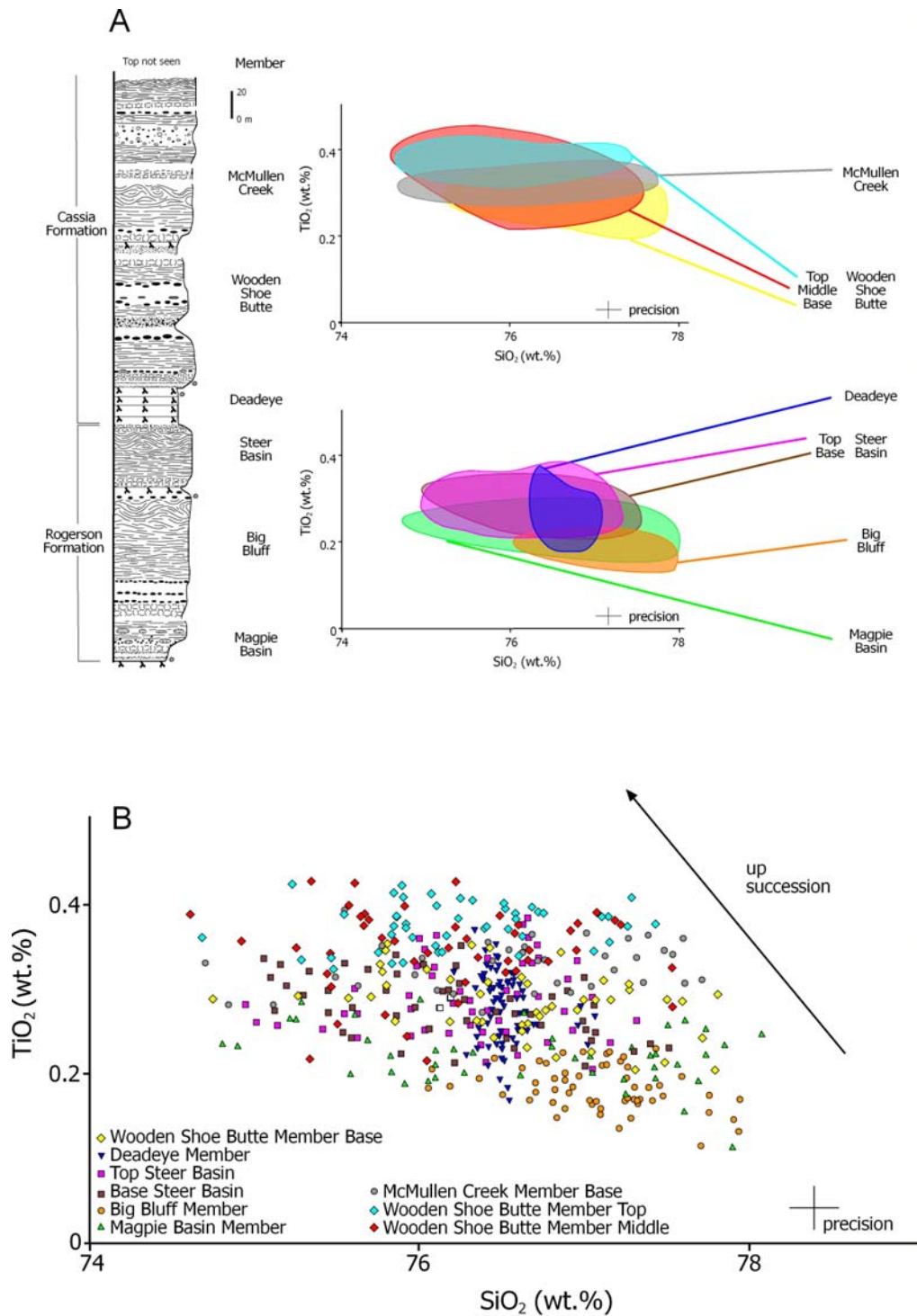


Figure 2.14 A. Variation in glass chemistry with height through the Cassia Mountains, with units becoming less silicic with height until the McMullen Creek Member which is more silicic than the trend would predict. **B.** Data showing the change in TiO_2 v SiO_2 with height from which **A.** was created.

Unit	Magpie Basin Member basal vitrophyre n = 59	Big Bluff Member basal vitrophyre n = 60	Steer Basin Member basal vitrophyre n = 55	Steer Basin Member upper vitrophyre n = 59	Deadeve Member n = 80	Wooden Shoe Butte Member basal vitrophyre n = 56	Wooden Shoe Butte Member medial vitrophyre n = 58	Wooden Shoe Butte Member upper vitrophyre n = 60	McMullen Creek Member basal vitrophyre n = 51	Representative Absolute Error (2 sigma)
SiO ₂	75.80	77.18	76.16	76.31	75.95	76.35	76.17	76.11	76.76	0.26
TiO ₂	0.25	0.18	0.28	0.30	0.37	0.29	0.34	0.37	0.36	0.05
Al ₂ O ₃	11.85	11.82	11.78	11.93	12.29	12.03	12.18	12.08	12.24	0.09
Cr ₂ O ₃	0.01	0.01	0.01	0.01	0.01	0.00	0.00	0.01	0.01	0.04
FeO	2.24	1.77	1.94	1.96	1.94	1.86	1.68	1.63	1.90	0.08
MnO	0.03	0.03	0.03	0.03	0.03	0.04	0.03	0.02	0.04	0.03
MgO	0.10	0.02	0.09	0.07	0.09	0.08	0.12	0.06	0.04	0.02
CaO	0.66	0.67	1.00	0.92	0.88	0.82	1.00	0.56	0.78	0.04
Na ₂ O	2.38	2.83	2.32	2.36	2.61	2.86	2.46	2.31	3.06	0.10
K ₂ O	6.56	5.39	6.24	6.01	5.77	5.57	5.92	6.78	4.73	0.08
NiO	0.01	0.01	0.01	0.00	0.00	0.00	0.01	0.01	0.01	0.01
F	0.14	0.19	0.18	0.14	0.12	0.16	0.14	0.14	0.16	0.18
Cl	0.04	0.04	0.04	0.03	0.01	0.02	0.02	0.04	0.05	0.03
SO ₃	0.03	0.05	0.05	0.02	0.01	0.01	0.01	0.02	0.02	0.04
Total	100	100	100	100	100	100	100	100	100	

Table 2.2 Averaged electron microprobe analyses for major element abundances from single glass shards or glass matrix where welding prevented identification of individual shards. Results present are averages of >50 analyses with representative errors on typical analyses shown on the right. All analyses assume Fe as FeO, normalised to 100% anhydrous and using the method detailed in the text to reduce sodium loss.

Mineral Chemistry

Pyroxene

Clinopyroxene is present within all the eruption units in the Rogerson and Cassia formations as euhedral phenocrysts up to 500 μm across (compositional data presented in Tables 2.3 and 2.4). In the lower units, the Magpie Basin and Big Bluff members, only augite is present (with fayalite present in place of pigeonite) whereas the younger units contain both pigeonite and augite. Within individual ignimbrites there are a number of discrete compositional modes, in both the pigeonite and augite (Fig. 2.15). In some ignimbrites the variability in pyroxene composition is considerable, for example between the two cooling units of the Wooden Shoe Butte Member (Fig. 2.9), pigeonite varies between 9.5–14 wt.% MgO and 29–35 wt.% FeO. The fallout deposits of the Wooden Shoe Butte Member contain pigeonite, augite and orthopyroxene (which is otherwise absent in the Cassia Mountain succession). The pigeonite in the fallout deposit has the same composition as one of the populations in the underlying Steer Basin Member whereas the augite composition is not seen in the Steer Basin Member. Although some of the ignimbrites of the McMullen Creek Member are reported to contain orthopyroxene (Wright et al. 2002), no orthopyroxene was found in the McMullen Creek sample analysed in this study. Magnesium numbers in pigeonites range from ~30 to 46 and from 17 to 53 in augite.

The pigeonites and augites are individually homogeneous (unzoned), with average changes from rim to core of less than 1% Wo, based on multiple analyses of rim and cores per phenocryst on > 20 individual crystals. Thus, the distinct compositional groups do not represent variation within a crystal (Fig. 2.16 A).

Clinopyroxenes are also found within the ignimbrites of the Cassia Mountains as crystal aggregates which commonly also contain feldspar and iron oxides. The compositions of the clinopyroxenes within the aggregates are identical to the compositions of clinopyroxenes present as individual crystals in the ignimbrite (Fig. 2.17). Intriguingly, the glomerocrysts only preserve a single compositional mode of pigeonite and augite, even in ignimbrites that have multiple compositional modes.

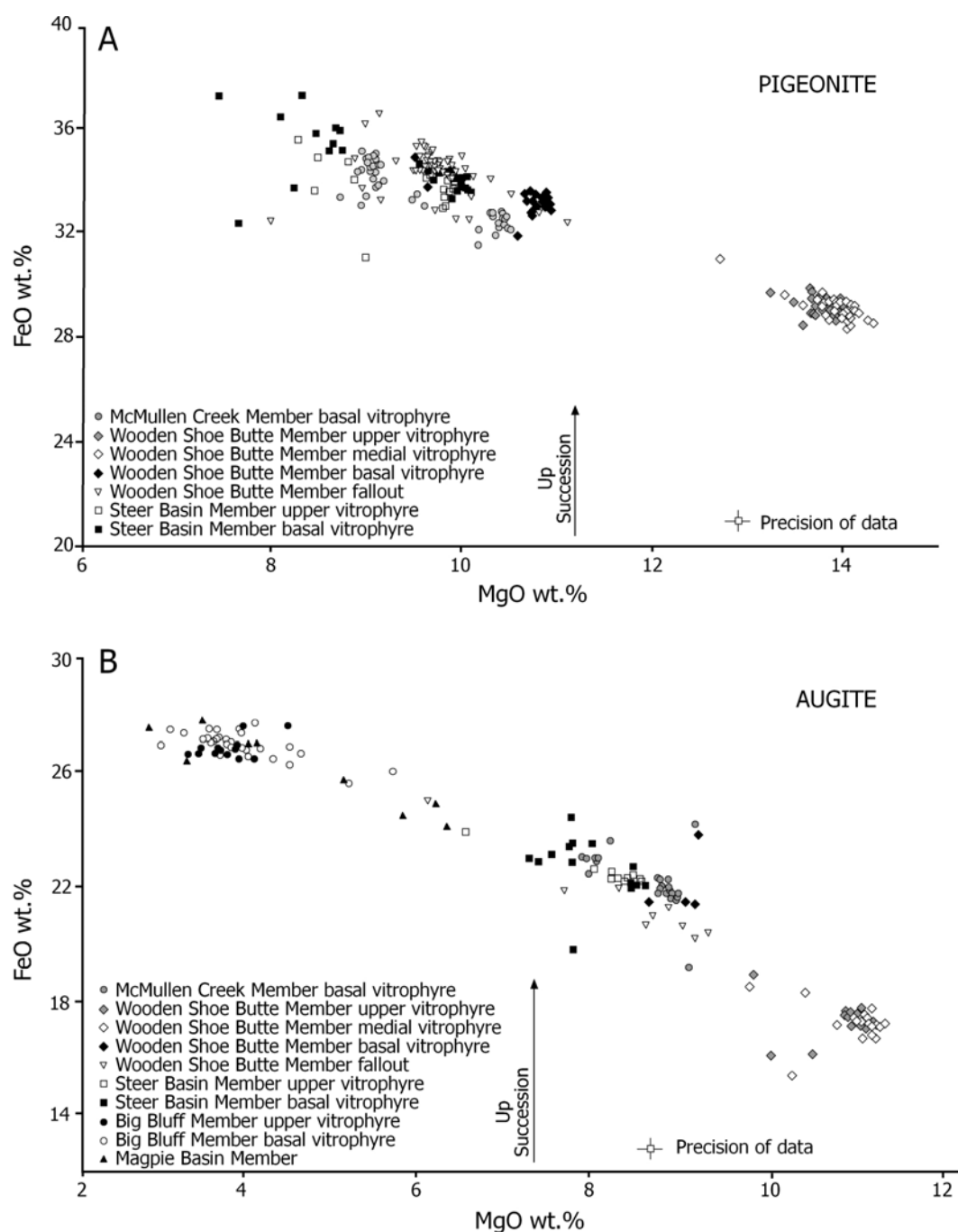


Figure 2.15 Clinopyroxene compositions for the Cassia Mountain ignimbrites. **A.** Compositional modes present in pigeonite showing that ignimbrites may contain multiple modes of pigeonite and a trend towards higher MgO (wt.%) and lower FeO (wt.%) up succession until the McMullen Creek Member. **B.** Compositional modes in augite, again showing that multiple modes may be present in a unit, with the same trend to increasing MgO (wt.%) and decreasing FeO (wt.%) up succession and the same break in the trend for the McMullen Creek Member.

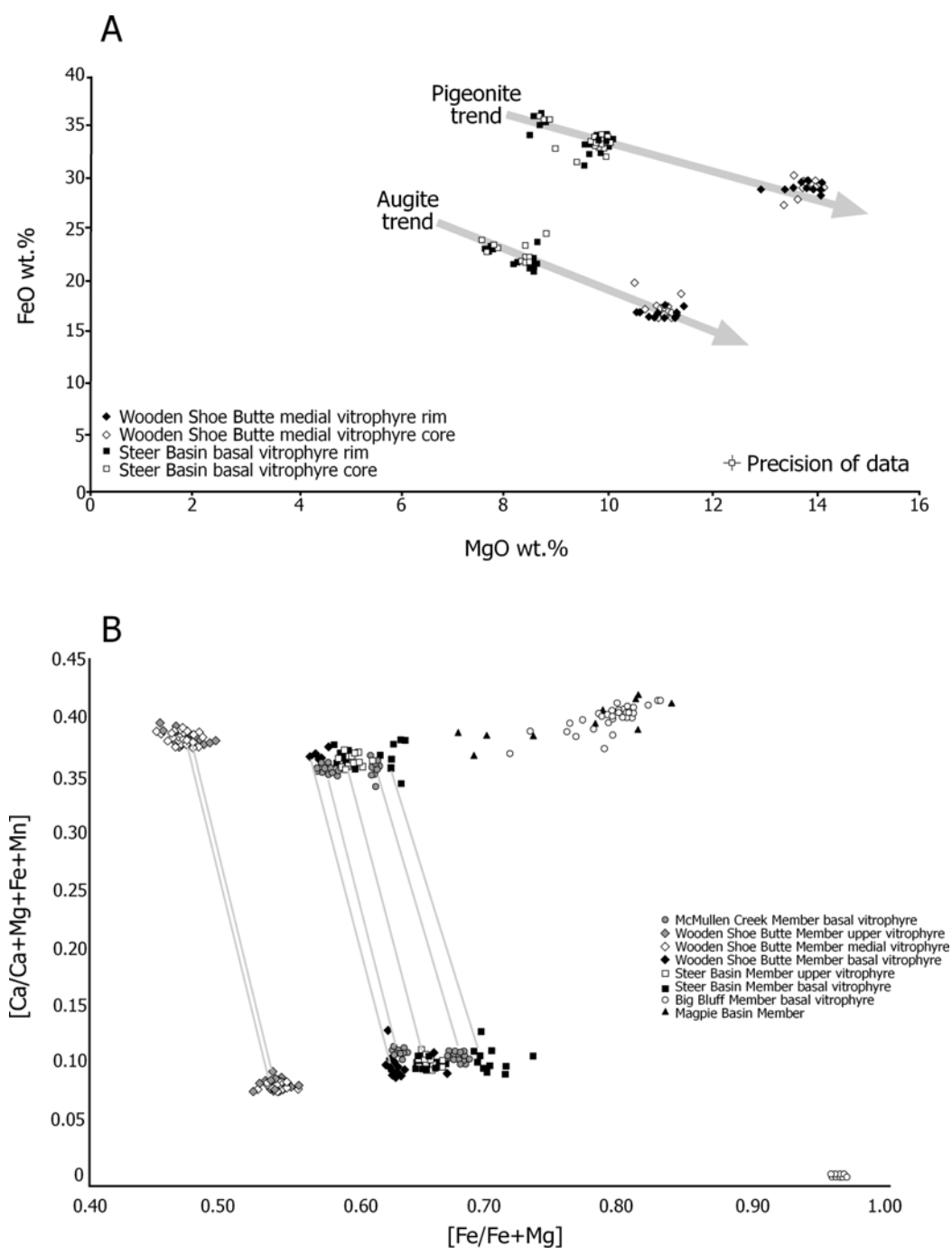


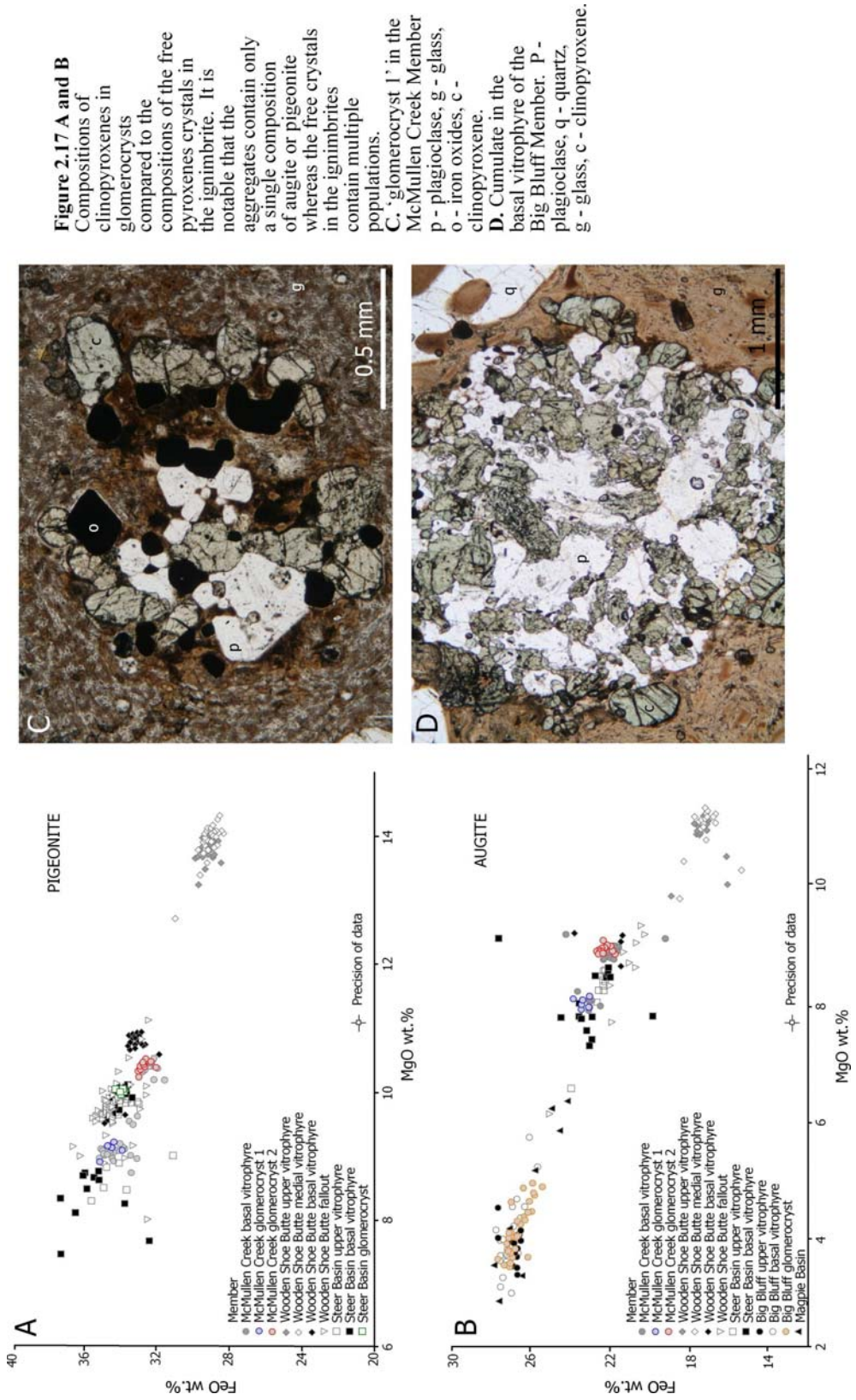
Figure 2.16 A. Rim and core compositions of the pyroxene phenocrysts from the base of the Steer Basin Member and the middle vitrophyre of the Wooden Shoe Butte Member. The two compositional populations of pigeonite in the Steer Basin Member are repeated in both rim and core analyses, showing that the multiple populations are not related to differences in a single phenocryst. **B.** Compositional relations between the pigeonites and augites within a single sample, illustrating that the pigeonite and augite compositions are consistent with being in equilibrium with each other.

	n	SiO ₂	TiO ₂	Al ₂ O ₃	FeO	MnO	MgO	CaO	Na ₂ O	K ₂ O	NI0	Total
McMullen Creek Member basal vitrophyre	17	50.37 (0.24)	0.35 (0.07)	0.90 (0.04)	21.83 (0.38)	0.76 (0.09)	8.85 (0.10)	16.59 (0.16)	0.23 (0.04)	0.00	0.00	100
McMullen Creek Member basal vitrophyre	7	50.26 (0.24)	0.34 (0.07)	0.81 (0.04)	23.01 (0.40)	0.80 (0.10)	8.01 (0.09)	16.62 (0.16)	0.22 (0.04)	0.00	0.00	100
Wooden Shoe Butte Member upper vitrophyre	18	51.35 (0.24)	0.35 (0.07)	0.93 (0.04)	17.29 (0.30)	0.54 (0.07)	11.09 (0.12)	18.10 (0.18)	0.26 (0.04)	0.02 (0.01)	0.00	100
Wooden Shoe Butte Member medial vitrophyre	16	51.48 (0.24)	0.34 (0.07)	0.95 (0.04)	17.40 (0.30)	0.53 (0.06)	10.94 (0.12)	18.04 (0.18)	0.27 (0.04)	0.02 (0.01)	0.00	100
Wooden Shoe Butte Member basal vitrophyre	5	49.93 (0.24)	0.30 (0.06)	0.91 (0.04)	21.56 (0.37)	0.63 (0.08)	9.03 (0.10)	17.44 (0.17)	0.21 (0.03)	0.00	0.00	100
Wooden Shoe Butte Member fall deposit	9	50.27 (0.24)	0.31 (0.06)	1.03 (0.04)	21.03 (0.37)	0.62 (0.08)	8.66 (0.10)	17.58 (0.17)	0.25 (0.04)	0.06 (0.04)	0.00	100
Steer Basin Member upper vitrophyre	12	50.45 (0.24)	0.33 (0.07)	0.88 (0.05)	22.34 (0.39)	0.57 (0.07)	8.30 (0.09)	16.62 (0.16)	0.24 (0.04)	0.04 (0.02)	0.00	100
Steer Basin Member basal vitrophyre	9	50.04 (0.24)	0.31 (0.07)	0.76 (0.04)	23.12 (0.40)	0.59 (0.07)	7.73 (0.09)	17.12 (0.17)	0.21 (0.03)	0.02 (0.01)	0.00	100
Steer Basin Member basal vitrophyre	7	49.98 (0.24)	0.32 (0.07)	0.84 (0.04)	22.22 (0.39)	0.59 (0.07)	8.48 (0.09)	17.00 (0.17)	0.21 (0.03)	0.00	0.00	100
Big Bluff Member upper vitrophyre	14	49.19 (0.23)	0.35 (0.07)	0.69 (0.03)	26.74 (0.47)	0.61 (0.08)	3.74 (0.04)	18.41 (0.18)	0.23 (0.04)	0.03 (0.01)	0.00	100
Big Bluff Member basal vitrophyre	29	48.98 (0.23)	0.34 (0.07)	0.68 (0.03)	27.10 (0.47)	0.63 (0.08)	3.85 (0.04)	18.26 (0.18)	0.24 (0.04)	0.01(0.01)	0.00	100
Magpie Basin Member basal vitrophyre	6	49.87 (0.23)	0.31 (0.11)	0.76 (0.03)	25.32 0.44)	0.65 (0.08)	5.47 (0.06)	17.60 (0.17)	0.23 (0.04)	0.02 (0.01)	0.01 (1.10)	100
Magpie Basin Member basal vitrophyre	4	49.06 (0.23)	0.53 (0.06)	0.81 (0.04)	26.97 (0.47)	0.74 (0.09)	3.34 (0.04)	18.42 (0.18)	0.25 (0.04)	0.01 (0.01)	0.00	100

Table 2.3. Median compositions (in wt.%) of the compositional populations of augite from ignimbrites within the Cassia succession, recalculated to 100%. n represents the number of analyses for each population. Figures quoted in brackets represent the error at 2 sigma.

	n	SiO ₂	TiO ₂	Al ₂ O ₃	FeO	MnO	MgO	CaO	Na ₂ O	K ₂ O	NI0	Total
McMullen Creek Member basal vitrophyre	3	49.98 (0.24)	0.25 (0.08)	0.47 (0.03)	33.27(0.45)	1.21 (0.11)	9.51 (0.10)	5.18 (0.11)	0.09 (0.05)	0.01 (0.01)	0.00	100
McMullen Creek Member basal vitrophyre	17	49.93 (0.24)	0.23 (0.08)	0.48 (0.03)	32.41 (0.44)	1.14 (0.11)	10.38 (0.11)	5.16 (0.11)	0.07 (0.04)	0.00	0.00	100
McMullen Creek Member basal vitrophyre	22	49.56 (0.24)	0.21 (0.07)	0.39 (0.02)	34.50 (0.47)	1.24 (0.12)	9.03 (0.09)	4.94 (0.11)	0.07 (0.04)	0.01 (0.01)	0.00	100
Wooden Shoe Butte Member upper vitrophyre	34	51.24 (0.24)	0.19 (0.06)	0.39 (0.02)	29.09 (0.39)	0.95 (0.09)	13.98 (0.15)	3.97 (0.09)	0.07 (0.04)	0.01 (0.01)	0.00	100
Wooden Shoe Butte Member medial vitrophyre	31	51.37 (0.25)	0.18 (0.06)	0.38 (0.02)	29.18 (0.40)	0.92 (0.09)	13.84 (0.14)	3.96 (0.09)	0.07 (0.04)	0.01 (0.01)	0.00	100
Wooden Shoe Butte Member basal vitrophyre	24	49.72 (0.24)	0.12 (0.04)	0.39 (0.02)	33.30 (0.45)	0.95 (0.09)	10.78 (0.11)	4.55 (0.10)	0.07 (0.04)	0.00	0.00	100
Wooden Shoe Butte Member fall deposit	59	49.60 (0.24)	0.19 (0.06)	0.31 (0.02)	34.57 (0.47)	1.03 (0.10)	9.69 (0.10)	4.38 (0.09)	0.10 (0.06)	0.02 (0.01)	0.00	100
Steer Basin Member upper vitrophyre	6	49.46 (0.24)	0.25 (0.08)	0.64 (0.04)	34.39 (0.47)	0.92 (0.09)	8.63 (0.09)	5.30 (0.11)	0.11 (0.06)	0.05 (0.02)	0.01 (0.26)	100
Steer Basin Member upper vitrophyre	13	50.04 (0.24)	0.20 (0.07)	0.40 (0.02)	33.89 (0.46)	0.92 (0.09)	9.83 (0.10)	4.65 (0.10)	0.08 (0.05)	0.00	0.00	100
Steer Basin Member basal vitrophyre	11	49.31 (0.24)	0.19 (0.06)	0.49 (0.03)	35.85 (0.49)	0.98 (0.09)	8.44 (0.09)	4.71 (0.10)	0.07 (0.04)	0.02 (0.01)	0.00	100
Steer Basin Member basal vitrophyre	27	49.71 (0.24)	0.20 (0.06)	0.40 (0.02)	33.91 (0.46)	0.94 (0.09)	9.94 (0.10)	4.78 (0.10)	0.07 (0.04)	0.01 (0.01)	0.00	100

Table 2.4 Median compositions (in wt.%) of the pigeonite modes of the different populations within the Cassia succession, recalculated to 100%. N represents the number of analyses for each population. Figures quoted in brackets represent the error at 2 sigma.



Feldspars

Euhedral feldspar crystals up to 5 mm in length are common. Broken crystals are present, but less abundant. All the ignimbrites in the Cassia Mountains contain plagioclase and some also contain sanidine (Fig. 2.18). In the Big Bluff Member, sanidine is intergrown with quartz in a myrmekitic texture. The plagioclase composition changes with stratigraphic height; oligoclase (An₂₁ to An₃₀) in the Big Bluff Member and andesine (An₃₂ to An₄₃) occurs in the units above (Fig. 2.18). The potassium-rich feldspars are sanidines, Or₅₄ to Or₅₉ (Table 2.5). Many of the feldspars host melt inclusions, typically 50 µm in diameter and creating a sieve texture. Rims and cores of individual feldspar phenocrysts were analysed with no significant compositional change seen between rims and cores.

Geothermometry

The intense welding and rheomorphism seen in the Cassia Mountain Formation suggests that magmas were emplaced at high temperature and produced from magmas of high magmatic temperature (e.g. 900 to 1100 °C), as is recorded by other SR-type rhyolites (Ekren et al. 1984; Honjo et al. 1992; Cathey and Nash, 2004; Andrews et al. 2008). Electron microprobe data from phenocryst rims were used for Fe-Ti oxide, two pyroxene or two feldspar geothermometry calculations (methods of Stormer 1983; Andersen et al. 1993; Lindsley 1983; Fuhrman and Lindsley 1988; Ghiorso 1984). The use of phenocryst rims for geothermometry assumes that the edges of the crystals were in equilibrium with the surrounding liquid even if the cores of the crystals were not.

Where possible, magmatic temperatures for each individual eruption unit were estimated using two thermometers and were calculated using an assumed pressure of 5 kbar to allow comparison with previous work. Changing the assumed pressure in the thermometer from 5 kbar to 1 kbar (at a constant assumed temperature) results in little change of results (e.g. 951 ± 66 to 955 ± 56). Other studies (e.g. Honjo et al. 1992; Cathey and Nash 2004; Andrews et al. 2008) suggest that the QUILF pyroxene thermometer (Andersen et al. 1993) provides the most reliable estimates of magmatic temperature for Snake River rhyolites minimising the uncertainty in the calculated

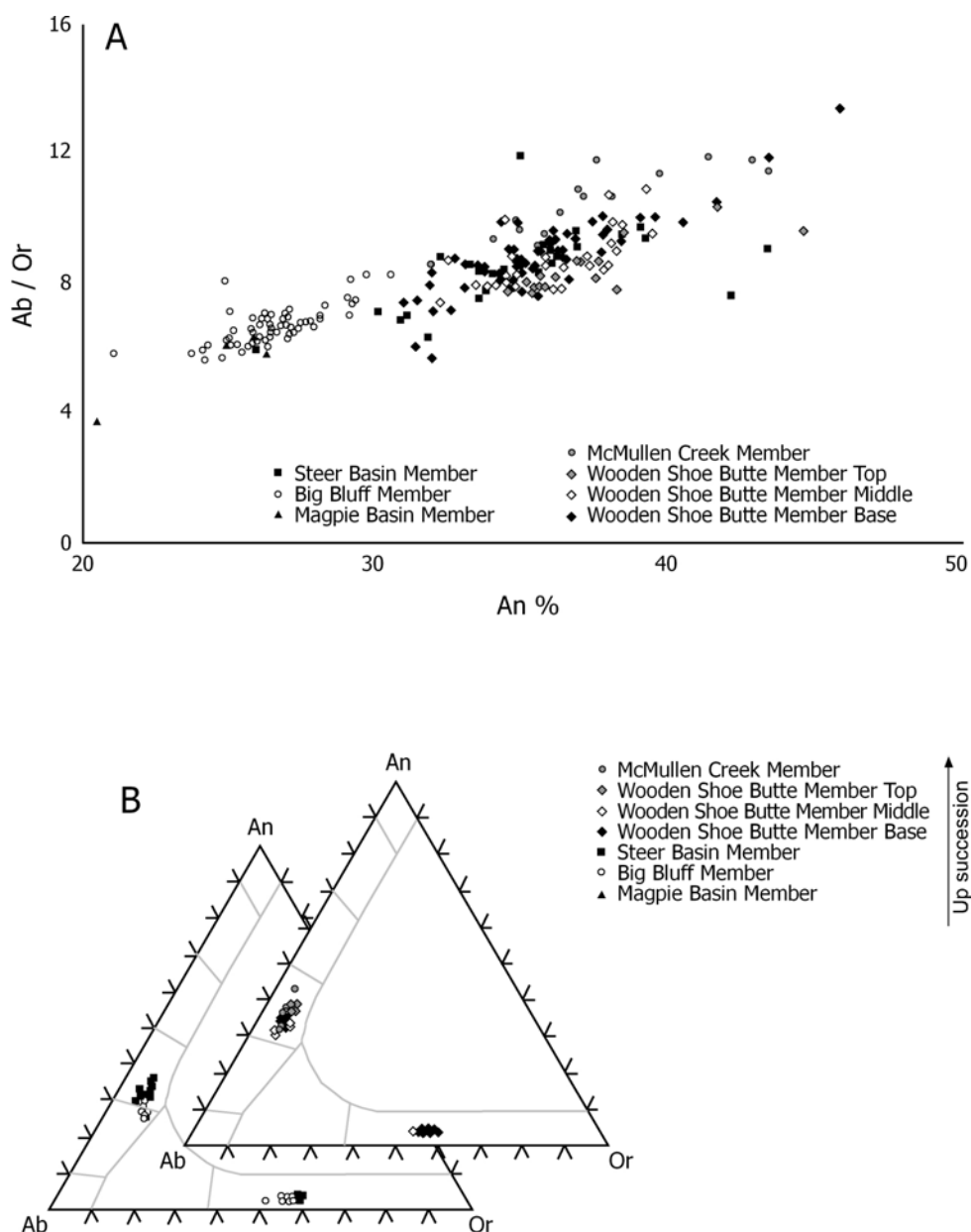


Figure 2.18 **A.** Plagioclase compositions in the Cassia Mountain succession showing the trend towards more calcic plagioclase compositions up succession. **B.** Ternary feldspar plots showing the increase in anorthite content up succession and the absence of sanidine in the upper units of the Cassia Mountains.

	n	SiO ₂	TiO ₂	Al ₂ O ₃	FeO	MnO	MgO	CaO	Na ₂ O	K ₂ O	NiO	Total
Plagioclase												
McMullen Creek Member basal vitrophyre	16	59.78 (0.27)	0.02 (0.07)	24.52 (0.18)	0.46 (0.07)	0.01 (0.02)	0.02 (0.02)	7.68 (0.13)	6.42 (0.13)	1.00 (0.05)	0.01 (0.03)	100
Wooden Shoe Butte Member upper vitrophyre	17	59.30 (0.27)	0.02 (0.07)	24.52 (0.18)	0.67 (0.08)	0.01 (0.02)	0.04 (0.03)	7.71 (0.13)	6.44 (0.13)	1.17 (0.05)	0.01 (0.03)	100
Wooden Shoe Butte Member medial vitrophyre	34	59.53 (0.27)	0.02 (0.07)	24.59 (0.18)	0.51 (0.07)	0.01 (0.02)	0.05 (0.03)	7.47 (0.12)	6.63 (0.13)	1.17 (0.05)	0.01 (0.03)	100
Wooden Shoe Butte Member basal vitrophyre	65	59.86 (0.27)	0.02 (0.07)	24.54 (0.18)	0.46 (0.07)	0.02 (0.03)	0.02 (0.02)	7.31 (0.11)	6.57 (0.13)	1.14 (0.05)	0.01 (0.03)	100
Steer Basin Member basal vitrophyre	33	60.41 (0.28)	0.03 (0.06)	24.19 (0.18)	0.50 (0.07)	0.01 (0.02)	0.03 (0.03)	6.87 (0.10)	6.44 (0.13)	1.46 (0.05)	0.00 (0.01)	100
Big Bluff Member basal vitrophyre	69	61.98 (0.28)	0.01 (0.07)	23.16 (0.17)	0.30 (0.07)	0.00 (0.01)	0.00 (0.01)	5.51 (0.10)	7.32 (0.14)	1.68 (0.05)	0.00 (0.01)	100
Magpie Basin Member basal vitrophyre	3	62.13 (0.28)	0.03 (0.07)	22.95 (0.17)	0.32 (0.07)	0.00 (0.01)	0.00 (0.01)	5.36 (0.10)	7.33 (0.14)	1.85 (0.05)	0.00 (0.01)	100
Sanidine												
Wooden Shoe Butte Member basal vitrophyre	3	65.90 (0.29)	0.07 (0.07)	19.28 (0.16)	0.18 (0.06)	0.01 (0.04)	0.00 (0.01)	0.70 (0.05)	4.53 (0.11)	9.27 (0.13)	0.00 (0.01)	100
Steer Basin Member basal vitrophyre	3	65.90 (0.29)	0.10 (0.08)	19.30 (0.16)	0.23 (0.06)	0.02 (0.04)	0.00 (0.01)	0.61 (0.05)	4.22 (0.10)	9.55 (0.14)	0.01 (0.03)	100
Big Bluff Member basal vitrophyre	35	65.70 (0.29)	0.04 (0.04)	19.35 (0.16)	0.14 (0.06)	0.01 (0.04)	0.00 (0.01)	0.74 (0.05)	4.56 (0.11)	9.42 (0.14)	0.01 (0.03)	100
Magpie Basin Member basal vitrophyre	9	65.75 (0.29)	0.11 (0.08)	19.37 (0.16)	0.21 (0.06)	0.00 (0.01)	0.00 (0.01)	0.83 (0.06)	5.07 (0.12)	8.64 (0.15)	0.01 (0.03)	100

Table 2.5 Average compositions of feldspar phenocrysts within the Cassia succession, recalculated to 100%. n represents the number of analyses for each unit. Figures quoted in brackets represent the error at 2 sigma.

temperature by allowing the ferrosilite (Fs) value to vary freely (Cathey and Nash, 2004). The graphical pyroxene thermometer of Lindsley (1983) was also used, and results agreed well with the QUILF thermometer (Fig. 2.19). Results from each thermometer were within error of each other and gave estimates of temperature ranging from 910 to 970°C (Fig. 2.19).

Feldspar thermometry using the SOLVCALC software of Wen and Nekvasil (1994) provided results with considerable variation (c. 200 °C) between the models of Fuhrman and Lindsley (1988) and Ghiorso (1984). The model of Ghiorso (1984) produced higher estimated magmatic temperatures but given that the model of Fuhrman and Lindsley (1988) shows better agreement with the other thermometers (Fig. 2.18), these estimates are considered more realistic.

Temperatures using the Fuhrman and Lindsley (1988) thermometer range from 860 to 880 °C (Fig. 2.19).

Zircon saturation thermometry (Watson and Harrison 1983) (Fig. 2.19), agrees well with the co-existing mineral thermometers and although there is no error quoted with the thermometer, here the error is assumed to be 50 °C (Fig. 2.19). The temperatures produced by the zircon saturation thermometer show little variation, ranging between 897 °C for the McMullen Creek Member and 925 °C for the Deadeye Member.

The abundance of titanium in quartz can be used as a thermometer, with titanium substituting for silica in a temperature dependent process (Wark and Watson 2006). Despite the titanium-in-quartz thermometer being developed using a system which had rutile as a phenocryst phase, it can be used when rutile is absent if the titanium activity of the melt is adjusted downward. Reducing the titanium activity of the melt from 1 to 0.5 results in a decrease in calculated temperature of around 100°C for a given titanium content. For the Bishop Tuff which contains ilmenite and magnetite, Wark et al. (2007) use an a_{TiO_2} of 0.6 based on titanium saturation experiments. Given that most SR-type ignimbrites contain ilmenite and titanomagnetite, an activity of titanium of 0.6 was taken when calculating temperatures. Errors on abundances of titanium in quartz, as determined from electron microprobe analyses, range between 10 and 44%

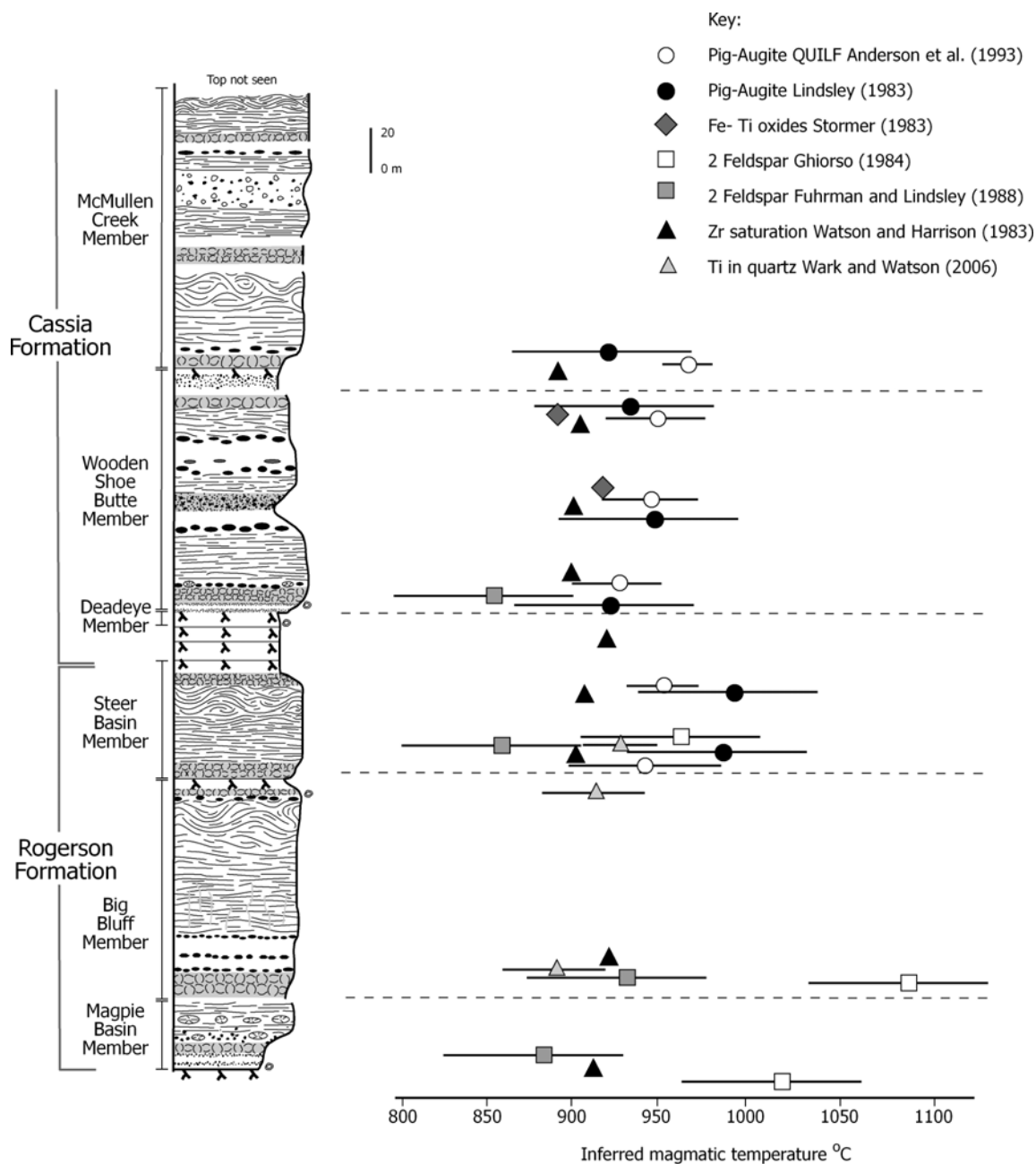


Figure 2.19 Magmatic temperature estimates of the Cassia Mountain succession from a variety of thermometers. Data from two mineral thermometers are based on averages of numerous (normally 20) pairs of co-existing phenocryst rim analyses. The zircon saturation thermometer (Watson and Harrison 1983) has no quoted error associated with it, so here it is taken as being ± 50 °C. Some units show a slight upward increase in temperature, but the magmatic temperatures of the whole succession remain relatively constant.

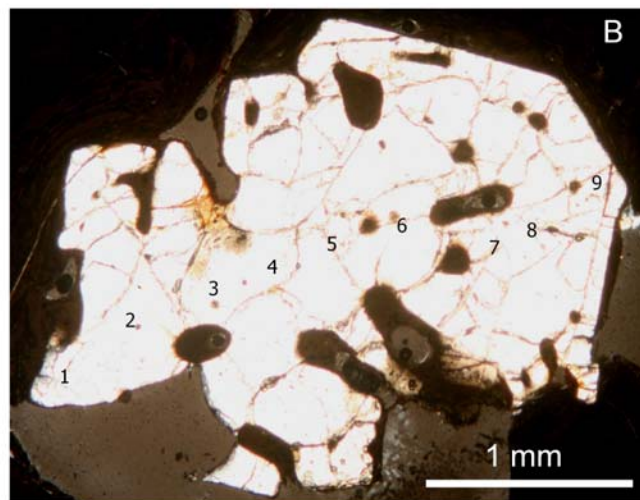
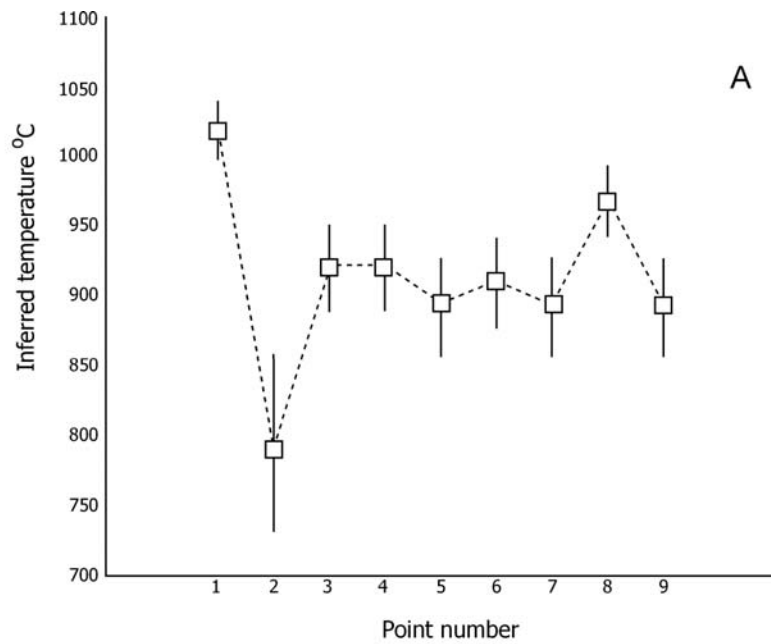


Figure 2.20 A. Thermometry in quartz results across an individual quartz grain in the basal vitrophyre of the Big Bluff Member, showing the variation derived from a single grain
B. Locations on the quartz grain analysed shown in A.

of the total abundance at 2σ . These errors translate into approximately $\pm 35^\circ\text{C}$. Temperatures determined using the titanium in quartz thermometer agree well with the other thermometers,

giving results around 900 °C for the Cassia Mountain rhyolites (Fig. 2.19). Considerable variation occurs within individual quartz phenocrysts, some of which show significant variations in estimated temperature. Some of the quartz phenocrysts show evidence of resorption features (Fig. 2.20) which may indicate that they had complex growth histories.

Geothermometry reveals the high magmatic temperature of these units ~ 900 °C (Fig. 2.19). All the thermometers are in agreement, with the exception of the two feldspar thermometer of Ghiorso (1984). Within individual units, the inferred magmatic temperature remains relatively constant. Temperatures are similar, even in the Wooden Shoe Butte Member where the compositions of the pigeonite and augite vary significantly with height, suggesting that most of the magma volumes were thermally homogeneous.

Neodymium isotopes:

Ignimbrites of the Cassia Mountains are known to have values amongst the lowest ϵ_{Nd} from the Snake River Plain (Nash et al. 2006), with values ranging from -7 to -5.9 (Wright et al. 2002). Using the Neodymium crustal index of De Paolo et al. (1992):

$$NCI = [\epsilon_{Nd(g)} - \epsilon_{Nd(m)}] / [\epsilon_{Nd(c)} - \epsilon_{Nd(m)}]$$

with g, m and c, representing glass, mantle and crust respectively; ϵ_{Nd} of the mantle is taken as -3 and ϵ_{Nd} of the crust is taken as -15 following Cathey and Nash (2004). The value of -15 for the crust is taken as the average of the continental crust east of the terrain boundary (Fleck 1990) and the value of -3 for the mantle is based on values derived from basalts by Leeman et al. (1992) east of the terrain boundary. The ignimbrites show an increasing mantle component with time, with the trend extending from the Bruneau-Jarbidge eruptive centre to the Twin Falls eruptive centre (Fig. 2.21). Some of the values of ϵ_{Nd} used here (McCurry unpublished data) were determined on crystal separates rather than glass. However, the results should be similar to those produced from glass separates, and there is good agreement with other studies (e.g. Nash et al. 2006). Interestingly the McMullen Creek Member, which shows anomalous behaviour in terms

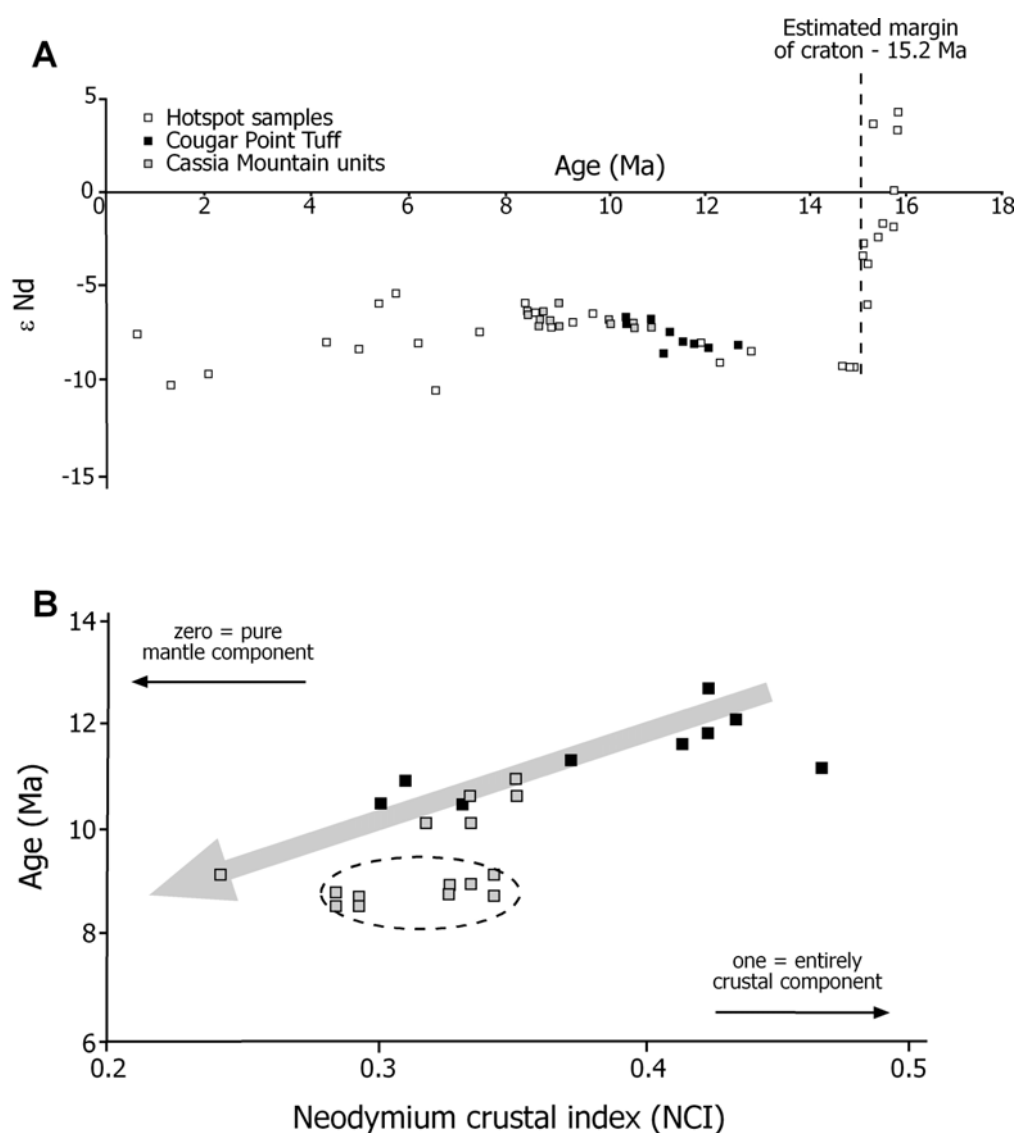


Figure 2.21 A. ϵ_{Nd} plotted against age (Ma) showing the change in ϵ_{Nd} throughout the history of the Yellowstone hotspot, (redrawn from Nash et al. (2006), with additional data from Wright et al. (2004) and McCurry unpublished). B. Neodymium crustal index of De Paolo (1992) showing an increase in mantle component through time from the Bruneau Jarbidge eruptive centre to the Twin Falls eruptive centre. The McMullen Creek Member (with the dotted circle) shows a greater crustal component than would be expected following the trend indicated with the arrow. This is in agreement with the distinct changes in glass and pyroxene chemistry seen in the McMullen Creek Member.

of its whole rock compositions and clinopyroxene compositions, has the least negative ϵ_{Nd} of all the data from the Bruneau-Jarbidge and Twin Falls eruptive centres. The mantle component of

the McMullen Creek Member is less than would be expected from the trend seen in the rest of the data (Fig. 2.21 B).

Discussion

The ignimbrites of the Cassia Mountains record volcanism in the central Snake River Plain from the Yellowstone hotspot spanning the period of ~11 to 8 Ma. The two distinctive features of the Cassia Mountain succession are (1) the multiple compositional modes of the pigeonites and augites within different eruption units and (2) the overall trend towards less silicic compositions of pyroxenes, feldspar and glass up succession. In the section below, these features are discussed and compared to the earlier (12.7-10.5 Ma), Bruneau-Jarbidge eruptive centre (Fig. 2.1).

Cause of pyroxene modal compositions

A detailed examination of Cassia Mountain pyroxene phenocryst data reveals that individual eruptive units may contain discrete compositions of both augite and pigeonite (Fig. 2.15). Possible explanations for the presence of these compositional modes are explored below.

Incorporation of partially melted material

The multiple populations of both pigeonite and augite may represent re-incorporated restitic material which could originate from a variety of sources. Patino-Douce (1997) showed experimentally that A-type granites with strong similarities to the Twin Falls rhyolites can be produced by dehydration melting of calc-alkaline protoliths at depths of 14.5 – 29 km. Although these melting experiments produced two pyroxenes, no pyroxene was present in the initial mineral assemblage of the protolith, arguing against the incorporation of pre-existing clinopyroxenes from a calc-alkaline source.

A second possible source of restite would be the incorporation of previously emplaced mafic intrusions. Pigeonite is commonly absent in intrusive rocks, having inverted to form augite and

orthopyroxene, such as at Bushveld (Buchanan 1978), Freetown (Wells and Bowles 1981), Skaergaard (Brown and Vincent 1963) and Grove Mountains, Antarctica (Liu et al. 2003). If the source of the restite was partially melted plutons, then the compositional modes and gaps in the clinopyroxene data would be difficult to explain as compositional modes and gaps are commonly absent in plutonic rocks (Cathey and Nash 2004). Although intrusive rocks have been reported from the Snake River Plain, their relationship with the rhyolites is uncertain. The best exposed intrusive unit is the 6.7 ± 0.4 Ma (Ferns 1989) Graveyard Point Sill, which contains both basaltic and rhyolitic compositions. The clinopyroxenes in the Graveyard Point Sill differ from those in the Cassia succession in terms of TiO_2 and FeO contents and by being strongly chemically zoned (Markl and White 1999), a feature not recorded from the Cassia succession.

The magnesium numbers of the clinopyroxenes in the Cassia succession (Mg numbers of 29.9 to 46 for pigeonite and 17 to 53 for augite) agree well with those projected from the whole rock compositions (Fig. 2.22) based on $^{\text{Fe/Mg}} K_{\text{D min/liq}} 0.35$ (Sisson and Grove 1993; Reubi and Nicholls 2005) and are consistent with crystallisation from a silicic magma. Using $^{\text{Ca/Na}} K_{\text{D min/liq}}$ values in the range of 2-5.5 following Reubi and Nicholls (2005), calcium numbers (Molar $\text{Ca}/(\text{Ca}+\text{Na}) \times 100$) of plagioclases (43 to 58) are also similar to those projected from whole rock compositions (Fig. 2.23), again reflecting the likelihood that they were formed in a silicic rock; calcium numbers modelled on average compositions of Twin Falls basalts (Bonnichsen and Godchaux 2002) are significantly higher (89–94) than those measured from the Cassia Mountain plagioclases.

The compositions of the pigeonite and augite are consistent with them having been in equilibrium (Fig. 2.16 B). This situation could occur if both the phases were of restite origin, however it is hard to reconcile an origin by reincorporation of partially melted material with the evidence that the clinopyroxenes follow the whole rock, glass, and feldspar trends throughout the Cassia Mountain succession.

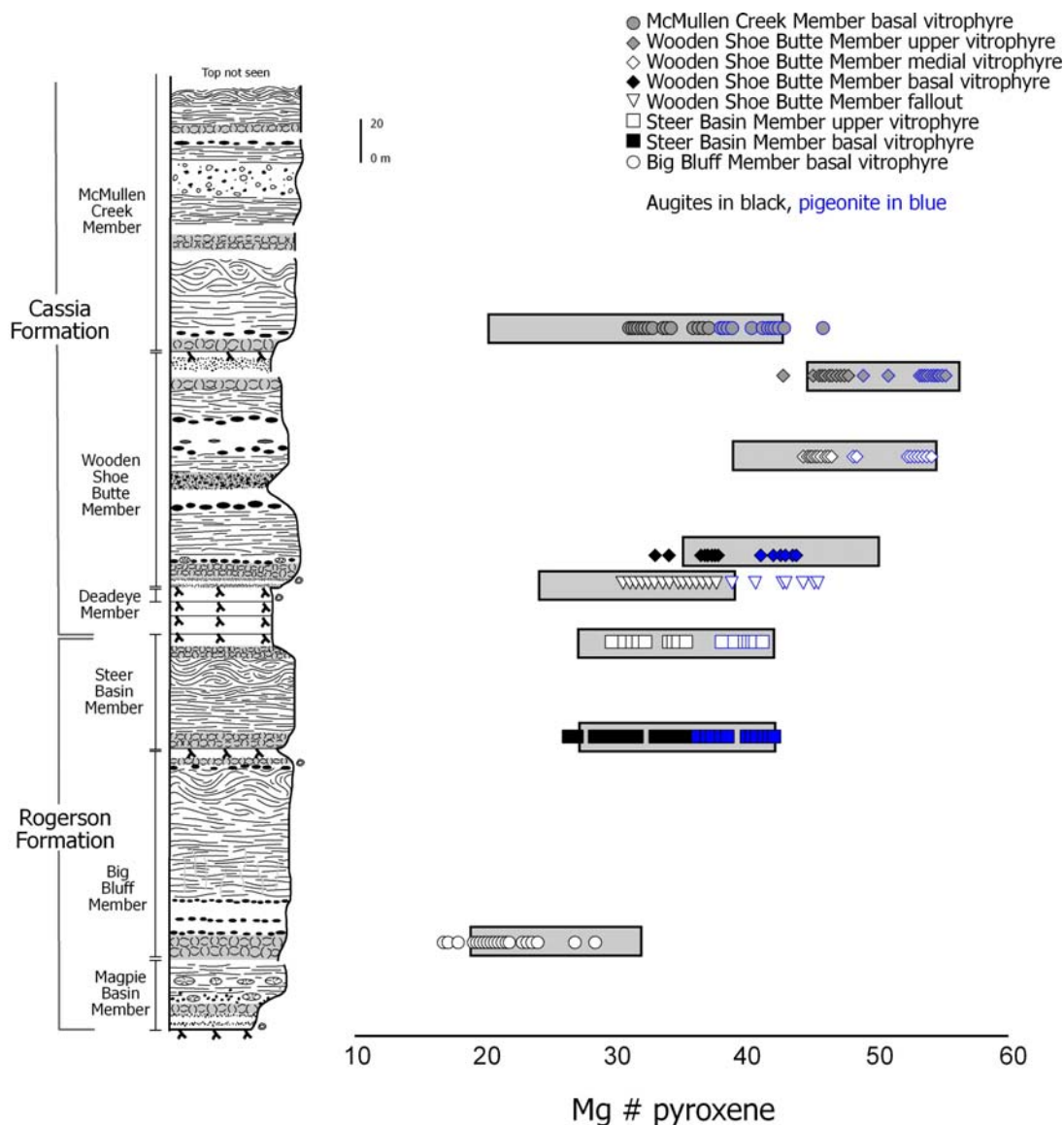


Figure 2.22 Clinopyroxene compositions projected from whole rock data (filled bars), compared with measured compositions. Projected values are based on $F_{Fe/Mg} Kd_{min/liq}$ of 0.35 for analysed whole rock compositions, following Reubi and Nicholls (2005). Some whole rock data for the McMullen Creek Member are from Wright et al. (2002). The units with the least agreement in the Wooden Shoe Butte Member have the least whole rock data available. The Mg number of the clinopyroxenes suggests that they are not from a basaltic source.

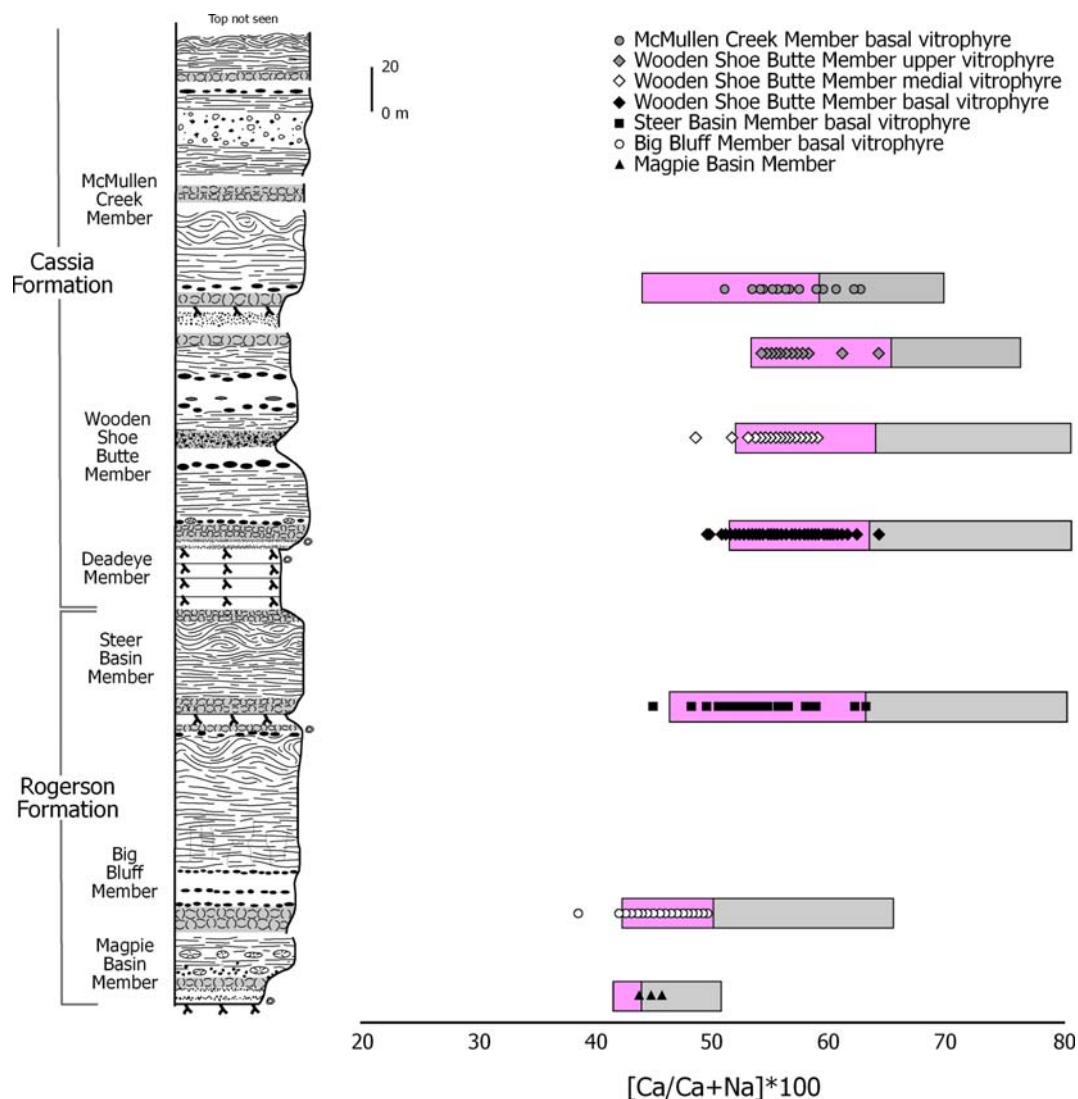


Figure 2.23 Compositions of plagioclase phenocrysts (symbols) compared with the modelled compositions based on the whole rock compositions using the $Ca/Na Kd_{min/liq}$ of 2 (pink) and 5.5 (grey), Reubi and Nicholls (2005). Using average compositions of Twin Falls basalts (from Bonnicksen and Godchaux 2002) to predict Ca numbers of plagioclases gives an estimated range from 89 to 96, suggesting that the plagioclases analysed crystallised from a silicic magma. The better agreement of the actual compositions with the pink fields suggests that 2 is more appropriate value of $Ca/Na Kd_{min/liq}$ for these rhyolites.

Wall rock assimilation

Addition of material from the margins of a magma chamber could explain the distinct modes in the pyroxene compositions, perhaps with one mode being magmatic and the others being

incorporated from elsewhere. Despite disequilibrium features in some of the other phenocrysts (e.g. resorption in quartz and melt inclusions in plagioclases) the clinopyroxenes appear to be euhedral, suggesting that they were phenocrysts. If the multiple modes of pyroxene relate to assimilating wall rock from the magma chamber, then this process must have occurred variably during the history of the magmatic system, because some ignimbrites contain only a single mode of pigeonite and augite (e.g. Wooden Shoe Butte Member) whereas others containing multiple modes (e.g. McMullen Creek Member). Glomerocrysts, the material most likely to represent wall rock, do not contain the multiple modes of clinopyroxene.

Oxygen fugacity conditions

Elsewhere, changes in the oxygen fugacity of a magma chamber have been invoked as a cause of changing compositions of Mg/Fe ratio in clinopyroxene (Grunder and Mahood 1988; Streck and Grunder 1997). During oxidising conditions, the presence of iron as Fe^{3+} rather than Fe^{2+} enables it to substitute for Al rather than Mg in the structure of clinopyroxene. Oxygen fugacity conditions are unlikely to explain the distinct populations in the Cassia Mountain succession for a number of reasons. Firstly, the augite compositions throughout the Wooden Shoe Butte upper cooling unit are identical (see Fig. 2.15) while the oxygen fugacity as determined from the iron oxide thermometer varies from -12.19 units to -13.52 units from the base to the top. Secondly, the Cougar Point Tuff, which shows approximately the same overall variation in MgO and FeO in pyroxenes, shows a variation in $f\text{O}_2$ of 5.2 log units without any apparent correlation between the oxygen fugacity and the composition of the pyroxenes in the unit (Cathey and Nash 2004). This suggests that the multiple modes of pyroxene are not simply a reflection of different conditions of oxygen fugacity.

Glomerocryst compositions

Glomerocrysts within the McMullen Creek and Steer Basin Members contain pigeonite, augite, plagioclase and opaque minerals (Fig. 2.17). Individual glomerocrysts contain only one population of pigeonite and one population of augite, whereas in the case of the McMullen Creek

Member, three populations of pigeonite and two of augite occur within the ignimbrite. In the case of ‘glomerocryst 1’ (Fig. 2.1.6) in the McMullen Creek Member, 6 individual pigeonites are present, and if the glomerocryst was sampling all the pyroxenes found in the ignimbrite, at their relative proportions as currently known, the probability of all the pigeonites in glomerocryst 1 being of the same composition is < 0.5%. Applying this to the augites in glomerocryst 1, the probability of all the augites being of the same composition is 6%. So considered together, this combination of pyroxenes is unlikely if the whole range of pyroxenes were available to the glomerocryst. This suggests that at the time of formation of ‘glomerocryst 1’ in the McMullen Creek Member, only one composition of pigeonite and one composition of augite were available. Moreover, the fact that the high FeO pigeonite and the high FeO augite are found in the same glomerocryst, whereas the high MgO pigeonite and the high MgO augite are found in another glomerocryst indicates that they are cognate to the magma of the ignimbrite that contains them.

The restricted composition of clinopyroxene in glomerocrysts compared to the range of clinopyroxene present in the ignimbrite as a whole suggests that the magma was efficiently segregated prior to eruption. Two possibilities could explain this:

- 1) A single magma chamber in which stratification was very efficient and the various compositions of pigeonite and augite were restricted to a single layer of the chamber;
- 2) The magmas crystallised in separate chambers and were subsequently mingled during the eruption after crystallisation of clinopyroxene.

A stratified magma chamber

Zoned or stratified magma chambers are often inferred based on vertical zonation within the deposit of a single eruption. This zonation is commonly in the form of chemical composition of juvenile clasts for example Mazama (Bacon and Druitt 1988) or Los Humeros (Ferriz and Mahood 1987; Carrasco-Nuñez and Branney 2005). A stratified magma chamber, as invoked for the Bruneau-Jarbidge eruptive centre (Cathey and Nash 2004) appears unlikely for the origin of the Cassia Mountain ignimbrites. Some of the ignimbrites appear to reflect a large volume of homogeneous magma, for example the Big Bluff Member contains a single composition of augite

both in the basal and upper vitrophyres. In the units which contain multiple modes of pigeonite, there is little evidence for zonation of a single magma chamber. For example, the Steer Basin Member has two populations of augite in the basal vitrophyre, but one composition in the upper vitrophyre. Of the two modes of pigeonite in the Steer Basin Member, the high Mg mode comprises 68% of the pigeonite in the base of the unit (n=38) and 71% of the pigeonite in the upper vitrophyre (n=19), which again does not appear to suggest zonation of a magma volume. This may reflect zonation in terms of crystal content, but not in terms of composition. Only in the Wooden Shoe Butte Member does the composition of pigeonite and augite change markedly between the base and the top which may reflect the upper and lower units being from separate eruptions as the contact between the two is not exposed and may contain a palaeosol.

Multiple magma chambers

An alternative hypothesis is simultaneous eruptive withdrawal from multiple smaller chambers containing batches of similar but slightly different magmas. Multiple magma chambers contributing to single explosive eruptions have been reported from other areas (e.g. Ontake, Japan, Kimura and Yoshida, 1999; Taupo Volcanic Zone, Nakagawa et al. 1998; Bali, Reubi and Nicolls 2005; Neapolitan Yellow Tuff, Pabst et al. 2007; Tenerife, Edgar et al. 2007) and of course, the presence of multiple magma chambers would not preclude some of the chambers from being zoned. An alternative suggestion for the production of the starkly different compositions of the pigeonite and augite between the lower and upper Wooden Shoe Butte using the multiple magma chamber model would be that the eruption began tapping a single magma chamber, as it progressed collapse of the caldera allowed eruption of a second volume of magma which contained the pyroxene compositions seen in the upper Wooden Shoe Butte unit. More likely, the strong variation in compositions may reflect two separate eruptions.

The restricted nature of clinopyroxene compositions within a single glomerocryst suggest pre-eruptive conditions in which the compositional modes of pigeonite and augite were not mixing freely, consistent with the multiple magma chamber model. Geothermometry of pigeonites and augites in different glomerocrysts suggests that the more evolved clinopyroxenes (higher FeO,

lower MgO) represent a cooler magma than the more mafic glomerocrysts (a difference of ca. 30 °C although the temperatures overlap within error). If the two magma chambers were of different size then the smaller chamber (all other things being equal) would cool faster and produce the more evolved, higher FeO pyroxenes. Alternatively the magma chambers could have been of similar volume but different shapes with a more spherical chamber retaining its heat and crystallising the more mafic, higher MgO pyroxenes and a more sill-like chamber cooling faster and crystallising the higher FeO pyroxenes. Another possibility is that the magma chambers formed at different depths in the crust. The eastern Snake River Plain contains a mid crustal sill located at approximately 12 km depth (e.g. Peng and Humphreys 1998), if such a feature were present under the central Snake River Plain, then the depths of magma chambers would be limited to < 12 km. Given that pressure variations have little effect on the QUILF thermometer (see earlier), and the glomerocrysts suggest differences in temperature of up to 30 °C derived using the QUILF thermometer, it seems unlikely that a difference in pressure would lead to the compositional variation observed.

A final possibility is that the magma chambers were produced at different times from the same parental magma. The higher FeO clinopyroxene magma chamber could have been produced earlier (and spent longer cooling) than the higher MgO clinopyroxene magma chamber, resulting in a greater degree of fractionation and more evolved compositions.

Trend towards more mafic compositions

Whole rock, glass, feldspar, pigeonite and augite data all show an overall trend towards more mafic compositions in the later erupted units, with the notable exception of the McMullen Creek Member. Possible ways in which progressively more mafic phenocryst compositions may occur within a single eruption and through the whole succession are explored below:

Changing amount of crustal melting over time:

Rhyolites within the Snake River Plain are generally considered to result from melting of crustal materials (e.g. Bonnicksen and Citron 1982), about which little is known. Crustal xenoliths have been used to determine the age of the craton, which decreases from 3.2 to 2.5 Ga passing from

east to west (Leeman et al. 1985; Wolf et al. 2005), but neodymium isotopes rule out a significant role for such old materials at the protolith. Neodymium isotopes (Fig. 2.20; Nash et al. 2006) suggest an increasing mantle component in the younger rocks of the Cassia Mountain succession; however this is based on the assumption that the crustal component being assimilated always retains the same isotopic composition. How the changing proportion of crust being melted affects clinopyroxene compositions is however, unclear. In the case of the Cougar Point Tuff (12.7 to 10.5 Ma on Fig. 2.20) there is no relationship between the degree of crustal melting and the composition of clinopyroxene.

The temperature contrast between a magma chamber and its surroundings may also play a role in the degree of fractionation the magma undergoes. The first magma passing through a crust would be cooled by conduction of heat to the country rock and fractionate. Magmas following this first batch through the same magmatic system pass up into crust which has been heated by the presence of the first magma, so the thermal gradient between the magma and the chamber walls will be much reduced. This reduction in cooling is considered to cause a decrease in fractionation and produce less silicic magmas. This scenario may explain the progressively less silicic compositions of the rhyolites from the Magpie Basin Member to the Wooden Shoe Butte Member, but it cannot explain the large time gap between the Wooden Shoe Butte Member and the McMullen Creek Member.

Melting of a progressively more mafic source:

In this scenario as melting of the craton progresses, the craton is progressively depleted in felsic minerals, as melting of the protolith continues, only the refractory material remains causing the rhyolites to become progressively more mafic. The McMullen Creek Member could represent the melting of 'fresh' crust starting the cycle again and producing more evolved rhyolite.

Duration of residence in the magma reservoir:

If the duration of crystallisation in the magma chamber(s) prior to eruption varied then the amount of cooling and fractionation would vary, and be reflected in different compositions of

pigeonite and augite. The lowest exposed unit in the Cassia Mountains is the Magpie Basin Member, estimated as being between 11.7 and 11.5 Ma (Bonnichsen et al. 2008). So, taking 11.6 Ma as the age of the Magpie Basin Member, the repose periods between the major eruptions progressively decreases from 700,000 years (between the 11.6 Ma Magpie Basin Member and the 10.91 Ma Big Bluff Member) to < 300,000 years (between the Deadeye and the 10.13 Ma Wooden Shoe Butte members). During this time, the compositions of the rhyolites become progressively less silicic until the eruption of the McMullen Creek Member which is much more evolved than the preceding Wooden Shoe Butte Member. The hiatus between the Wooden Shoe Butte and McMullen Creek Members is variously estimated at between 1.2 and 1.6 Ma (Perkins et al. 1995; Nash et al. 2006). This extended hiatus is associated with the increasing FeO and decreasing MgO in the pigeonite and augite of the McMullen Creek Member. The length of time in the magma reservoir is based on the assumption that the period between eruptions represents the period of fractionation within a magma chamber.

Given that there are no constraints on the basaltic input, the main driving force of the system, it is difficult to speculate on the cause of the trend towards less silicic compositions in the rhyolites over time. As previously mentioned, the variation in time crystallising could explain the small-scale variation in compositions of the clinopyroxenes within an individual eruption unit. However, the good correlation between length of repose between eruptions agrees with the whole rock and mineral compositions of the ignimbrites, especially the McMullen Creek Member, this would seem to be the most likely cause of the trend to less silicic compositions. The other possibilities are not readily testable.

Comparison with the Bruneau-Jarbidge eruptive centre

The ignimbrites from the Cougar Point Tuff succession are similar in appearance, whole rock chemistry and mineralogy to those of the Cassia Mountain stratigraphy. The ignimbrites are intensely welded and highly rheomorphic in places, and inferred to have been produced from high-temperature magmas. Both successions are of SR-type and contain anhydrous phenocryst assemblages dominated by plagioclase, sanidine, quartz, pigeonite, augite and iron oxides with

accessory zircon and apatite. A difference between the two successions is that the Cougar Point Tuff ignimbrites commonly contain fayalite whereas this is rare in the Cassia Mountain succession. However, despite the similarities, there are some significant differences between the centres:

Clinopyroxenes

The ignimbrites of the Cougar Point Tuff contain numerous compositional modes of both pigeonite and augite (Cathey and Nash 2004). The ranges of compositions of pigeonite and augite in the Cougar Point tuffs are almost identical to those of the Cassia Mountains, but there are some significant differences. Firstly there is no systematic progression towards more mafic compositions of clinopyroxenes through time at the Bruneau-Jarbidge eruptive centre (Fig. 2.24). The compositions of pigeonites and augites in Cougar Point Tuff ignimbrites were repeatedly erupted in a number of different ignimbrites which does not occur with the Cassia Mountain succession, where compositions of clinopyroxene are not repeated, with the exception of the fall deposit of the Wooden Shoe Butte Member.

Feldspars

Feldspar compositions in the Cougar Point Tuff and the Cassia Mountain ignimbrites are similar in overall composition (Fig. 2.25). Cathey and Nash (2004) note little compositional difference between the rims and cores of the feldspars in the Cougar Point Tuff succession, further emphasising the similarity in feldspar composition from each of the two eruptive centres. In contrast to the Cassia Mountain succession, there is no apparent compositional trend in plagioclase compositions (which vary from An₂₄ to An₃₆) with height through the Cougar Point Tuff succession (Fig. 2.25).

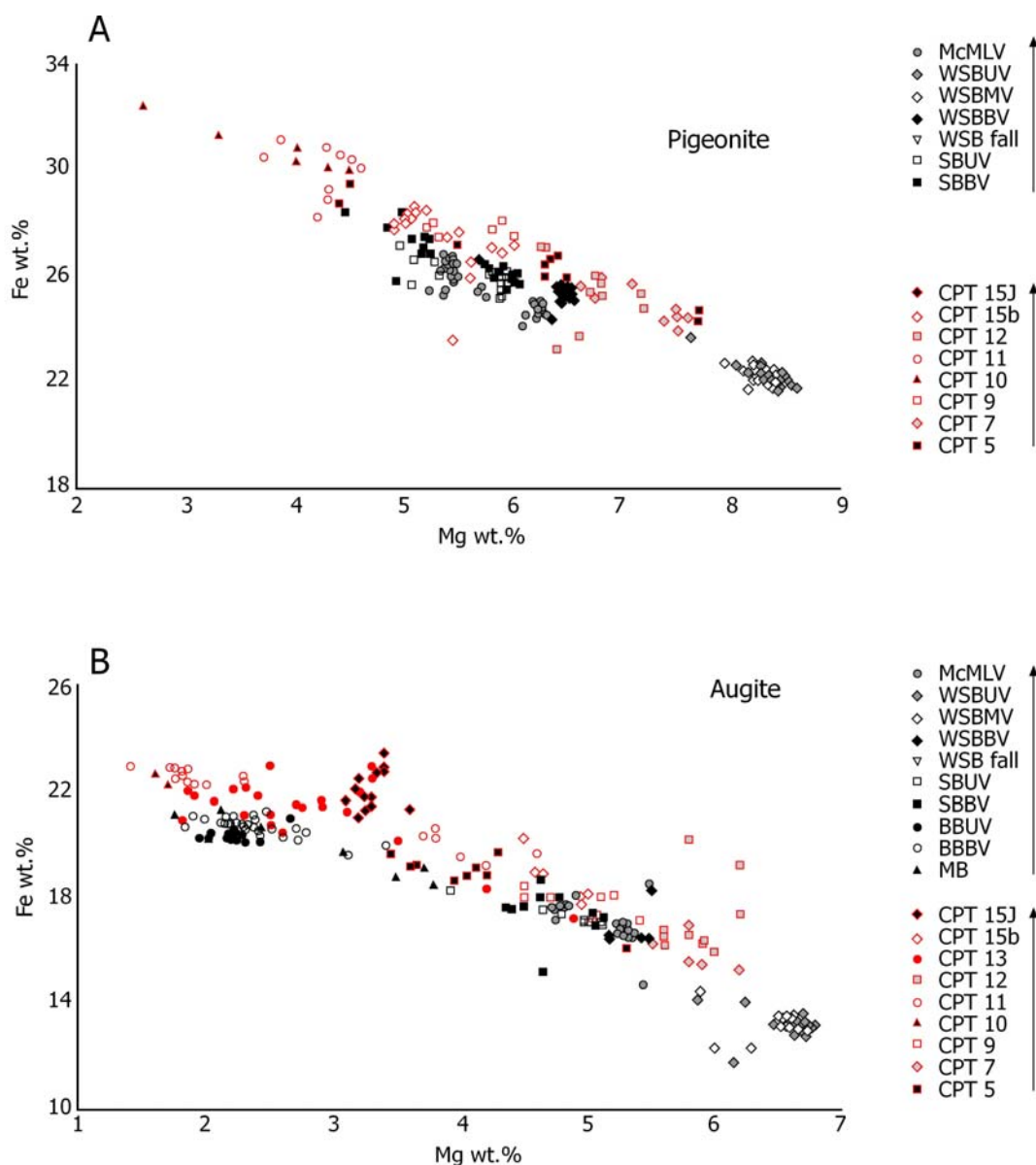


Figure 2.24 Comparison of the clinopyroxene modes in the Cassia succession and in the Cougar Point Tuff (replotted from Cathey and Nash 2004). Abbreviations for the units are CPT - Cougar Point Tuff followed by the number of the unit, MB -Magpie Basin, BBBV - Big Bluff basal vitrophyre, BBUV - Big Bluff upper vitrophyre, SBBV - Steer Basin basal vitrophyre, SBUV - Steer Basin upper vitrophyre, WSB - Wooden Shoe Butte, WSBBV - Wooden Shoe Butte basal vitrophyre, WSBMV - Wooden Shoe Butte medial vitrophyre (basal vitrophyre of the upper Wooden Shoe Butte flow unit), WSBUV - Wooden Shoe Butte upper vitrophyre, McMLV - McMullen Creek lower vitrophyre. **A.** Pigeonite compositions contrasting the trend of increasing Mg wt.% with increasing stratigraphic height in the Cassia Mountains to the random variation in the Cougar Point Tuff. **B.** Augite compositions, showing the same lack of trend in the Cougar Point Tuff in contrast to the Cassia Mountain succession. Note that the Cassia succession reaches lower values of Fe wt.% and higher values of Mg wt.% than the Cougar Point Tuff. The arrows represent younging in each succession.

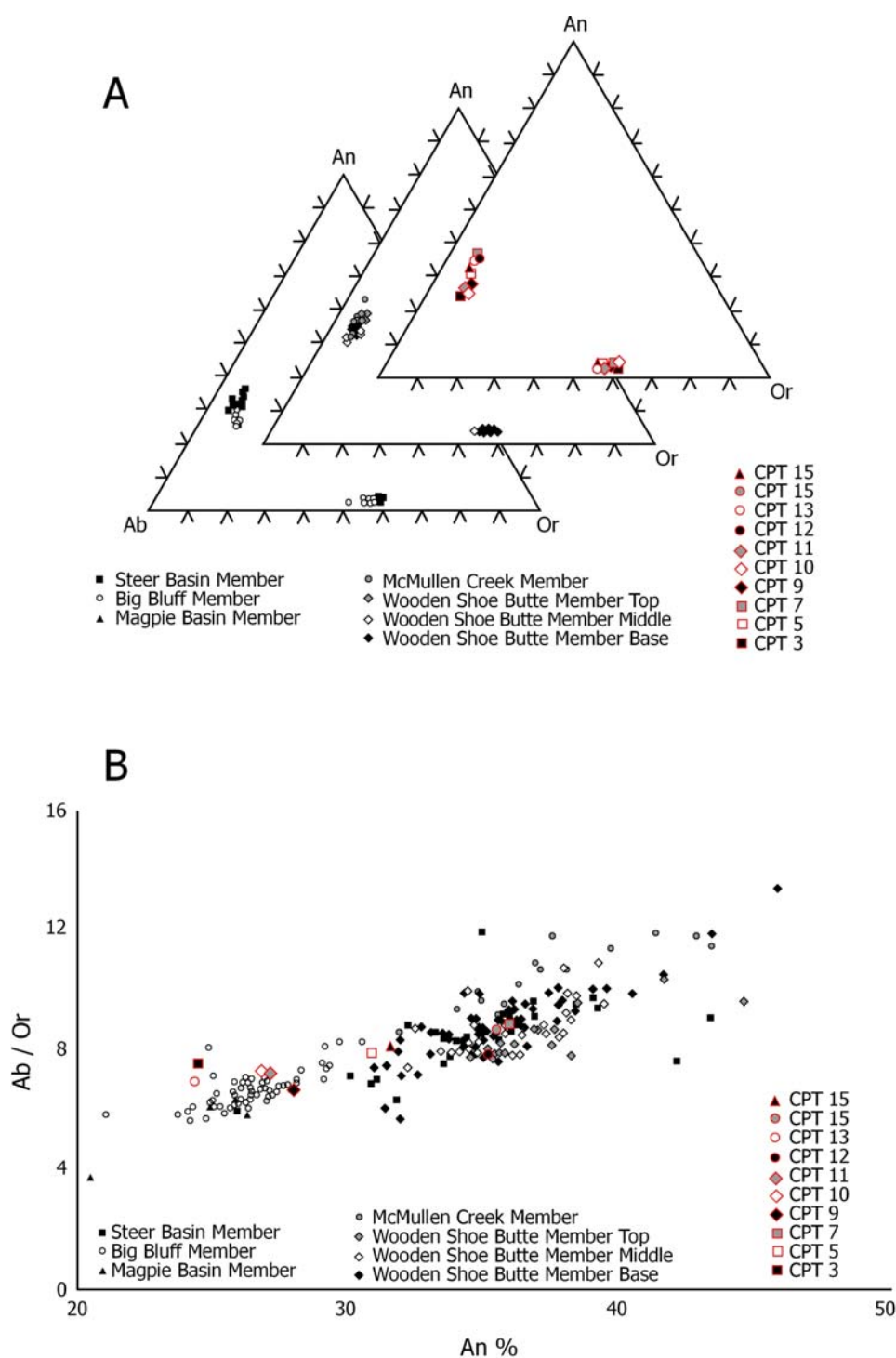


Figure 2.25 **A.** Ternary feldspar plots of the Cassia Mountain and Cougar Point Tuff successions, showing overall similarity between the two successions. **B.** Diagram showing the lack of a compositional trend in the Cougar Point Tuff feldspars (replotted after Cathey and Nash 2004) in comparison with the feldspars from the Cassia Mountains.

Glass

Cougar Point Tuff median glass compositions are similar to those of the Cassia Mountain ignimbrites (Fig. 2.26). However, the range in glass composition in the Cougar Point Tuffs is less than that in the Cassia succession, both through the succession as a whole and within individual units. This difference could be due to the relative lack of published data from each of the Cougar Point Tuffs (ranges shown in Fig. 2.26 represent individual shards for the Cougar Point Tuff) in comparison with the Cassia succession for which every sample contains > 50 data. The glass data from the Cougar Point Tuff succession are separated into three groups by Cathey and Nash (2004) on the basis of their Fe-number and iron content; as can be seen from Figure 2.26, the Cassia glasses plot to a generally higher FeO wt% content. The glass data of Cathey and Nash (2004) were obtained using a single analysis run, in contrast to the two run methodology used here. To ensure that the divergence in results is not a function of analytical method, 50 analyses of the glass from the fallout deposits of Cougar Point Tuff 13 were analysed and they plotted close to the groups proposed by Cathey and Nash (2004) suggesting that the difference in the glass analyses is real rather than an artefact of analysis.

Bruneau-Jarbidge model

The repetition of pyroxene modes is interpreted by Cathey and Nash (2004) as reflecting the successive tapping of a single, long-lived and strongly thermo-chemically zoned magma chamber, this model with a series of layers each containing a discrete composition of pigeonite and augite, in equilibrium with the surrounding magma. The magma chamber is inferred to have persisted for at least the duration of the Cougar Point Tuff succession, at least 2.2 million years (c. 12.7-10.5 Ma). Such a magma chamber must have been very large volume: estimates for volumes of individual Cougar Point Tuff ignimbrites ranging up to 700 km³ (Cathey and Nash 2004) or up to 1,800 km³ (Leeman et al. 2008).

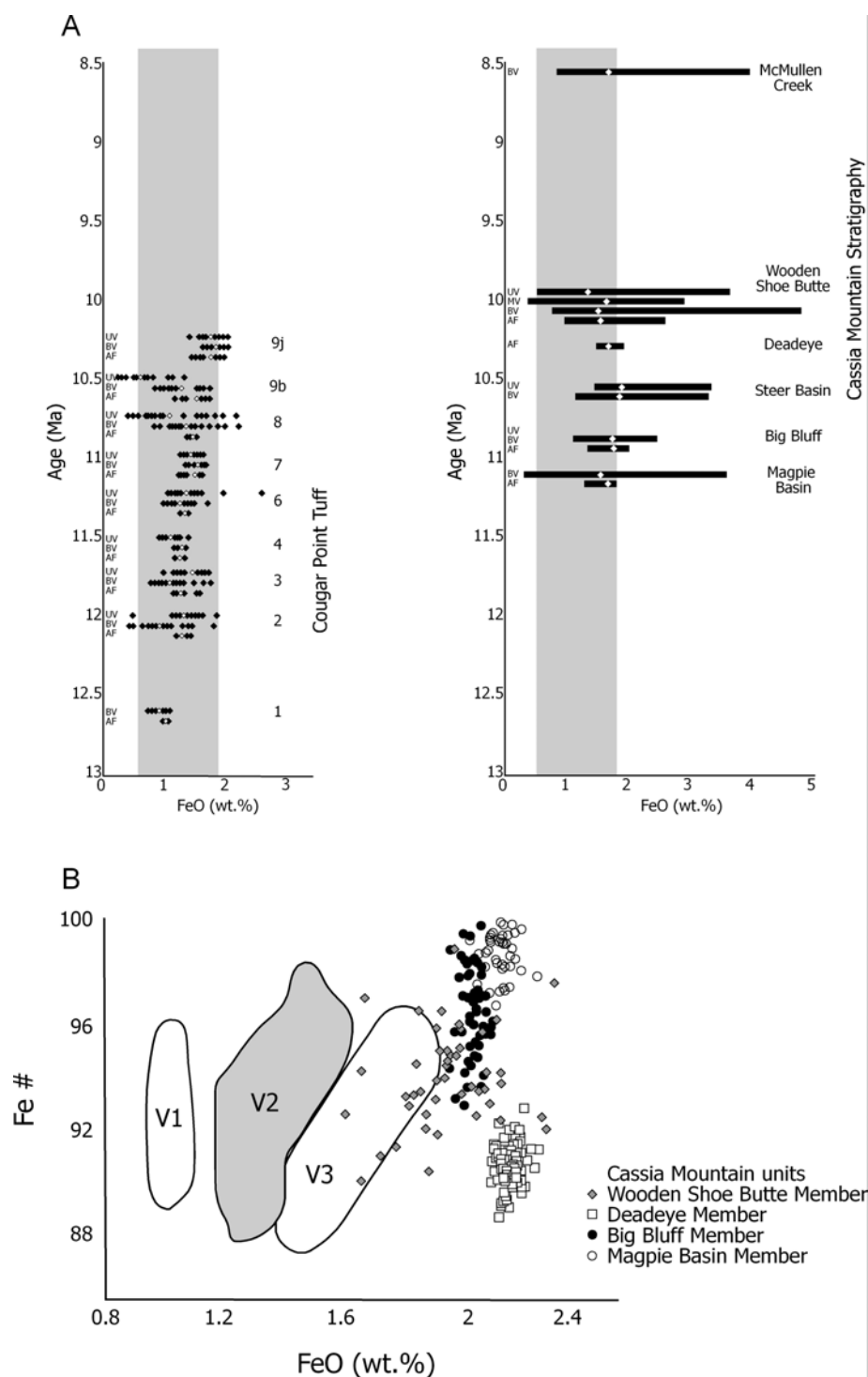


Figure 2.26 A. Comparison of glass compositions between the Cougar Point Tuff succession and the Cassia Mountain succession showing the greater range in glass compositions in the Cassia Mountain deposits (see text). Abbreviations are: af - airfall, bv - basal vitrophyre, mv - medial vitrophyre and uv - upper vitrophyre. **B.** Compositional change of fall deposits through time becoming progressively richer in FeO (wt.%) from the Cougar Point Tuff to the Cassia Mountain deposits. V1, V2 and V3 are compositional trends inferred for the Cougar Point Tuffs (Cathey and Nash 2004)

Twin Falls eruptive centre model

The multiple compositions of pigeonite and augite and the compositions of glomerocrysts are interpreted as representing a magmatic system whereby multiple batches of similar magma evolved in parallel. The magma chambers are of subtly different size or shape which results in slightly different temperatures of the chambers and the variation in compositions of the pigeonite and augite. Only the marked change in clinopyroxene compositions in the Wooden Shoe Butte Member are suggestive of a zoned magma chamber, although the sharp change in compositions between the two flow units are more easily explained as the result of separate eruptions. Of course the presence of multiple magma chambers does not preclude the possibility of the chambers being zoned, although few of the ignimbrites suggest this. This model has the magmas sharing a conduit, thoroughly mixing the multiple compositions of clinopyroxene and allowing them to be deposited together, creating the heterogeneity seen in hand specimen (Fig. 2.27). An alternative to this model involves the magmas ascending different conduits and mixing during transport in a pyroclastic density current. The conduit mixing model is favoured as the mixing of the multiple compositional modes is thorough and is seen at numerous localities (e.g. Chapter 3).

The variation in the number of pyroxene modes is interpreted as reflecting the changing nature of the magmatic system between eruptions, with the Big Bluff Member explained by a single homogeneous magma chamber whereas the Steer Basin Member, containing two modes of pigeonite is interpreted as resulting from two magma chambers. The model of creating new magmatic plumbing systems for each eruption is consistent with the broadly time-transgressive nature of the volcanism, with the centres of volcanism overlapping and gradually migrating east. This contrasts with the previous models of volcanism that suggest a stationary magma chamber producing volcanism lasting for some 2.5 Ma before the locus of volcanism moved some 75 km to the proposed Twin Falls eruptive centre.

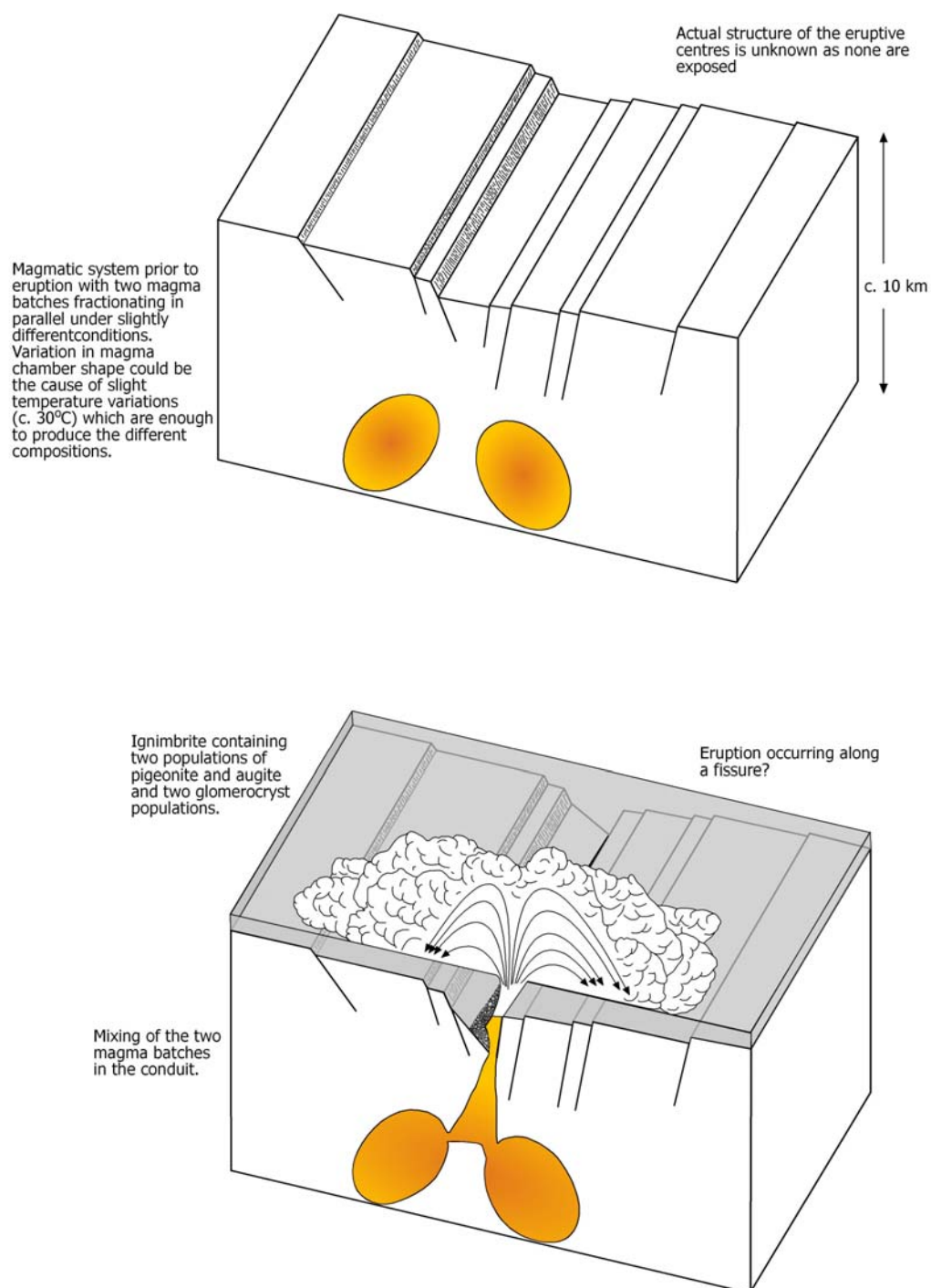


Figure 2.27 Block diagram showing the preferred model for the origin of the heterogeneity in the ignimbrites of the central Snake River Plain. An alternative model would have the magma chambers stacked vertically and sharing the same conduit where mixing could occur, however the thermometry by QUILF suggests that changing the pressure has little effect on the composition of the clinopyroxenes.

Conclusions:

The Cassia Mountain succession, thought to record products of the Twin Falls eruptive centre is dominated by a series of intensely welded ignimbrites separated by a variety of non-welded rhyolitic pyroclastic deposits and rhyolitic volcanoclastic sediment. The welded ignimbrites are the product of high temperature (900-950°C) magmas inferred to have been erupted from a source within the plain in the vicinity of Twin Falls (Fig. 2.1, 2.19). The magmatic system that produced the explosive eruptions is inferred to have been dynamic, and changed between eruptions. Ignimbrites of this succession become progressively less silicic up-succession and variably contain multiple compositions of pigeonite and augite. A model that explains the main features of the magmatic system is proposed that invokes a parental magma that ponds in a number of magma chambers prior to eruptive withdrawal. This model is supported by the compositions of pigeonite and augite in various units and glomerocrysts suggesting that the magmas were separated prior to eruption. The trend towards less silicic compositions supports the work of Bonnicksen et al. (2008) which shows a similar trend for the Snake River Plain as a whole. However, the McMullen Creek Member represents a fundamental change in the system as shown by clinopyroxene compositions and the whole rock chemistry: and after a long (1.2-1.8 Ma) period of repose, more evolved rhyolites were again erupted. This model contrasts with that proposed for the Bruneau-Jarvis eruptive centre (Cathey and Nash 2004) which could reflect the eastward increasing thickness of the craton favouring the production of multiple smaller magma chambers in the eastern CSRP rather than a single long-lived system in the western CSRP.

Chapter 3: Eruptive volumes of Snake River-type ignimbrites

Abstract

The central Snake River Plain of southern Idaho and northern Nevada is surrounded by a number of massifs dominated by significant thicknesses (> 500 m) of intensely welded rhyolite. By correlating between adjacent massifs surrounding the central Snake River Plain, three new eruption units are defined in the period c. 11.4-10.5 Ma. Cougar Point Tuff 11, Big Bluff Tuff and Steer Basin Tuff are defined using a combination of techniques including field logging, magnetic polarity; whole rock, glass, clinopyroxene and feldspar chemistry; oxygen isotopes; and $^{40}\text{Ar}/^{39}\text{Ar}$ geochronology. Several Snake River Plain ignimbrites show compositional heterogeneity in that they contain multiple compositional modes of both pigeonite and augite phenocrysts which are useful for correlation. Bulk deposit volume estimates for the newly correlated eruption units range from 640 km³ for the Steer Basin Tuff to 1200 km³ for the Big Bluff Tuff, and are similar to DRE given the intensity of welding. These represent the first volume estimates for ignimbrites in the central Snake River Plain and are large enough to be considered as ‘super-eruptions’. They are comparable in volume to eruptions from the better studied Yellowstone plateau and Heise eruptive centres from the younger part of the Yellowstone hotspot.

Introduction

The Snake River Plain of southern Idaho and northern Nevada, USA, was the site of voluminous bimodal basaltic and silicic volcanism during the Miocene (Bonnichsen and Citron 1982; Pierce and Morgan 1992). Several buried eruptive centres (Fig. 3.1) within the centre of the plain are inferred sources. The silicic volcanism from the central Snake River Plain (CSRP) was sufficiently different from Plinian, ignimbrite-forming volcanism that it has been regarded as a different category of activity, ‘Snake River-type’ volcanism (Branney et al. 2008). Snake River (SR)-type volcanism was defined by a distinctive

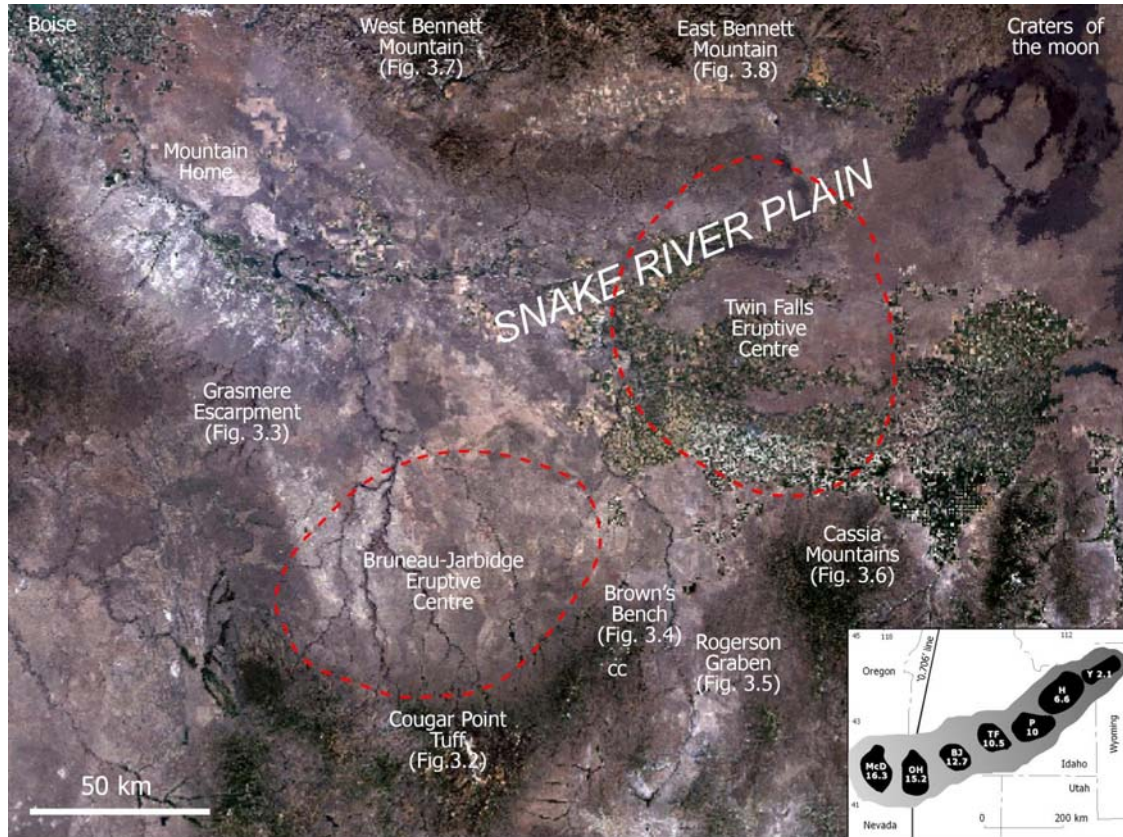


Figure 3.1 Composite satellite image showing the locations of the various massifs bounding the central Snake River Plain. Each massif is referenced to a generalised vertical section of that massif later in the chapter. The inset shows the locations of the proposed eruptive centres along the central Snake River Plain with the numbers reflecting the age of onset of activity at that eruptive centre (Pierce and Morgan 1992). The abbreviations are: McD - McDermitt, OH - Owyhee-Humboldt, BJ - Bruneau-Jarbidge, TF - Twin Falls, P - Picabo, H - Heise and Y - Yellowstone. CC is the approximate location of the Corral Creek section on Browns Bench, see Bonnichsen et al. (2008) for more information on this location.

association of several facies. SR-type ignimbrites are much better-sorted than ignimbrites from Plinian-forming volcanism ($\sigma\phi < 1.5$ compared to $\sigma\phi$ 2-5 for ‘typical’ ignimbrites), often lacking pumice lapilli and lithic lapilli. They are typically intensely welded and highly rheomorphic despite having metaluminous chemistry (Bonnichsen and Citron 1982; Cathey and Nash 2004; Christiansen and McCurry 2008; Branney et al. 2008). SR-type ignimbrites are thought to be large volume, with estimates ranging from tens to hundreds of cubic kilometres of material (Andrews et al. 2008; Branney et al. 2008; Leeman et al. 2008), but hitherto volumes have not been calculated.

Eruptive volume on the Yellowstone hotspot track:

Super-eruptions are defined as those having erupted volumes larger than 300 km^3 of non-vesicular rock, equivalent to 750 km^3 of volcanic ash (Sparks et al. 2005), or having erupted masses of larger than 10^{15} kg (Mason et al. 2004). The Yellowstone-Snake River Plain system has produced a number of super-eruptions (Christiansen 2001; Bindeman and Valley 2001; Morgan and McIntosh 2005). These include the $2,500 \text{ km}^3$ Huckleberry Ridge Tuff; the $1,000 \text{ km}^3$ Lava Creek Tuff and the 280 km^3 Mesa Falls Tuff from the Yellowstone plateau (Christiansen 2001). The ignimbrites from the older Heise eruptive centre (e.g. Fig. 3.1) vary in volume from the 300 km^3 Conant Creek Tuff to the $1,800 \text{ km}^3$ Kilgore Tuff (Morgan and McIntosh 2005).

The total volume of rhyolite in the central Snake River Plain is estimated as c. $7,000 \text{ km}^3$ on the basis that the thickness of rhyolite exposed in massifs bounding the plain is commonly 500 m or more and the area is $14,000 \text{ km}^2$ (Bonnichsen et al. 2008). Perkins and Nash (2002) suggest a volume of $10,000 \text{ km}^3$ for just the Cougar Point Tuff succession (see later). A ‘caldera-forming’ stage (although no calderas have yet been discovered from the CSRP) is proposed for the period 12.7-10.5 Ma wherein most of the volume was erupted followed by a volumetrically subordinate ‘rifting stage’ which is proposed to have occurred between 9.5-5.5 Ma (Bonnichsen et al. 2008). Volumes of individual eruptions from the central Snake River Plain are not well constrained, they vary from 0.25 km^3 to $1,800 \text{ km}^3$ (Andrews et al. 2008; Boroughs et al. 2005; Leeman et al. 2008) although many estimates are only accurate to an order of magnitude.

Regional Stratigraphy

The central Snake River Plain is bordered by a series of massifs (Fig. 3.1) composed of outflow ignimbrite sheets and poorly exposed, non-welded slope-forming sediments (Fig. 3.1), separated by areas of low topographic relief with limited exposure (e.g. Shoshone Basin). The massifs are fault bounded with major N-S trending faulting interpreted as

resulting from re-activation of pre-existing basin and range faults (e.g. Rodgers et al. 1990; Andrews et al. 2008) although recent work has suggested that extension may have been occurring in northern Nevada more recently (e.g. Colgan et al. 2004; 2006), removing the necessity of re-activation. Hitherto the stratigraphies of each massif have been considered separately and how these stratigraphies relate to each other has yet to be addressed. Some of the individual massifs are described below.

Bruneau Jarbidge

Bruneau and Jarbidge canyons (Fig. 3.2) expose a number of Snake River-type ignimbrites, collectively known as the Cougar Point Tuff succession, and a number of voluminous rhyolite lavas (Bonnichsen 1982b; Bonnichsen and Kauffman 1987). The products of the Bruneau-Jarbidge eruptive centre (Bonnichsen 1982) onlap the older Bieroth volcanics in northern Nevada, a relationship that is well exposed in Bruneau canyon (Bonnichsen and Citron 1982). Nine ignimbrites, named CPT III, V, VII, IX, X, XI, XII, XIII and XV were erupted over the period of 12.77 to c. 10.5 Ma as determined by $^{40}\text{Ar}/^{39}\text{Ar}$ geochronology (Cathey and Nash 2004; Bonnichsen et al. 2008). The ignimbrites are variously separated by little-studied fallout deposits, volcanoclastic sediments and palaeosols (although more may be present than are currently recorded). Intercalated within the succession beneath CPT XII is a lava flow, the Black Rock Escarpment Lava, exposed in Bruneau river canyon but absent in Jarbidge river canyon (see Chapter 5). The ignimbrites are high silica rhyolites containing plagioclase, sanidine, augite, pigeonite, fayalite, magnetite, ilmenite and quartz with accessory zircon and apatite (Cathey and Nash 2004). All are inferred to have had high magmatic temperatures of 740-960 °C (Cathey and Nash 2004) or 882-997 °C (Bonnichsen et al. 2008), and unusually low $\delta^{18}\text{O}$ values (Boroughs et al. 2005). Overlying the ignimbrite succession are abundant basaltic lavas erupted from within the Bruneau-Jarbidge eruptive centre (Bonnichsen 1982).

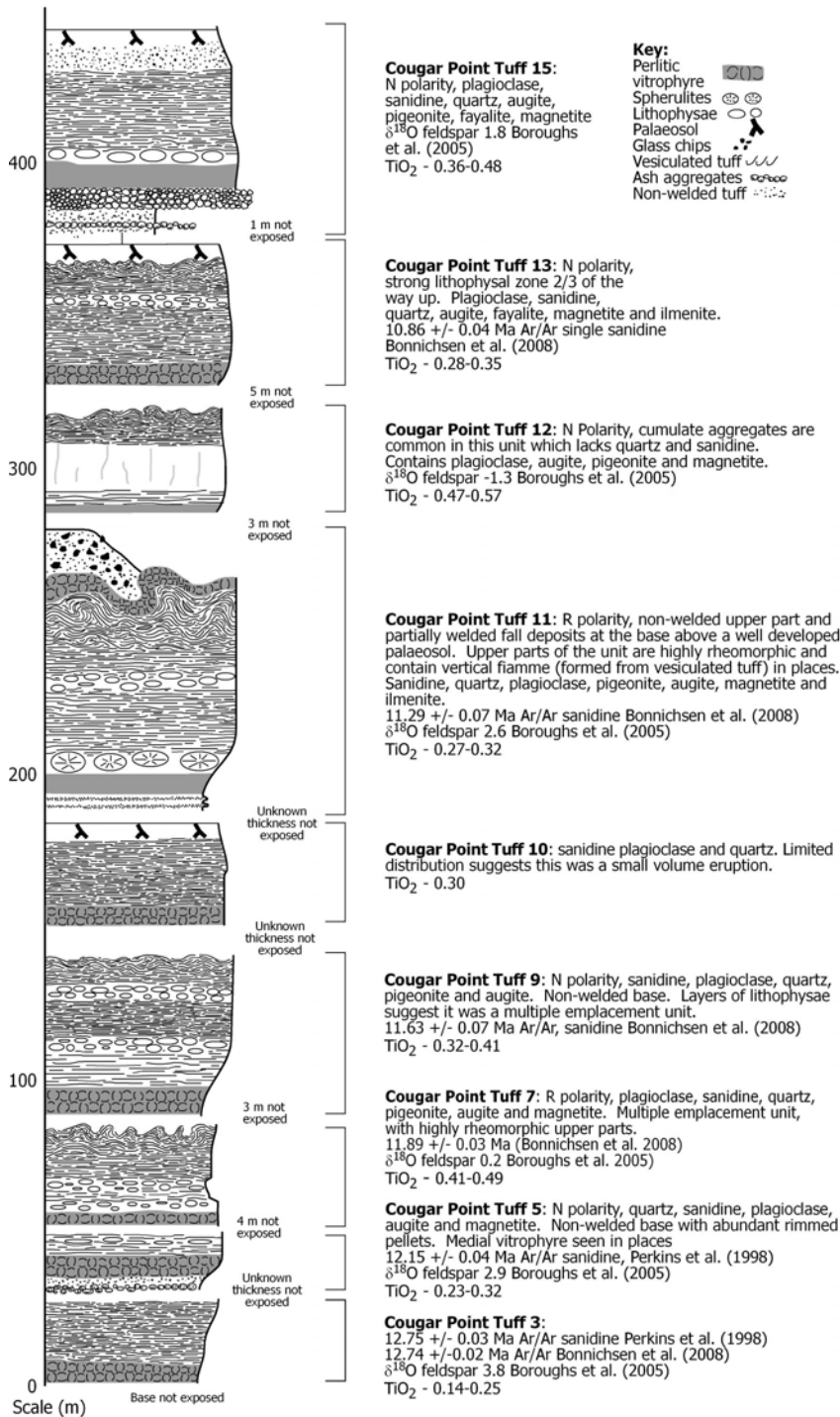


Figure 3.2 Generalised vertical section of the Cougar Point Tuff succession (Fig. 3.1) with ages corrected to Fish Canyon Tuff standard of age 28.02 Ma (Renne et al. 1998).

Grasmere Escarpment

The Grasmere Escarpment (Fig. 3.3), on the north-western margin of the Bruneau-Jarbridge eruptive centre exposes at least three SR-type rhyolitic ignimbrites, but the base of the succession is not exposed. These units are variably exposed along the length of the escarpment. The whole rock characteristics (74-75 wt.% SiO₂) of these units are described by Bonnicksen et al. (2008) but no phenocryst contents or geochronological is available for this poorly understood succession.

Browns Bench

The Browns Bench massif (Fig. 3.4) is fault bounded on its eastern margin exposing a succession of rhyolitic ignimbrites that extend from southern Idaho into northern Nevada. These units were numbered 1-12 in ascending order by Bonnicksen et al. (2008) who also provide physical descriptions of some of them and their whole rock chemistry. They are metaluminous rhyolites (72 to 77 wt.% SiO₂), characteristic of the central Snake River Plain (e.g. Bonnicksen et al. 2008; McCurry and Christiansen 2008). ⁴⁰Ar/³⁹Ar geochronology for two of the ignimbrites on Browns Bench is provided by Bonnicksen et al. (2008) with Unit 7 10.98 ± 0.07 Ma and Unit 9 10.29 ± 0.09 Ma. Phenocryst assemblages, dominated by quartz, plagioclase, sanidine, augite, pigeonite, iron oxides, zircon and apatite are reported by Bonnicksen et al. (2008) but details of the phenocryst and glass chemistries of these units has not yet been reported. Between the welded ignimbrites are poorly-exposed, non-indurated 'slope-forming' units, probably of volcaniclastic origin.

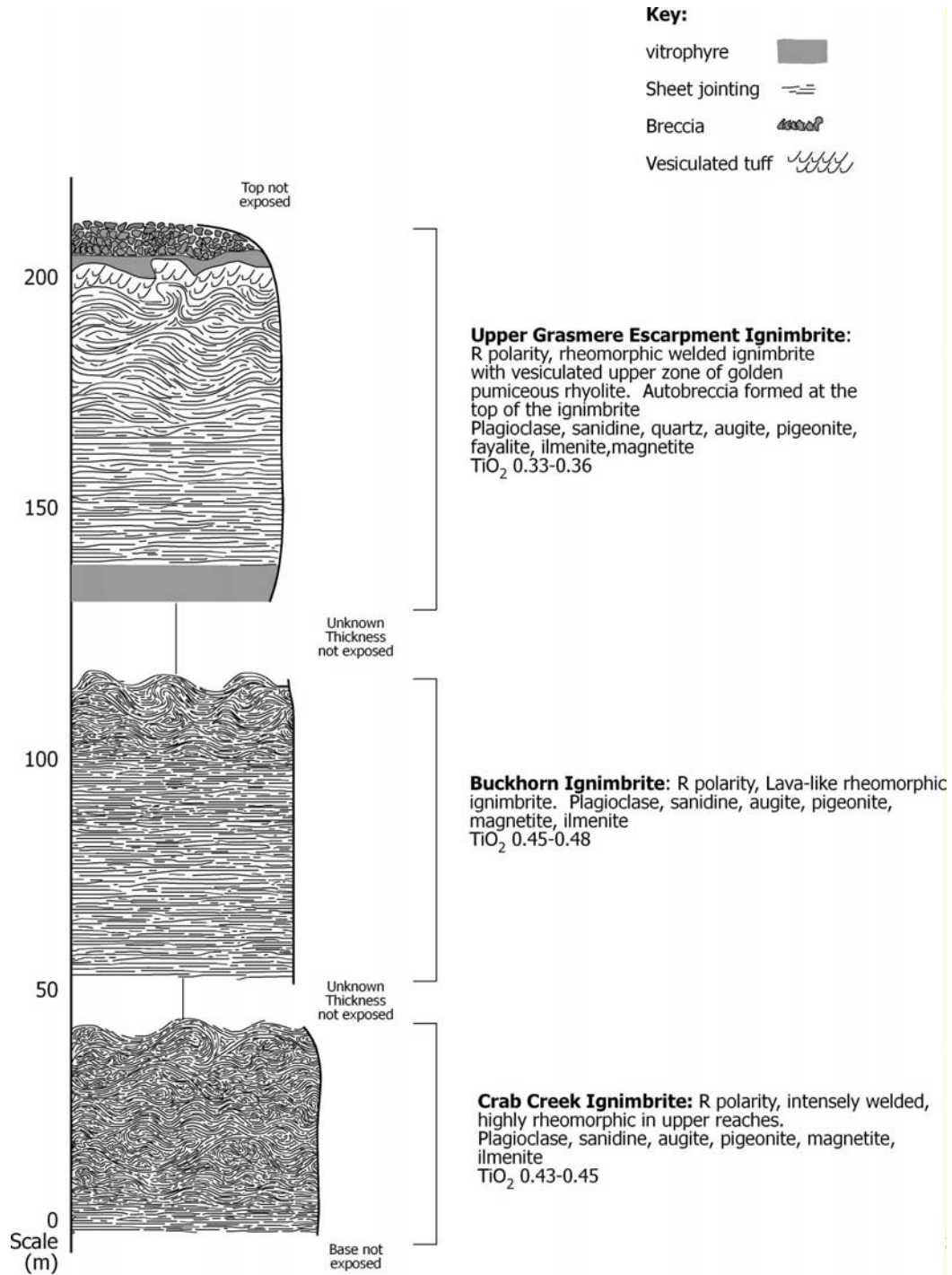


Figure 3.3 Generalised vertical section of the Grasmere Escarpment

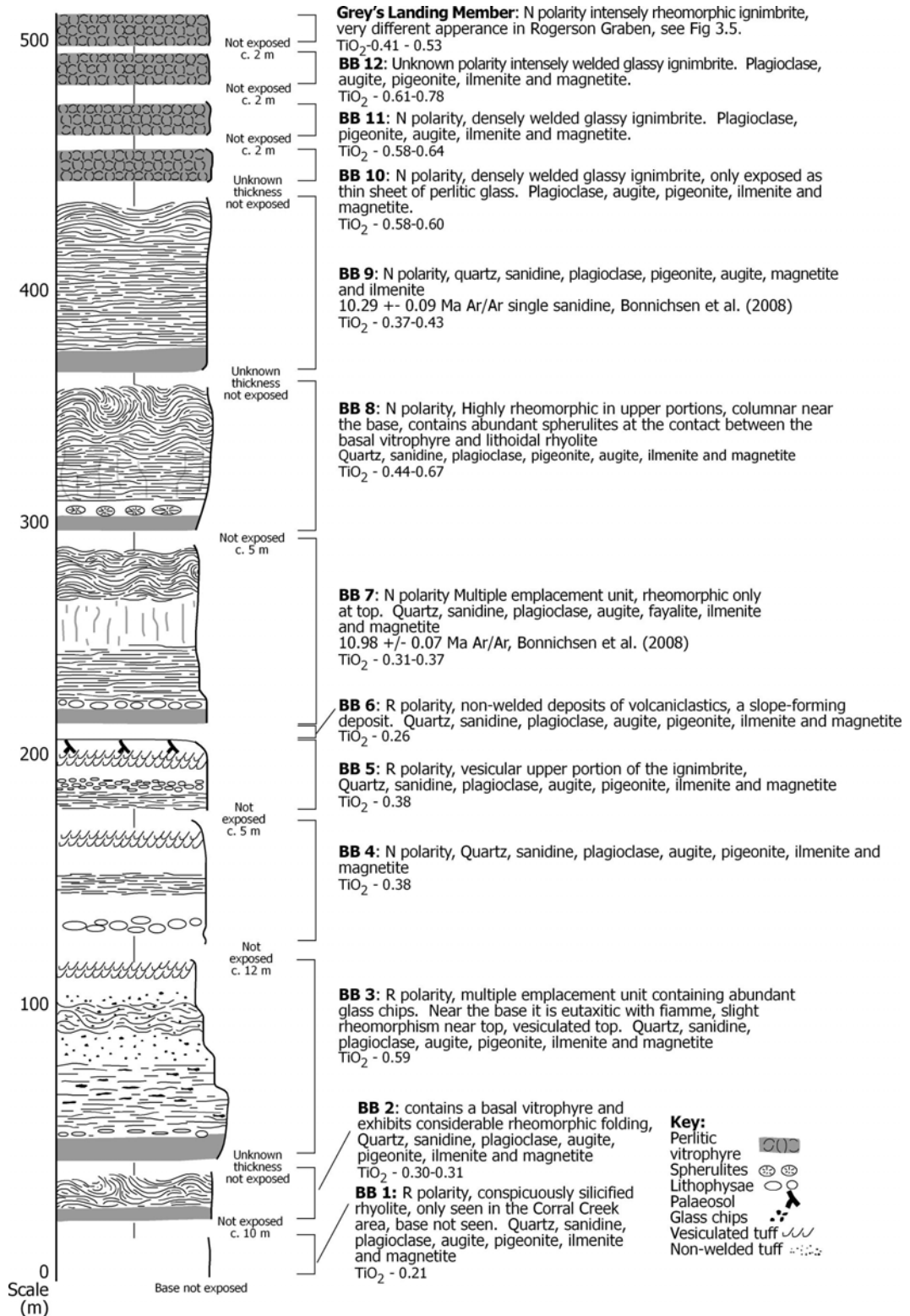


Figure 3.4 Generalised vertical section of the Browns Bench escarpment based on written descriptions in Bonnichsen et al. (2008) and this work. Ages recalculated to the Fish Canyon Tuff standard of 28.02 Ma (Renne et al. 1998).

Rogerson Graben

The Rogerson Graben (Fig. 3.5) exposes 7 rhyolitic ignimbrites that range in welding intensity from the lava-like Jackpot 1-5 to partially-welded Sand Springs Ignimbrite (Andrews et al. 2008). The base of the succession is not exposed and more units may be concealed. The ignimbrites are high silica rhyolites of high inferred magmatic temperature (> 900 °C; Andrews et al. 2008) containing plagioclase, sanidine, pigeonite, augite, quartz, magnetite, ilmenite with accessory zircon and apatite; separated by volcanoclastic sediments and palaeosols. One of the ignimbrites, the Grey's Landing, overtops the adjacent Browns Bench massif, making it an important regional stratigraphic marker. Glass, whole rock and phenocryst data are reported (Andrews et al. 2008), but only the Rabbit Springs ignimbrite has been dated with an $^{40}\text{Ar}/^{39}\text{Ar}$ age of 10.44 ± 0.13 Ma (Bonnichsen et al. 2008).

Cassia Mountains

The Cassia Mountains (Fig. 3.6) contain a succession of rhyolitic ignimbrites, which extend for tens of kilometres across southern Idaho. They are also separated by little-described 'slope-forming' volcanoclastic sediments and palaeosols. The most prominent of the ignimbrites are the Big Bluff (65 m thick) and Steer Basin Members (40-50 m thick). The Cassia Mountain ignimbrites unconformably overlie Permian limestones. The area was mapped by Williams et al. (1990) and Mytton et al. (1991) and subsequent work has been mostly on petrological aspects of individual ignimbrites (e.g. Watkins et al. 1996). The lower part of the Cassia Mountain stratigraphy, including phenocryst, whole rock and glass chemistry is described in Chapter 2. The upper part of the Cassia Mountain stratigraphy comprises a series of ignimbrites referred to as the McMullen Creek (Wright et al. 2002). The McMullen Creek Member is poorly understood; at least four units are distinguished but more may be present. It has distinctive whole rock and isotope chemistry that contrasts with underlying units and is inferred to represent a separate eruptive episode (Bonnichsen et al. 2008; Chapter 2).

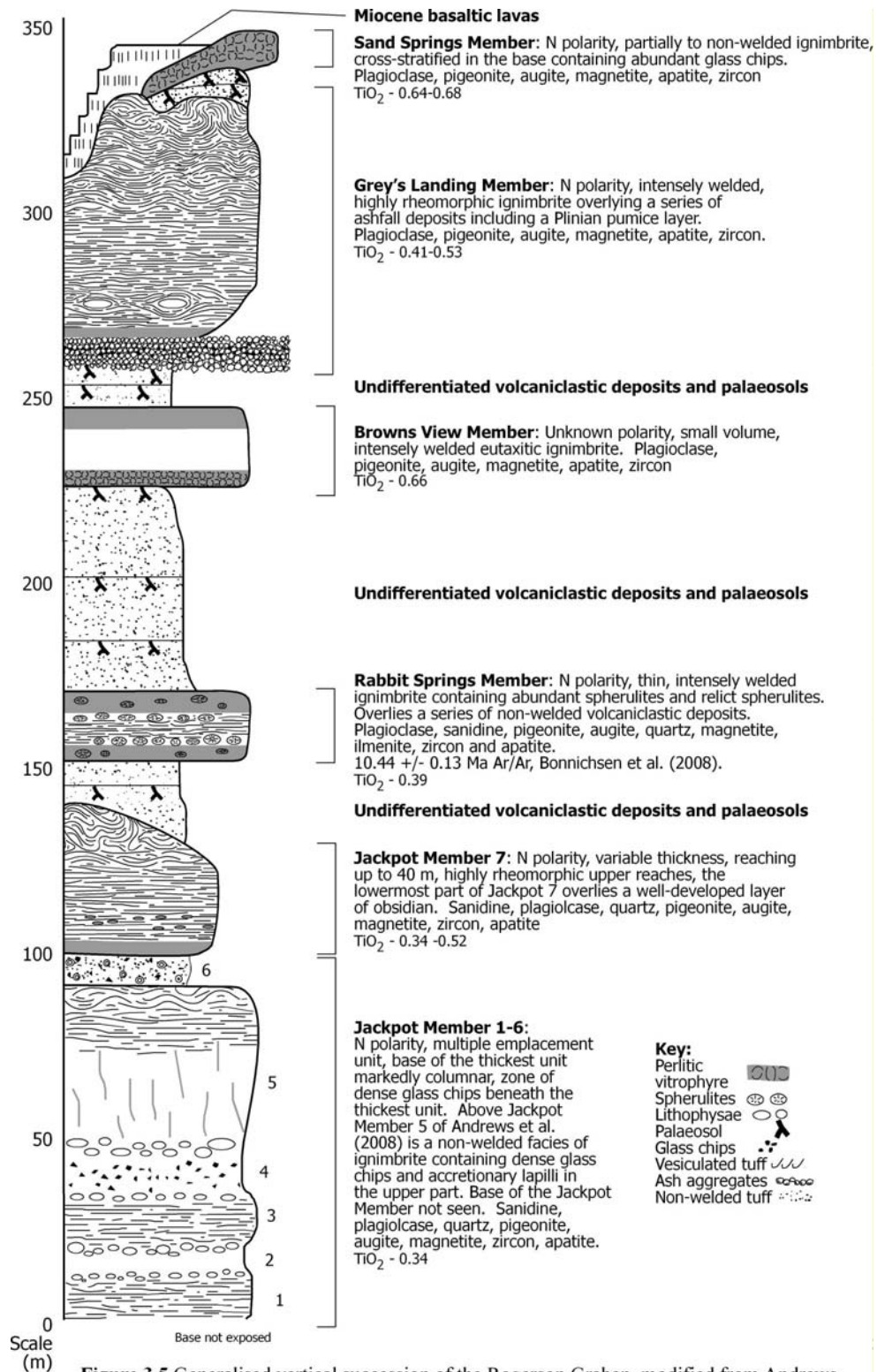


Figure 3.5 Generalised vertical succession of the Rogerson Graben, modified from Andrews et al. (2008) with the age of the Rabbit Springs Member (Bonnichsen et al. 2008) recalculated to the Fish Canyon Tuff standard age of 28.02 Ma (Renne et al. 1998).

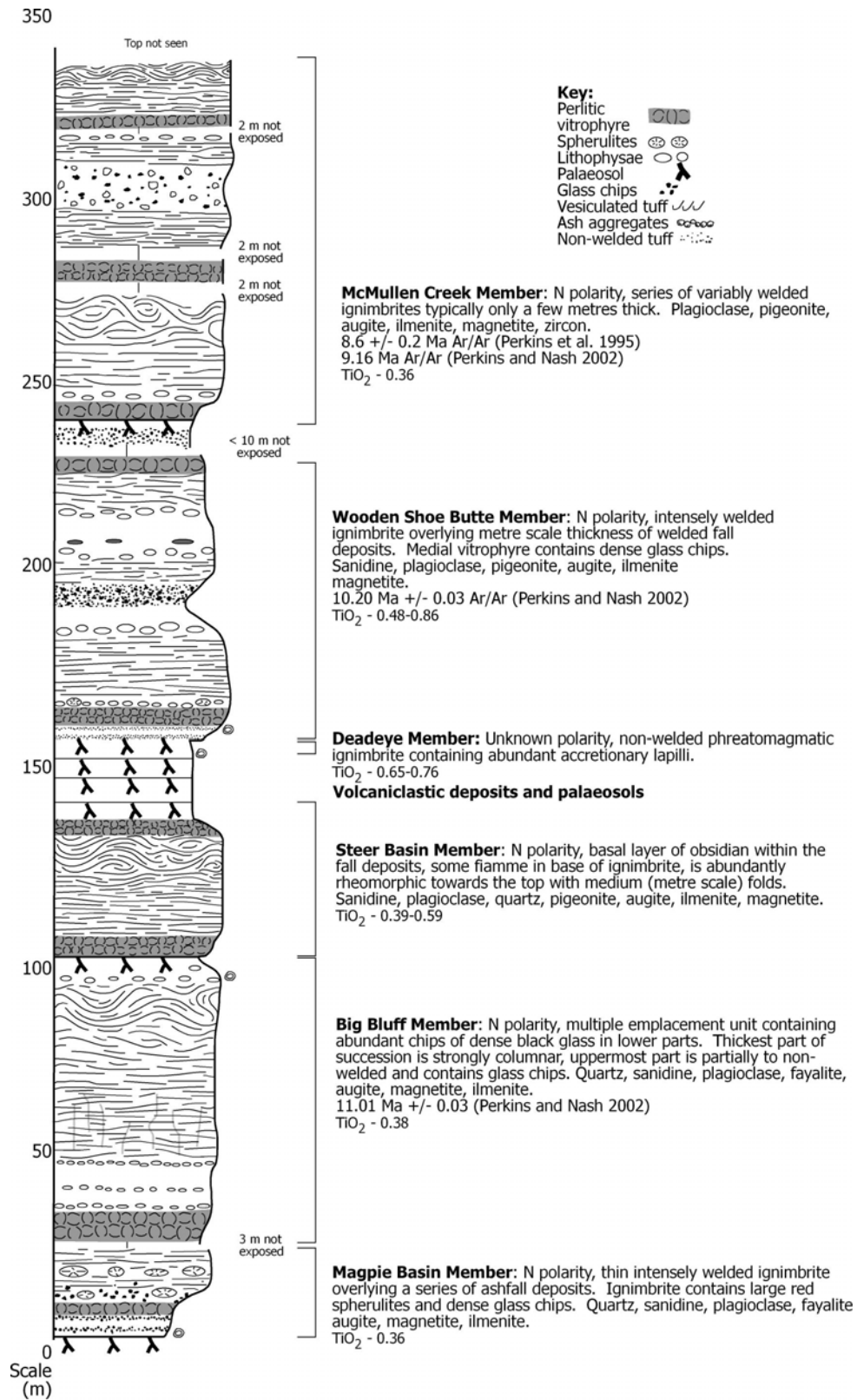


Figure 3.6 Generalised vertical section of the Cassia Mountains (Fig. 3.1)

West Bennett Mountain

The West Bennett Mountain region, on the north side of the Snake River Plain (Fig. 3.7) contains at least 8 rhyolitic units that are of equivocal origin. The base of the succession is not seen. The rhyolites in the West Bennett Mountain region are high silica rhyolites (SiO_2 73-76 wt.%) and have a phenocryst assemblage including sanidine, plagioclase, quartz, augite, pigeonite, ilmenite, magnetite and accessory zircon (Bonnichsen et al. 2008). The area was initially mapped by Wood and Gardener (1984), however recent work has proposed some revisions, suggesting that faulting has repeated the upper part of the stratigraphy that previously included the High Springs and Rattlesnake Springs, Frenchman Springs and Dive Creek units (Starkel *pers. comm*; Bonnichsen et al. 2008). The revised stratigraphy is illustrated in Figure 3.7. Geochronological data is sparse for this succession, the Windy Gap and High Springs rhyolites have K-Ar age determinations of 11.0 ± 0.6 and 10.0 ± 0.3 Ma respectively (Clemens and Wood 1993). No $^{40}\text{Ar}/^{39}\text{Ar}$ geochronology has been published.

East Bennett Mountain

The area north of the Snake River Plain surrounding Davis Mountain contains at least seven welded rhyolitic ignimbrites unusually intercalated with basalt and diatomite (Honjo et al. 1986; Oakley and Link 2006). The units are metaluminous rhyolites typical of the central Snake River Plain, with phenocryst assemblages containing; sanidine, plagioclase, quartz, pigeonite, augite, ilmenite and magnetite in addition to accessory zircon (Oakley and Link 2006; Bonnichsen et al. 2008). The uppermost ignimbrite in the East Bennett succession, the Tuff of the City of Rocks (Fig. 3.8), has relatively low SiO_2 content for a Snake River-type rhyolite c.70 wt.% compared to the more typical 75 wt.% (Bonnichsen et al. 2008). High precision $^{40}\text{Ar}/^{39}\text{Ar}$ ages using sanidine are available for the older rhyolitic units (Oakley and Link 2006; Figure 3.8) and K-Ar ages for some of the younger units (Armstrong et al. 1980). The 11.21-9.15 Ma Miocene ignimbrites (Fig. 3.8) overlie deposits of Eocene Challis volcanism (Honjo et al. 1986; Oakley and Link 2006).

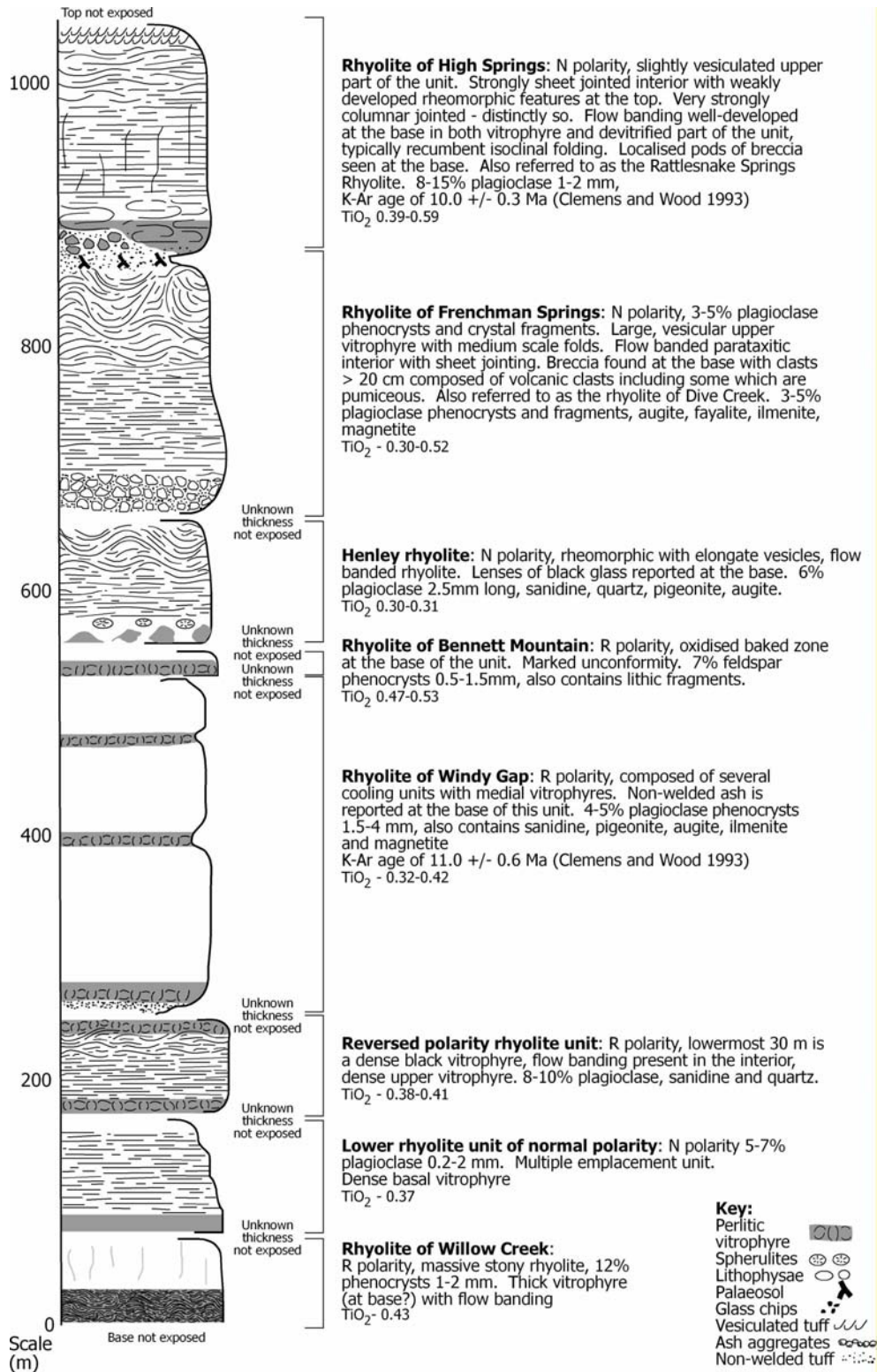


Figure 3.7 Generalised vertical section of the rhyolitic succession in the West Bennett Mountain region adapted from descriptions in Wood and Gardener (1984) and Bonnichsen et al. (2008)

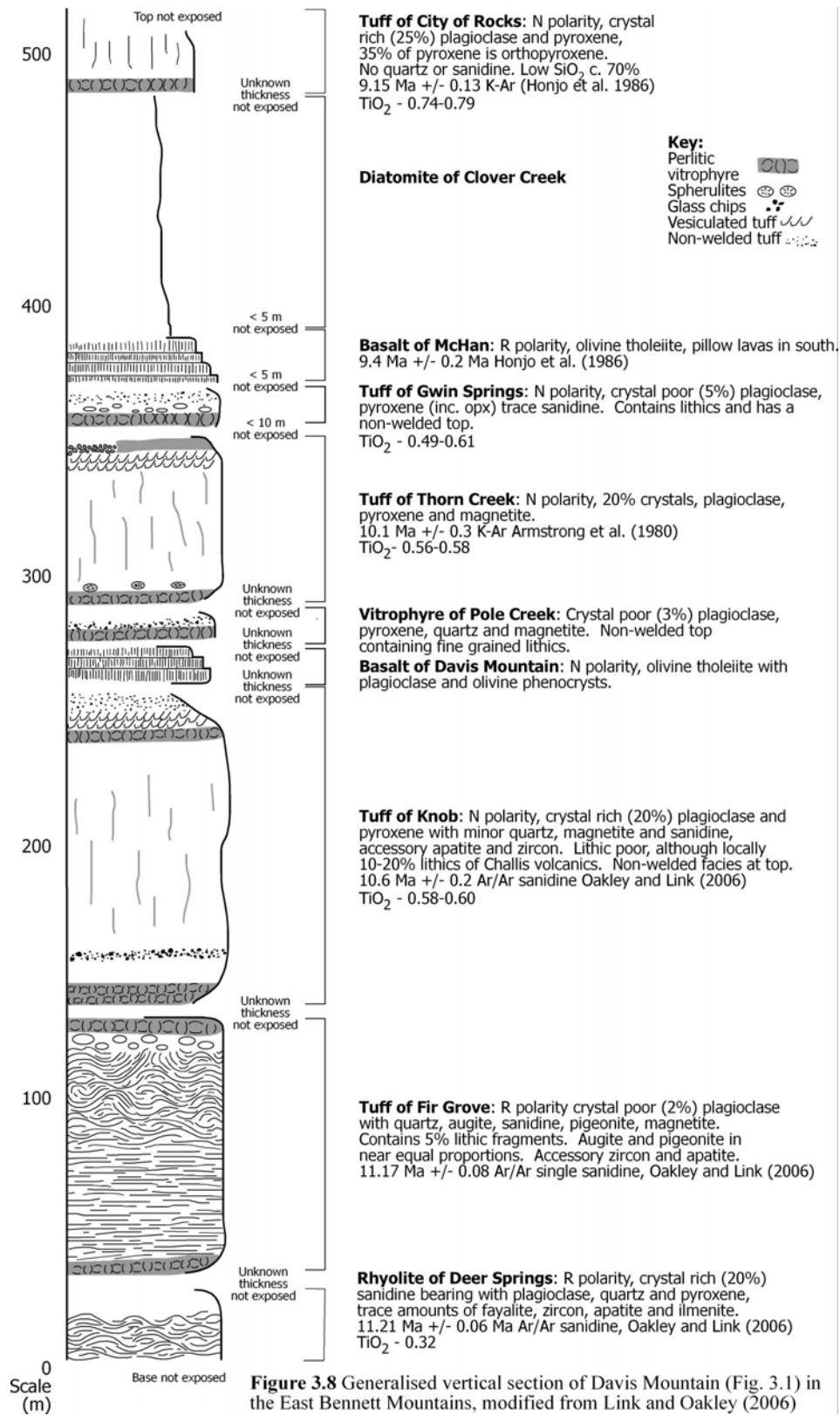


Figure 3.8 Generalised vertical section of Davis Mountain (Fig. 3.1) in the East Bennett Mountains, modified from Link and Oakley (2006)

The King Hill ignimbrite and Tuff of Dempsey Meadow are present between the West and East Bennett Mountain successions, little is known about these ignimbrites, except for whole rock chemical characteristics Bonnicksen et al. (2008). No correlations between these units and those in either the West or East Bennett Mountains have been determined.

Rationale for study

This work proposes and tests correlations along and across the central Snake River Plain. This has not been achieved hitherto because of the similarity of the welded ignimbrites in the region with few field characteristics sufficiently distinctive to establish correlations. The correlations proposed in this work, build on the proposed regional stratigraphy of Bonnicksen et al. (2008), which splits the Snake River Plain into CAT (composition and time) groups based on relative position, whole rock chemistry (particularly TiO₂ contents), magnetic polarity and age. Ignimbrites may exhibit significant changes in appearance over small distances particularly in response to palaeotopography. The Grey's Landing ignimbrite in the Rogerson Graben, for example, thickens from less than five metres thick at the graben margins to greater than sixty metres thick over less than a kilometre at the graben axis (Andrews et al. 2008). The most effective way to correlate ignimbrites is to characterise the associated fallout stratigraphy which changes thickness and grain size in a predictable manner regionally whilst retaining its internal layering and grading stratigraphy. However in the central Snake River Plain, fallout deposits are generally insufficiently well-exposed at the bases of the large ignimbrites so this method has limited applicability. The large scale of the province further complicates attempts at correlation, with massifs on either side of the plain 50 km apart with no exposure of rhyolitic rocks within the plain.

Zoning in ignimbrites

Correlation by geochemistry is complicated by the possibility that some of the ignimbrites may show vertical or sectorial variations in their chemical composition. Given that the emplacement of an ignimbrite can be spatially variable, compositional variation through a

deposit may be vertically through a single section or laterally over a distance. Many ignimbrites are chemically zoned (e.g. Mazama Tuff, Bacon and Druitt 1988; Arico Ignimbrite, Brown et al. 2003; Zaragoza Ignimbrite, Carrasco-Nunez and Branney 2005), including ones that record large volume eruptions (e.g. Bandelier Tuff, Smith and Bailey 1966; Bishop Tuff Hildreth 1979, Hildreth and Wilson 2007; and the Valley of Ten Thousand Smokes Ignimbrite, Hildreth 1983, Fierstein and Wilson 2005).

Whereas medium-volume ignimbrites (e.g. Mazama and Zaragoza ignimbrites) are strongly zoned (e.g. from rhyolite to andesite), large volume ignimbrites tend to be more subtly zoned. The ignimbrites of the central Snake River Plain are more strikingly heterogeneous in mineral chemistry than they are zoned. Vertical zoning occurs in some Snake River Plain ignimbrites as recorded by a subtle change in the proportions of compositional modes of clinopyroxenes (Cathey and Nash 2004). Crucially, the zoning exhibited takes the form of changes in the proportion of pigeonite and augite compositional modes rather than the compositions of these modes. In rare cases the phenocryst compositions may vary (e.g. Wooden Shoe Butte Member, Chapter 2), however the Wooden Shoe Butte Member is composed of two discrete members which each have separate but internally consistent homogeneous clinopyroxene populations.

Analytical techniques

To test correlations proposed on the basis of fieldwork, rocks were analysed for whole rock chemistry by X-ray fluorescence (technique as described previously). Glass and crystal chemistry were determined using electron microprobe (electron microprobe technique as described previously; Chapter 2). FeO, SiO₂, TiO₂, CaO and MgO are considered to be the most reliable oxides as determined from glass analyses due to the potential problems in analysing Na₂O (see Chapter 2). A subset of samples in this study underwent age determinations at the Scottish Universities Environmental Research Centre (SUERC) in East Kilbride using ⁴⁰Ar/³⁹Ar geochronology. Correlations were further tested by determining the oxygen isotopic characteristics of the units within a correlation with analysis at the University of Oregon.

Argon dating methodology

Preparation

Samples for $^{40}\text{Ar}/^{39}\text{Ar}$ dating were collected during fieldwork in 2006 and 2007. Samples were prepared at the University of Leicester where they were split, and then crushed using a fly-press, before being wet-sieved to obtain a size fraction appropriate to the feldspar grain size of the sample, typically 355-500 μm and 500-710 μm . Sanidine separates were then hand-picked under a binocular microscope to pick crystals that had no adhering glass, melt inclusions or visible alteration. The selected crystals were cleaned in acetone (to remove any hydrocarbons from the surface) in an ultrasonic bath for twenty minutes, rinsed in deionised water and placed in deionised water in an ultrasonic bath for a further twenty minutes. This process was repeated using 2% nitric acid to remove any adhering glass or altered material from crystal surfaces or fractures.

Each sample was packed in a 6 mm Cu-foil packet by SUERC staff, stacked and interspersed with packages containing a mineral standard. All packets were held in place in a 6 mm ID quartz tube. The quartz tube with samples and monitors was placed into a 25 mm OD Al irradiation tube. The monitor mineral standard was Taylor Creek Rhyolite sanidine (TCR2a) with a $^{40}\text{Ar}/^{39}\text{Ar}$ age of 28.34 Ma (Renne et al. 1998). Samples and monitors were irradiated for 1 hr in a Cd-lined facility (RODEO) at the Petten HFR, Netherlands on the 12th February 2007.

Analysis

After irradiation and cooling, laser $^{40}\text{Ar}/^{39}\text{Ar}$ single fusion experiments were carried out by Dan Barfod in the NERC Argon Isotope Laboratory, East Kilbride, Scotland. Samples were loaded onto a 52 mm diameter Cu-sample tray that contained circular machined depressions (2 mm deep, 2 mm diameter), and placed in a UHV laser cell. The laser cell is fitted with a zinc-selenide, doubly-pumped UHV-window for transmission of IR laser light.

A 25W CO₂ laser was used to heat samples in two steps at ca. 3% and 15% power. At these settings 15% laser power setting was sufficient to fuse the samples, typically extracting >95% of the remaining argon. Argon evolved from samples was stripped of active gases using SAES getters running hot (ca. 250°) and at room temperature. System blanks were measured every 2-4 grains and found to have been stable through the course of analysis. The laser firing, gas handling and mass spectrometer were controlled by in-house and GVI software. Data were collected on a multi-collector mass spectrometer (GVI instruments Argus) using a variable sensitivity faraday collector array in static (non-peak hopping) mode.

Comparison of ⁴⁰Ar/³⁹Ar ages

To correlate between the adjacent massifs along the margins of the central Snake River Plain it is necessary to incorporate data from a number of sources, in terms of ⁴⁰Ar/³⁹Ar geochronology, most of the data available is from Bonnicksen et al. (2008) and Perkins et al. (1998). Both of these studies use the Fish Canyon Tuff as a standard and use an age of 27.84 Ma for the Fish Canyon Tuff (McIntosh *pers. comm.*). To be able to compare results, these ages were increased by a factor of 1.00646 (28.02/27.84) to compensate for the use of the older standard (28.02 Ma, Renne et al. 1998) in the more recent work. All the ages in this chapter are recalculated and quoted to the original reference.

Oxygen isotopes

Methodology

Oxygen isotope analyses were performed at the University of Oregon stable isotope laboratory, using CO₂-laser fluorination and a 35 W laser. Samples ranging in weight from 0.6 to 2 mg were reacted in the presence of purified BrF₅ reagent to liberate oxygen. The gases generated were purified through cryogenic traps and a small mercury diffusion pump to remove traces of fluorine gas. Oxygen was converted to CO₂ gas by a small platinum-graphite converter, the yield was measured, and then CO₂ gas was analyzed on a MAT 253

mass spectrometer. Four to seven standards were analyzed together with the unknowns during each analytical session with the San Carlos olivine ($\delta^{18}\text{O} = 5.35\text{‰}$) and Gore Mountain garnet ($\delta^{18}\text{O} = 5.75\text{‰}$) used as standards. Day-to-day $\delta^{18}\text{O}$ variability on standards ranged from +0.1‰ to -0.3‰, and these values were added or subtracted to the unknowns to correct for day-to-day variability. Values are reported on a standard mean ocean water scale.

Rhyolites from the central Snake River Plain have been found to contain a significant depletion in $\delta^{18}\text{O}$ with feldspar values ranging from -1.4 to 3.8‰ (Boroughs et al. 2005). This range of $\delta^{18}\text{O}$ is significantly depleted compared to the typical values 7-10‰ reported for rhyolites (Taylor 1968). The range in $\delta^{18}\text{O}$ observed in the CSRP (5.2‰) allied to the precision on the measurements (0.1‰) allows oxygen isotopes to be used as a correlative tool in addition to the methods previously described.

Results

$^{40}\text{Ar}/^{39}\text{Ar}$

Results of the $^{40}\text{Ar}/^{39}\text{Ar}$ experiments are shown in Table 3.1. Individual single crystal ages derived from a sample gave results with a wide scatter. The scatter is likely to reflect geological causes; for example the lack of fallout deposits meant that it was necessary to sample ignimbrites which may have entrained xenocrystic material or accidental material into the pyroclastic density currents, or contain slightly altered feldspars. To determine the validity of the individual ages, linear probability plots (Fig. 3.9) were used to assess ages to include in the calculation of the final age. Given that all the ignimbrites in this study are of known magnetic polarity (Bonnichsen et al. 2008), the geomagnetic polarity time scale may be used to investigate the possibility of older xenocrystic material being incorporated into the ignimbrite. The geomagnetic polarity timescale is based on the correlation of the sequence of magnetic deposits from the ocean-floor with deposits on land which have been dated (e.g. Cande and Kent 1995). This timescale is then calibrated against astronomical

	Unit	Age (Ma)	Error (2σ)	MWSD	Number
Cassia Mountains	Steer Basin Member	10.48	0.09	0.65	8
	Big Bluff Member	10.91	0.07	1.02	14
Rogerson Graben	Jackpot 7	10.4	0.09	2	7
	Jackpot 5	10.95	0.16	0.31	3
Browns Bench	Browns Bench 8	10.56	0.09	0.69	7
	Browns Bench 5	11.34	0.08	0.83	9
	Browns Bench 3	11.98	0.64	6.1	4
Grasmere Escarpment	Buckhorn Ignimbrite	11.50	0.18	0.48	6
	Upper Grasmere Escarpment Ignimbrite	11.68	0.59	8	6
West Bennett Mountain	Frenchman Springs	10.96	0.09	0.49	11
	Windy Gap	10.98	0.08	0.86	11

Table 3.1 Summary of $^{40}\text{Ar}/^{39}\text{Ar}$ age data, full dataset and locations of samples are provided in Chapter 3 appendix.

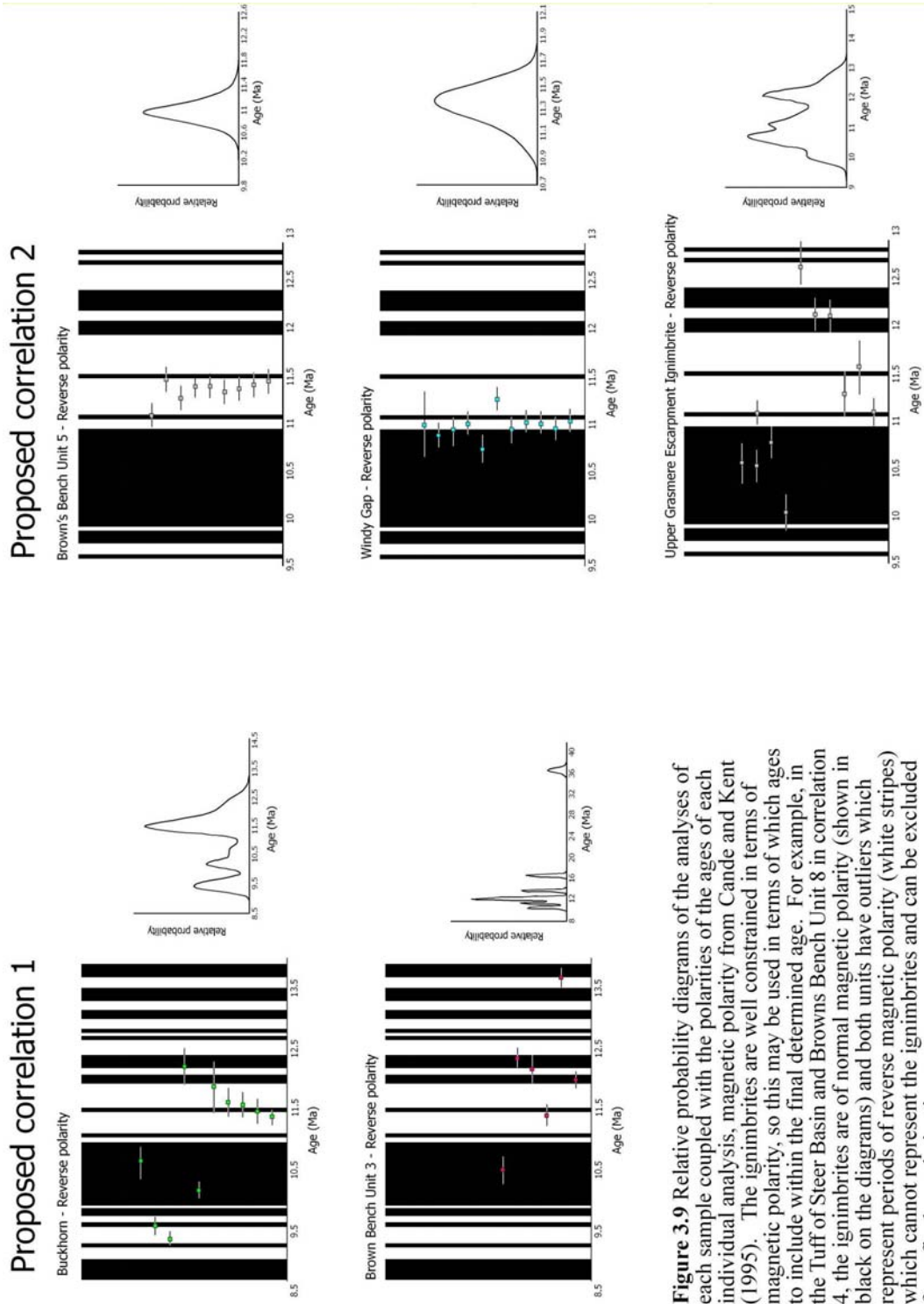
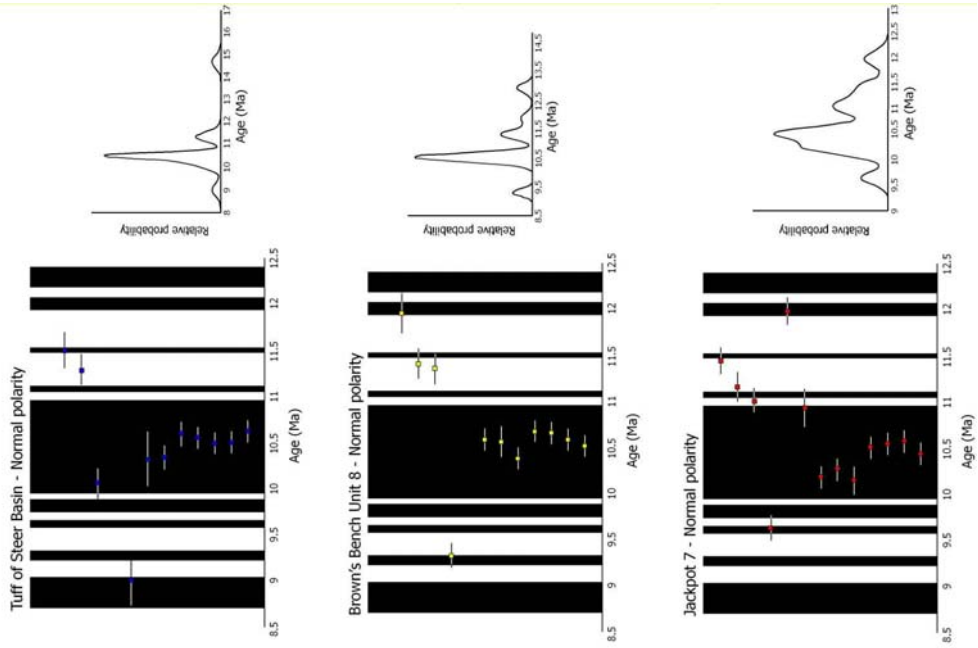
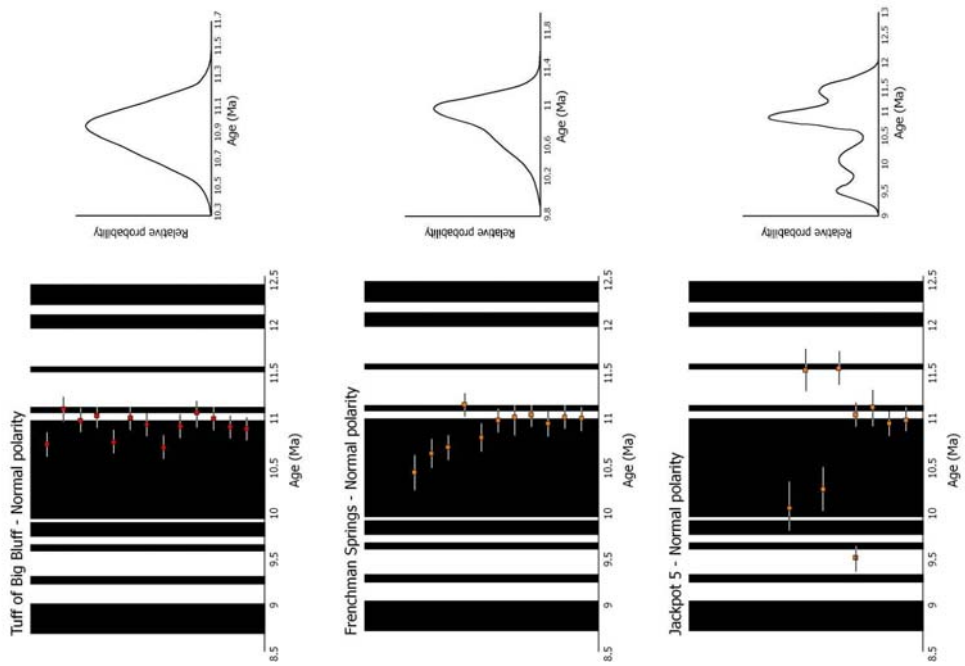


Figure 3.9 Relative probability diagrams of the analyses of each sample coupled with the polarities of the ages of each individual analysis, magnetic polarity from Cande and Kent (1995). The ignimbrites are well constrained in terms of magnetic polarity, so this may be used in terms of which ages to include within the final determined age. For example, in the Tuff of Steer Basin and Browns Bench Unit 8 in correlation 4, the ignimbrites are of normal magnetic polarity (shown in black on the diagrams) and both units have outliers which represent periods of reverse magnetic polarity (white stripes) which cannot represent the ignimbrites and can be excluded from final age derivations.

Proposed correlation 4



Proposed correlation 3



timings (e.g. Baksi 1993). Thus, using this timescale, any ages of crystals that represent a polarity opposing the known polarity of the ignimbrite may be discounted from the final age derivation (e.g. Fig. 3.9). The samples were split into a series of proposed correlations, which will be considered individually, starting with the oldest.

Proposed correlation 1: Buckhorn Ignimbrite, Cougar Point Tuff 7 and Browns Bench 3

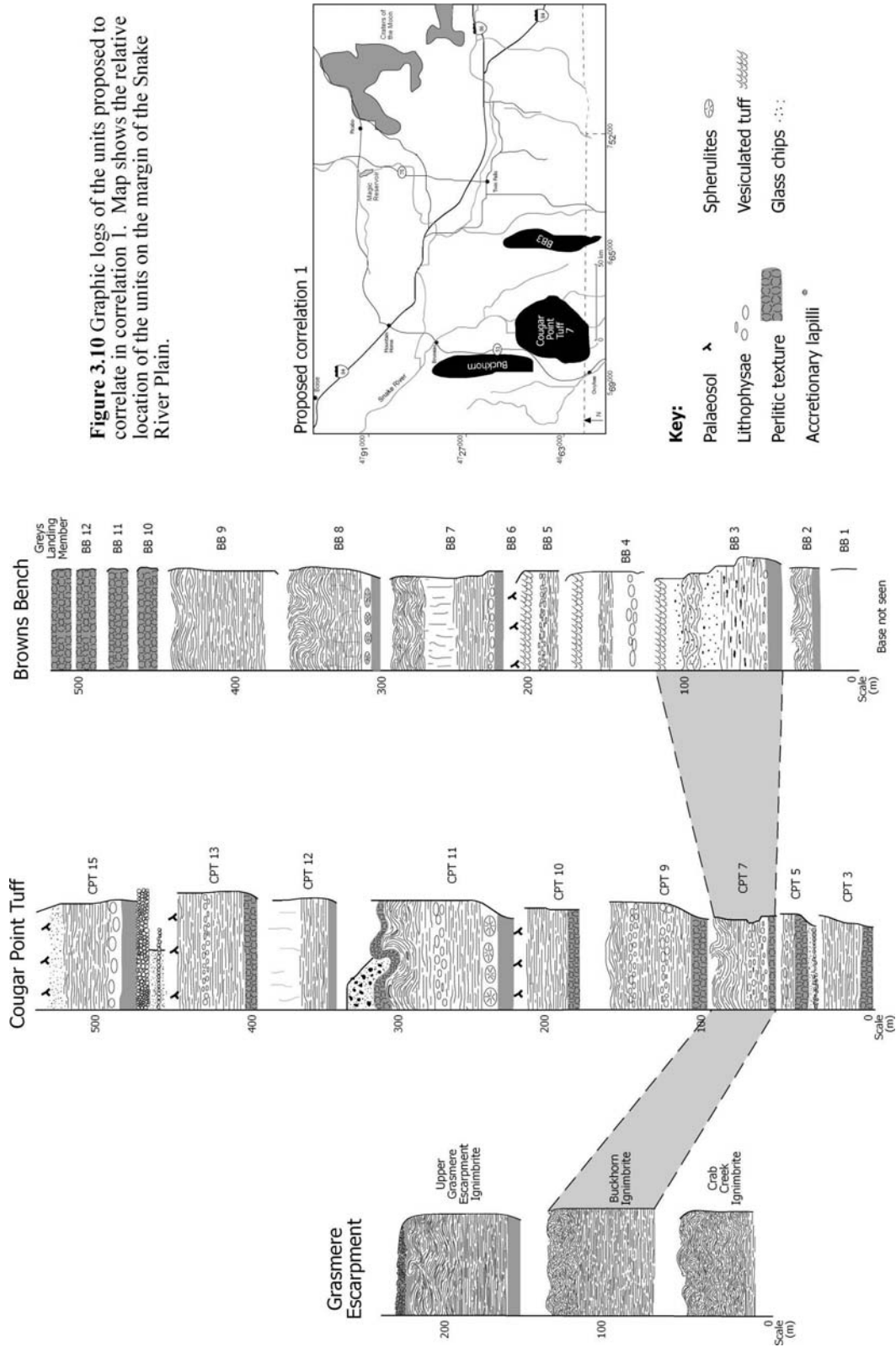
The three ignimbrites of proposed correlation 1 (Fig. 3.10) are within CAT group 3, which is characterised by units with whole rock TiO₂ contents of 0.38-0.59 wt. % and reverse magnetic polarity (Bonnichsen et al. 2008). CAT group 3 lies within ‘Stage A’, which is thought to represent the first major period of eruptive activity during the evolution of the central Snake River Plain (Bonnichsen et al. 2008).

Physical description

The Buckhorn Ignimbrite (Fig. 3.11) is a lava-like rhyolitic ignimbrite composed of a slightly rheomorphic, welded and devitrified centre and an upper vesiculated zone that is poorly exposed along the Grasmere Escarpment (Fig. 3.1). The base of the Buckhorn ignimbrite is not exposed.

Cougar Point Tuff 7 is a rheomorphic rhyolitic ignimbrite (Fig. 3.11 E) composed of multiple zones of different weathering characteristics (Bonnichsen and Citron 1982). The upper reaches of Cougar Point Tuff 7 are sheet jointed and pass upwards into a highly rheomorphic zone. It contains quartz, sanidine, plagioclase, augite, pigeonite, ilmenite and magnetite.

Browns Bench 3 (Fig. 3.11 A) is an intensely welded ignimbrite, with lithophysal horizons that indicate more than one cooling unit (e.g. Smith 1960) reflected in the step-like character of the unit. The lowermost zone of the ignimbrite contain abundant fiammé of



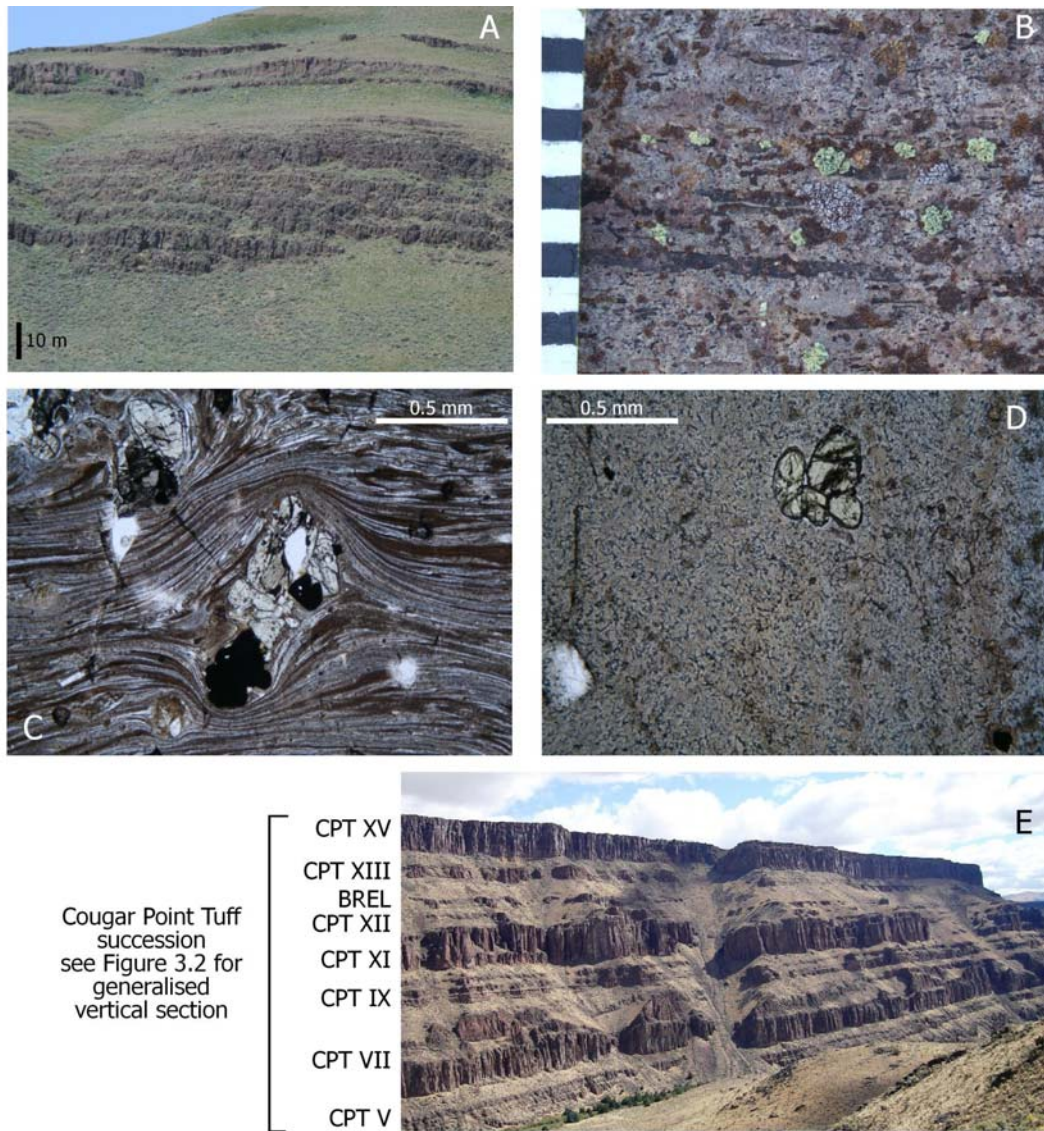


Figure 3.11 **A.** Outcrop of Browns Bench 3 on the Browns Bench escarpment near Corral Creek, showing the multiple step-like cliffs of Browns Bench 3, reflecting the differences in erosional characteristics of the layers. Fiamme present in the base of Browns Bench 3, fiamme are unusual in Snake River-type rhyolites.
B. Fiamme present in the lower half of Browns Bench 3, showing the irregular outlines of the fiamme (black) in the welded matrix.
C. Flow banding and folding from the base of Browns Bench 3 illustrating the rheomorphic nature of the unit.
D. Lava-like groundmass of the Buckhorn unit, showing no evidence of pyroclastic texture.
E. Cougar Point Tuff succession showing the majority of the units in the succession from Black Rock, CPT abbreviations relate to units of the Cougar Point Tuff succession (e.g. Bonnicksen and Citron 1982; Cathey and Nash 2004) and BREL is the Black Rock Escarpment Lava (see Chapter 5).

black glass (Fig. 3.11 B) which have a lower crystal content than the surrounding ignimbrite and have classical flame shapes with ragged edges. Fiammé are rare in Snake River-type ignimbrites due to the lack of pumice lapilli (Branney et al. 2008). Above the eutaxitic zone is a zone of ignimbrite rich in chips of angular to sub-angular non-vesicular glass < 3 cm in size. This passes up into a slightly rheomorphic zone and the upper part of the ignimbrite is vesiculated with prolate vesicles.

Glass and phenocryst characteristics

Microprobe analysis of glass in these ignimbrites shows that they cannot be distinguished on the basis of major element compositions of their glass (Fig. 3.12 A). FeO contents ranging from 0.5-2.5 wt.% and CaO contents between 0.2 and 2 wt.% for all the units.

With respect to phenocryst populations, Browns Bench 3 contains a single mode of pigeonite, the Buckhorn Ignimbrite contains two modes of pigeonite and Cougar Point Tuff 7 contains three. The two pigeonite modes of the Buckhorn Ignimbrite (average FeO 29.9 and 31.5 wt.%) do not overlap with the pigeonite composition of Browns Bench 3 which has an average FeO content of 32.8 wt.% (Fig. 3.13) with typical errors at 2σ for this abundance of FeO being c. 0.4 wt.%. Augite is much less common and the compositions again do not overlap. Both the Buckhorn Ignimbrite and Browns Bench 3 contain plagioclase with overlapping compositional ranges (An_{41} to An_{58} ; Fig. 3.13).

$^{40}\text{Ar}/^{39}\text{Ar}$ ages

Cougar Point Tuff 7 has been dated as 11.89 ± 0.03 Ma by $^{40}\text{Ar}/^{39}\text{Ar}$ (Bonnichsen et al. 2008). Ages of individual crystals from Browns Bench 3 show significant scatter with the range of ages spanning three million years (Fig. 3.9; Table 3.1). This range of ages of individual sanidines means that the age as determined here has a very large error, 12.3 ± 1 Ma. The MWSD of the Browns Bench 3 age is 6, suggesting that the $^{40}\text{Ar}/^{39}\text{Ar}$ age is

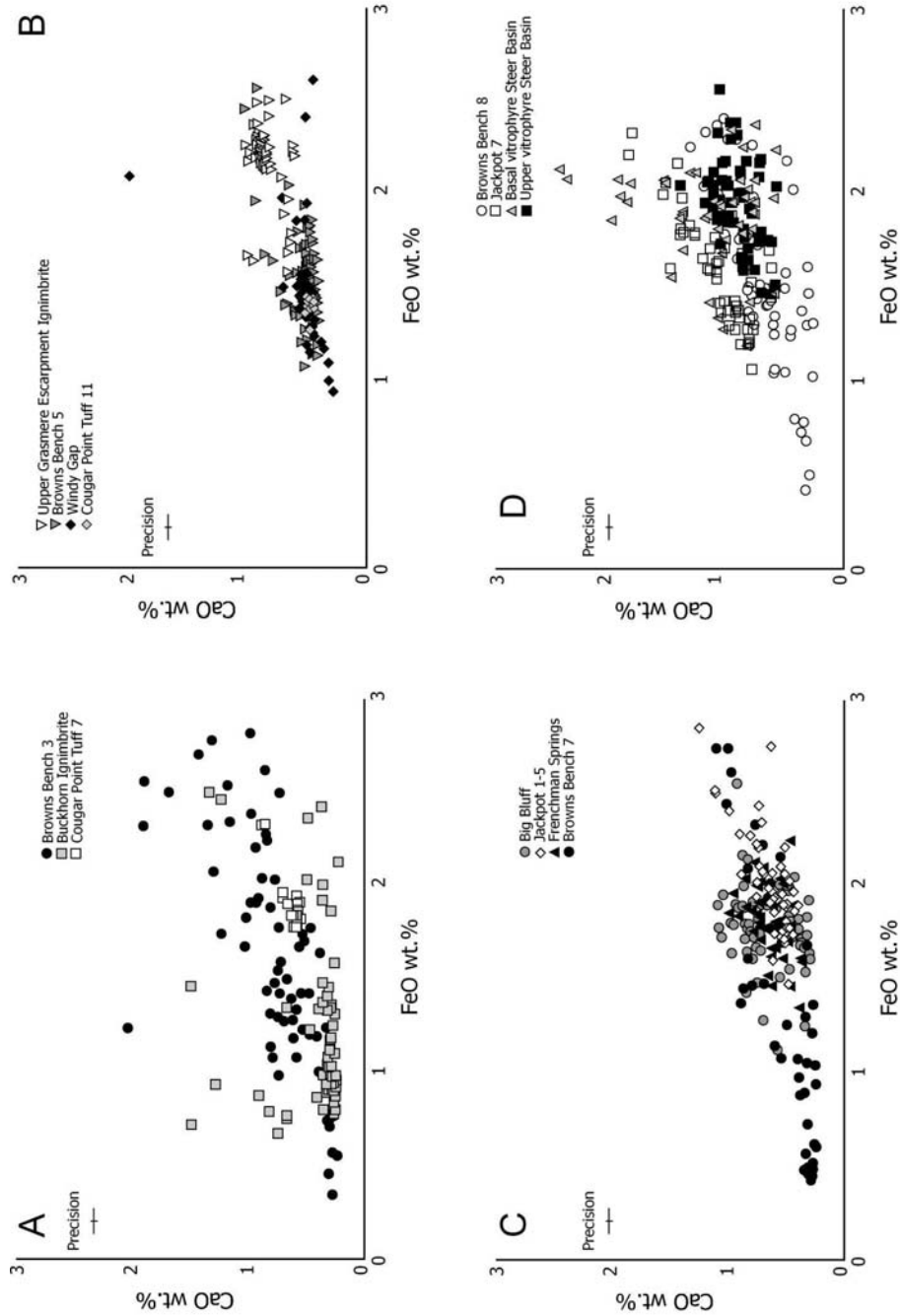


Figure 3.12 Major element chemistry of the glasses from the correlations proposed, **A**, Proposed correlation 1, **B**, Proposed correlation 2, **C**, Proposed correlation 3, **D**, Proposed correlation 4. As can be seen the glass chemistries in correlation 2 suggest that the Upper Grasmere Escarpment Ignimbrite does not correlate with any other unit in that correlation, while C and D illustrate that the correlations proposed cannot be disproved on the basis of glass chemistry

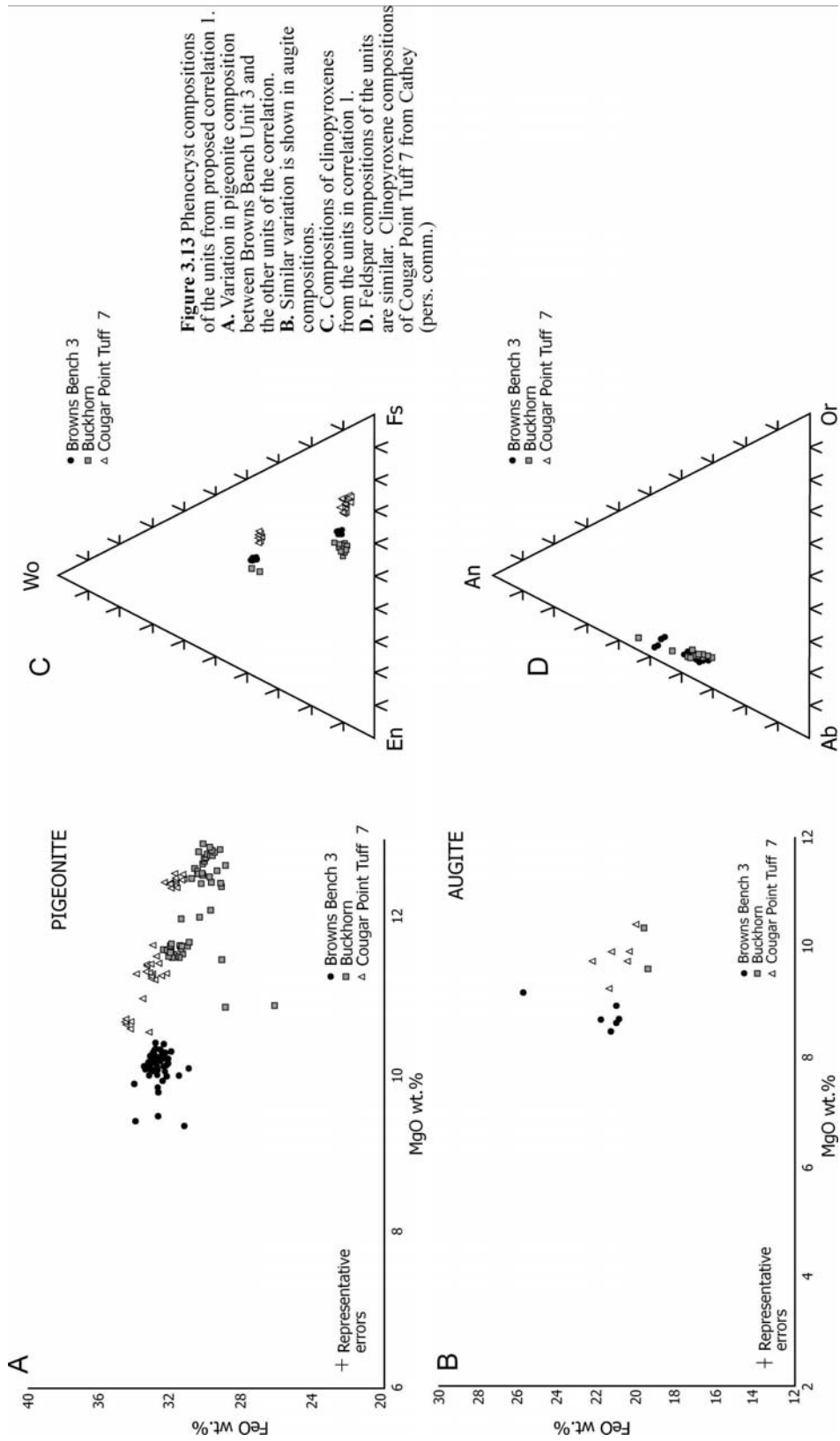


Figure 3.13 Phenocryst compositions of the units from proposed correlation 1. **A.** Variation in pigeonite composition between Browns Bench Unit 3 and the other units of the correlation. **B.** Similar variation is shown in augite compositions. **C.** Compositions of clinopyroxenes from the units in correlation 1. **D.** Feldspar compositions of the units are similar. Clinopyroxene compositions of Cougar Point Tuff 7 from Cathey (pers. comm.)

unreliable. The Buckhorn Ignimbrite has a $^{40}\text{Ar}/^{39}\text{Ar}$ age of 11.56 ± 0.17 Ma, which does not correlate with the older Cougar Point Tuff 7.

Oxygen isotopes

The Buckhorn Ignimbrite has an average $\delta^{18}\text{O}$ of 2.06 ‰, and Browns Bench 3 has an average $\delta^{18}\text{O}$ of 0.64 ‰. Boroughs et al. (2005) analysed feldspars from Cougar Point Tuff 7 and determined a $\delta^{18}\text{O}$ of 0.20 ‰ (Fig 3.14).

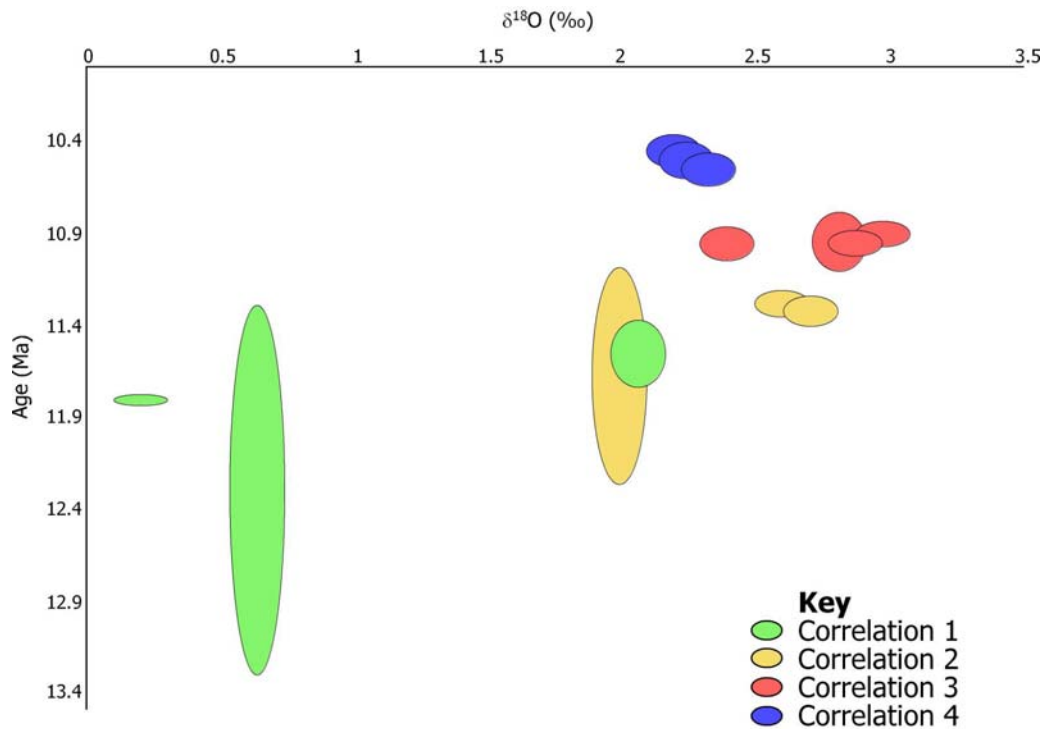


Fig. 3.14 Diagram showing the ages and oxygen isotopic characteristics of the units in all correlations. The unit in correlation 3 which does not overlap with the others is the Frenchman Springs rhyolite.

Interpretation

A difference in clinopyroxene compositions suggests that Browns Bench 3 does not correlate with either the Buckhorn Ignimbrite or Cougar Point Tuff 11. The clinopyroxene compositions of Cougar Point Tuff 11 differ slightly from those in the Buckhorn Ignimbrite and the units have $^{40}\text{Ar}/^{39}\text{Ar}$ ages which do not overlap within error. However, the age of the Buckhorn Ignimbrite is poorly constrained and the clinopyroxene compositions are not strikingly different. The oxygen isotopic characteristics of the units are different outside of the error of measurement, suggesting that these three ignimbrites represent three different units.

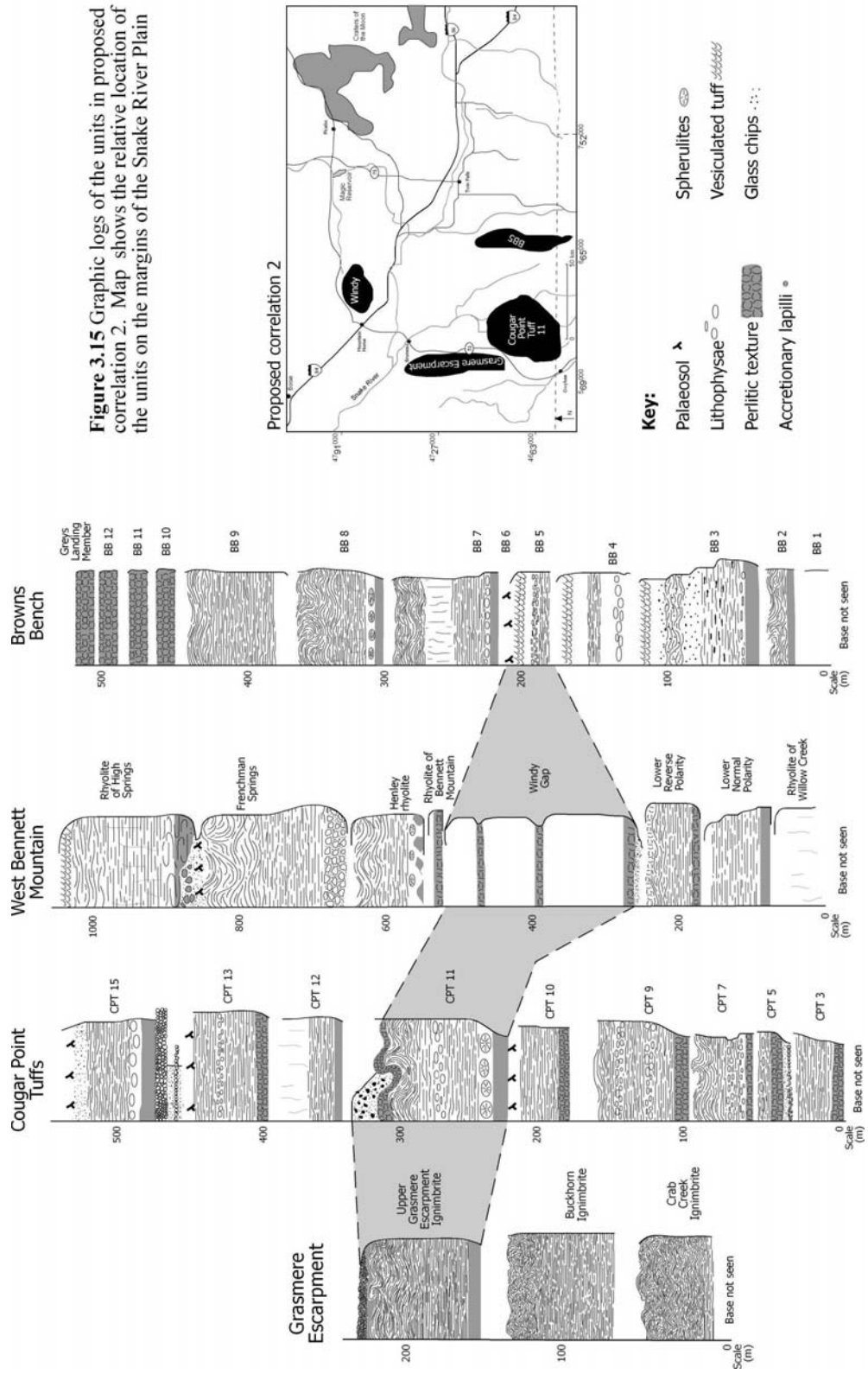
Proposed correlation 2: Browns Bench 5, Upper Grasmere Escarpment Ignimbrite, Windy Gap and Cougar Point Tuff 11

CAT group 5 of Bonnicksen et al. (2008) contains all the units in proposed correlation 2 (Fig. 3.15). They have similar whole rock chemistry, TiO_2 contents (between 0.26 and 0.43 wt%) and reverse magnetic polarity. CAT group 5 is estimated to contribute around 25% of the erupted volume of the central Snake River Plain (Bonnicksen et al. 2008).

Physical description

Browns Bench 5, is an intensely welded (Fig. 3.16 F), locally lava-like ignimbrite well exposed in the Corral Creek section of Browns Bench (Fig. 3.1). The uppermost part of the ignimbrite is vesiculated tuff overlain by a well-developed palaeosol (Fig. 3.4). It has a low phenocryst content $\leq 5\%$ and contains sanidine, plagioclase, quartz, augite, pigeonite, ilmenite and magnetite.

The Upper Grasmere Escarpment Ignimbrite extends for at least 25 km along the Grasmere Escarpment to the north of the Bruneau-Jarbidge eruptive centre, where it has localised good exposure (Fig. 3.16 D). It is rheomorphic with a stony, devitrified centre, and



medium-scale folds in the upper third of the ignimbrite. The uppermost part is a highly vesiculated (pumiceous) zone, golden brown in colour.

The Windy Gap Ignimbrite is c. 300 m thick, (Wood and Gardener 1987; Fig. 3.7), in the Bennett Mountains to the north of the Snake River Plain (Fig. 3.1). It is composed of a succession of lithoidal rhyolite layers and the presence of medial vitrophyres suggests that it is a compound cooling unit. Non-welded ash is reported at the base of the unit (Wood and Gardener 1987) but it is unclear whether this is an ashfall deposit or a non-welded lower part of the ignimbrite. The Windy Gap Ignimbrite is characterised by coarse plagioclases, 3-4 mm in diameter (Bonnichsen et al. 2008).

Cougar Point Tuff 11 (Bonnichsen and Citron 1982) is a voluminous, intensely welded rhyolitic ignimbrite which typically develops erosional pillars (Fig. 3.16 A). It is widely the thickest of the Cougar Point Tuffs ranging from c. 40 m thick in Bruneau canyon to up to 100 m thick in Jarbidge canyon (Bonnichsen and Citron 1982). Its uppermost part is highly rheomorphic and contains fiammé (Fig. 3.16 C) which follow the rheomorphic folds. Its phenocryst assemblage includes quartz, sanidine, plagioclase, augite, pigeonite, fayalite, ilmenite and magnetite (Bonnichsen and Citron 1982; Cathey and Nash 2004).

Glass and phenocryst characteristics

Windy Gap and Browns Bench 5 have average glass FeO contents of 1.48 and 1.55 wt.% respectively whereas the Upper Grasmere Escarpment Ignimbrite has an average FeO content of 2.14 wt.%, and given that the error on FeO analysis in glass at 2σ is 0.08 wt.% (e.g. Fig 3.12) it appears unlikely these units correlate (Fig. 3.12 B). Cougar Point Tuff 11 has identical glass compositions to Windy Gap Ignimbrite and Browns Bench 5.

Pyroxene phenocrysts are relatively rare in all the ignimbrites considered in this proposed correlation. Upper Grasmere Escarpment Ignimbrite has a single population of augite with

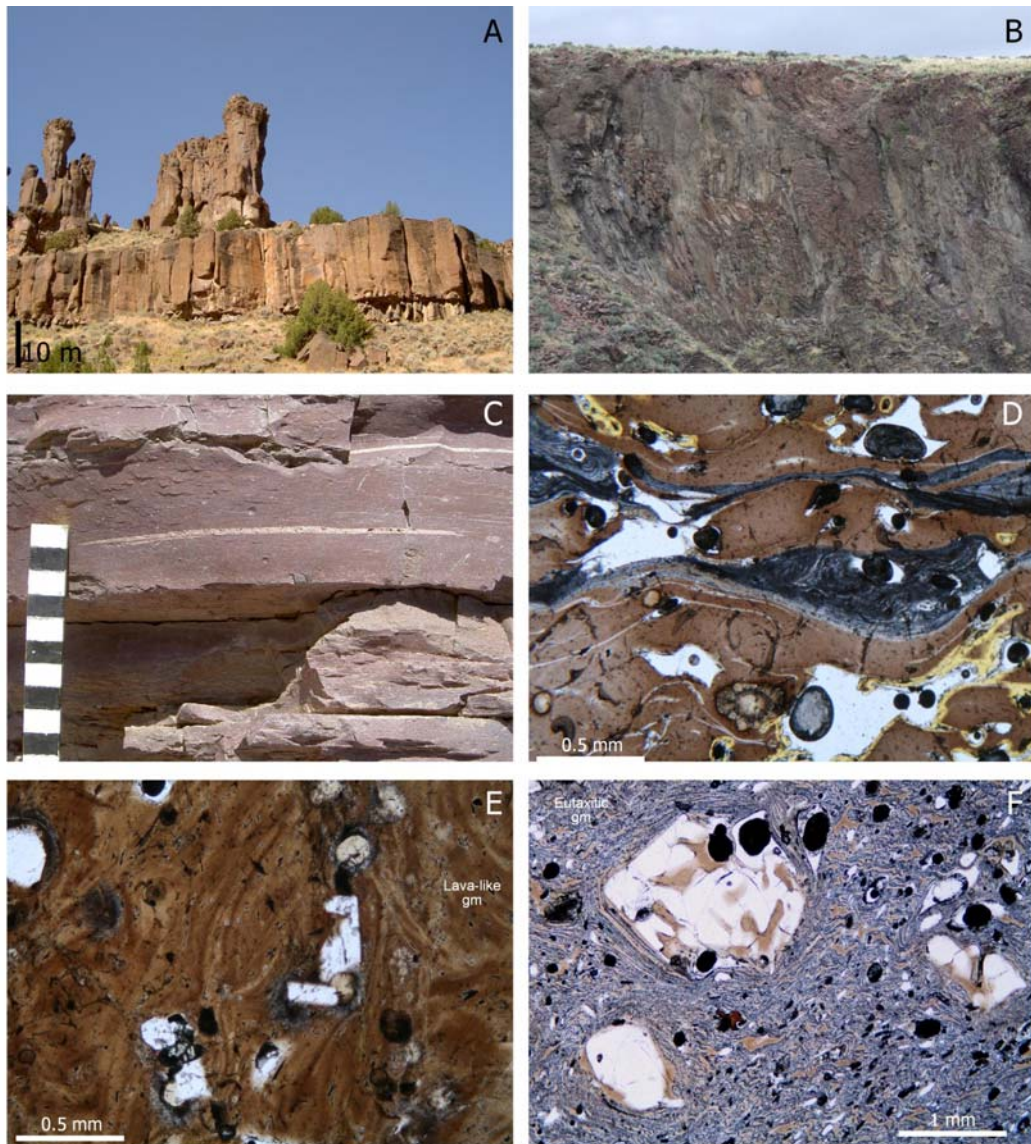


Fig. 3.16 **A.** Characteristic erosional pillars in Cougar Point Tuff 11, Jarbidge canyon. **B.** Upper Grasmere Escarpment Ignimbrite showing large scale folds in the upper part of the ignimbrite. **C.** Fiamme representing vesiculated tuff in the upper reaches of Cougar Point Tuff 11. **D.** Photomicrograph of vesiculated, intensely welded Upper Grasmere Escarpment Ignimbrite. **E.** Photomicrograph of the Windy Gap unit showing a lava-like, flow banded groundmass. **F.** Photomicrograph of Browns Bench Unit 5 showing the eutaxitic fabric composed of deformed glass shards which are wrapping an embayed quartz phenocryst.

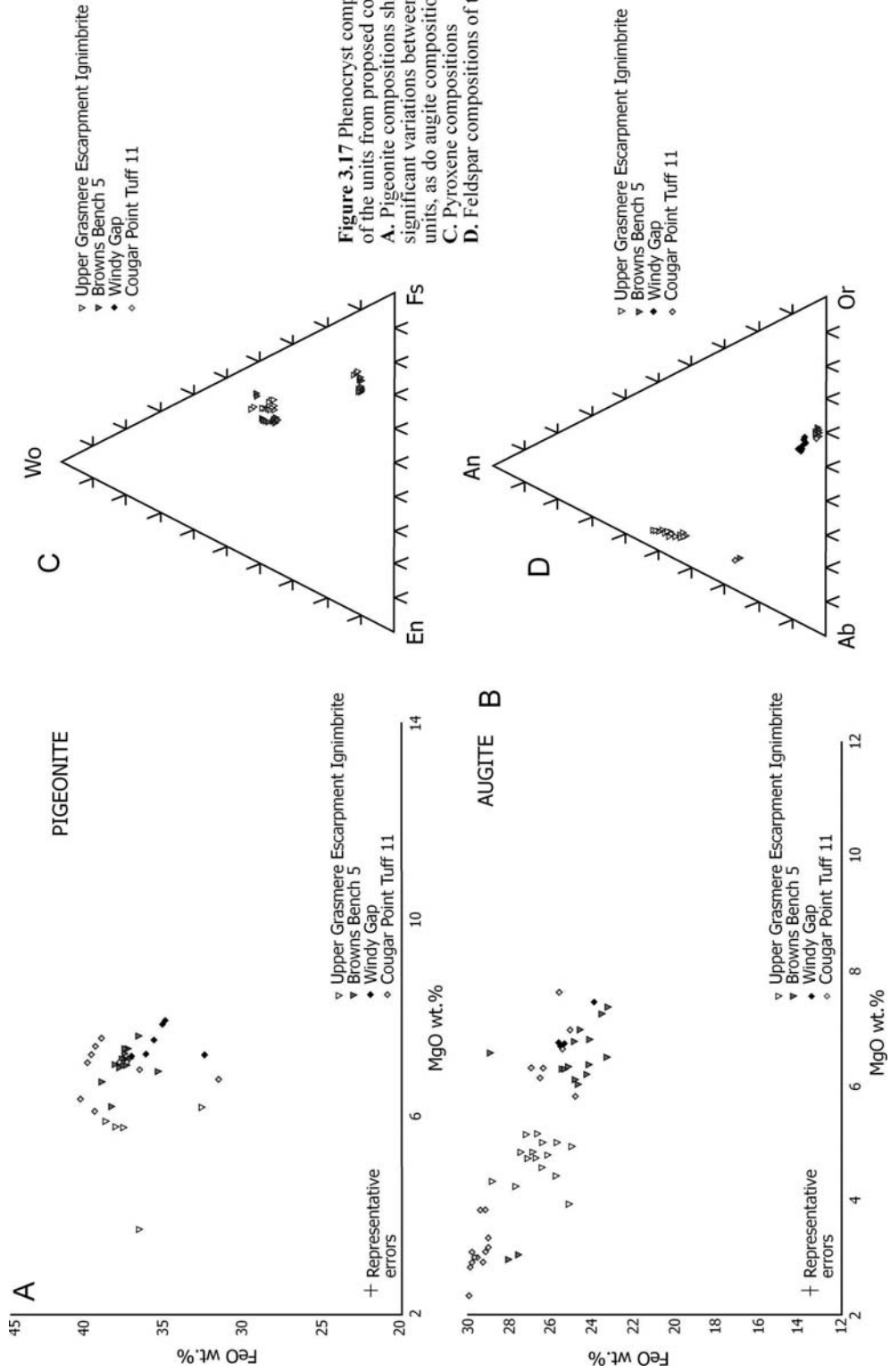


Figure 3.17 Phenocryst compositions of the units from proposed correlation 2. A. Pigeonite compositions show significant variations between ignimbrite units, as do augite compositions in B. C. Pyroxene compositions in B. D. Feldspar compositions of the units

an average MgO content of 4.77 wt.%, whereas Browns Bench 5 has two compositional modes with average MgO contents of 6.56 and 3.00 wt.%, similar to the values of the two modes in Cougar Point Tuff 11 (Fig. 3.17). The compositions of pigeonite and augite in the Windy Gap Ignimbrite appear to be similar (although there are insufficient data exist to test whether two compositional modes of augite are present). Plagioclase to sanidine proportions and plagioclase compositions suggest that the Upper Grasmere Escarpment Ignimbrite unit is distinct again, with more calcic plagioclase than the other units (Fig. 3.17 D).

⁴⁰Ar/³⁹Ar ages

Browns Bench 5 has a ⁴⁰Ar/³⁹Ar age of 11.34 ± 0.08 Ma while the Windy Gap Ignimbrite has a ⁴⁰Ar/³⁹Ar age of 10.98 ± 0.08 Ma. Cougar Point Tuff 11, which is a prospective correlative of these units has a ⁴⁰Ar/³⁹Ar age of $11.29 \text{ Ma} \pm 0.07$ (Bonnichsen et al. 2008). Ages derived from crystals taken from the Upper Grasmere Escarpment Ignimbrite show a large scatter, (Fig. 3.9; Table 3.1) resulting in an age of 10.68 ± 0.59 . The MWSD of the age of UGEL is 8, which suggests that the age is not reliable.

Oxygen isotopes

Browns Bench 5 has $\delta^{18}\text{O}$ of 2.72 ‰ which overlaps with the 2.60 ‰ of the Cougar Point Tuff 11 as reported by Boroughs et al. (2005) within the estimated error of the measurements (0.1 ‰). The Upper Grasmere Escarpment Ignimbrite has $\delta^{18}\text{O}$ of 1.99 ‰ distinctly lower than the values for Browns Bench 5 and Cougar Point Tuff 11 (Fig 3.14).

Interpretation

The Upper Grasmere Escarpment Ignimbrite is distinct from the other ignimbrites in terms of both glass and clinopyroxene compositions. These data do not favour a correlation despite the very poor precision of the ⁴⁰Ar/³⁹Ar age. The age of the Windy Gap unit does not overlap with the age of Browns Bench 5 or Cougar Point Tuff 11 suggesting that the

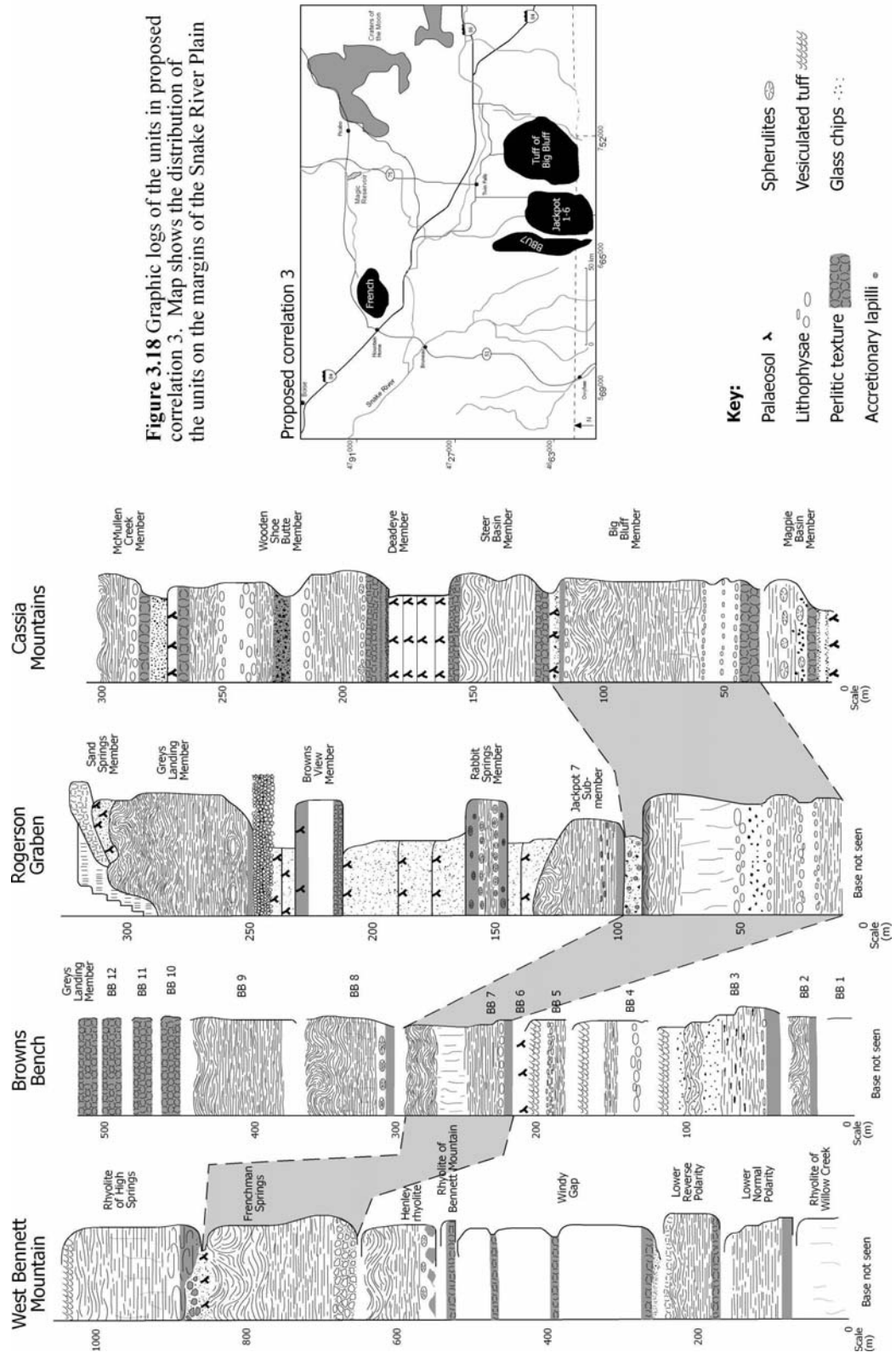
Windy Gap is a different eruptive unit. The phenocryst and glass compositions of Cougar Point Tuff 11 and Browns Bench 5 are identical and their ages overlap within error. The oxygen isotopic characteristics of Browns Bench 5 overlap with those of Cougar Point Tuff 11, and are distinct from the $\delta^{18}\text{O}$ characteristics of UGEL. Given the similarities of Browns Bench 5 and Cougar Point Tuff 11 in terms of glass, clinopyroxene compositions age and oxygen isotopic character, these units are considered to correlate.

Proposed correlation 3: Big Bluff Member, Jackpot 1-6, Browns Bench 7 and Frenchman Springs Rhyolite

A possible correlation between the Big Bluff Member, Jackpot 1-6, Browns Bench 7 and the Frenchman Springs Rhyolite is proposed because all these units are within the same CAT group, with normal magnetic polarity and have whole rock TiO_2 abundances between 0.22 and 0.38 wt.% (Bonnichsen et al. 2008). The Big Bluff Member and Jackpot 1-6 Member of Andrews et al. (2008) are thick units which are low in their respective successions on the south side of the central Snake River Plain.

Physical description

The Big Bluff Member in the Cassia Mountains (Chapter 2) is a thick, intensely welded, rhyolitic ignimbrite. Overlying the basal ashfall deposits (Fig. 3.21), the ignimbrite is composed of a succession of massive layers with different weathering characteristics, separated by lithophysal horizons (Fig. 3.18). Near the base of the ignimbrite, abundant non-vesicular clasts of black angular glass < 5 cm occur. The uppermost unit is the thickest (40 m), and is slightly rheomorphic near the top, where there is a thin (< 1 m thick), black to dark grey, perlitic vitrophyre containing spherulites with characteristic green chalcedony fills. This sub-unit is overlain by a yellow to pink, non-welded massive lapilli-tuff containing abundant chips of non-vesicular black glass and pumice clasts up to a few centimetres in diameter.



The Jackpot Member of Andrews et al. (2008) is composed of seven sub-units and located within the Rogerson Graben where its base is not exposed. The lower five sub-units are intensely welded and variably lava-like (*sensu* Branney and Kokelaar 1992). The majority of the thickness of the Jackpot Member is within sub-units 1-5, with each sub-unit separated by lithophysal horizons. At the base of sub-unit 4 of Andrews et al. (2008) is a layer of centimetre-scale (< 2 cm), angular chips of non-vesicular black glass (Fig. 3.19), identical to those in the Big Bluff Member. The upper part of sub-unit 5 is slightly rheomorphic and has a thin (metre scale) perlitic vitrophyre which is folded by the rheomorphism. Above this vitrophyre is a zone of non-welded material referred to by Andrews et al. (2008) as 'Jackpot 6'. This non-welded material becomes progressively more fused downwards towards the vitrophyre at the top of Jackpot 5. The non-welded facies contains abundant angular chips of non-vesicular glass and concentric-laminated accretionary lapilli, < 2 cm in diameter. Some of the accretionary lapilli have the angular glass clasts as cores (Fig. 3.19). The accretionary lapilli become more abundant upwards in Jackpot 6, and are rare in the basal metre or so of the ignimbrite. The Jackpot Member contains 10-15% phenocrysts of sanidine, plagioclase, clinopyroxene, quartz and magnetite with zircon and apatite present as accessories.

Browns Bench 7 also contains several different weathering horizons which are in places separated by lithophysal horizons, and the upper part of the thickest sub-unit is slightly rheomorphic, but both the top and lower contact of Browns Bench Unit 7 are not exposed.

The Frenchman Springs Rhyolite is a lava-like, flow-banded deposit < 100 m thick, containing 3-5% phenocrysts (Fig. 3.18). It is entirely massive and lacks any internal stratigraphy. It exhibits a basal breccia containing large clasts up to 20 cm in diameter (Fig. 3.19), many of which are vesiculated, indicative of an autobreccia. Although autobreccias may occur locally at the bases of rheomorphic ignimbrites (e.g. Sumner and Branney 2002), they are much more common at the base of rhyolitic lavas, and their extensive development has been used as a diagnostic criterion for an effusive origin (Bonnichsen and Kauffman 1987; Henry and Wolff 1992; Branney and Kokelaar 1992).

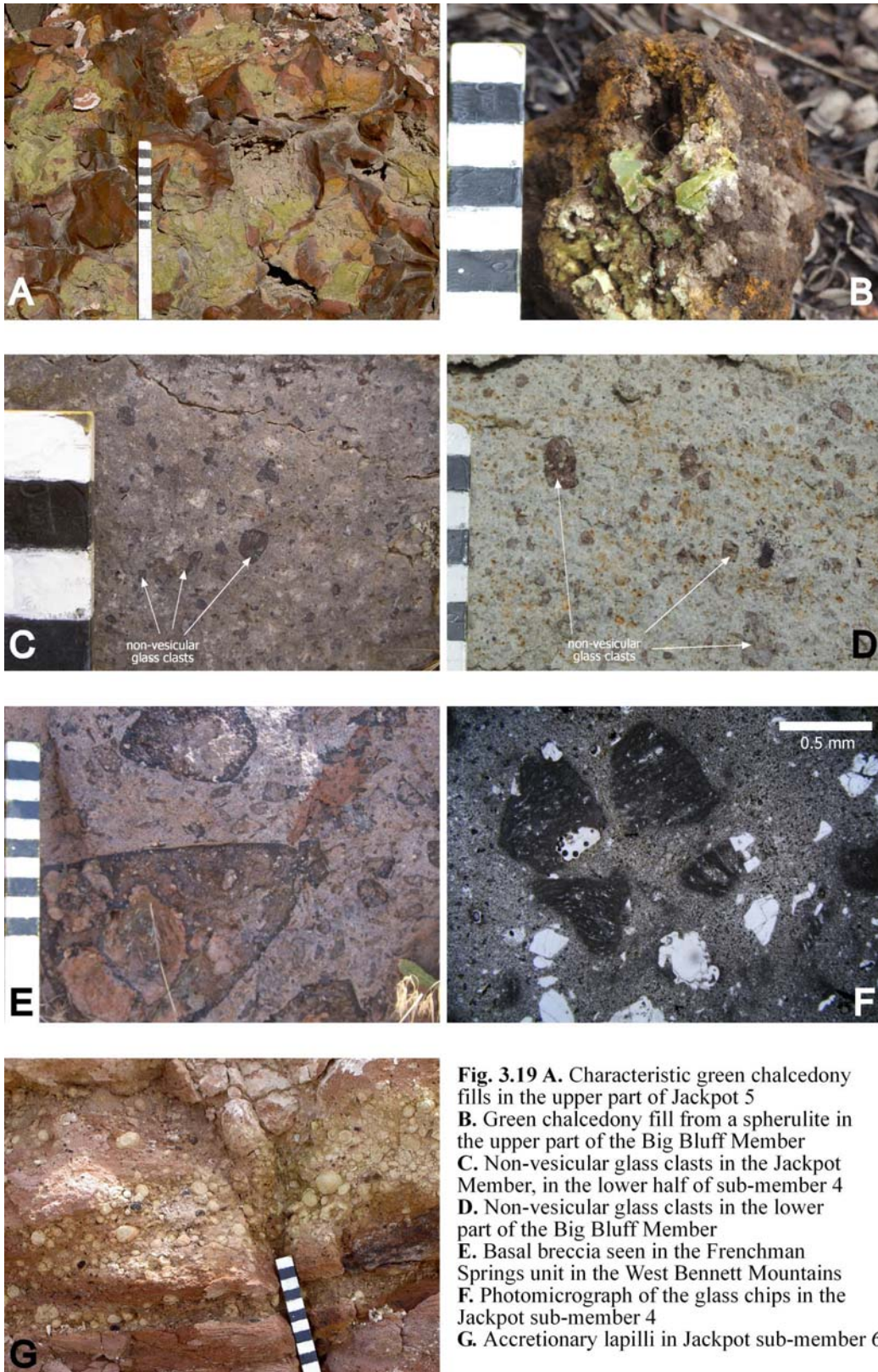


Fig. 3.19 A. Characteristic green chalcedony fills in the upper part of Jackpot 5
 B. Green chalcedony fill from a spherulite in the upper part of the Big Bluff Member
 C. Non-vesicular glass clasts in the Jackpot Member, in the lower half of sub-member 4
 D. Non-vesicular glass clasts in the lower part of the Big Bluff Member
 E. Basal breccia seen in the Frenchman Springs unit in the West Bennett Mountains
 F. Photomicrograph of the glass chips in the Jackpot sub-member 4
 G. Accretionary lapilli in Jackpot sub-member 6

Unfortunately, the lateral extent of the autobreccia at the base of the Frenchman Springs Rhyolite has not been determined.

Glass and phenocryst characteristics

The Big Bluff Member and proposed correlative units have similar glass chemistry in terms of SiO₂, TiO₂, FeO and CaO, although Browns Bench 7 shows a wider range of FeO than the other units (Fig. 3.12 C) with values less than 1 wt.% FeO.

The pyroxene compositions of the Big Bluff Member and proposed correlatives are distinctive throughout the Snake River Plain as a whole. Most Snake River-type rhyolites contain both augite and pigeonite, whereas the Big Bluff Member, Browns Bench 7 and Frenchman Springs contain augite, and rarely fayalite but lack pigeonite. However, the pyroxenes in Jackpot 1-6 are too altered to analyse (e.g. Andrews et al. 2008; this study). The lack of pigeonite in the other three units separates them from the overlying ignimbrites both at the Rogerson Graben and Cassia Mountains where pigeonite is ubiquitous in the younger ignimbrites (Andrews et al. 2008; Chapter 2). Feldspar compositions and morphology in the 4 units of proposed correlation 3 are similar; plagioclase is present in all, with compositions overlapping as oligoclase An₂₄₋₃₀ (Fig. 3.20). These compositions are distinct from those of overlying ignimbrites in both the Rogerson Graben and Cassia Mountains which contain andesine (Andrews et al. 2008; Chapter 2). All the four units contain sanidine with compositions, Or₅₃₋₅₇ (Fig 3.20) similar to the compositions of sanidine in other central Snake River Plain rhyolites. With respect to crystal textures, Jackpot 5 contains sanidines with myrmekitic textures, which in the Rogerson Graben are unique to the Jackpot Member (Andrews et al. 2008), and identical textures are seen in the upper parts of the Big Bluff Member in the Cassia Mountains.

The Big Bluff Member and Jackpot 1-6 both contain some ilmenite and a greater abundance of titanomagnetite which are not in equilibrium, using the criteria of Bacon and

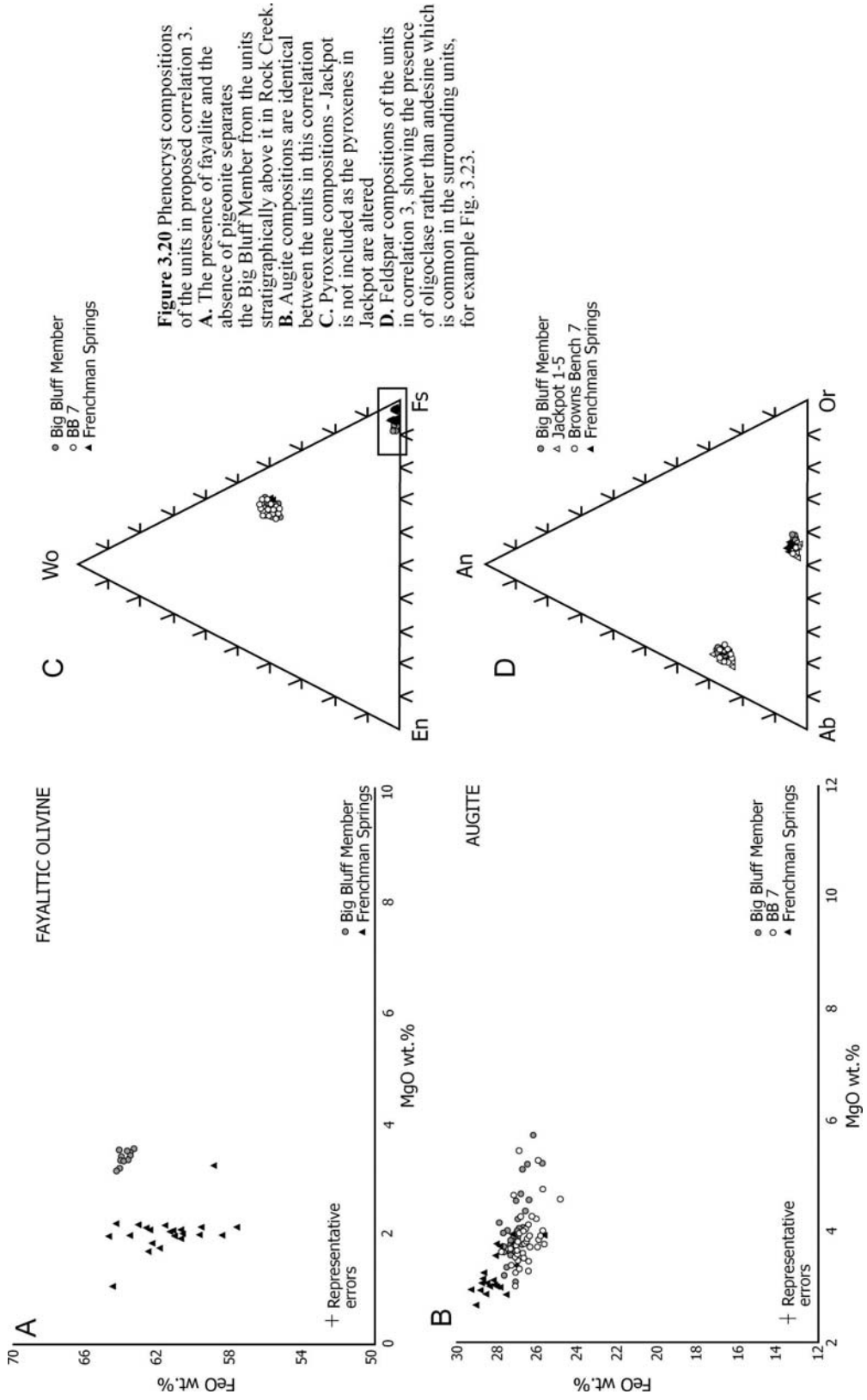


Figure 3.20 Phenocryst compositions of the units in proposed correlation 3. A. The presence of fayalite and the absence of pigeonite separates the Big Bluff Member from the units stratigraphically above it in Rock Creek. B. Augite compositions are identical between the units in this correlation. C. Pyroxene compositions - Jackpot is not included as the pyroxenes in Jackpot are altered. D. Feldspar compositions of the units in correlation 3, showing the presence of oligoclase rather than andesine which is common in the surrounding units, for example Fig. 3.23.

Hirschmann (1988). In contrast, the Frenchman Springs Rhyolite contains ilmenite and rare titanomagnetite.

⁴⁰Ar/³⁹Ar ages

Browns Bench 7 has an ⁴⁰Ar/³⁹Ar of 10.98 ± 0.07 Ma as derived from single crystal sanidine by Bonnicksen et al. (2008). The Big Bluff Member has been dated by ⁴⁰Ar/³⁹Ar as 10.83 ± 0.03 Ma (Perkins et al. 1995) on an assumed correlative distal ashfall, the same age was later refined to 10.93 ± 0.03 Ma, Perkins et al. (1998) and further corrected here to an age of 11.01 ± 0.03 Ma. This study uses a sample from the Big Bluff ignimbrite to give an ⁴⁰Ar/³⁹Ar age of 10.91 ± 0.07 Ma (Fig. 3.25). The Frenchman Springs Unit has an age of 10.96 ± 0.09 and the Jackpot 1-6 unit has an ⁴⁰Ar/³⁹Ar age of 10.95 ± 0.16 Ma (Table 3.1).

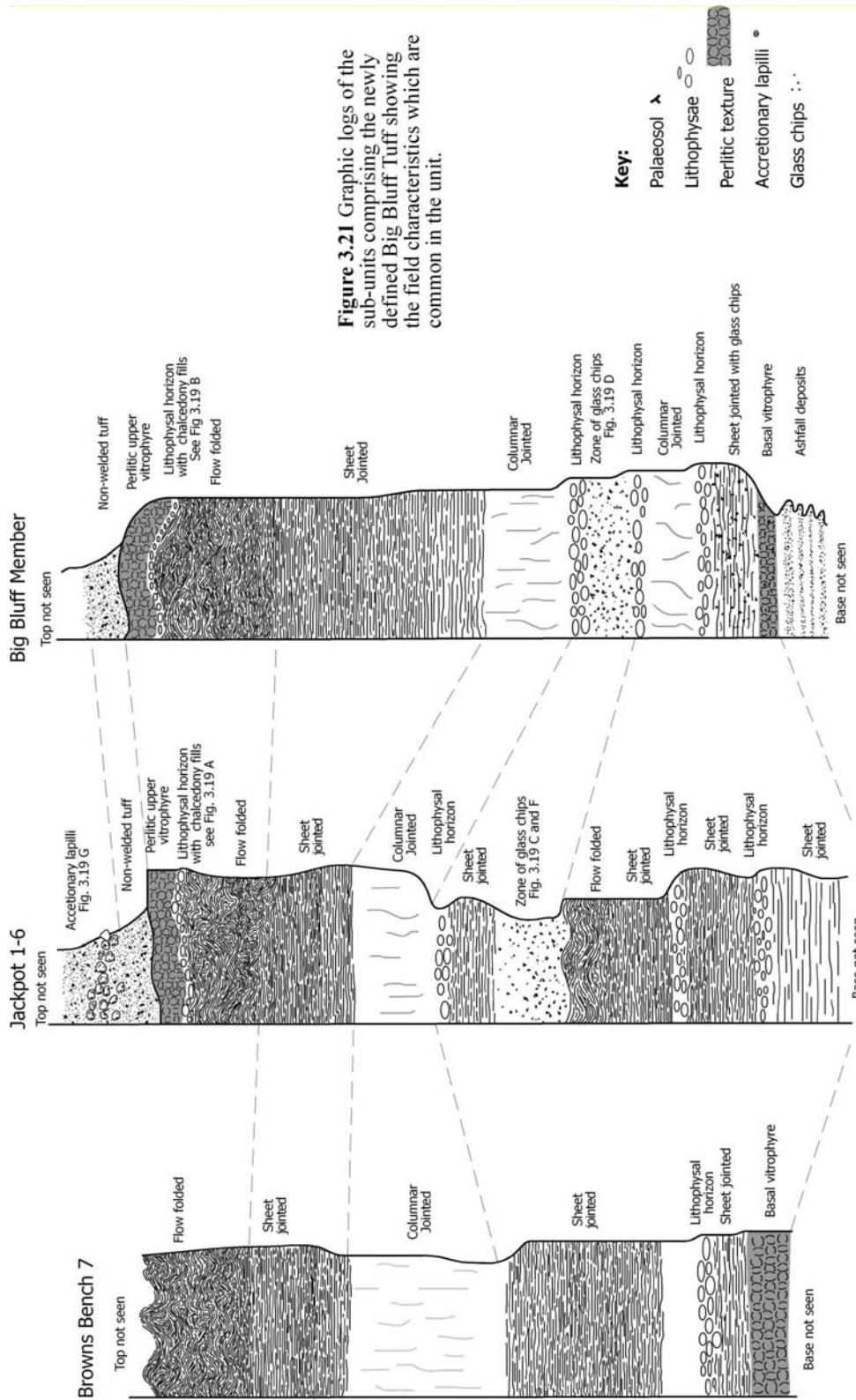
Oxygen isotopes

The Tuff of Big Bluff has a $\delta^{18}\text{O}$ of 2.98 ‰, the Jackpot 1-6 unit has $\delta^{18}\text{O}$ of 2.81 ‰ and Browns Bench 7 has $\delta^{18}\text{O}$ of 2.86 ‰. The Frenchman Springs unit in the West Bennett Mountains has a distinctly lower $\delta^{18}\text{O}$ of 2.39 ‰ (Fig. 3.14).

Interpretation

The ages of all units in this correlation overlap within error of the analysis. The Big Bluff Member, Jackpot 1-6 and Browns Bench 7 are now considered to be the same unit (Fig. 3.21), which I name the Big Bluff Tuff. Although the Frenchman Springs Rhyolite overlaps with the Tuff of Big Bluff within error of the age determination, it is considered to be a lava which was erupted at around the same time, for the following reasons:

(1) The Frenchman Springs Rhyolite has a basal autobreccia composed of vesiculated blocks which is not present in the Big Bluff Tuff. Widespread basal autobreccias are characteristic of rhyolitic lavas but breccias can be locally developed in intensely rheomorphic ignimbrites.



(2) The phenocryst content of the Frenchman Springs unit is c. 2%, significantly lower than the 15% recorded in the Big Bluff Member or correlatives.

(3) The Frenchman Springs unit contains little titanomagnetite, whereas in the Big Bluff Member it is more common than ilmenite.

(4) All the units which comprise the Big Bluff Tuff overlap within error in terms of oxygen isotopes whereas the Frenchman Springs unit is isotopically distinct.

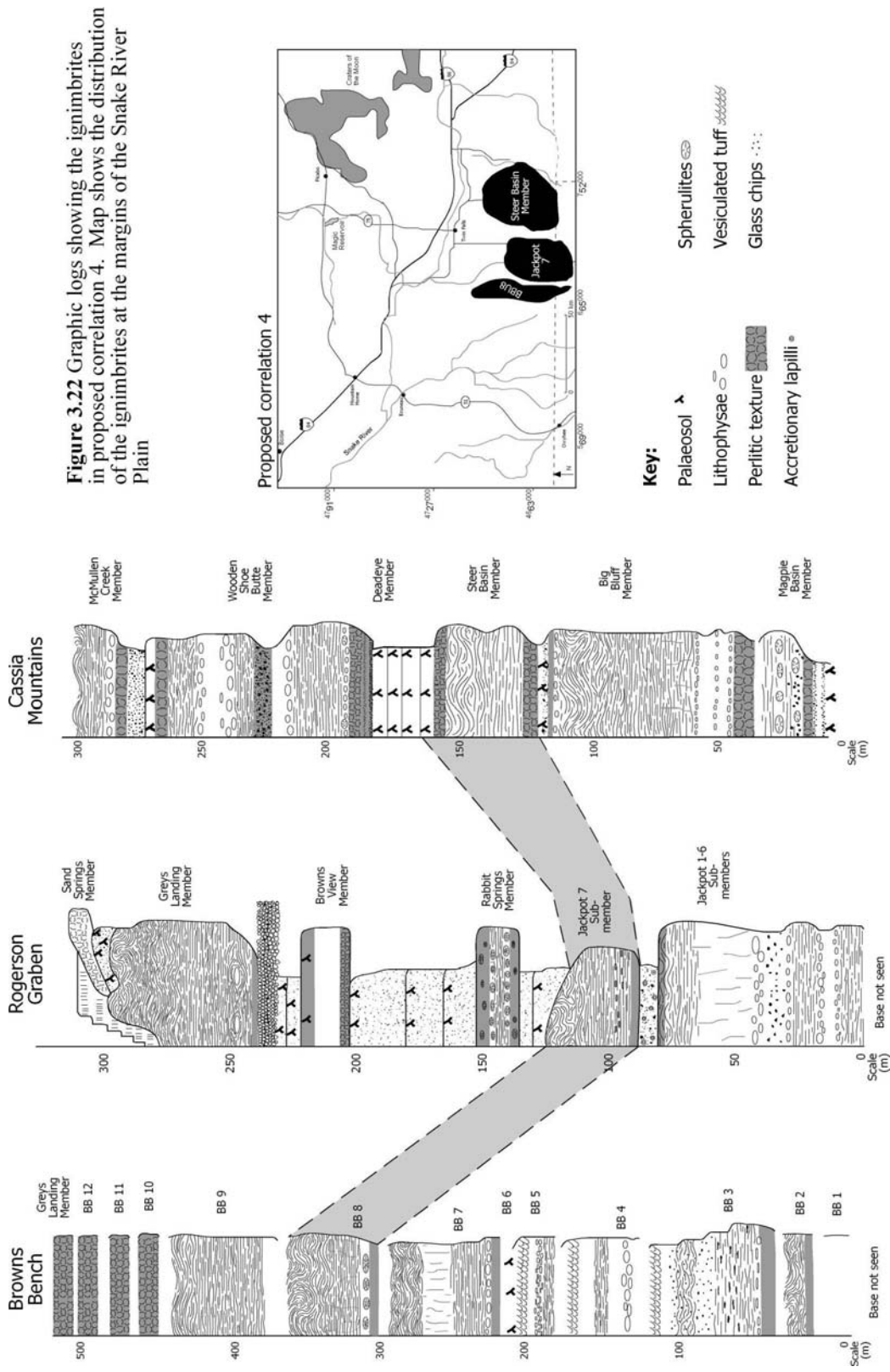
Proposed correlation 4: Steer Basin Member, Jackpot 7 and Browns Bench 8

Proposed correlation 4 involves the ignimbrites directly above those in correlation 3 in their respective massifs (Fig. 3.22). The Steer Basin Member, Jackpot 7 and Browns Bench 8 (BBU8) are all found within CAT group 8A with TiO₂ contents of between 0.39 and 0.67, and normal magnetic polarity (Bonnichsen et al. 2008).

Physical description

The Steer Basin Member is an intensely welded, highly rheomorphic ignimbrite in the Cassia Mountains (Chapter 2), between 40 and 50 m thick. The lowermost exposure includes a distinctive layer of aphyric obsidian (Fig. 3.23 A), used by Native Americans as a source of tool points (Williams et al. 1990). Directly above this obsidian layer is a crystal rich basal vitrophyre which passes up into intensely welded lithoidal rhyolite containing fiammé (Fig. 3.23 C) probably formed by the post-welding vesiculation of tuff. The uppermost part of the ignimbrite is highly rheomorphic, containing metre to decimetre-scale open folds, picked out by flow banding and partly by sheet-jointing. A thin (< 1 m thick) perlitic upper vitrophyre lies on the rheomorphic zone and passes upwards into a non-welded facies (c. 2 m thick) of ignimbrite overlain by a palaeosol (Fig. 3.26).

The Jackpot 7 ignimbrite in the Rogerson Graben is an intensely welded ignimbrite, thirty to forty metres thick (Andrews et al. 2008). It overlies a deposit of obsidian interpreted as fused ashfall (Fig. 3.23 B), overlain by the ignimbrite's basal vitrophyre. The interior of



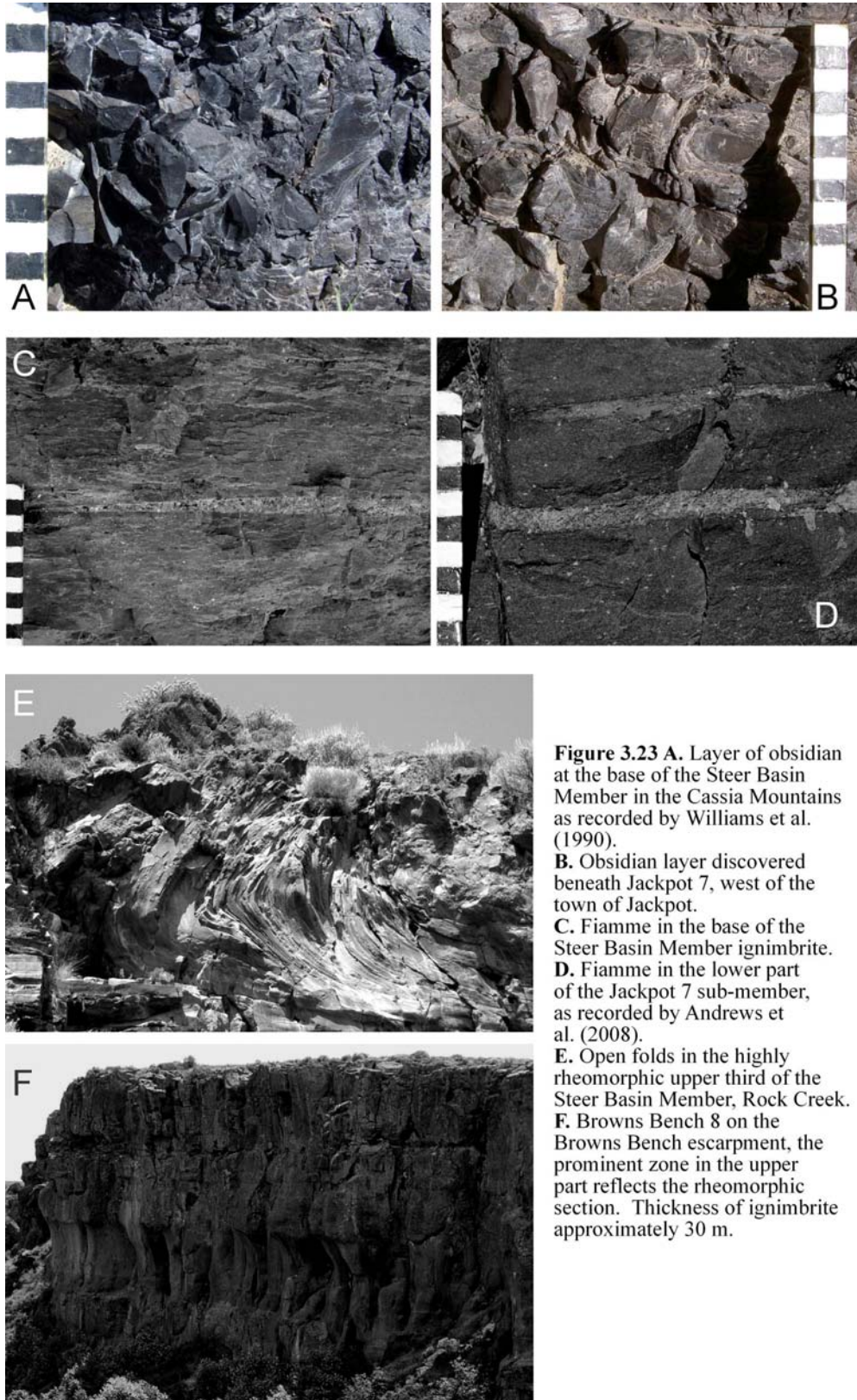


Figure 3.23 A. Layer of obsidian at the base of the Steer Basin Member in the Cassia Mountains as recorded by Williams et al. (1990).
 B. Obsidian layer discovered beneath Jackpot 7, west of the town of Jackpot.
 C. Fiamme in the base of the Steer Basin Member ignimbrite.
 D. Fiamme in the lower part of the Jackpot 7 sub-member, as recorded by Andrews et al. (2008).
 E. Open folds in the highly rheomorphic upper third of the Steer Basin Member, Rock Creek.
 F. Browns Bench 8 on the Browns Bench escarpment, the prominent zone in the upper part reflects the rheomorphic section. Thickness of ignimbrite approximately 30 m.

Jackpot 7 contains fiammé (Fig. 3.23 D) near the base reaching several centimetres, interpreted as post-welding vesiculated tuff (Andrews et al. 2008) which passes up into lithoidal sheet-jointed rhyolite. The uppermost part of the deposit is lithoidal and highly rheomorphic.

Browns Bench 8 is an extremely high-grade rheomorphic ignimbrite with a prominent upper rheomorphic zone. The base of the ignimbrite is not exposed but abundant obsidian occurs in float beneath the ignimbrite, suggesting the presence of a non-exposed fused ashfall layer.

Glass and phenocryst characteristics

Microprobe analyses of glass show that the Steer Basin Member, Jackpot 7 and Browns Bench 8 are identical in terms of most major element oxides. TiO₂ contents in all 3 units range from 0.2-0.35 wt.% and SiO₂ contents are similar (74-77.5 wt.%). The FeO and CaO contents are shown in Figure 3.12 D with Browns Bench 8 having a larger range of FeO and CaO than the Steer Basin Member and Jackpot 7.

All three ignimbrites contain both pigeonite and augite crystals, with pigeonite more abundant than augite. Identical compositional modes in both pigeonite and augite are recorded from all the ignimbrites (e.g. Chapter 2; Fig. 3.24). The compositional groups are outside of analytical error and are significantly different from the compositions of pyroxenes in the ignimbrites of correlation 3. The clinopyroxene compositions are unique in the Snake River Plain, in that the compositions of pigeonite and augite may overlap with other units, only the units within this correlation have the exact same combination of modes in both pigeonite and augite.

The feldspars within ignimbrites of this proposed correlation are similar, in both proportion and composition; plagioclase is much more abundant than alkali feldspar. The plagioclase in all these units is oligoclase to andesine An₃₂ to An₃₈ (Fig. 3.24) in contrast with the

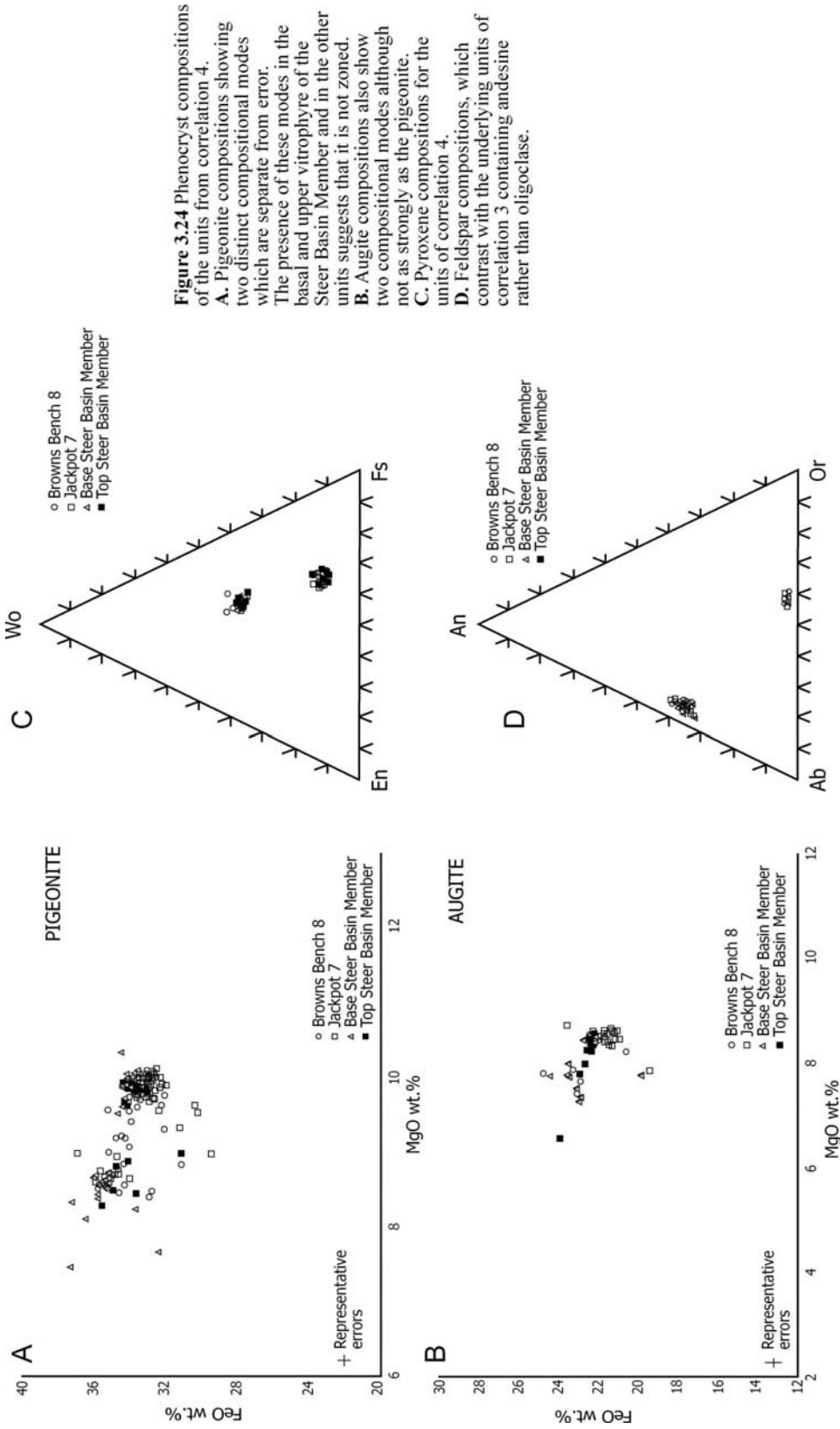


Figure 3.24 Phenocryst compositions of the units from correlation 4.
A. Pigeonite compositions showing two distinct compositional modes which are separate from error. The presence of these modes in the basal and upper vitrophyre of the Steer Basin Member and in the other units suggests that it is not zoned.
B. Augite compositions also show two compositional modes although not as strongly as the pigeonite.
C. Pyroxene compositions for the units of correlation 4.
D. Feldspar compositions, which contrast with the underlying units of correlation 3 containing andesine rather than oligoclase.

oligoclase in the stratigraphically lower Big Bluff Tuff. Units of this proposed correlation all contain sanidine with Or₅₅ to Or₅₉ and these compositions overlap.

⁴⁰Ar/³⁹Ar ages

The Steer Basin Member has a ⁴⁰Ar/³⁹Ar age of 10.48 ± 0.09 Ma, the Jackpot Member 7 units of Andrews et al. (2008) has a ⁴⁰Ar/³⁹Ar age of 10.4 ± 0.09 Ma and the Browns Bench 8 has a ⁴⁰Ar/³⁹Ar age of 10.56 ± 0.09 Ma (Table 3.1). All of these ages overlap within error of the measurements (Fig. 3.25) and even more compellingly, the spread of ages for all three units in this proposed correlation are similar, with all three units containing an older component of c. 11.5 Ma (Fig. 3.9).

Oxygen isotopes

All the units in correlation 4 have similar depletion in δ¹⁸O; the Steer Basin Member has 2.24 ‰, the Jackpot 7 unit has δ¹⁸O of 2.20 ‰ and Browns Bench 8 has δ¹⁸O of 2.32 ‰ (Fig. 3.14).

Interpretation

Stratigraphically, these units overlie the ignimbrites of the previous correlation and have numerous similar physical features such as the presence of a basal layer of obsidian (Fig. 3.26). The identical clinopyroxene compositions which are preserved vertically through a section (e.g. Chapter 2) are a strong indication that the Steer Basin Member, Jackpot 7 and Browns Bench 8 are correlatives. This is supported by the similarities in glass and feldspar compositions. The ⁴⁰Ar/³⁹Ar geochronology for these units produces ages which overlap and have the same distribution of ages. Underlying and overlying units have ⁴⁰Ar/³⁹Ar ages which are different outside of analytical uncertainty. All the units in this correlation have oxygen isotopic characteristics which overlap within error of the measurement. Given this weight of evidence, the Steer Basin Member, Jackpot 7 and Browns Bench 8 are considered

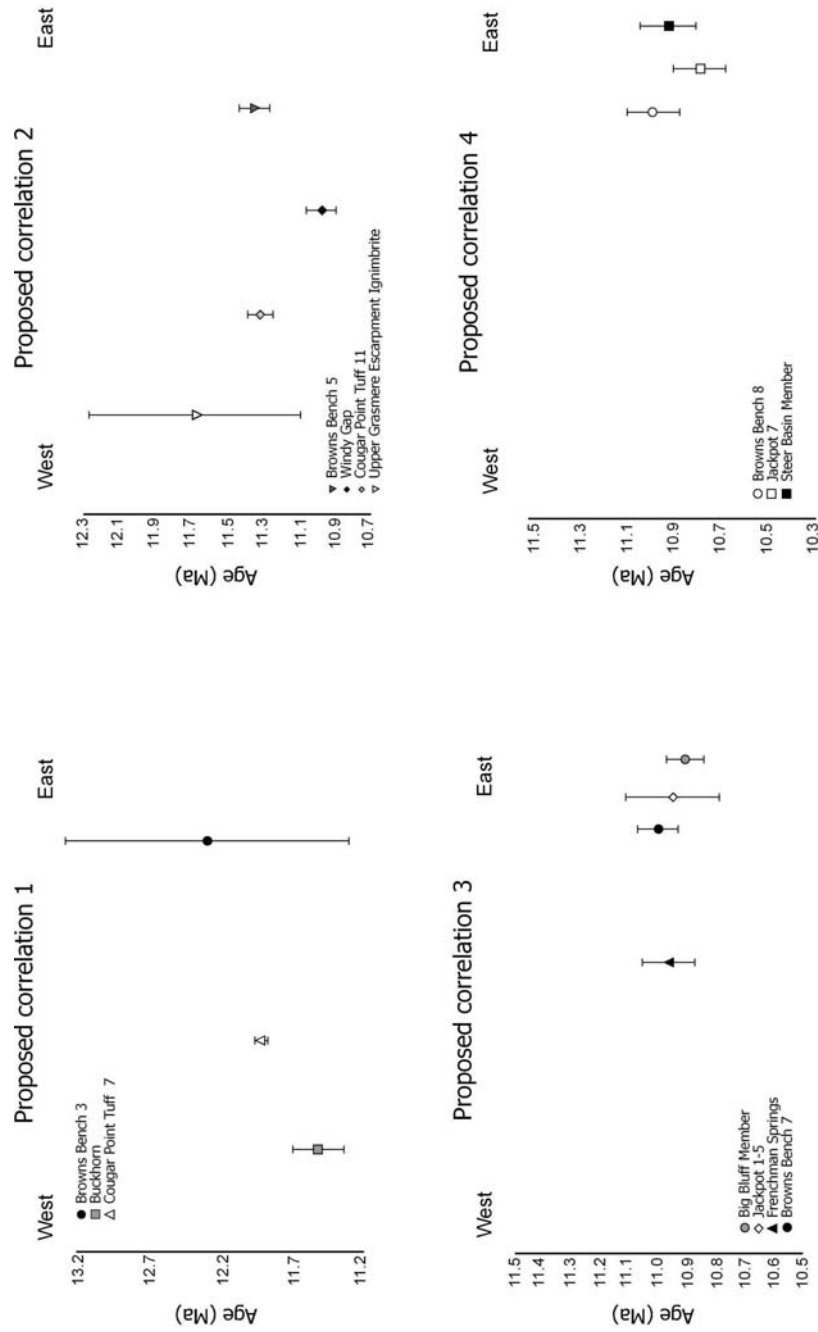
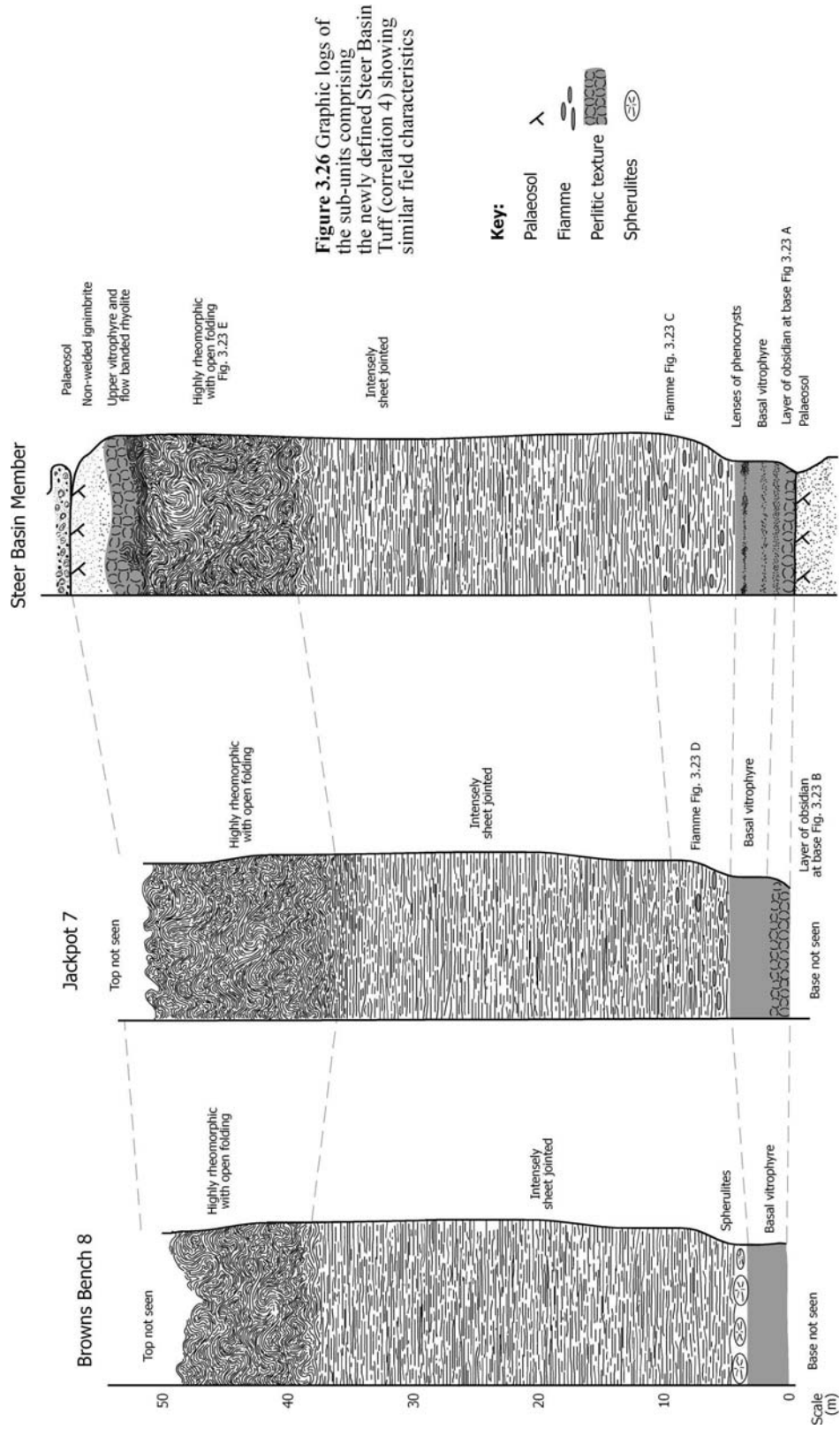


Figure 3.25 Diagrams show the ages of the units in each proposed correlation. In proposed correlation 1, the difference in age between Cougar Point Tuff 7 and the Buckhorn ignimbrite is shown. Proposed correlation 2, shows the overlap in age between Browns Bench 5 and Cougar Point Tuff 11. Proposed correlation 3 and correlation 4 show the good agreement in age between all the units in these correlations.



to correlate, and are interpreted as from a single eruptive unit. This new unit is hereby termed the Steer Basin Tuff.

Discussion:

Correlation of local units into three widespread ignimbrites, here termed Cougar Point Tuff 11, the Big Bluff Tuff and the Steer Basin Tuff is compelling because the regional representation of each correlation has good agreement in terms of mineral compositions, whole rock chemistry, magnetic polarity, geochronology, oxygen isotopic composition and glass chemistry in each correlation. The volumes of these units and their significance will be explored in the following section.

Eruptive volumes:

In this study it is inferred that three widespread ignimbrites; Cougar Point Tuff 11, Big Bluff Tuff and the Steer Basin Tuff represent the products of individual large eruptions. Estimations of the erupted volumes of each are presented below:

Cougar Point Tuff 11:

This unit contains the sub-units of Cougar Point Tuff 11 in the Bruneau-Jarbidge eruptive centre (Bonnichsen 1982; Bonnichsen and Citron 1982; Cathey and Nash 2004) and Browns Bench 5 (Bonnichsen et al. 2008). The volume of Cougar Point Tuff 11 has been estimated at between 50 and 1800 km³ (Boroughs et al. 2005; Leeman et al. 2008), although no distribution of the unit is given. The inferred distribution for Cougar Point Tuff 11 stretches from the Bruneau-Jarbidge eruptive centre to the Browns Bench escarpment (Fig. 3.1), an area of approximately 6,180 km³. The thickness of the unit varies between 75 and 30 m, so 50 m thick is taken as an average and produces an extracaldera volume of 309 km³. The intracaldera deposits of well-known ignimbrites have been considered to be of equivalent volume to the outflow volumes, and ashfall deposits have also been considered to be of similar volume (e.g. Rose and Chesner 1987; Wilson 2001;

Mason et al. 2004). Although this is not necessarily the case, it seems a reasonable approximation for the central Snake River as large volume calderas have been identified from the eastern Snake River Plain and Yellowstone (e.g. Morgan and McIntosh 2005; Christiansen 2001). Furthermore, the ashfall deposits from Snake River-type eruptions are widely recorded in the intermontane basins of the western United States (e.g. Perkins et al. 1998; Perkins and Nash 2002) with deposits recorded > 1000 km to the east in Nebraska (e.g. the Ogallala Formation, Rose et al. 2003). Following the above assumption, that the extracaldera volume is equal to the intracaldera volume which is equal to the ashfall volume, the estimated volume for Cougar Point Tuff 11 is 927 km³.

The Big Bluff Tuff:

The Big Bluff Tuff includes the Big Bluff Member (Williams et al. 1991), the majority of the Jackpot Member (Andrews et al. 2008) and Browns Bench 7 (Fig. 3.21; Bonnicksen et al. 2008). No volume estimates have been made for the Big Bluff Member but the Jackpot Member has an estimated minimum volume of >> 22.5 km³ (Andrews et al. 2008). The newly correlated Big Bluff Tuff is exposed in the Cassia Mountains, Rogerson Graben and on Browns Bench (Fig. 3.1), covering an area of c. 5,335 km² (Fig. 3.18), and is typically 75 m thick (a conservative estimate as the base of the Jackpot Member is not exposed). This gives a volume of 400 km³. Typical volume assumptions normally involve radial distributions from a central vent; however this assumption is not followed here because in the successions to the north of the Plain no units are currently known which have the same characteristics (discounting the Frenchman Springs unit as discussed above). This produces an estimated total volume of c. 1200 km³ for the Big Bluff Tuff.

The Steer Basin Tuff:

The outcrop area is approximately the same as the Big Bluff Tuff, however, the unit is typically only 40 m thick (Fig. 3.26) making the volume of the exposed Tuff of Steer Basin

213 km³. Using the same assumptions as for the Big Bluff Tuff, the overall volume of the Steer Basin Tuff is estimated at ~640 km³.

Volume or magnitude?

Historically the volume of volcanic eruptions has been measured using the semi-quantitative Volcanic Explosivity Index (VEI) of Newhall and Self (1992). The VEI is based on a combination of observations on eruptive behaviour and the bulk volume of the deposit. Using this scale, the Big Bluff Tuff has a VEI of 8 and the Steer Basin Tuff has a VEI of 7. However, measuring the volume of deposits over-estimates the volume of non-welded deposits when compared with welded rocks, to avoid this a dense rock equivalent was used (e.g. Carey and Sigurdsson 1986; Mason et al. 2004). The magnitude system of Mason et al. (2004) uses the eruptive mass of the deposit to generate a magnitude for the eruption. To determine the mass of the deposit the MAGMA program (Wohletz 1999) was used, assuming anhydrous conditions with the chemistry of the magma and the inferred magmatic temperature to calculate rock density and then the method of Mason et al. (2004) was followed. The results gave estimated magnitudes of 8.47 for the Big Bluff Tuff, 8.36 for Cougar Point Tuff 11 and 8.15 for the Steer Basin Tuff (Table 3.2). For ease of comparison, and using the same method of estimating volume (e.g. I = O = A), the Big Bluff Tuff is estimated to be slightly larger than the Cerro Galan ignimbrite (Sparks et al. 1985 and De Silva 1989) whereas the Steer Basin Tuff is estimated to be slightly larger than the Oruanui eruption (Wilson 2001).

The Yellowstone hotspot track:

The Yellowstone hotspot track has produced a number of eruptions large enough to be classified as super-eruptions (> 750 km³ and 300 km³ DRE; Sparks et al. 2005) from both the Yellowstone plateau and the Heise eruptive centre (Christiansen 2001; Morgan and McIntosh 2005). The Tuff of Big Bluff and the Tuff of Steer Basin are both of similar size to known eruptions from the Yellowstone hotspot (Fig. 3.27). The Big Bluff Tuff is of equivalent magnitude to the Blacktail Tuff of Morgan et al. (1984) and represents one of

Rank	Deposit name	Volume basis	Min. Magnitude	Age (Ma)	Reference
1	Fish Canyon Tuff	O + I	9.1	27.8	Lipman (1997)
2	Younger Toba Tuff	O + I + A	8.8	0.074	Rose and Chesner (1987)
3	Lund Tuff	O + I	8.7	29	Maughan et al. (2002)
4	Huckleberry Ridge Tuff	O + I	8.6	2	Christiansen (1984, 2001)
5	Atan Ignimbrite	O + I	8.6	4	Lindsay et al. (2002)
6	Millbrig Big Bentonite	A	8.6	454	Huff et al. (1996)
7	Green Tuff	O + A	8.6	28-30	Ukstins Peate et al. (2003)
8	Blacktail Tuff	O + I	8.5	6.5	Morgan et al. (1984)
9	Kneeling Nun Tuff	O	8.5	33	Elston et al. (1975)
10	Carpenter Ridge Tuff	O + I	8.5	27.5	Lipman et al. (1973)
11	Timber Mtn - Rainier Mesa Member	O	8.5	11.6	Farmer et al. (1991)
12	Paintbrush Tuff - Topopah Springs Member	O	8.5	13.4	Farmer et al. (1991)
13	Apache Springs Tuff	O	8.5	29-28	Ratte et al. (1984)
14	Big Bluff Tuff	O + I + A	8.47	10.9	This study
15	Cerro Galan Ignimbrite	O + I + A	8.4	2.2	Sparks et al. (1985)
16	Kinneville Bentonite	A	8.4	454	Francis et al. (1989)
17	Bloodgood Canyon Tuff	O	8.4	29-28	Huff et al. (1996)
18	Deicke Bentonite	A	8.4	454	Ratte et al. (1984)
19	Dillon/Sapinero mesa	O	8.4	28.5	Huff et al. (1996)
20	Sapinero Mesa Tuff	O+I	8.4	28.5	Lipman et al. (1973)
21	Paintbrush Tuff - Tiva Canyon Member	O	8.4	12.9	Farmer et al. (1991)
22	Mitchell Mesa Rhyolite	I+O	8.4	32-33	Henry and Price (1984)
23	Cougar Point Tuff 11	O+I+A	8.36	11.35	This study
24	Lava Creek Tuff	O	8.3	0.6	Christiansen (1984, 2001)
25	Timber Mountain Ammonia Tanks Mbr	I+O	8.3	11.4	Farmer et al. (1991)
26	Oldest Toba Tuff	I+A	8.3	0.79	Lee et al. (2004)
27	Kilgore Tuff	O+I	8.3	4.3	Morgan et al. (1984)
28	Panizos Ignimbrite	O+I	8.2	6.1	Ort (1993)
29	Barrel Springs	O	8.2	36	Parker and McDowell (1979)
30	Wild Cherry Formation	O	8.2	36	Parker and McDowell (1979)
31	Sifon Ignimbrite	O	8.2	8.3	De Silva (1991)
32	Steer Basin Tuff	O + I + A	8.15	10.5	This study
33	Huaylillas	O + I	8.1	5	De Silva (1991)
34	La Jara	O + I	8.1	30	Lipman (1975)
35	Oruanui	O + I + A	8.1	0.0265	Wilson (2001)

Table 3.2 Magnitudes of the Tuff of Big Bluff and the Tuff of Steer Basin compared to those of super-eruptions from elsewhere, as compiled by Mason et al. (2004). Volumes are based on O - outflow, I - intracaldera and A - ashfall. It should be noted this table does not include some of the large units from places such as Etendeka.

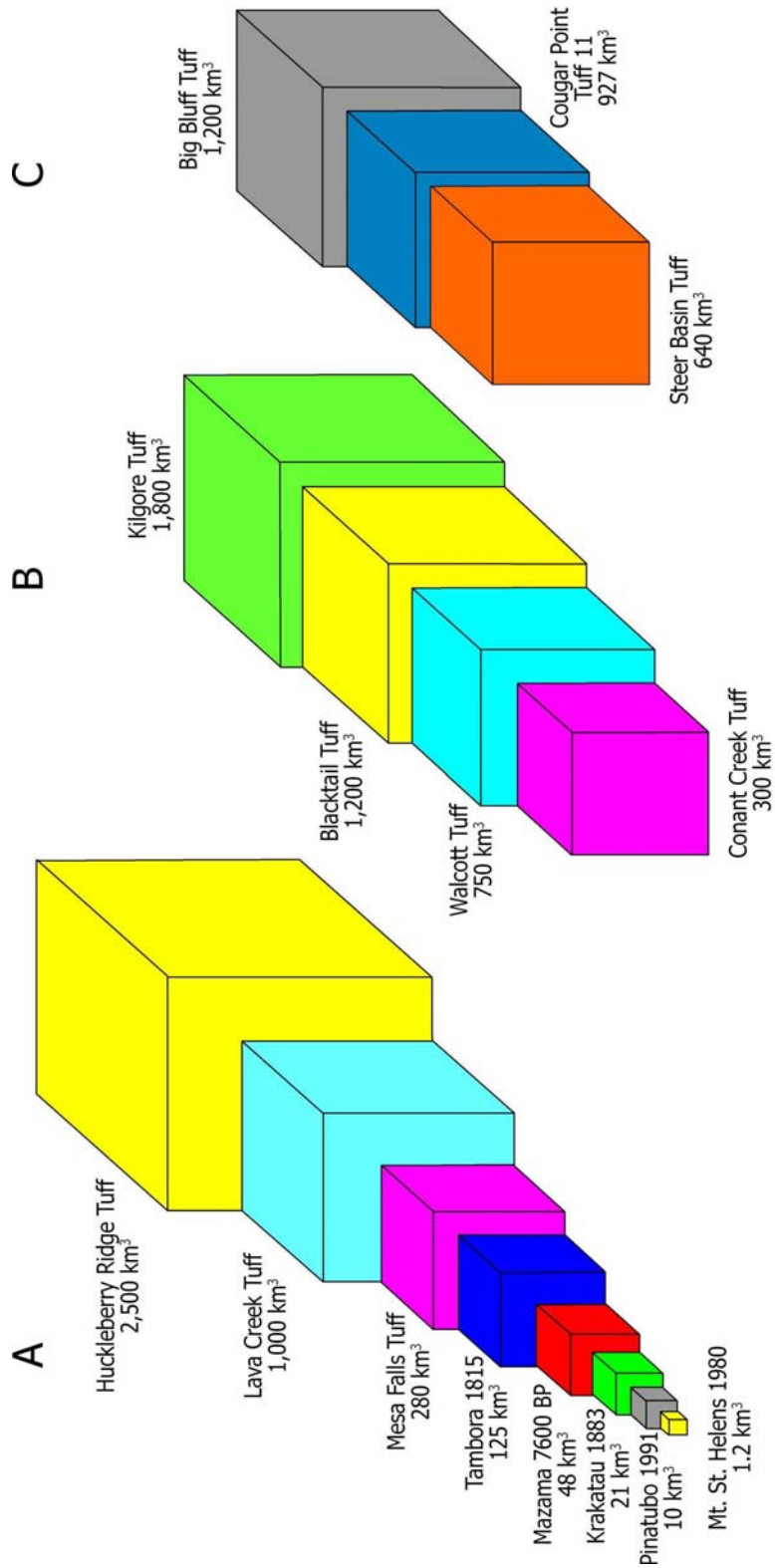


Figure 3.27 A. Volumes of well known eruptions from a variety of volcanic fields. B. Volumes of eruptions from the Heise eruptive centre (Morgan and McIntosh 2005). C. Volumes of newly recognised super-eruptions from the earlier part of the hotspot track (correlations 2-4; this study).

the largest eruptions from the Yellowstone hotspot. The volume of the Steer Basin Tuff is most similar to the Walcott Tuff from the Heise eruptive centre (Morgan and McIntosh 2005). However, as discussed above, as it has a greater intensity of welding, the Steer Basin Tuff is of greater magnitude.

The total erupted volume of the central Snake River Plain is significantly larger than the Yellowstone plateau. The Yellowstone plateau erupted $\sim 3,800 \text{ km}^3$ of rhyolite over a period of 2.2 million years (Christiansen 2001) whereas in the 2.2 million years from 12.7-10.5 Ma, estimates for the amount of rhyolite erupted in the central Snake River Plain are between 7-14,000 km^3 (Perkins and Nash 2002; Bonnicksen et al. 2008). This suggests that during the early part of the hotspot history the Yellowstone hotspot was approximately three times more productive than the Yellowstone plateau.

Eruption frequency

The new correlations in the central Snake River Plain reduce the number of eruptions from the Miocene Yellowstone hotspot. Hitherto 56 ignimbrites, 19 lavas and 15 rhyolites of equivocal (explosive or effusive) origin from the central Snake River Plain erupted between 13-5.5 Ma (Bonnicksen et al. 2008). Assuming half (8) of the unknown rhyolites are ignimbrites, and given that in the record of events that allow unequivocal interpretation the ratio of ignimbrites to lavas is $\sim 3:1$ this is conservative, the tally for the central Snake River Plain is 64 ignimbrites spanning a period of 7.5 million years. This equates to 8.5 ignimbrite-forming eruptions per million years. This is in marked contrast with the younger volcanic fields of Heise, which had 5 explosive eruptions over 2.2 Ma, a rate of 2.27 eruptions per million years. The Yellowstone plateau has produced 6 explosive eruptions in the past 2.2 Ma, with the tuffs of Sulphur Creek, Bluff Point and Lyle Spring in addition to the three large volume eruptions (Christiansen 2001). The Yellowstone plateau has experienced explosive eruptions at an average rate of 2.72 eruptions per million years.

The new correlations in this work reduces the known number of ignimbrites from the central Snake River Plain by five, giving 59 ignimbrite-forming eruptions at a rate of 7.4 per million years, or one explosive eruption per 135,000 years. The ‘ignimbrite flare-up’ of the central Snake River Plain (Bonnichsen et al. 2008) is best represented by the Cougar Point Tuff succession of the Bruneau-Jarbidge eruptive centre which had an ignimbrite forming eruption every 200-300 ka (Cathey and Nash 2004; Bonnichsen 2008). As the entirety of the Cougar Point Tuff may be seen vertically stacked in steep canyon sections (e.g. Fig 3.11 E), the frequency of these eruptions cannot be reduced by correlation. Given that the Cougar Point Tuff succession represents part of the ‘flare-up’ event, the relative eruptive frequencies suggest that there are numerous other correlations that have yet to be made.

Other possible correlations

The new geochronological data available here allows speculation on further correlations based on the CAT groups of Bonnichsen et al. (2008). Some possible correlatives are suggested below; all require further work:

Big Bluff Tuff and Cougar Point Tuff 13

It is possible that the Big Bluff Tuff has a correlative unit further west within the Cougar Point Tuff succession. The most likely candidate is Cougar Point Tuff 13 as both units are within CAT group 7 of Bonnichsen et al. (2008). Cougar Point Tuff 13 contains fayalite and augite and lacks pigeonite similar to the Big Bluff Tuff (Fig. 3.28). In terms of age, Cougar Point Tuff 13 has a $^{40}\text{Ar}/^{39}\text{Ar}$ age of 10.86 ± 0.06 Ma (Bonnichsen et al. 2008) which is an average of three $^{40}\text{Ar}/^{39}\text{Ar}$ age determinations (10.89 ± 0.06 , 10.7 ± 0.06 and 10.82 ± 0.07 Ma). Previously it was thought that the Big Bluff Tuff did not correlate with Cougar Point Tuff 13 because the $^{40}\text{Ar}/^{39}\text{Ar}$ age of the Big Bluff Tuff quoted was that of Perkins et al. (1998) as 11.01 ± 0.03 Ma. The $^{40}\text{Ar}/^{39}\text{Ar}$ age of the Big Bluff Tuff as determined here, 10.91 ± 0.07 Ma, overlaps with all three ages of Cougar Point Tuff 13 from Bonnichsen et al. (2008). Only the age of the Tuff of Big Bluff as determined by Perkins et al. (1998) does not agree with the ages of the later studies. Some of the ages

attributed by Perkins et al. (1995), the original paper from which the age was recalculated, have been shown to have been correlated incorrectly. Given the good agreement between the ages and chemistry of the Tuff of Big Bluff and Cougar Point Tuff 13, it is suggested here that these units correlate. The compositions of the augites and ages of all the units are shown in Figure 3.28. If the Big Bluff Tuff and Cougar Point Tuff 13 correlate then the resultant volume of that eruption would be the largest erupted from the Yellowstone hotspot and one of the largest eruptions known.

Steer Basin Tuff, Cougar Point Tuff 15 and the Tuff of Knob

If the Big Bluff Tuff correlates with Cougar Point Tuff 13 to the west, it is possible that the overlying Steer Basin Tuff also correlates further west to Cougar Point Tuff 15 which is thought to be ~ 10.5 Ma (Perkins et al. 1998; Perkins and Nash 2002; Bonnicksen et al. 2008) based on interpolation between units of known age. The constituent units of the Steer Basin Tuff all have ages which overlap with 10.5 Ma (Fig. 3.29). Cathey and Nash (2004) identify two units that they suggest represent Cougar Point Tuff 15, referred to as 15b and 15j reflecting their relative outcrop in Bruneau and Jarbidge canyons respectively. Clinopyroxene compositional data in Cathey and Nash (2004) suggests that it is the CPT 15b unit that may correlate with the Steer Basin Tuff (Fig 3.29). It is also possible that the Steer Basin Tuff correlates to the north side of the Snake River Plain with the Tuff of Knob in the Davis Mountain area (Fig. 3.8) (Oakley and Link 2006) as this has a similar crystal content and assemblage, whole rock chemistry and $^{40}\text{Ar}/^{39}\text{Ar}$ age. The Tuff of Knob contains 10-20% lithics of Eocene Challis volcanics but the Challis calderas lie north of the Snake River Plain, so these lithics could have been incorporated locally. The Tuff of Knob has a $^{40}\text{Ar}/^{39}\text{Ar}$ age of 10.6 ± 0.2 Ma (Oakley and Link 2006; Fig. 3.8). If the Steer Basin Tuff does indeed correlate with the Tuff of Knob in the Davis Mountain area, this would greatly increase the volume of the unit, likely making it larger than the Big Bluff Tuff. If these units all correlate, then the estimated erupted volume would be $3,060 \text{ km}^3$. Further work is needed.

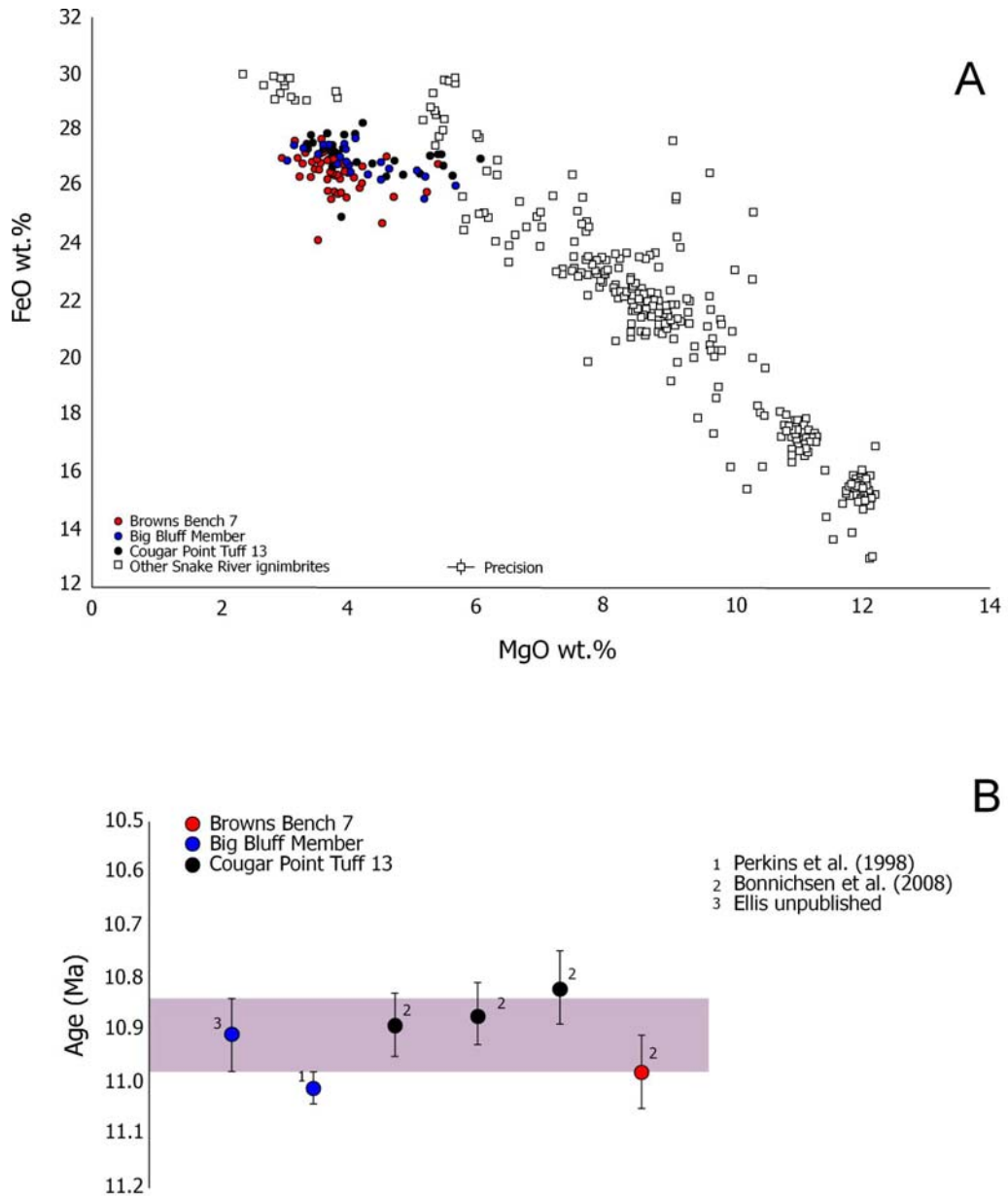


Figure 3.28 **A.** Diagram showing the augite compositions from the Big Bluff Tuff compared to those from Cougar Point Tuff 13 and other ignimbrites from the central Snake River Plain. **B.** Ages of all the units which are relevant to the proposed correlation. The age of the Big Bluff Member from Perkins et al. (1998) was revised from Perkins et al. (1958) and is further revised here. Ages from Perkins et al. (1998) and Bonnichsen et al. (2008) are revised relative to the Fish Canyon Tuff age of 28.02 Ma.

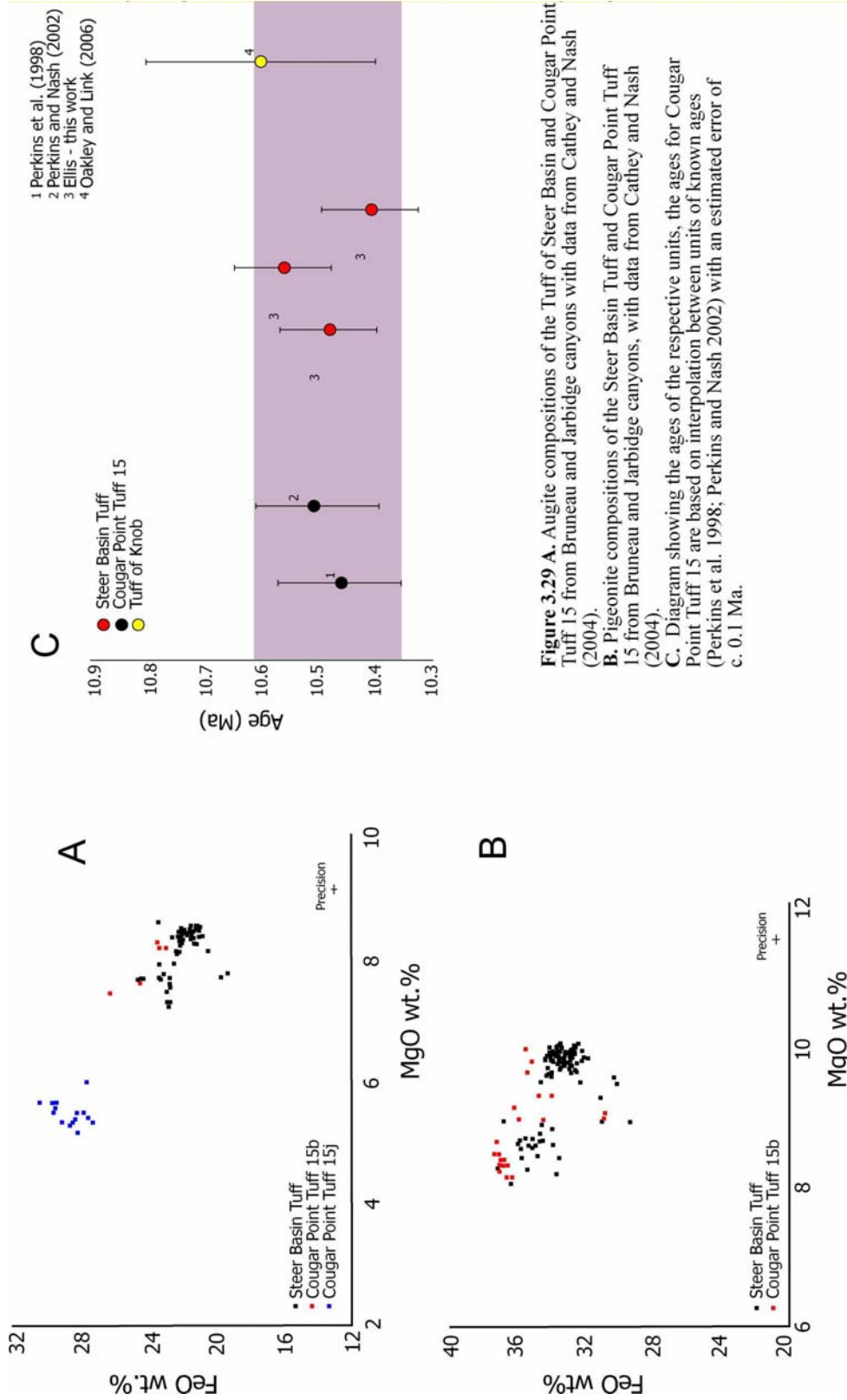


Figure 3.29 A. Augite compositions of the Tuff of Steer Basin and Cougar Point Tuff 15 from Bruneau and Jarbidge canyons with data from Cathey and Nash (2004).
B. Pigeonite compositions of the Steer Basin Tuff and Cougar Point Tuff 15 from Bruneau and Jarbidge canyons, with data from Cathey and Nash (2004).
C. Diagram showing the ages of the respective units, the ages for Cougar Point Tuff 15 are based on interpolation between units of known ages (Perkins et al. 1998; Perkins and Nash 2002) with an estimated error of c. 0.1 Ma.

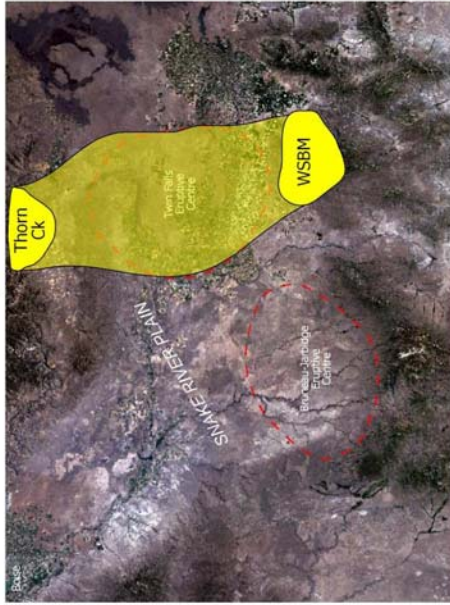
Wooden Shoe Butte Member and Tuff of Thorn Creek

The 10.20 ± 0.03 Ma Wooden Shoe Butte Member (WSB) (Perkins and Nash 2002) may correlate across the plain to the Tuff of Thorn Creek which has a K/Ar age of 10.1 ± 0.3 Ma (Armstrong et al. 1980). The location of the units suggest that they may correlate (Fig. 3.30) and despite the fact that the WSB and Tuff of Thorn Creek are in different CAT groups, WSB is in group 9 and Thorn Creek in 10, there remains the possibility of correlation. The two units have similar whole rock TiO_2 contents, WSB average 0.63 wt.% (n=15) and Tuff of Thorn Creek 0.56 wt.% (n=3; Bonnicksen et al. 2008) and similarities in terms of their reported abundances of Zn and Nb (Oakley and Link 2006). However, better resolution is required for the geochronology, along with more detailed characterisation of the phenocryst chemistry to test this hypothesis.

Eruptive centres:

Ignimbrites in the CSRP have been thought to have originated from discrete eruptive centres along the axis of the Snake River Plain with activity moving eastwards from centre to centre with time (Pierce and Morgan 1992; McCurry et al. 1996). Inferred eruptive centres thought to be the source of ignimbrites described in this chapter are the Bruneau-Jarbidge centre in the west (Bonnicksen 1982) and the Twin Falls eruptive centre further east (McCurry et al. 1996). The increasing amount of geochronology (e.g. Oakley and Link 2006; Bonnicksen 2008; this work) suggests that volcanism was more widely distributed along the central Snake River Plain in the Miocene. Deposits in the East Bennett Mountain region are of 11.2 Ma (e.g. Fig. 3.8), located at least 150 km north east of the proposed Bruneau-Jarbidge centre, yet considerably older than the proposed onset of activity from the Twin Falls eruptive centre (Pierce and Morgan 1992). This suggests that either the sources of the eruptive activity were more dispersed than the eruptive centre model currently suggests, or that the density currents produced from these eruptions were very far-travelled.

C. Wooden Shoe Butte Member (WSBM) and Tuff of Thorn Creek



A. Big Bluff Tuff and Cougar Point Tuff 13



B. Steer Basin Tuff and Cougar Point Tuff 15

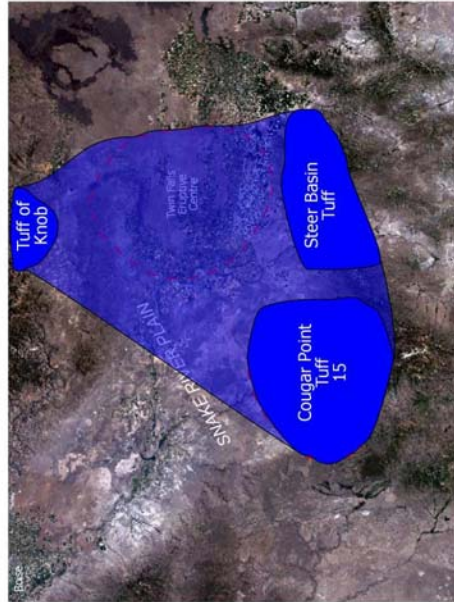


Figure 3.30 Showing the locations of the correlations which are proposed as a result of this work. **A.** The proposed correlation between the newly defined Big Bluff Tuff and Cougar Point Tuff 13. **B.** The proposed correlation between the newly defined Steer Basin Tuff, Cougar Point Tuff and the Tuff of Knob from the East Bennett Mountains. **C.** The locations of the Wooden Shoe Butte Member (WSBM) in the Cassia Mountains and the Tuff of Thorn Creek in the East Bennett Mountains.

Conclusions:

Different ignimbrites from the central Snake River Plain contain different phenocryst populations, often including multiple compositional modes of clinopyroxene. These multiple modes of both augite and pigeonite are sufficiently variable between ignimbrites to act as ‘fingerprints’ of individual eruptive units, yet appear to remain relatively constant within an eruptive unit. Using clinopyroxene compositions in concert with whole rock chemistry; magnetic polarity; glass and feldspar chemistry; oxygen isotopes and $^{40}\text{Ar}/^{39}\text{Ar}$ geochronology, has allowed correlation of ignimbrites between adjacent massifs (for the first time). Three super-eruptions have been identified with volumes of 640 km^3 , 927 km^3 and $1,200\text{ km}^3$ comparable in magnitude to the well-known eruptions from the younger Yellowstone and Heise volcanic fields. In addition, a number of predicted correlations have been disproved on the basis of the combination of field and geochemical evidence.

The frequency of eruptions from the central Snake River Plain is thought to be approximately three times higher than that recorded at the Yellowstone plateau. Given the number of ignimbrite units recorded by Bonnicksen et al. (2008) and the timespan in question, it is likely that deposits of more super-eruptions may be present in the central Snake River Plain, and the techniques detailed here demonstrate how such correlations may be achieved.

In addition to the change in eruption frequency through the history of the hotspot, the deposits from most eruptions in the central Snake River Plain are significantly different to those from the Yellowstone plateau (e.g. Branney et al. 2008). The central Snake River Plain is dominated by well-sorted (lacking pumice and lithic lapilli), intensely welded, lava-like ignimbrites of high-inferred magmatic temperature, which contrasts with the non to poorly-welded, poorly-sorted, pumice-bearing deposits from Yellowstone and Heise. This illustrates how the eruptive behaviour of hotspot volcanism may vary through time both eruption frequency and eruptive style.

Chapter 4: The Deadeye Member: a rhyolitic phreatomagmatic eruption from the Yellowstone hot spot track

Abstract

The Deadeye Member records a large (1.3 km³), rhyolitic phreatomagmatic eruption from the Yellowstone-Snake River Plain volcanic province. It is a single, 6 m thick soil-bound eruption unit, comprising a succession of fallout deposits overlain by a non-welded ignimbrite containing abundant accretionary lapilli, flattened mud clumps and exhibiting local cross-stratification. Two distinct pumice fall beds contain four populations of glass: black pumice, white pumice, grey macroscopic cusped shards and non-vesicular black glass fragments. The populations exhibit broadly similar chemical characteristics, but reflect magmas that had different histories prior to the Deadeye eruption; some interpreted as juvenile and others as accessory. The magma of the Deadeye eruption was similar to those that formed the typical ‘Snake River-type’ intensely welded ignimbrites which dominate the central Snake River Plain as indicated by similar whole rock and glass compositions, estimated magmatic temperature and oxygen isotope characteristics. The different (e.g. non-welded) lithofacies of the Deadeye Member are interpreted as the result of a different eruptive style whereby water interacted with already fragmenting rhyolitic magma resulting in a phreatomagmatic eruption. The Deadeye Member is one of several non-welded ‘slope-forming’ deposits that separate cliff-forming welded ignimbrites and lavas along the margins of the Snake River Plain. These deposits have received little attention, and it is possible that silicic phreatomagmatic behaviour in the Miocene Yellowstone Snake River Plain volcanic province was more common than has been appreciated.

Geological Background

The Yellowstone-Snake River Plain volcanic province (YSRP) of southern Idaho and northern Nevada is a bimodal continental igneous province, dominated by basalt and rhyolite. Large volumes of rhyolite are thought to have erupted from discrete eruptive centres that young eastwards reflecting westward movement of the North American plate over the Yellowstone hotspot (Pierce and Morgan 1992; McCurry et al. 1996; Fig. 4.1 inset). The explosive rhyolitic eruptions date from c. 16 Ma in the west (the McDermitt caldera, Nevada; Henry et al. 2006) to 639 ka in the east (Yellowstone, Wyoming; Lanphere et al. 2002). At each location along the hotspot track the rhyolitic volcanism was followed by extensive effusions of basalt lava (Greeley 1982; Godchaux and Bonnicksen 2002) and so the ‘eruptive centres’ (Bonnicksen 1982) are poorly constrained as they are buried by the younger basalt lavas (Godchaux and Bonnicksen 2002).

‘Snake River-type’ volcanism

The rhyolitic volcanism in the central Snake River Plain was sufficiently different from ‘typical’ Plinian and ignimbrite-forming rhyolitic volcanism elsewhere (deposits described in Bond and Sparks 1976; Walker 1981) that a new category of volcanism, ‘Snake River (SR)-type volcanism’ has been defined (Branney et al. 2008) with a type area that includes the inferred Bruneau-Jarbidge and Twin Falls eruptive centres (Fig. 4.1 inset). SR-type volcanism is defined by an unusual association of volcanic facies, including intensely welded and commonly lava-like, rheomorphic ignimbrites with high inferred magmatic temperatures (830-1050 °C; Honjo et al. 1992; Cathey and Nash 2004; Chapter 2), and large volume, extensive rhyolite lavas (Bonnicksen 1982b; Bonnicksen and Kauffman 1987).

SR-type fall deposits are unusually fine-grained compared with Plinian pumice fall deposits elsewhere and yet are significantly thicker than distal Plinian deposits of equivalent grain-size.

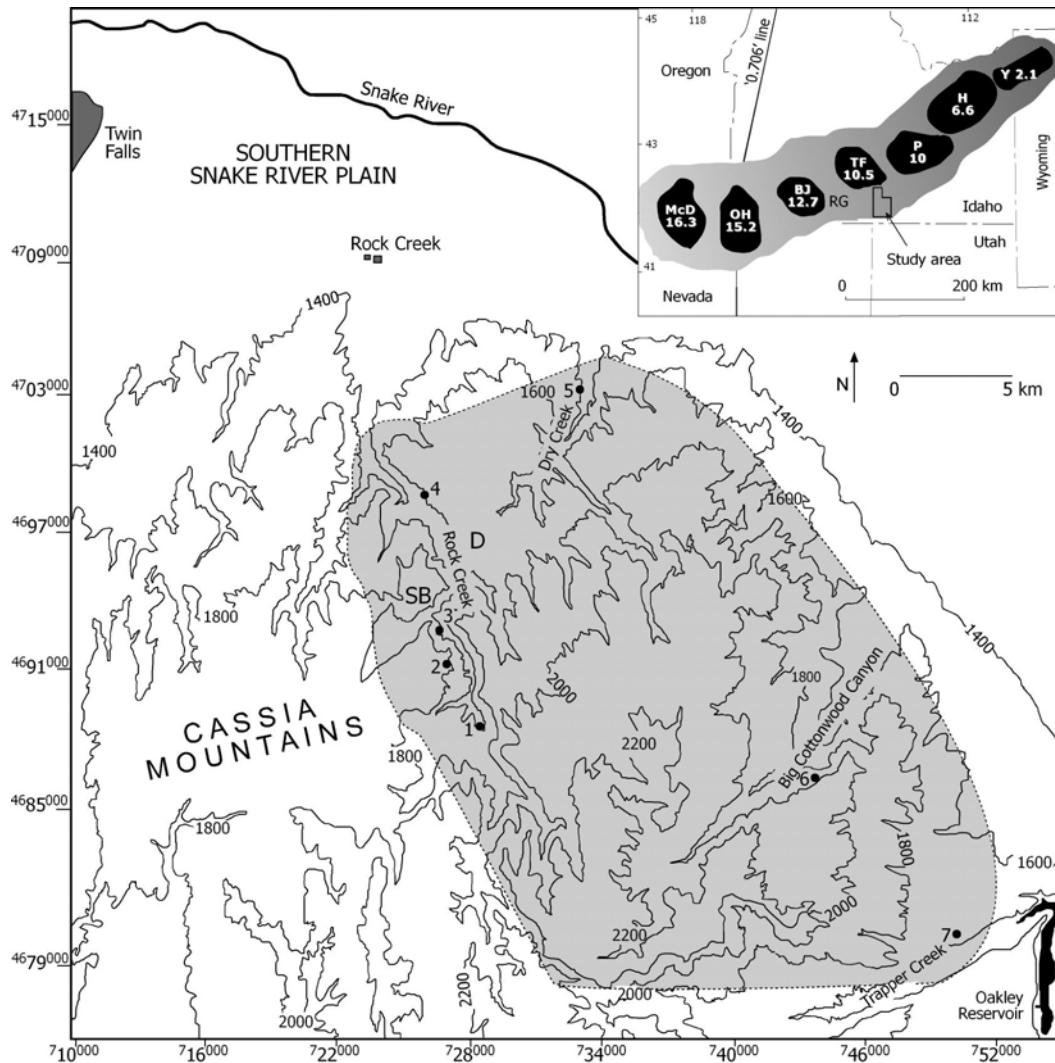


Figure 4.1 Distribution (including inferred subcrop) of the Deadeye Member (grey shading) in the Cassia Mountains. Numbers relate to the locations of logged sections (Fig. 4.6). Inset shows inferred silicic eruptive centres along the Snake River Plain with ages of onset of activity in millions of years at the centre: McD - McDermitt, OH - Owyhee Humboldt, BJ - Bruneau-Jarbridge, TF - Twin Falls, P - Picabo, H - Heise, Y - Yellowstone (after Pierce and Morgan 1992). RG is the Rogerson Graben, SB is the Steer Basin campground, the type section of the Deadeye Member and D shows the location of the Deadeye, the place name used for the member is located at D.

SR-type ignimbrites are better sorted than ignimbrites from ‘typical’ rhyolitic eruptions. Both the fall deposits and ignimbrites commonly contain few if any lithic clasts, but centimetre-scale clasts of non-vesiculated black volcanic glass are however common. Pumice lapilli are rare in SR-type deposits and both ignimbrites and the fall deposits are

dominated by ash (Branney et al. 2008). Ash aggregates (both pellets and accretionary lapilli) are common in products of Snake River-type volcanism, for example in Jackpot 6 (Andrews et al. 2008), the Wooden Shoe Butte Member (Chapter 2), Cougar Point Tuff XV and the Dry Gulch ignimbrite.

Aims

The intensely welded ignimbrites that typify Snake River-type volcanism are well-exposed at steep sided canyons and escarpments, forming cliffs. The welded ignimbrites are separated by poorly exposed slope-forming units which have hitherto received scant attention, generally being referred to as volcanoclastic sedimentary intervals (e.g. Bonnicksen and Citron 1982; Williams et al. 1990; Andrews et al. 2008).

This chapter investigates the non-welded pyroclastic deposits associated with Snake River-type volcanism, with reference to a newly discovered, non-welded ignimbrite within the Cassia Mountains. The poorly exposed nature of the deposits presents a particular challenge to interpreting the physical volcanology, for example hindering construction of isopach maps, resolution of deposit architecture and estimating volumes of individual deposits.

The Cassia Formation

The Deadeye Member is part of the Cassia Formation (Chapter 2), a Miocene succession dominated by pyroclastic units exposed in the Cassia Mountains in southern Idaho south of the Snake River Plain (Fig. 4.1). The Cassia Formation overlies the ignimbrites and sediments of the Rogerson Formation (Andrews et al. 2008; Chapter 2), which unconformably overlies Permian limestone (Williams et al. 1990; Mytton et al. 1990). The basal part of the Cassia Formation conformably overlies the Steer Basin Member (Fig. 4.2) which is equivalent to the Jackpot 7 sub-member in the Rogerson Graben (Andrews et al. 2008). The base of the Cassia Formation is formed of a series of volcanoclastic fluvio-lacustrine deposits that are overlain by the Deadeye Member (Fig 4.2). The entire

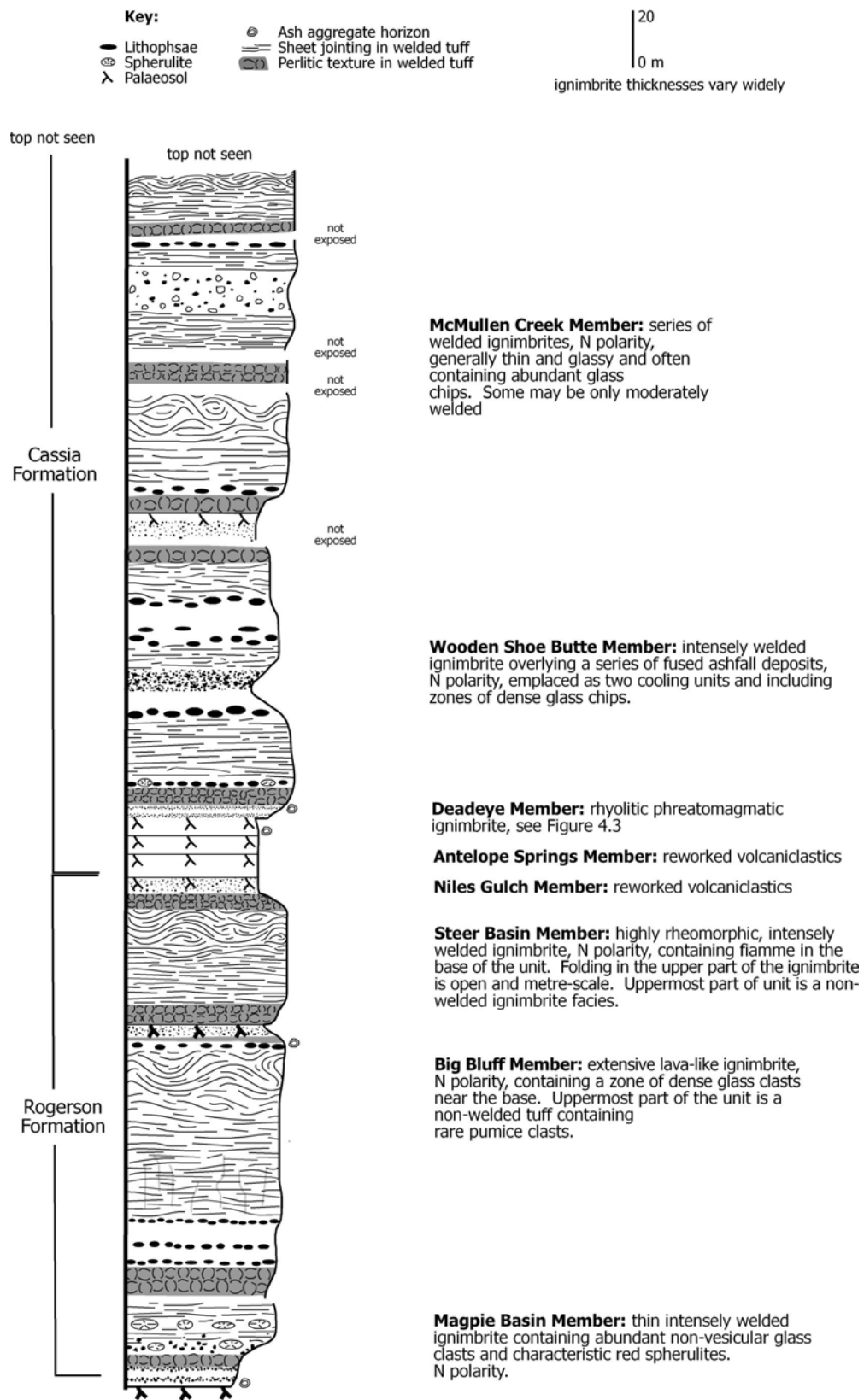


Figure 4.2 Generalised vertical section from the Cassia Mountains showing units from the Rogerson and Cassia Formations.

succession between the Steer Basin and Wooden Shoe Butte Members (Fig. 4.2) was mapped as ‘reworked volcanoclastic sediment and airfall tuff’ by Williams et al. (1990).

The Deadeye Member

The Deadeye Member (new name) lies on a palaeosol developed in sediments (Fig. 4.3). It is subdivided into three sections based on the lithofacies present in the unit. Section A is the lowest section, typically 1 m thick and composed of a series of thinly bedded deposits interpreted to be of ashfall origin. Section B is approximately 3 m thick, variably massive to cross-stratified and interpreted as the deposits of a pyroclastic density current. Overlying section B, section C is a metre thickness of parallel-bedded deposits inferred to represent fallout. At the top of section C, a strong palaeosol is developed in the top of the Deadeye Member.

Lithofacies of the Deadeye Member

The Deadeye Member exhibits several lithofacies (Table 4.1) which are distinguished on the basis of grain size, sorting, composition, sedimentary structures and geometry (partly following Sohn and Chough 1989; Brown et al. 2007). Lithofacies interpreted as sedimentary are described using sedimentological terms (e.g. sand) whereas those interpreted as pyroclastic are described using volcanic terminology (e.g. ash; White and Houghton 2006). Lithofacies codes are adapted from Branney and Kokelaar (2002).

Clast-supported pumice bedded lapilli (bpL) facies

Description

The clast-supported pumice bedded lapilli lithofacies is composed of well-sorted, centimetre-sized framework-supported pumice lapilli, abundant chips of dense black glass, large millimetre to centimetre-sized, bubble-wall glass shards and lesser amounts of euhedral sanidine crystals. Alteration is common and gives the facies a characteristic

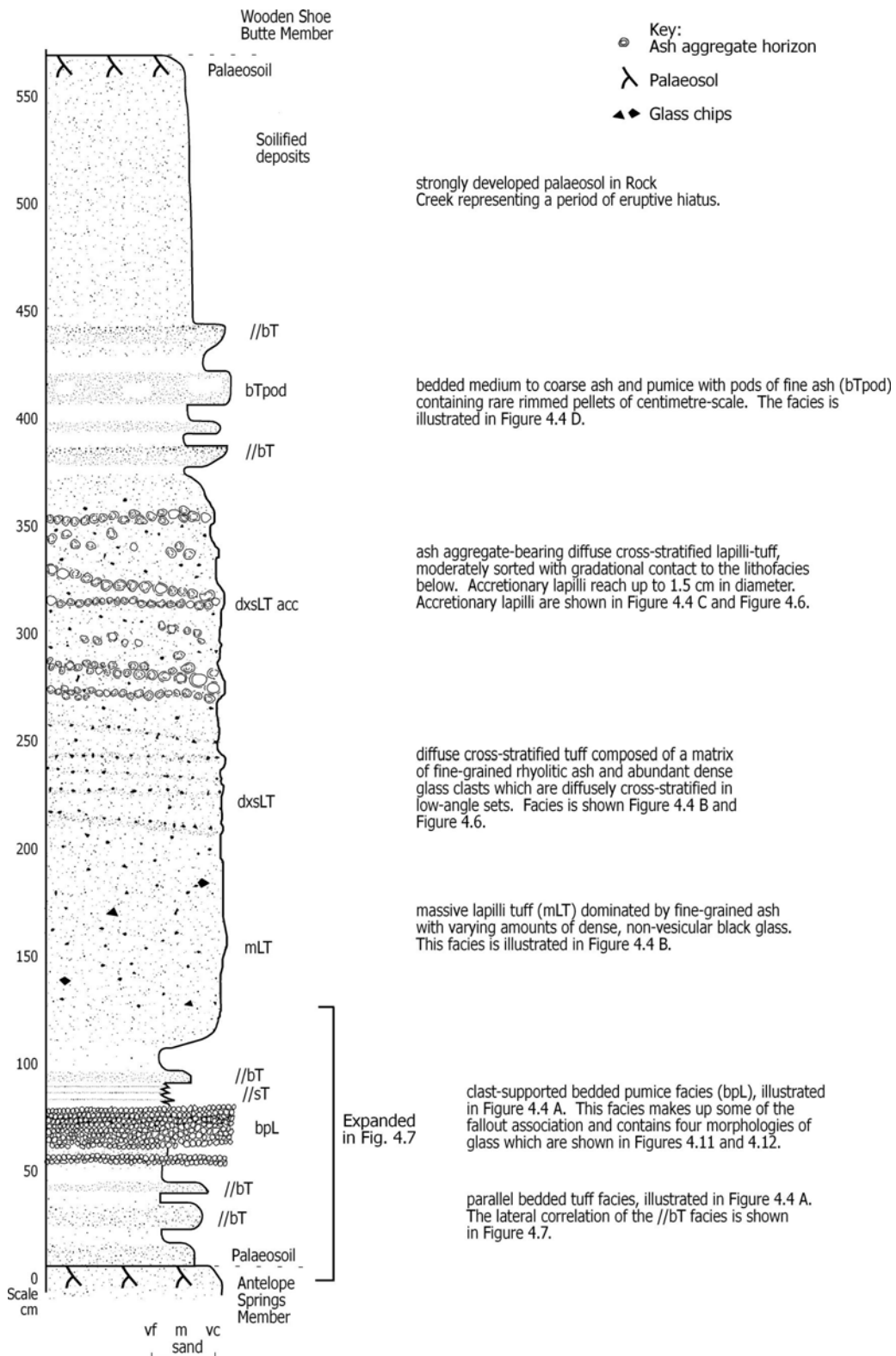


Figure 4.3 Generalised vertical section of the Deadeye Member, based on its appearance at the type locality, the Steer Basin campground (GR 11T 4684191E 725831N). The lithofacies codes shown in this figure relate to lithofacies in Table 4.1.

yellow colour and obscures the outlines of individual pumice clasts. Beds up to 20 cm thick maintain an even thickness across an exposure with sharp contacts and non-erosive bases. The bpL lithofacies contains four varieties of glass clasts (described later): black pumice, white pumice, macroscopic shards and dense black clasts. The bpL facies is interbedded with the bedded tuff (//bT) lithofacies (Fig. 4.3; Fig. 4.4 A).

Interpretation

The well-sorted, clast-supported and angular nature of the pumice lapilli suggests deposition by fallout. This is consistent with the absence of erosive bases and constant thickness across an exposure. These deposits likely correspond to an eruption of Plinian style, but restricted outcrop precludes definition on the basis of fragmentation / dispersal index (see Fig. 4.10). Similar facies are common in other volcanic provinces (e.g. Vesuvius, Barberi et al. 1989; Tenerife, Brown et al. 2003).

Parallel-bedded coarse to fine ash (//bT) lithofacies

Description

The parallel-bedded coarse to fine ash facies is composed of brown to grey, well-sorted glass shards in beds 2-15 centimetres thick. These ash shards are mostly thick walled bubble-wall remnant shards of coarse to fine ash with minor amounts of crystals of feldspar and pyroxene also present. This facies is variably normal to reverse graded and contacts between beds are dominantly sharp and non-erosional. Individual beds maintain their thickness and internal stratigraphy across an exposure. The facies appears well-sorted although lithification has prevented granulometric analysis. In Rock Creek this facies composes 75% of section A (pre-ignimbrite) of the Deadeye Member (e.g. Fig. 4.9) and is found interbedded with the bpL facies.

Interpretation

The parallel-bedded coarse to fine ash facies is interpreted as the product of fallout from an eruption column on the basis of the high degree of sorting, the maintenance of thickness of individual beds and the lack of erosional bases to beds. The facies shows no evidence of cross-stratification and in the Rock Creek area, the facies is interbedded with the clast-supported pumice bedded lapilli facies, which is also interpreted as being of fallout origin. The facies shows no evidence of reworking (e.g. scours or ripples).

Clast-supported pumice bedded lapilli with ash pods and parallel-bedded coarse to fine ash with ash pods (bpL pod and bT pod)*Description*

The clast-supported pumice bedded lapilli with ash pods and parallel-bedded coarse to fine ash with ash pods are grouped together as the main feature is the presence of pods of fine ash within the two facies previously described. Both the bpL pod and bT pod facies are parallel-bedded and well-sorted containing abundant pods of white fine ash. These pods may reach five centimetres in diameter and have shapes which range from irregular to ovoid. The pods contain no internal stratigraphy and are separated from the surrounding deposit by a sharp boundary. Rare millimetre-scale coated pellets are found in the same bed as the pods (e.g. Fig. 4.4 D). Neither the bpL pod nor bT pod facies show any evidence of having an erosive base or cross-stratification. The bpL pod and bT pod facies are both only found in section C of the Deadeye Member.

Interpretation

This facies has close similarities to the parallel-bedded coarse to fine ash facies and is similarly interpreted as ashfall. The planar geometry of this facies combined with the absence of erosional bases, supports this interpretation. However, the strongly bimodal grain size distribution of the deposit is atypical of fallout deposits. The origin of the fine-grained, well-sorted material which comprises the pods is enigmatic, it may be a fraction of

the eruption column within the main eruption cloud, or it may be the result of lofting of the pyroclastic density current adding fine ash to the atmosphere. The fine ash in the eruption column is interpreted to have aggregated under the influence of moisture, causing the fine ash particles to cling together and the aggregate to have the properties of a much larger clast. This process has been previously described from 'wet' eruptions e.g. (Walker 1981b; Talbot et al. 1994; Palladino and Taddeucci 1998). The Oruanui eruption from the Taupo volcanic zone contains a range of depositional styles from those interpreted as dry to 'wet-flushed' (Wilson 2001) and the pods of fine ash in the Deadeye Member most closely resemble features inferred to be 'moisture flushed' from the Oruanui deposits (Wilson 2001).

Although the density current deposits contain abundant ash aggregates in the form of accretionary lapilli and coated pellets, the pods are unlikely to be the result of collapse of either coated pellets or accretionary lapilli. Many of the pods are orders of magnitude larger than any ash aggregate within the density current deposit.

Deposits have been reported with local complexities which are laterally traceable into typical fallout deposits and are interpreted to represent deposition of pyroclastic material initially deposited on vegetation and subsequently deposited some time later. In the proximal deposits of the Rotongaio ash of the Taupo volcanic zone, this redeposited material is coarser pumices within a fine-grained matrix, whereas in most distal areas the redeposited material is a finer pumiceous ash (Smith and Houghton 1995). This mechanism appears unlikely for the production of the pods seen in the Deadeye Member as all the pod-bearing beds are stratigraphically above the pyroclastic density current deposits which are up to three metres in thickness. No casts of vegetation have been observed in the pyroclastic density current deposits, and vegetation taller than 3 m is rare in southern Idaho today.

Parallel-laminated fine to medium ash (//sT) facies*Description*

The parallel-laminated ash (//sT) facies is well-sorted white to grey, fine to medium ash with 1-5 millimetre thick laminations picked out by sharp changes in grain size (Fig 4.4 F). Individual laminations extend across exposures for as much as a metre without truncations or thickness changes. The facies is a volumetrically subordinate facies of the Deadeye Member (always less than 2% of any succession in Rock Creek) and occurs as units < 5 cm thick (Fig. 4.1). In Rock Creek (Fig. 4.1) it is associated with the parallel-bedded tuff facies, whereas further east in Trapper Creek the facies is associated with the scour-dominated sand (ScS) and well-sorted, fine sand and silt (bT *b*) facies.

Interpretation

In Rock Creek, where it is associated with other facies which are clearly sub-aerial, the //sT facies is interpreted as a fallout deposit with the laminations being produced by small scale changes in the eruption column. In Trapper Creek, where the laminated ash facies is associated with the scour-dominated sand, it may also represent a subaerial ashfall deposit. It may also represent a fallout deposit through shallow water that may have been periodically present in the Trapper Creek location (Perkins et al. 1995). The addition of material to shallow water by remobilisation of recently deposited fine ash by wind is not discounted. No desiccation cracks (e.g. Branney 1991), reflecting periods of drying of the substrate have been observed and an interpretation as an ashfall deposit is preferred.

Massive lapilli-tuff (mLT)*Description*

The massive lapilli-tuff lithofacies is white to grey, non-graded, and commonly forms a unit 0.5-1.5 metres thick. It is composed of well-sorted ($\sigma\phi$ 1.1-1.7; Fig. 4.5) medium to coarse ash with abundant chips of non-vesicular dense black glass up to 3 centimetres in size. These glass clasts are angular to sub-angular and form up to 5% of the lithofacies.

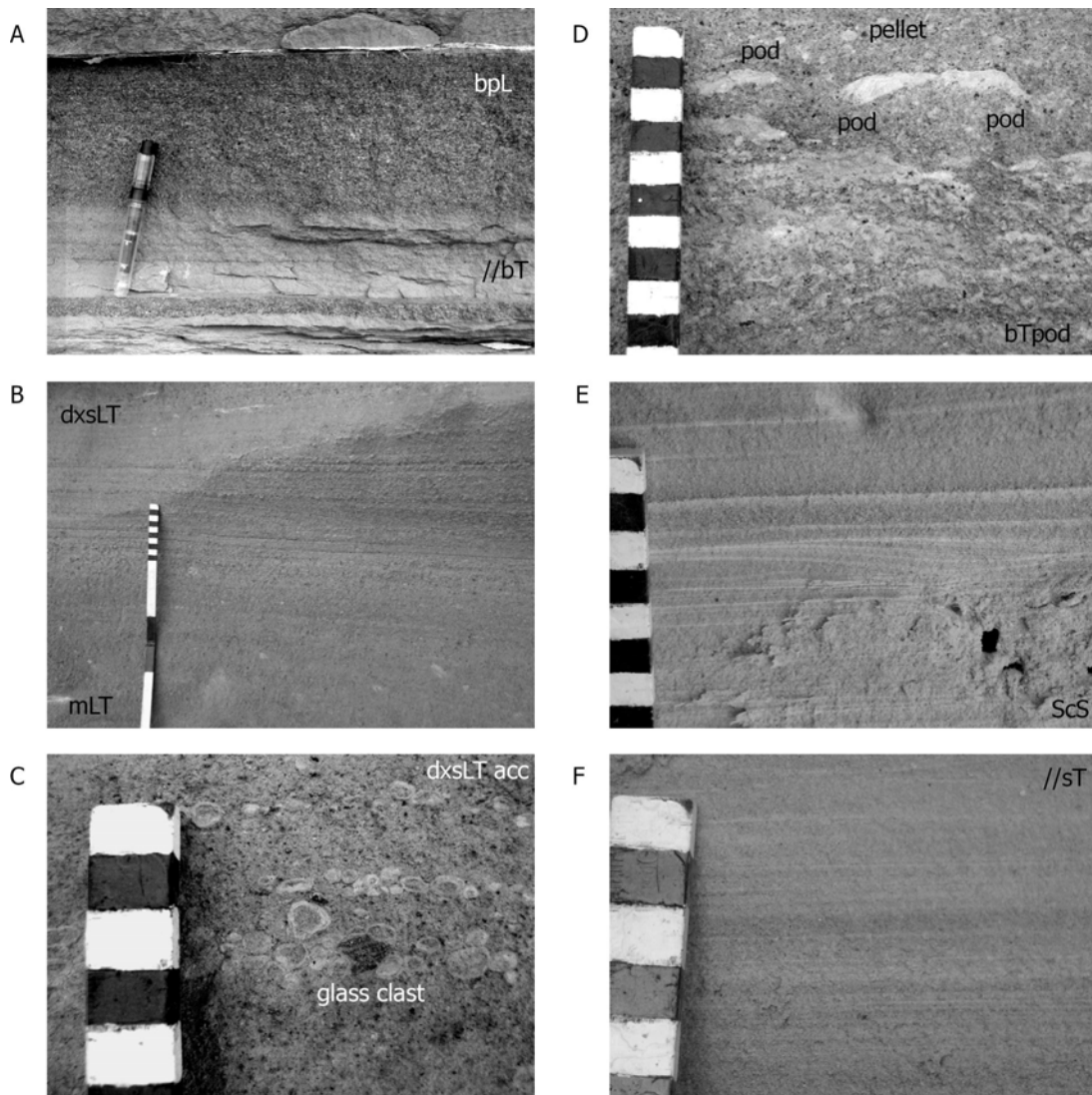


Figure 4.4 Illustrations of facies of the Deadeye Member, **A.** Parallel-bedded coarse to fine ash (//bT) and clast-supported pumice bedded lapilli (bpL) from the basal fallout succession in Rock Creek. **B.** Massive and diffusely cross-stratified tuff facies (mLT and dxsLT) in the lower part of the ignimbrite. **C.** The upper region of the ignimbrite showing the abundant accretionary lapilli and a centimetre-scale clast of dense black glass. **D.** Parallel bedded coarse to fine ash and pumice with pods of fine ash (bTpod) facies showing the size of the pods of finer grained ash within the bedded tuff. **E.** scoured sand facies (ScS), note the small scale of the structures and the fine-grained drapes on the top. **F.** Parallel-laminated fine to medium ash, clearly seen with white laminae.

No clasts of other lithologies have been observed. The lithofacies contains <3% by volume euhedral feldspar crystals up to 5 mm in length. The massive lapilli-tuff facies commonly grades upwards into diffuse cross-stratified lapilli-tuff (dxsLT) and ash aggregate-bearing

diffuse cross-stratified tuff (dxsLT acc) facies. The mLT lithofacies has a lenticular geometry and is absent in some locations (e.g. Fig 4.8).

Interpretation

Massive lapilli-tuff is interpreted as a primary pyroclastic deposit as it is dominantly composed of rhyolitic glass and overlies a series of deposits interpreted as deposited by ashfall. The presence of accretionary lapilli, higher in the deposit (e.g. Fig. 4.3) is also indicative of a pyroclastic deposit. The mLT facies represents a pyroclastic density current deposit (i.e. an ignimbrite) on the basis of the lateral, non-systematic variability in thickness and the gradational transformation into a diffuse cross-stratified facies (e.g. Fig. 4.4 B; 4.6 A). The massive nature and absence of tractional bedforms suggest deposition was from a granular fluid-based type of pyroclastic density current in which any turbulence was dampened within the lower flow-boundary zone by high particle concentrations (Branney and Kokelaar 1992; 1997; 2002). Like most SR-type ignimbrites the mLT facies of the Deadeye Member is better sorted than typical (non SR-type) ignimbrites, which have sorting of $\sigma\phi$ 2.5-3.5 (Walker 1971; Branney and Kokelaar 2002).

Diffuse cross-stratified lapilli-tuff (dxsLT)

Description

The diffuse cross-stratified lapilli-tuff facies is composed of well-sorted, white to grey, medium to coarse grained vitric ash with abundant chips of dense black glass, identical to those in the mLT facies. The thickness of the facies varies from tens of centimetres to several metres (Fig. 4.3). The stratification is typically low angle (5-10°) and is picked out by the changes in the abundance of glass chips which reach 30 vol.%. Accidental lithics of other lithologies (e.g. basalt or sedimentary clasts) are absent. Individual beds persist for tens of centimetres to metres laterally before truncation. This lithofacies grades vertically into the massive lapilli-tuff (mLT) and ash aggregate-bearing diffuse cross-stratified tuff (dxsLT acc) as shown in Figure 4.4 B.

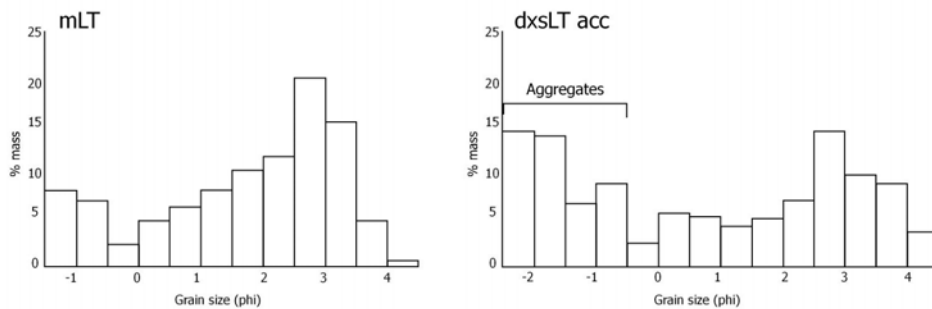
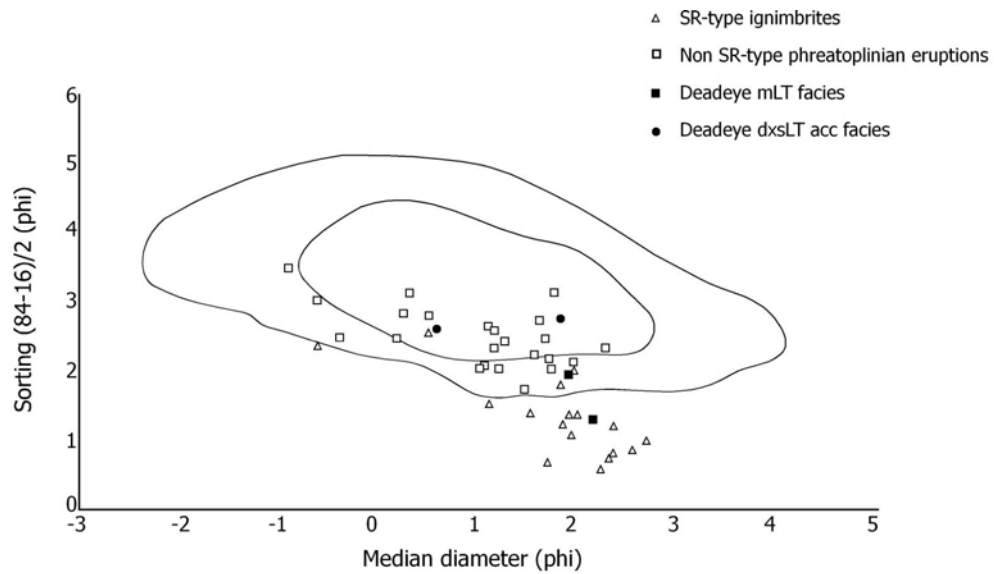


Figure 4.5 Granulometry of the Deadeye Member, showing that the massive lapilli-tuff facies is better sorted than the ash aggregate-bearing diffuse cross-stratified tuff facies due to the lack of accretionary lapilli. Data for phreatoplinian ignimbrites from elsewhere is plotted, Vesuvius (Barberi et al. 1989) and Kos Plateau Tuff (Allen and Cas 1998) are plotted on the diagram of Walker (1971) along with SR-type ignimbrites (Branney et al. 2008).

Interpretation

The gradational contact between the mLT facies and the dxsLT facies requires that the interpretation for the mLT facies be consistent with that for the dxsLT facies. The cross-

stratified nature of the deposit requires deposition from a current. The upwards facies change from massive to diffusely cross-stratified reflects a change in the properties of the flow-deposit boundary zone. Cross-stratification results from the impingement of turbulent eddies on the flow-deposit boundary (Branney and Kokelaar 2002) suggesting with time the flow boundary zone became less concentrated allowing greater influence of turbulence. The diffuse nature of the cross-stratification is the result of small-scale unsteadiness at the flow deposit boundary, which may be the result of one or more of the following processes: (1) successive surges of a pulsating current (2) periodic impingement of turbulence on the flow deposit boundary zone (3) intrinsic frictional effects due to a thickening granular flow-dominated boundary zone (Branney and Kokelaar 2002). Each of the cross-stratified layers which are reversely graded with ash-dominated bases and dense glass chips at the top, may represent the stratigraphy within the base of the Deadeye density current at various periods through the history of the current. The grain size segregation is preserved in the deposit by the fluctuations in shear stress acting on the flow deposit boundary, causing freezing of the basal grainflow layers (e.g. Branney and Kokelaar 1992; 2002).

Ash aggregate-bearing diffuse cross-stratified lapilli-tuff (dxsLT acc)

Description

The ash aggregate-bearing diffuse cross-stratified lapilli-tuff lithofacies is well-sorted ($\sigma\phi$ 2.5; Fig. 4.5) with similarities to the massive lapilli-tuff and diffuse cross-stratified lapilli-tuff facies. Abundant accretionary lapilli and coated pellets ranging from 0.3 to 1.5 cm in diameter are supported in a matrix of fine to medium ash (Fig. 4.5). Both the accretionary lapilli and the coated pellets have an unstructured core of medium to coarse ash (350-500 μm), where the core is surrounded by multiple layers of white fine (125-180 μm) ash it is termed an accretionary lapillus, where it exhibits a single coating it is termed a coated pellet. The accretionary lapilli are more abundant than the coated pellets and occur in low-angle cross-sets with the same attitude as the cross-stratification in the diffuse cross-stratified tuff facies. Ash aggregates are so abundant as to be clast supported in some layers and some show evidence of soft-state deformation. As with the massive lapilli-tuff

and the diffuse cross-stratified lapilli tuff facies, the ash aggregate-bearing cross-stratified lapilli tuff lithofacies contains some large (up to 3 cm) clasts of dense black glass, often containing euhedral crystals of feldspar.

Interpretation

The gradational contact between the dxsLT and dxsLT acc facies (Fig. 4.6) requires a consistent interpretation. The lithofacies is interpreted in a similar way to the diffuse cross-stratified tuff facies, i.e. as the deposit of a pyroclastic density current in which turbulence periodically dominated the flow-boundary zone (Branney and Kokelaar 2002). The soft-state deformation of the ash aggregates suggests that they were deposited from a cool, moist current, which allowed them to retain their moisture to the point of deposition. Recent work on Tenerife (Brown et al. 2008; Branney et al. in prep) has suggested that the different morphologies of ash aggregates reflect growth histories in differing environments. The Brown et al. (2008) model suggests that coated pellets (ash cores surrounded by a single finer-grained rim) are representative of fallout deposits (e.g. Brown and Branney 2004) whereas accretionary lapilli (those with numerous rims) are characteristic of density current deposits. The presence of both coated pellets and accretionary lapilli within the dxsLT acc facies may be indicative of a complex depositional environment. The aggregates with single rims within the deposit may suggest that the density current was either pulsatory, in which case the ash aggregates were deposited between pulses of the current and were never entrained by the current or that the coated pellets fell through a dilute current wake, which helped acquire the coating on the pellet. The accretionary lapilli are interpreted as pellets which fell into the density current closer to source and were transported for a distance, acquiring multiple rims, before being deposited. Similar deposits, of locally occurring lenses of fallout within what are primarily density current deposits are reported from Roccamonfina (Valentine and Gianetti 1995).

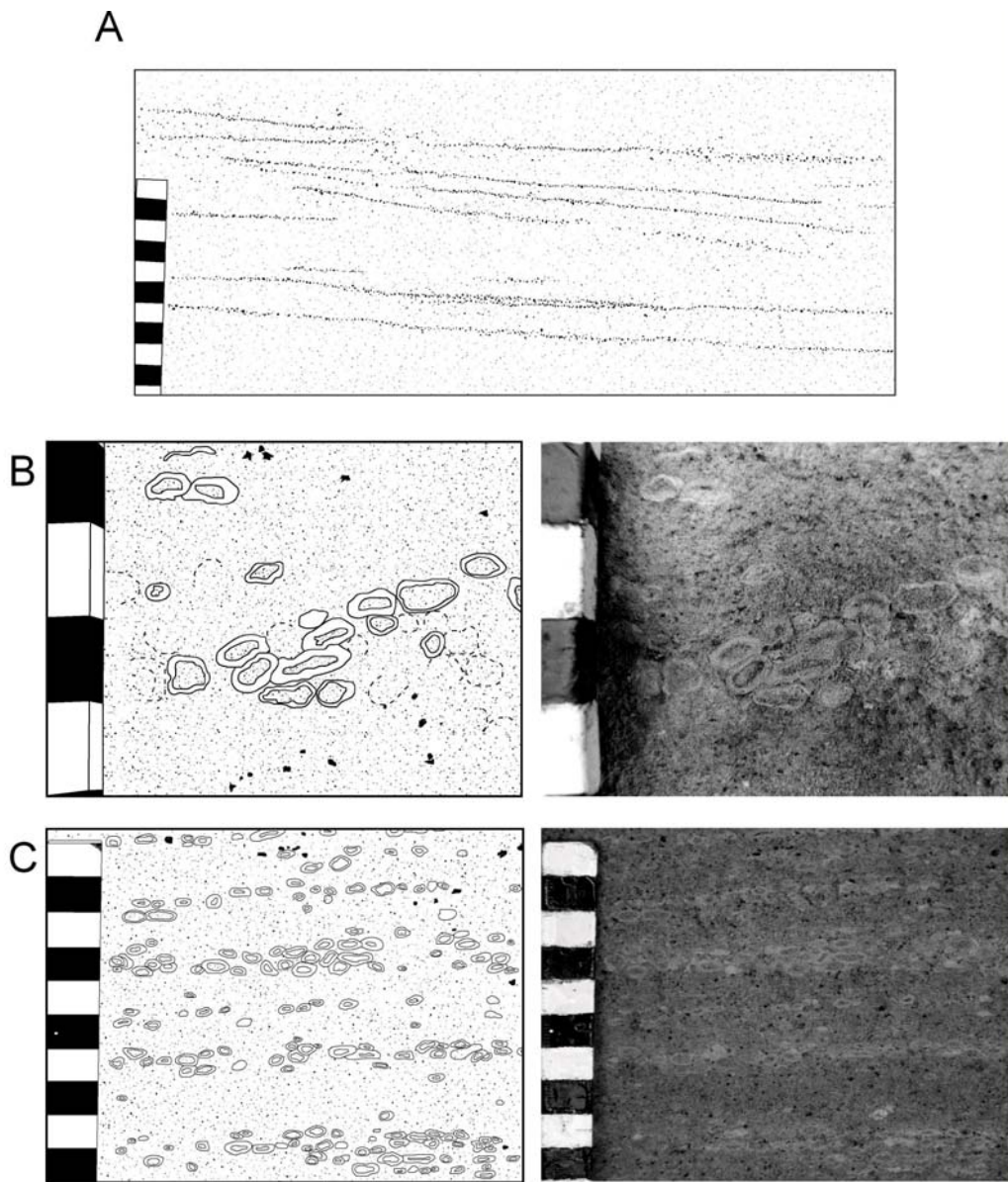


Figure 4.6 Facies of the density current deposits of the Deadeye Member. **A.** The diffuse cross-stratification in the dxsLT facies. **B.** Details of the accretionary lapilli showing soft-sediment deformation, suggesting that they were moist on deposition. **C.** Cross-stratification of the accretionary lapilli within the upper reaches of the Deadeye ignimbrite.

Scoured, fine sand and silt lithofacies (ScS)*Description*

The scoured, fine sand and silt lithofacies, is composed of well-sorted, rhyolitic glass shards and crystals. Abundant scour surfaces erode into the substrate to millimetre to centimetre depth, and have white silt drapes which are thinner than a millimetre (e.g. Fig 4.4 F). The ScS facies is found in lenticular beds which are typically centimetre-scale thickness, reaching a maximum of ten centimetres. It is only recorded in the Trapper Creek locality (Fig. 4.1) where it is found interbedded with the bedded sand of irregular thickness facies.

Interpretation

This facies is interpreted as reworking of the parallel-bedded fall deposits (bT and //sT facies) with periodic erosion, causing the scours, and periodic deposition causing the deposit to be preserved. This facies is thought to represent a series of small-scale scours and rills as seen in other areas (e.g. Branney 1991), with small, ephemeral streams being established on the new deposit surface. The suppression of bedforms is due to the high particle concentration in the streams (e.g. Leeder 1999; Fisher et al. 2008) and the fine grained material represents the last very thin (millimetre-scale) covering of the deposit allowing the finest sediment to settle. It would be difficult to produce such an evenly deposited and fine-grained drape under sub-aerial conditions with reworking by aeolian processes and none of the scours show reverse grading as is common in aeolian ripples (Anderson and Bunas 1993).

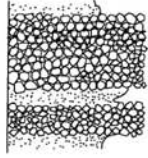
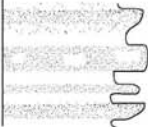
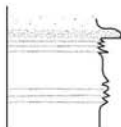
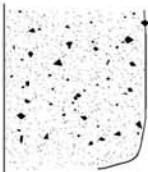
Bedded sand of irregular thickness (bS)*Description*

The bedded sand of irregular thickness facies is dominated by well-sorted, medium to coarse sand composed of brown to grey volcanic glass fragments. Grading within this facies may be normal or reverse and contacts are variably sharp and gradational. This

facies shows thickness variations across a single exposure with low angle truncations which may only be observed with good lateral continuity of outcrop. This facies is very similar to the bT facies in terms of composition and bed thickness and where continuity of outcrop is poor, the two facies may be indistinguishable.

Interpretation

The close similarities between the bedded sand of irregular thickness facies and the parallel-bedded coarse to fine ash facies suggest that these two facies are related, however the variations in thickness seen in the bS facies cannot be reconciled with an origin by fallout. These thickness variations range up to 25% of the thickness of that bed, although commonly the variation is less. Massive deposits may be produced by a variety of depositional processes; turbidity currents commonly produce massive deposits and are often found in areas of volcanic activity (Bouma 1962; Fisher 1984; Kneller and Branney 1995). The origins of turbidity currents may be slope instabilities (e.g. Masson 1996), direct input of pyroclastic density currents to marine or lacustrine environments (Trofimovs et al. 2006) or by vertical density currents (e.g. Manville and Wilson 2004). The thin nature of the beds would be consistent with turbidite deposits in distal areas although distal volcanoclastic turbidites have an overall tendency to a fining upwards succession and abundant ripples (e.g. Bouma 1962; Schneider et al. 2001). An alternative possibility is that the reworking of the parallel-bedded coarse to fine ash facies occurred by a series of hyperconcentrated flows (HCF), which are high particle concentration flows (20-60% e.g. Lavigne and Suwa 2004; 40-70% e.g. Mulder and Alexander 2001 or 40-80% e.g. Smith 1986). The massive to crudely stratified nature, scale and thickness changes of individual beds are all consistent with deposition from HCF. Although some hyperconcentrated flow deposits are poorly sorted (e.g. Kataoka and Nakajo 2002), the well-sorted nature of the deposits reflects the nature of the available material, dominantly ash which had already been well-sorted due to initial deposition as fallout. The variable nature of the grading seen in the bS facies is also consistent with hyperconcentrated flow deposits (Giordano et al. 2002; Svendsen et al. 2003). In the Trapper Creek succession (Fig. 4.1; Fig 4.8) the sub-ignimbrite succession (comprising the bS, ScS and //sT facies) reaches at least 2.8 m

Description	Interpretation	
	<p>Clast-supported pumice lapilli (bpL) Well sorted, centimetre-scale framework supported pumice clasts. This facies contains four glass morphologies, macroscopic shards, dense glass clasts, white pumice (which comprises the majority of the facies) and black pumice. The black pumice often is a golden colour. This facies is commonly altered to a yellow clay.</p>	<p>Deposition by pumice fallout indicated by clast support, sorting and laterally consistent preservation of bed thickness (e.g. Fig. 4.4 A).</p>
	<p>Parallel-bedded fine to coarse ash (//bT) Well sorted ash in massive beds Dominated by bubble wall-type with rare crystals and small chips of black glass. Individual beds reach up to ten centimetres in thickness.</p>	<p>Interpreted as an ashfall deposit based on the high degree of sorting and lateral preservation of thickness along an exposure. Grading within this facies is taken to represent the waxing and waning of the eruption column with time. Interbedded with bpL facies (e.g. Fig. 4.4 A)</p>
	<p>Clast-supported pumice bedded lapilli with ash pods and parallel-bedded coarse to fine ash with pods of fine ash (bpL pod & bT pod) Well sorted, coarse ash to pumice clasts which are found in parallel-bedded layers. The facies contains irregularly shaped pods of white, fine to medium ash within it. The facies also contains rare rimmed pellets.</p>	<p>This facies is interpreted as the product of fallout from an eruption column during moist conditions. The pods of finer white ash are interpreted as aggregation of the finer material in the column enhanced by moisture. The 'mud clumps' then behave as a single large particle and fall under gravity. The irregular shapes are produced as the clumps shatter on impact.</p>
	<p>Parallel-laminated fine to medium ash (//sT) A volumetrically subordinate facies of the Deadeye Member, the parallel-laminated ash facies is well sorted and composed of medium and fine grained ash. The laminae are millimetre scale, picked out by changes in grain size. The laminae are parallel throughout an outcrop and are never seen to truncate other laminae. This facies is < 5 cm in thickness. This facies may be found associated with both the bT facies and the ScS facies.</p>	<p>Ashfall deposit, deposited during quiescent period with small scale pulses in the column reflected in lamination, or in shallow quiet water preserving laminations.</p>
	<p>Massive lapilli-tuff (mLT) White to grey, well sorted, massive lapilli-tuff. Medium to coarse ash containing some large c. 3 cm chips of dense black volcanic glass. Clasts of other lithologies are absent. Thickness ranges from 0.5 - 1.5 m. Strongly associated with dxsLT and dxsLT acc with common intergradations.</p>	<p>Deposit of a granular fluid-based pyroclastic density current at a fluid escape dominated boundary (sensu Branney and Kokelaar 2002). Escaping fluid from the recently deposited ignimbrite supports a high concentration of grains in the flow boundary zone sufficient to suppress turbulence and inhibit the development of stratification during deposition.</p>

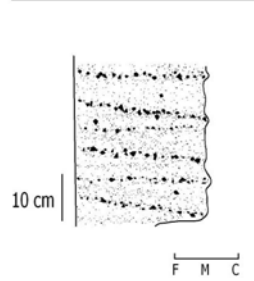
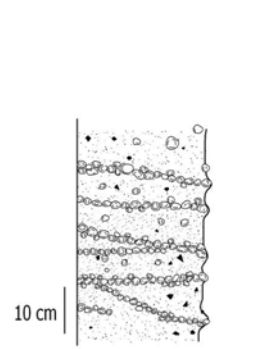
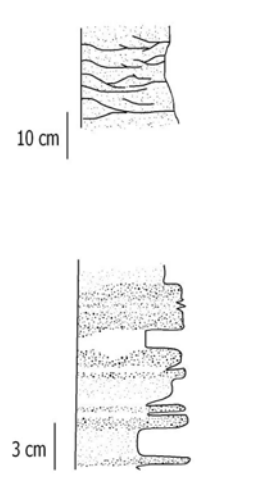
	Description	Interpretation
	<p>Diffuse cross-stratified lapilli-tuff (dxs LT) White to grey, well sorted, medium to coarse ash containing abundant chips of dense black glass, but lacking lithics of any other lithology. The glass chips pick out low-angle cross-stratification (Fig. 4.6 A). Thickness ranges between 1 and 2 m. Associated with mLT and dxsLT acc.</p>	<p>Deposit of a pyroclastic density current, with periodic impingement of turbulence on the flow boundary. The diffuse nature of the cross-stratification reflects small-scale unsteadiness at the flow boundary.</p>
	<p>Ash aggregate-bearing diffuse cross-stratified lapilli-tuff (dxsLT acc) Well to moderately sorted, similar to the mLT and dxsLT facies but contains a variety of ash aggregates including accretionary lapilli with multiple coatings or rimmed pellets with a single coating of finer, white ash around a core of medium ash. The aggregates are in low-angle cross-stratified layers and are locally clast-supported; some are deformed. Dense glass chips are also present in this facies.</p>	<p>Same overall interpretation as the dxsLT facies but with the addition of ash aggregates. The ash aggregates are a hybrid of accretionary lapilli and rimmed pellets suggesting a variety of processes occurring simultaneously. The deformation of the aggregates suggests they were moist upon emplacement and the current was cool.</p>
	<p>Scour-dominated fine sand and silt (ScS) Well-sorted fine sand to silt grade rhyolitic material containing abundant scours surfaces which are typically centimetre scale and commonly have drapes composed of fine white silt. This facies is rarely seen in the Deadeye member, only in the Trapper Creek outcrop.</p>	<p>Volcaniclastic sediment derived from reworking of fine grained rhyolitic material, in shallow quiet water conditions indicated by the lack of wave ripples.</p>
	<p>Bedded sand of irregular thickness (bS) Well-sorted sand grade deposits with normal or reverse grading present. Very similar in appearance to the //bT facies but showing variations in thickness across a single exposure. Where exposure is not sufficiently continuous this facies may be indistinguishable from the //bT facies.</p>	<p>Reworking of the bT facies involving water producing hyperconcentrated flow deposits. The well-sorted nature of the facies reflects the material being reworked was initially well-sorted. Associated with the ScS facies and only recorded in Trapper Creek locality.</p>

Table 4.1 Summary of the lithofacies recorded in the Deadeye Member.

thickness (the base of the succession is not exposed) which is considerably thicker than the next closest locality which has a sub-ignimbrite succession of 1.2 m (Fig. 4.10). The limited data available from the isopach map (Fig. 4.10) suggests that this amount of thickening is not a primary feature, which is consistent with the interpretation of the majority of the Trapper Creek succession as representing reworked volcanoclastic deposits. Distinguishing between primary and reworked volcanoclastic deposits is often problematic (e.g. Branney 1991; Manville and Wilson 2004; Sohn et al. 2008) and how common this lithofacies is in the Trapper Creek section is difficult to quantify for the reasons given above. The interpretation of this facies is based on its associated with other lithofacies which represent reworking of primary pyroclastic material particularly the interbedding of the bS lithofacies with the ScS lithofacies at Trapper Creek.

Lithofacies associations

Associations between the lithofacies of the Deadeye Member (Figs. 4.3 and 4.4 and Table 4.1) assist in interpretations of processes and environments.

Fallout deposit association //bT, bpL, //sT, //bT pod ± bpL pod

The massive to parallel-bedded coarse to fine ash (//bT), clast supported pumice (bpL), parallel laminated ash (//sT) and both pod-bearing facies (//bT pod and bpL pod) comprise the fall deposit association (Fig. 4.7). The //bT, bpL and //sT facies are commonly found interbedded with each other in section A of the Deadeye Member. The fall deposit association is also seen above the density current deposit of the Deadeye Member (section C) where the facies containing the pods of ash may be present. This association is termed fallout because all the facies exhibit features typical of fallout deposits e.g. parallel-bedding, maintenance of grain size and thickness, a good degree of sorting and a lack of erosional scours.

Pyroclastic density current deposit association mLT, dxsLT, dxsLT acc

The mLT, dxsLT and dxsLT acc facies are intergradational. The change in facies in the pyroclastic density current deposit association (PDCDA) represents the changing conditions in the pyroclastic density current through time and space. The massive lapilli-tuff facies represents a granular fluid-based current whereby the concentration of grains dampened the effect of turbulence to such a degree that massive deposits resulted (Branney and Kokelaar 2002). The gradational transformation to a diffusely cross-stratified lapilli tuff represents the intermittent influence of turbulence on the fluid boundary layer, giving the deposit its diffuse characteristics. This upwards change in facies could be the result of an increase in unsteadiness of the current, which allowed turbulence to variably influence the flow boundary zone, or a decrease in particle concentration in the current which would allow a fixed degree of turbulence to have a greater effect on depositional facies (Branney and Kokelaar 2002). The appearance of ash aggregates in the upper reaches of this association is a common feature of pyroclastic deposits (e.g. Cole and Scarpati 1993; Wilson 2001; Brown and Branney 2004; Brown et al. 2008). The lower part of the pyroclastic density current deposits, contain no ash aggregates, taken as reflecting deposition occurring from the density current (to give the mLT and dxsLT facies) occurring in the time taken for the ash to aggregate in the atmosphere. The ash pellets then fall into the density current where they are inferred to acquire their fine-grained rims prior to deposition (Brown and Branney 2004). The deformation of the accretionary lapilli suggests that the pyroclastic density current into which the pellets fell was not sufficiently hot to cause the lapilli to dry and harden. The dxsLT acc facies is interpreted in the same way as the dxsLT facies with periodic influence of turbulence on the flow boundary zone. The combination of coated pellets and accretionary lapilli in a single deposit is unusual and may reflect a pulsating current whereby the coated pellets were deposited primarily during the period between pulses of the current. Alternatively the pellets could have fallen through the wake of a very dilute current with little influence of the current on the morphology of the aggregate.

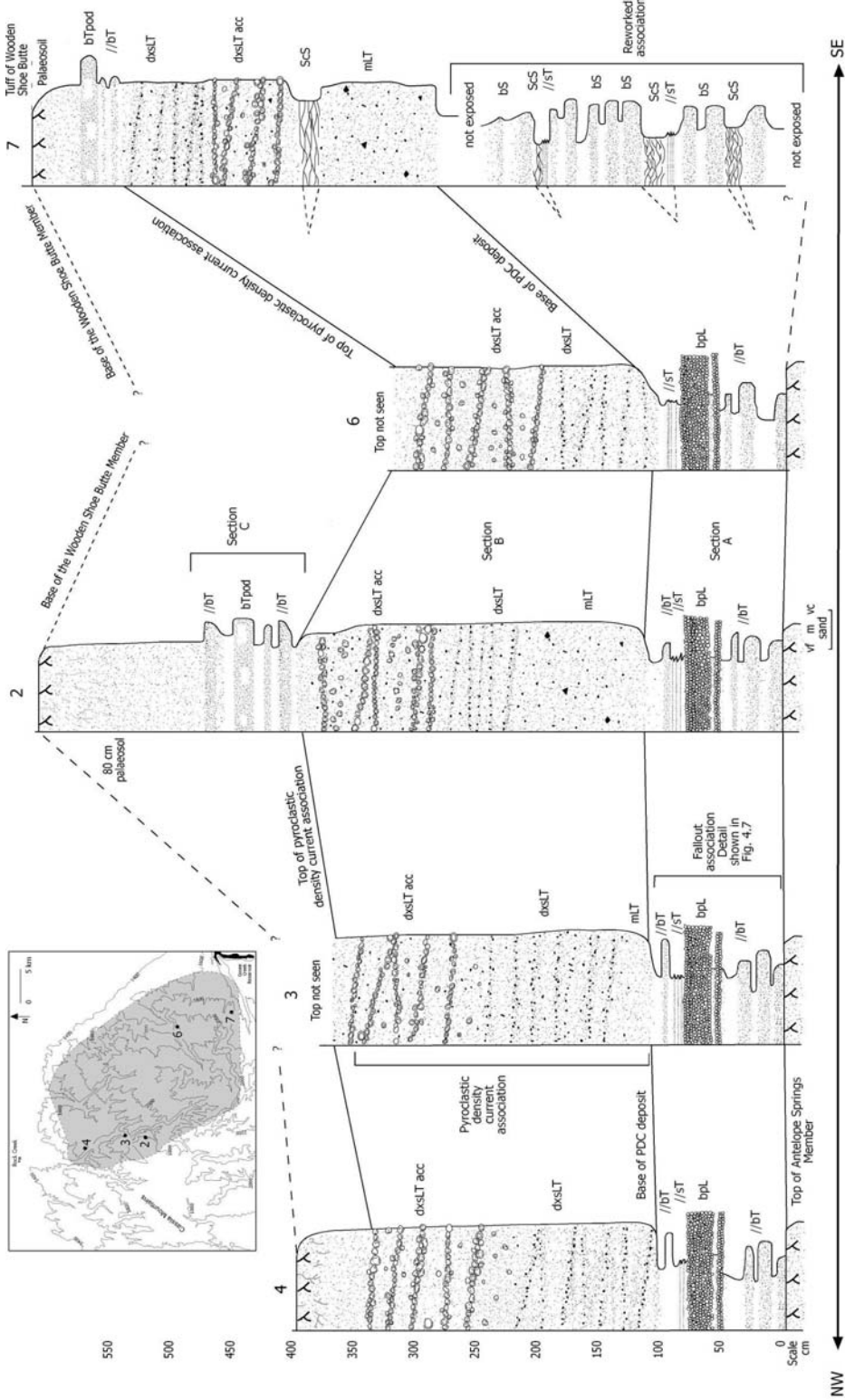


Figure 4.8 Fence diagram showing the change in the proportion of facies in the Deadeye Member at different locations. Trapper Creek has a clearly different succession than the rest of the locations, reflecting different depositional conditions in that locality.

Reworked association ScS and bS

An association of the ScS and bS facies is observed only in the Trapper Creek region (location 7; Fig. 4.1). This association is dominated by lithofacies which are interpreted as not being of primary volcanic origin, and it is named the reworked association. Trapper Creek contains reworked deposits, tuffaceous shale and diatom-bearing deposits (Perkins et al. 1995), suggesting the presence, at least periodically, of a lake during the Miocene. Separating the Deadeye Member from the overlying Wooden Shoe Butte Member is a well-developed palaeosol containing calcified rootlets, indicating that periodic drying occurred. Even during these dry periods, significant reworking of the primary Deadeye deposits may have occurred through fluvial or mass-flow processes. The pre-ignimbrite fallout succession is much thicker at Trapper Creek than would be expected for this location (Figs. 4.8 and 4.9) considering the next closest succession in Big Cottonwood Canyon is less than half as thick (>2.5 m at Trapper Creek to 1.18 m). This indicates that Trapper Creek was a local depocentre with sedimentary input (e.g. bS and ScS facies) thickening the succession. Big Cottonwood Canyon was separated from Trapper Creek by a palaeotopographic high which would have allowed the presence of different depositional environments in these two locations. The proportion of facies pre-ignimbrite in the Deadeye Member is shown in Figure 4.9 and for the member as whole in Figure 4.10.

Source of the Deadeye Member

As with most of the ignimbrites in the central Snake River Plain, the source area of the Deadeye Member is not exposed. None of the lithofacies associated with the Deadeye Member are indicative of proximal areas; e.g. large lithic clasts (e.g. Pittari et al. 2006), well-developed cross-bedding (e.g. Rowley et al. 1985 Mount St. Helens), impact sags resulting from ballistically emplaced blocks (e.g. Pfeiffer 2001; Geshi et al. 2002). Isopachs of the pumice-lapilli fall deposit in the Deadeye Member (Figs. 4.7 and 4.11) tentatively suggest an eruption source somewhere within the Snake River Plain to the north east of the Cassia Mountains, although the data are insufficient to confirm this. As shown in Figure 4.11, the prevailing wind direction during the Miocene was westerly (Rose et al.

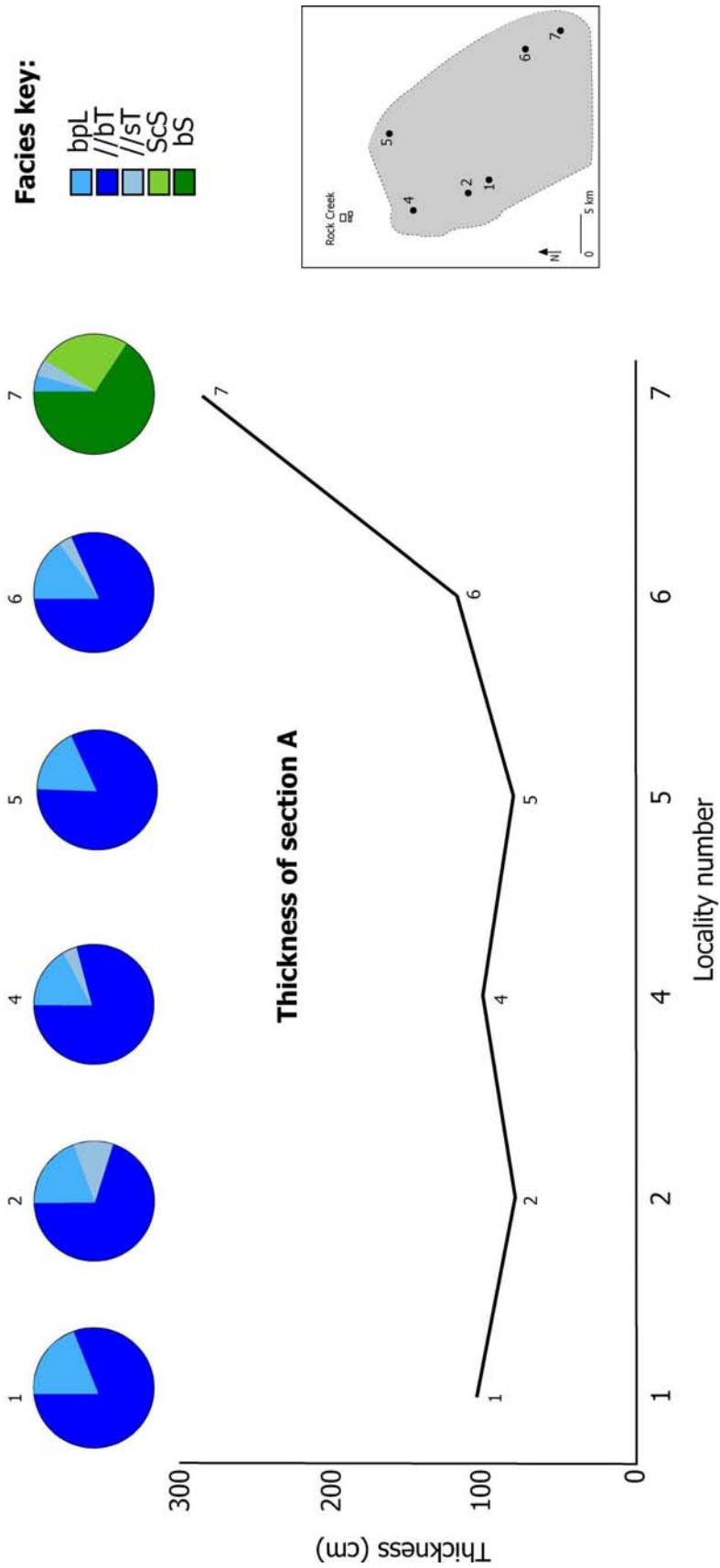


Figure 4.9 Proportion of facies in section A of the Deadeye Member and the thickness of the pre-ignimbrite stratigraphy at each of the localities. Inset shows the location of the sections (Fig. 4.1). The blue coloured facies represent the fallout association and the green coloured facies represent the reworked association. At Trapper Creek, the bS facies may be over-estimated due to the difficulty in distinguishing between the bS and //bT facies without good exposure, given the association at Trapper Creek with other reworked facies it is interpreted as the bS facies rather than //bT facies.

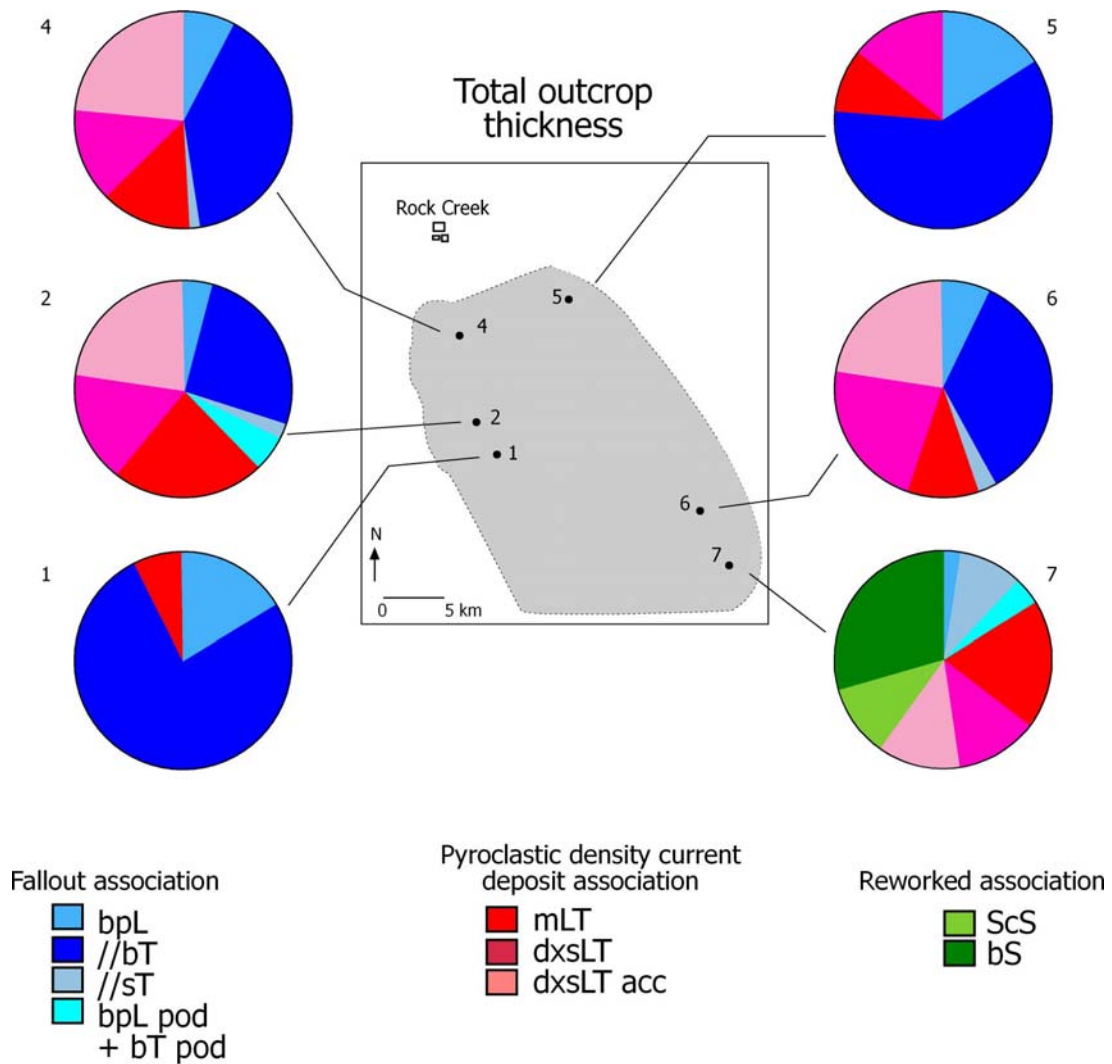


Figure 4.10 Proportion of facies at each locality for the Deadeye Member as a whole. The succession at Trapper Creek (locality 7) shows the abundance of reworked material. Inset shows the distribution of the localities (Fig. 4.1). The proportions of the facies at each location may be slightly misleading as only localities 2, 4 and 5 have exposed palaeosols at their upper and lower contacts.

2003). This is consistent with a source to the north of Rock Creek for the Deadeye Member, a source east or west of Rock Creek is possible, but is considered less likely because nothing is exposed to the east or west of the Cassia Mountains that is suggestive of an eruptive centre.

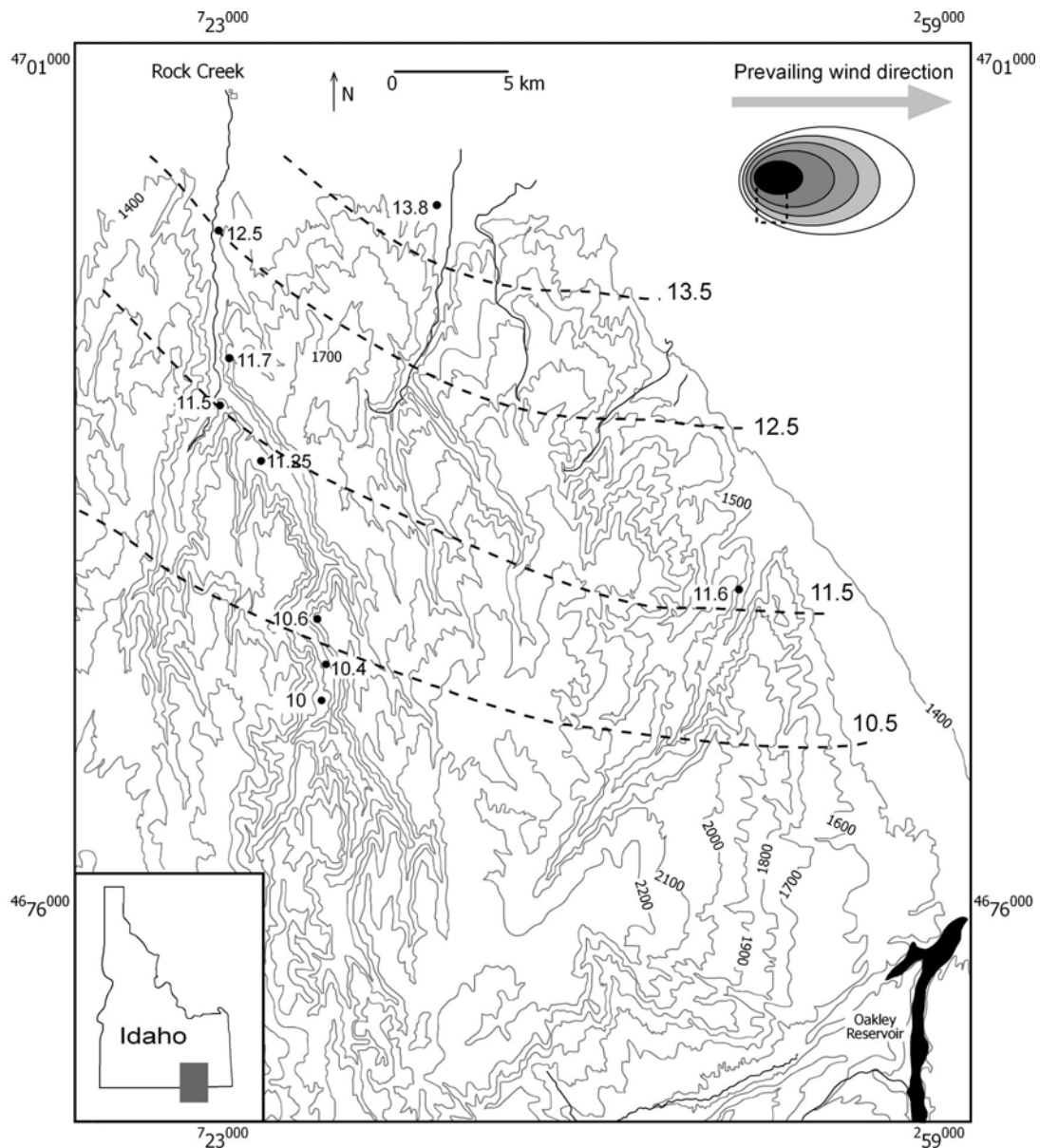


Figure 4.11 Partial isopach map of the coarse pumice fall layer of the Deadeye Member (Fig. 4.7), suggesting that either the source of the eruption or the dispersal axis was to the north of the Cassia Mountains, in the Twin Falls area. This is consistent with the Twin Falls eruptive centre being the source of the rhyolitic ignimbrites in the Cassia Mountains, as suggested by McCurry et al. (1996). The prevailing wind direction is from Rose et al. (2003).

Volume of the Deadeye Member

Using the typical 5 m thickness and the known distribution of 255 km², gives a minimum volume of 1.3 km³ for the Deadeye Member. It is possible that the erupted volume was

much larger, given that the unit is only exposed within a limited area, no intracaldera deposits are known and erosion of the non-welded deposit was likely. Within the Rogerson Graben to the west of the Cassia Mountains a sequence of reworked volcanoclastic deposits are found in a position stratigraphically equivalent to the Deadeye Member. The volcanoclastic deposits are located above the 10.44 ± 0.13 Ma Rabbit Springs Member in the Rogerson Graben (Andrews et al. 2008; Bonnichsen et al. 2008), however no primary pyroclastic deposits are present in this section, and it cannot be determined whether the reworked material was originally from the Deadeye eruption.

In terms of deposit architecture, the Plinian bed decreases in thickness to the south in the Cassia Mountains by approximately 30% of their initial thickness over a distance of > 10 km; more consistent with a sheet-like deposit geometry than a cone-like geometry. A sheet-like geometry would be consistent with a significantly larger volume for the Deadeye Member than that proposed here.

Geochemistry

Because the Deadeye Member contrasts in appearance to the other Snake River-type ignimbrites (e.g. non-welded, diffusely cross-stratified, fine-grained) whole rock chemistry and electron microprobe analyses were carried out to determine whether the Deadeye Member is chemically similar to other SR-type ignimbrites. The methodology for whole rock chemical analysis is described in Chapter 2.

Whole Rock Chemistry results

The Deadeye Member is a typical Snake River metaluminous rhyolite, whole rock chemistry of the Deadeye Member and other SR-type ignimbrites from the Cassia Mountain Group is shown in Table 4.2. It has high concentrations of TiO_2 , MgO and Fe_2O_3 and affinities with A-type granites (c.f. Bonnichsen and Citron, 1982; Cathey and Nash 2004; Andrews et al. 2008; Chapter 2).

Sample Name	Big Bluff Member Basal vitrophyre	Steer Basin Member Basal vitrophyre	Deadeye Fall deposit	Deadeye Ignimbrite	Deadeye Ignimbrite	Deadeye Ignimbrite	Wooden Shoe Butte Member Basal vitrophyre
	TBB	BVSB	PJFAS11	TCPU8 PJ	PJI1	TWSBBV	
SiO ₂	71.99	70.60	68.03	69.54	68.67	71.18	
TiO ₂	0.38	0.59	0.67	0.65	0.76	0.51	
Al ₂ O ₃	11.76	12.09	12.79	12.44	12.93	12.03	
Fe ₂ O ₃	3.10	3.89	4.98	3.73	4.67	3.53	
MnO	0.05	0.06	0.05	0.03	0.06	0.05	
MgO	0.14	0.40	0.35	0.12	0.13	0.39	
CaO	1.17	1.85	1.63	1.45	1.53	1.97	
Na ₂ O	3.14	2.57	1.18	2.05	1.74	2.79	
K ₂ O	5.795	6.29	4.76	5.31	5.41	6.09	
P ₂ O ₅	0.04	0.09	0.09	0.09	0.10	0.07	
Total	99.74	100.26	100.43	99.96	99.97	100.65	
L.O.I.	2.19	1.89	5.91	4.54	3.97	2.05	
Nb	53	43	51	43	47	44	
Zr	574	559	656	597	631	524	
Sr	59	92	92	84	89	88	
Y	81	67	63	64	68	66	
Rb	200	192	237	183	195	194	
Mo	3	4	3	4	3	3	
U	6	6	7	7	8	7	
Th	37	36	38	30	33	37	
Pb	29	24	22	26	28	25	
Cu	n.d.	n.d.	1.3	n.d.	n.d.	n.d.	
Ga	22	21	21	19	20	20	
Zn	79	62	72	61	68	54	
La	88	76	90	87	86	78	
Ce	169	145	164	167	170	145	
Nd	71	61	77	45	45	62	
Cs	2	1	5	n.d.	n.d.	5	
Ba	1189	1193	1210	1099	1114	1088	
Co	6	6	9	1	2	6	
Sc	6	6	7	8	9	4	
V	5	16	22	19	20	11	

Table 4.2 Whole rock chemical data from the Deadeye Member and enclosing units from the Cassia Mountains. The Deadeye Member, despite having a vastly different appearance to the other rhyolites in the area has similar whole rock chemistry.

Multiple glass populations

The pumice-lapilli fall deposits (bpL) within the lower parts of the Deadeye Member contain four visually distinct populations of glass: white pumice, black pumice, macroscopic shards and non-vesicular clasts. In order to determine whether these were chemically distinct, and which may be juvenile, the different populations were hand-picked, cleaned using deionised water and made into polished thin section for analysis using a JEOL JXA-8600S electron microprobe at the Geology Department of the University of Leicester. The methodology for analysing glass on the microprobe is the same as that used in Chapter 2.

White pumice population

Description

The white pumice population contains clasts 2-10 mm in diameter of microvesicular glass with a pearly lustre and containing abundant, mostly lineated, microvesicles. Some original clast outlines have been obscured by alteration; others can be seen in thin section (Fig. 4.12 A). Microvesicle walls are thin (Fig. 4.13 A), typically in the order of tens of micrometers ($< 50 \mu\text{m}$), and the vesicularity is typical of pumice in rhyolitic Plinian deposits elsewhere (e.g. Vesuvius, Barberi et al. 1989). There is a wide range of SiO_2 (74.4-77.4 wt.%), FeO (1.63-4.03 wt.%) and TiO_2 (0.28-0.44 wt.%). The average abundances of Na_2O (1.67 wt.%) and K_2O (6.16 wt.%) are similar to the surrounding welded ignimbrites in the Cassia Mountains (Fig. 4.14). Using the aluminosity index of molar $\text{Al} / (\text{Ca} + \text{Na} + \text{K})$, the white pumice population span the range of metaluminous to peraluminous (Fig. 4.15 A).

Interpretation

The greater scatter in the glass compositions for the white pumice population may suggest either 1) that the white pumice population is more compositionally heterogeneous than the macroscopic shard population or 2) the pumiceous morphology has undergone a greater degree of alteration than the macroscopic shard population. The range of aluminosity (Fig.

4.15 A) indicates that the white pumice population has undergone sodium exchange, with hydration of the glass causing Na^+ to be exchanged for H^+ (e.g. Aramaki and Lipman 1965). The electron microprobe methodology was designed to reduce volatilisation of sodium, so the sodium exchange likely occurred prior to sampling. Sodium exchange would be promoted by the large surface area of the pumiceous population.

The microvesicular nature of this pumice may reflect a lower eruptive temperature than the macroscopic shard population, because such textures can be promoted when high viscosity prevents coalescence of bubbles; and viscosity of rhyolites is strongly temperature dependent (e.g. Murase and McBirney 1973). The multiple glass populations are present in a fallout deposit which appears to be of Plinian style. The abundance of the white pumice population in this Plinian deposit suggests that it is juvenile as most distal Plinian deposits are dominated by juvenile material with a sub-ordinate lithic component.

Black pumice population

Description

This pumice population is dominantly black, but varies to brown and bronze. It has a microvesicularity broadly similar to the white pumice and both pumice morphologies can commonly be found inter-mingled on a single clast. The ranges of SiO_2 (73.3-78.6 wt.%), CaO (0.37-1.04 wt.%) TiO_2 (0.28-0.43) and FeO (1.29-4.69 wt.%) are similar to those of the white pumice population (Fig. 4.14 B). The black pumice population spans a similar range of aluminosity (0.96-1.35) to that seen in the white pumice population (Fig. 4.15 A).

Interpretation

As with the white pumice population, the black pumice is similar to the surrounding welded ignimbrites in terms of major element chemistry (Fig 4.14). The black pumice has a spread of data similar to the white pumice population, which is also attributed to alteration due to its large surface area. Given the similarities in appearance and geochemistry between the

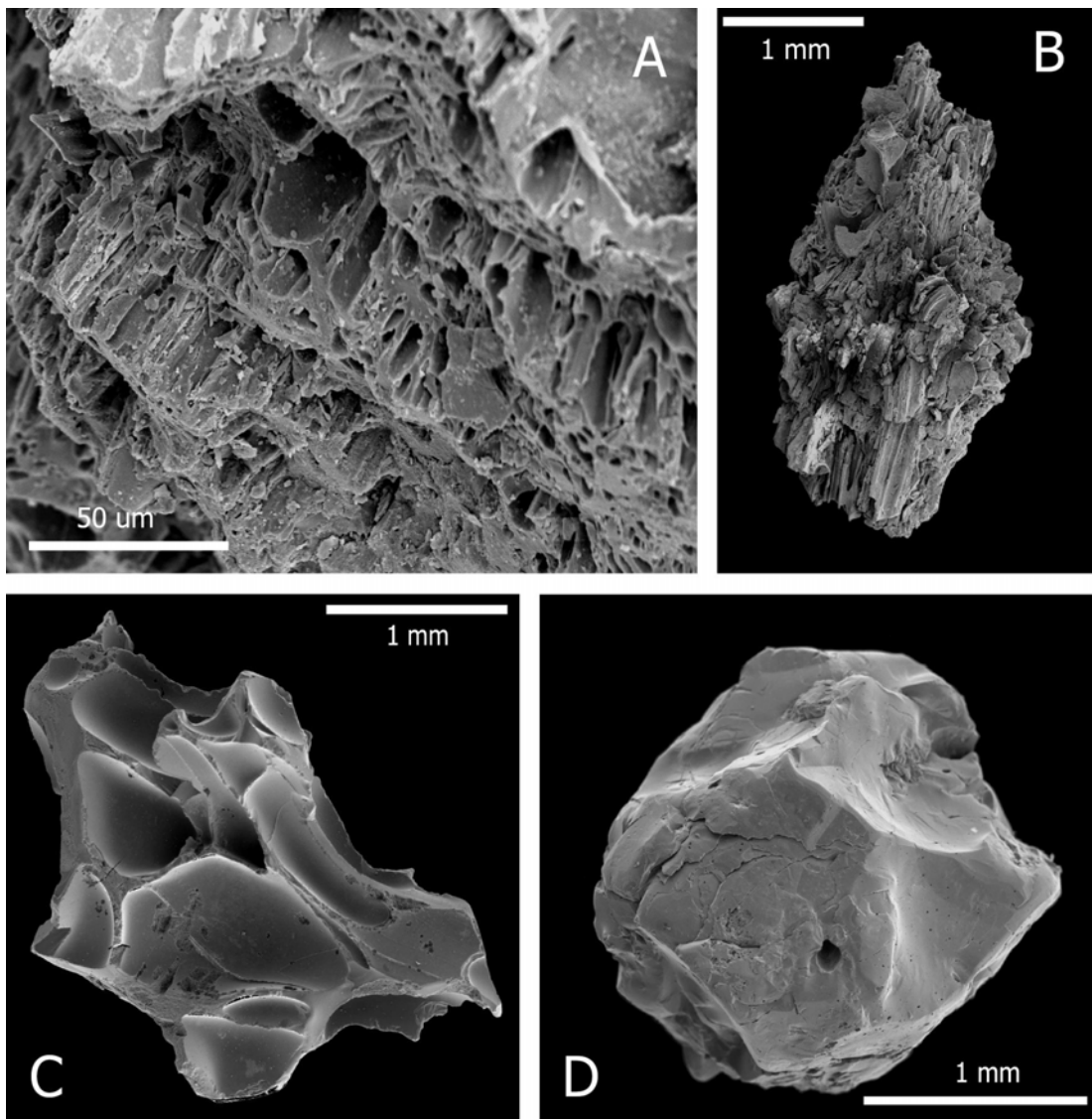


Figure 4.12 Morphologies of the four different shard populations in the Deadeye Member bed X. **A.** White pumice at higher magnification to show microvesicular texture **B.** Black pumice with lined vesicles **C.** Macroscopic shard with numerous bubble walls, note the thicker bubble walls 0.1 mm in contrast to the pumiceous populations **D.** Black, non-vesicular glass clast

black and white pumice populations, are interpreted as closely related. This is supported by the presence of black and white glasses mingled together in the same clast (Fig 4.15 B). The difference in their appearance which does not appear to be related to chemical composition could be explained by a subtle difference in vesicularity (Figs. 4.12 B and 4.13 B), with the black pumice population having slightly thicker bubble walls than the white

pumice population. As these two populations are intimately linked, the black pumice population is also interpreted as juvenile.

Macroscopic shard population

Description

The macroscopic shard population comprises dark grey shards bi and tri-cusate (in three dimensions) shards typically ≤ 7 mm. The shapes suggest that they represent chilled fragments of large walls of (~ 0.25 mm³) ellipsoidal to spherical bubbles that must have been present at the time of fragmentation (Fig. 4.12 C). The thickness of the bubble walls averages 634 microns, much thicker than the bubble walls of the white and black pumice populations (Fig. 4.12 C). Macroscopic shards of this type are a common feature of SR-type volcanism and also occur in the Magpie Basin Member, the Big Bluff Member, and the Dry Gulch ignimbrite. They are rhyolitic, with the most restricted range of chemistry of any of the shard populations and compositions similar to those of the surrounding ignimbrites in the Cassia Mountains (Fig. 4.14). The compositional range of SiO₂ (76.2-77.3 wt.%) is very restricted and this is the case for most of the other elements e.g. FeO (1.79-2.01 wt.%) and CaO (0.67-0.78 wt.%) the TiO₂ (0.17-0.37 wt.% e.g. Fig. 4.12 C) has a range similar to the other glass populations, but at a lower TiO₂ abundance. Given the number of analyses (n=79) the restricted range of major elements suggests, that the macroscopic shards are a single compositional mode (sensu Cathey and Nash 2004).

Interpretation

The macroscopic shards are interpreted as juvenile because of their high abundance, vesicularity and restricted compositional range. The morphology of the shards including large vesicles and thick bubble walls is similar to that seen in scoriaceous, more basaltic tephtras (e.g. Mangan and Cashman 1996). Such morphologies are promoted in magmas which are of sufficiently low viscosity to allow the coalescence of bubbles. Typically

rhyolitic magmas are too viscous to allow this to occur and this high viscosity promotes the micro-vesicular pumiceous texture common in rhyolitic pyroclasts.

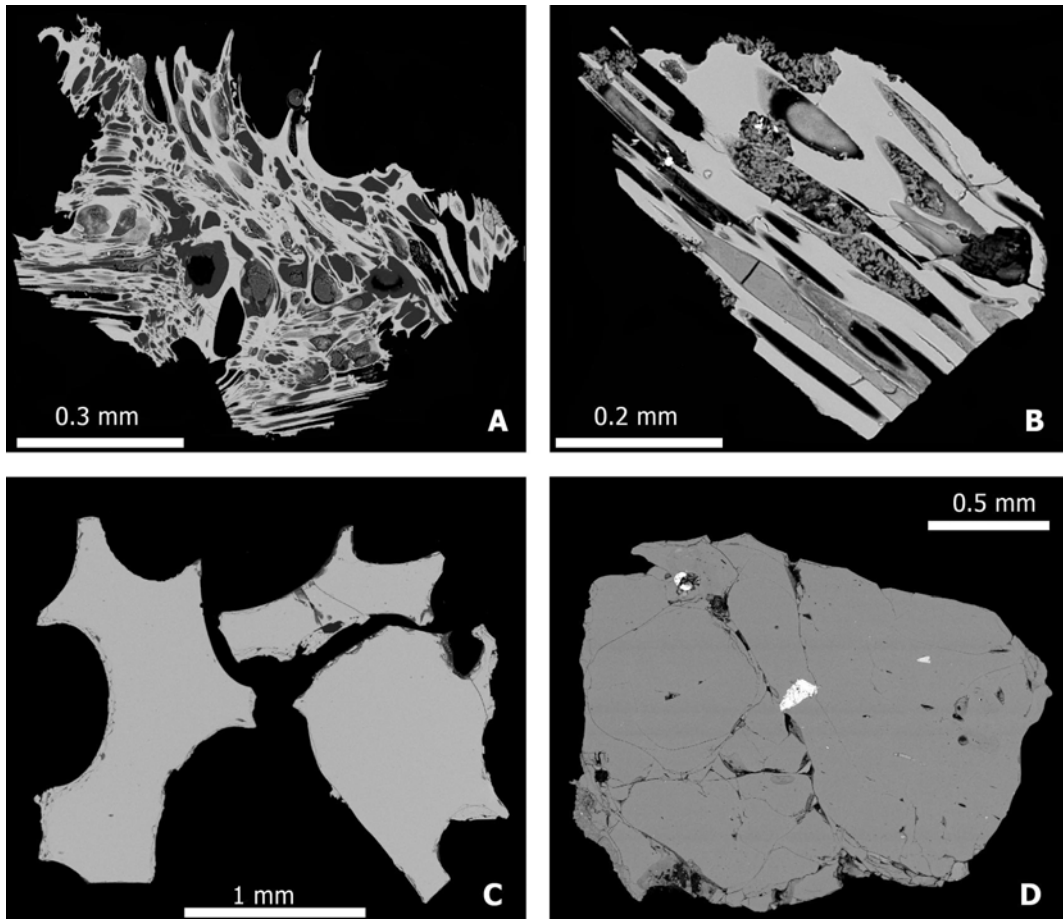


Figure 4.13 S.E.M. images of the four glass populations clearly showing the variation in vesicularity between them (note scale changes) **A.** White pumice with microvesicular texture. **B.** Black pumice **C.** Macroscopic shards with thick remnant bubble walls. **D.** Non-vesicular dense glass clast showing perlitic cracks.

Non-vesicular black glass population

Description

A population of non-vesicular glass clasts comprises angular to sub-rounded non-vesicular black glass (millimetre scale in the Plinian fall deposit, but reaching 3 cm in the overlying

ignimbrite). These clasts show no evidence of vesiculation, and contain a variable content of euhedral phenocrysts of feldspar. Perlitic cracks reflect partial hydration. Microprobe analysis shows that their composition overlaps with those of the other glass populations (Fig. 4.14). However, the dense black glass population has a large scatter in terms of SiO₂ (74.0-78.1 wt.%), FeO (0.8-3.6 wt.%), CaO (0.4-1.7 wt.%) and TiO₂ (0.27-0.59 wt.%) with aluminosity ranging from 0.88 to 1.23 (Fig. 4.15 A).

Interpretation

The origin of these non-vesicular glass fragments is enigmatic. If juvenile there are two possibilities;

- 1) They may represent pyroclastic material welded to the conduit walls, and then ejected as the eruption progressed and the vent flared, as suggested for obsidian clasts at Newberry volcano by Rust and Cashman (2007). However the obsidian from Newberry contains vesicles whereas that in the Deadeye Member does not and the largest obsidian clasts from Newberry reach 1 cm whereas those in the Deadeye Member may be considerably larger.
- 2) The non-vesicular black glass clasts could be similar to ‘blocky shards’ reported from explosive eruptions elsewhere (Rotongaio ash, Walker 1981b; Panum Crater deposits, Heiken and Wohletz 1985). This range in clast size (< 1mm to 3 cm in the ignimbrite) suggests the glass clasts are not ‘blocky shards’, which are generally found to be c. 300 microns in diameter (e.g. Wohletz et al. 1995).

If the dense glass clasts are not juvenile, then their origin must be explained in some other way. Smith and Houghton (2006) refer to anything that does not contribute energy to the eruption as ‘lithic’ so even glassy clasts could be ‘lithic’ in this sense. The non-vesicular glass clasts occur within both the fall deposits and the ignimbrite, so they were probably sourced from the vent rather than being entrained by a pyroclastic density current.

Abundant rhyolite lavas occur at eruptive centres (e.g. Bruneau-Jarbridge, Bonnicksen 1982b; Bonnicksen and Kauffman 1987) and such lavas could be the source of the non-vesicular glassy clasts. In other volcanic fields, non-vesiculated rhyolite clasts are common in eruptions which have blasted through pre-existing lava domes, including phreatoplinian

	Deadeye Member				Wooden Shoe Butte Member	Steer Basin Member	Big Bluff Member
	White pumice n = 48	Black pumice n = 52	Macroscopic shards n = 79	Non-vesicular clasts n = 50			
SiO ₂	76.37	76.61	76.50	75.95	76.35	76.16	77.14
TiO ₂	0.36	0.34	0.28	0.37	0.29	0.28	0.18
Al ₂ O ₃	11.99	12.13	11.99	12.28	12.03	11.78	11.82
Cr ₂ O ₃	0.01	0.01	0.01	0.01	0.00	0.01	0.01
FeO	2.27	2.03	1.88	1.94	1.86	1.94	1.77
MnO	0.03	0.06	0.03	0.03	0.04	0.03	0.03
MgO	0.14	0.12	0.10	0.09	0.08	0.09	0.02
CaO	0.85	0.78	0.74	0.88	0.82	1.00	0.67
Na ₂ O	1.67	2.36	2.91	2.61	2.86	2.32	2.83
K ₂ O	6.16	5.48	5.47	5.77	5.57	6.24	5.39
NiO	0.01	0.01	0.01	0.01	0.00	0.01	0.01
F	0.12	0.11	0.10	0.08	0.11	0.13	0.12
Cl	0.05	0.03	0.02	0.02	0.02	0.03	0.03
SO ₃	0.03	0.03	0.01	0.01	0.01	0.05	0.05
Total	100	100	100	100	100	100	100

Table 4.3 Electron microprobe analyses of the different clast types in bed X of the Deadeye Member compared with other glass analyses from ignimbrites elsewhere within the Cassia Mountains. All averages recalculated to 100% anhydrous. The compositions of the glass populations are shown in Figure 4.14.

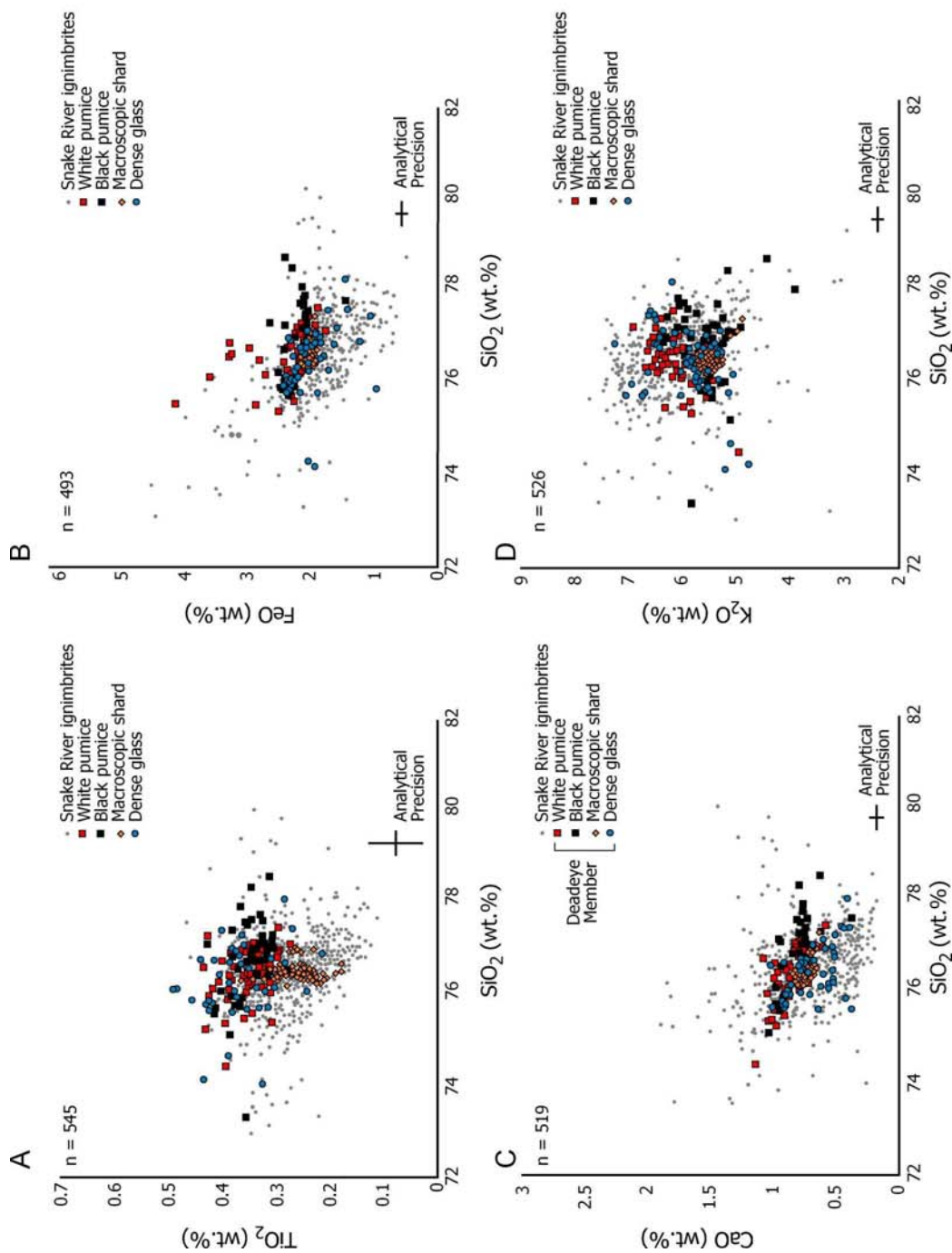


Figure 4.14 The compositions of the four glass populations in the Deadeye Member compared to other SR-type ignimbrites in terms of **A.** TiO_2 , **B.** FeO , **C.** CaO and **D.** K_2O . The four glass populations found in the bed X of the Deadeye Member have compositions identical to the welded rhyolites of the Cassia Mountains.

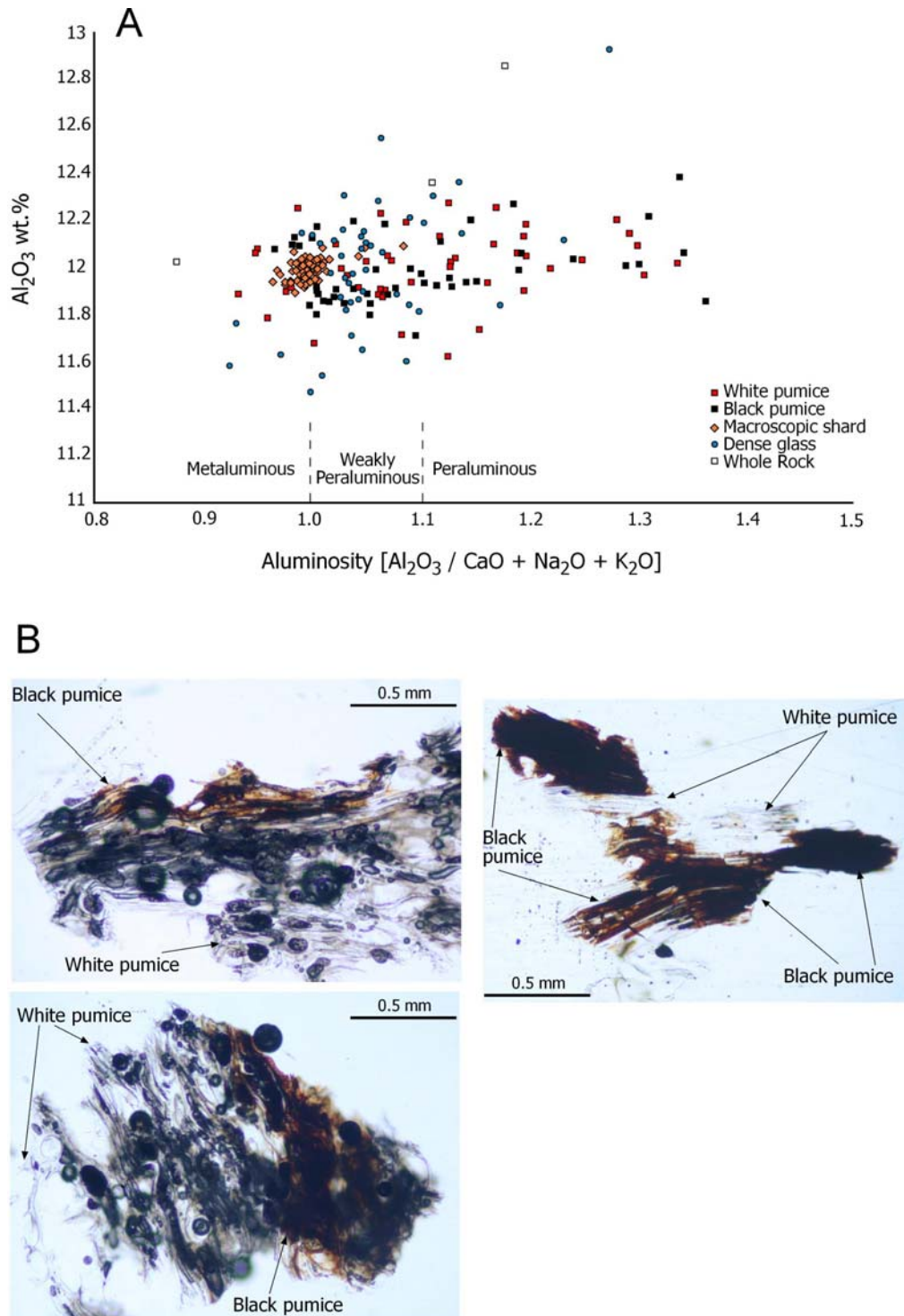


Fig. 4.15 A. Showing the range in aluminosity of the different glass populations in bed X of the Deadeye Member. The white and black pumice populations have a large range of aluminosity, probably due to sodium exchange promoted by their larger surface area. **B.** Three examples of mingling of the two pumice populations in the Deadeye Member.

eruptions (e.g. Rotongaio, Walker 1981b; Mascall ignimbrite; Streck and Fearn 2004). However only a small proportion (<5 %) of the volume of the lavas in the Snake River Plain are glassy, and by far the greater proportion is lithoidal whereas the Deadeye Member contains no clasts of lithoidal rhyolite. This suggests that the non-vesicular dense glass clasts are not simply lava entrained at the vent during the eruption, otherwise much more devitrified rhyolite would be expected.

An abundance of glassy rhyolite with little or no devitrified rhyolite could be present at the source if rhyolite there had been emplaced sub-aqueously and formed hyaloclastite by quenching. Although hyaloclastite originally referred to glassy fragments produced from basaltic pillow lavas, the term has since been extended to refer to any glass fragments formed by subaqueous spalling (e.g. Fisher 1984; White and Houghton 2006). Silicic hyaloclastites have been reported from Iceland (Furnes et al. 1980), Canada (De-Rosen Spence et al. 1980) and Japan (Maeno and Taniguchi 2006). In them, angular glass fragments range in size from less than a millimetre to 40 cm (Furnes et al. 1980).

The non-vesicular glass clasts in the Deadeye Member fallout deposits are tentatively interpreted as hyaloclastite, entrained at source by the Deadeye explosive eruption. Thus the clasts are lithics sensu White and Houghton (2006), although the term accidental seems more useful given that the clasts are glassy rather than lithoidal (Cas and Wright 1987).

Overview of the Deadeye Member

The Deadeye Member is the product of an explosive rhyolitic eruption, from a source probably located within the Snake River Plain, to the north of its outcrop area. After a period of quiescence during which a palaeosol developed at Rock Creek, the eruption began with an explosive eruption column that gave rise to widely dispersed ash and pumice fallout. Depositional environments varied across the region. In Trapper Creek, the ash was reworked with lithofacies dominated by scouring and lateral thickness variations whereas in

Rock Creek the deposition was subaerial as indicated by the primary ashfall deposits and lack of reworking features. Following the fallout, a fine-grained pyroclastic density current deposit was emplaced, over at least 255 km². Gradational variations in the ignimbrite between massive and diffusely-stratified facies reflecting variability in the flow boundary zone of the density current, between fluid-escape dominated (massive lithofacies) and periodic impingement of traction (diffusely-stratified lithofacies) conditions (Branney and Kokelaar 2002). The upper reaches of the density current deposits (section B) contain a variety of ash aggregates including both accretionary lapilli and coated pellets. These aggregates are in diffuse low angle cross-stratified layers and show soft-sediment deformation features indicating that they were moist at the time of deposition. These aggregates had varying pre-emplacment histories and reflect unsteadiness of the density current. Fallout deposition continued after the ignimbrite emplacement, with fine ash falling as clumps rather than individual grains, reflecting moisture in the atmosphere. The Deadeye eruption then ended and a palaeosol developed on the deposit.

Discussion

Being entirely non-welded and with a distinctly fine-grained ignimbrite, the Deadeye Member is significantly different in appearance to the surrounding intensely welded SR-type ignimbrites. Clearly the Deadeye Member erupted in a different style; but what caused this difference?

The non-welded nature of the Deadeye Member and the moist nature of the pellets and accretionary lapilli in the Deadeye Member suggest a low emplacement temperature. However thermometry using zircon saturation (Watson and Harrison 1983) suggests that the magmatic temperature of the Deadeye Member was ~925 °C, similar to those for the intensely welded ignimbrites within the Cassia Mountains (Fig. 4.16 and Chapter 2). The magma which erupted to form the Deadeye Member also had a depletion in $\delta^{18}\text{O}$ characteristic of Snake River-type rhyolites from elsewhere in the central Snake River Plain

area, with magmatic feldspar values for Snake River-type volcanic products ranging from -1.4‰ to 3.8‰ $\delta^{18}\text{O}_{\text{VSMOW}}$ (Boroughs et al. 2005), considerably depleted from the typical

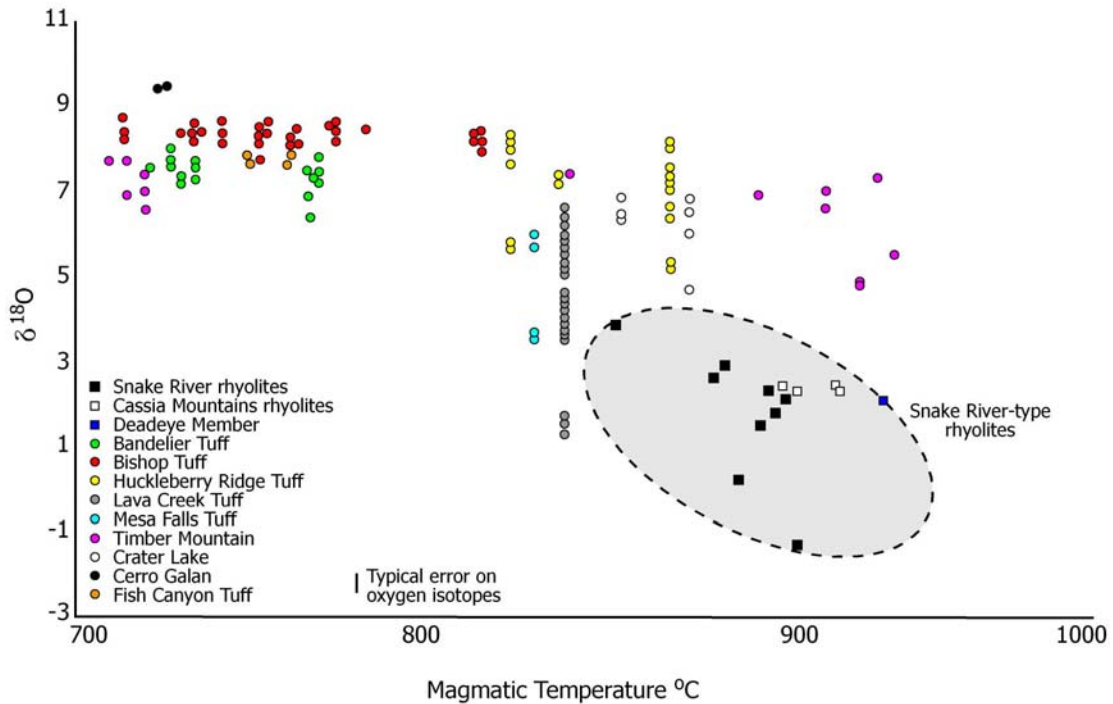


Figure 4.16 Graph showing the similarities in oxygen isotope signature and magmatic temperature between the Deadeye Member and other SR-type rhyolites. Oxygen isotope data from Boroughs et al. (2005) and Boroughs and Starkel (pers. comm.). Magmatic temperatures are based on zircon saturation thermometry (Watson and Harrison 1983). Data for ‘typical’ rhyolites shown are from Bindeman and Valley (2000; 2001; 2003); Spell et al. (1996); Bindeman et al. (2007); Wolff et al. (2002); Bacon et al. (1989) and Lipman and Friedman (1975). The Snake River-type magmas generally have higher magmatic temperatures and lower $\delta^{18}\text{O}$ than other rhyolites. Low $\delta^{18}\text{O}$ values seen for some of the Yellowstone ignimbrites are in part due to the analysis being of zircon.

range for rhyolites of 7‰ to 10‰ (Fig. 4.16). Major element chemistry of all four glass component types in the bpL facies is indistinguishable from the glass compositions of the surrounding SR-type welded ignimbrites of the Cassia Mountains (Fig. 4.14). Additionally, the whole rock compositions and inferred magmatic temperatures of the Deadeye Member are similar to those of the Snake River-type rhyolites. These similarities suggest that the magmas erupted in the Deadeye eruption was closely similar to those of the intensely

welded ignimbrites. Thus the contrast in deposit facies reflects a difference in eruptive style.

The relatively small volume (1.3 km³) of the Deadeye Member compared to other Snake River-type ignimbrites (e.g. the Big Bluff Tuff ~ 1200 km³ and Cougar Point Tuff 11 927 km³, Chapter 3) might favour the development of non-welded facies in that the smaller volume may allow a greater proportion of air to be ingested into the density current, cooling the pyroclasts and reducing the emplacement temperature. However, the central Snake River Plain does not exhibit a simple relationship between deposit volume and welding intensity, as some small-volume ignimbrites are intensely welded (e.g. the < 10 km³ Magpie Basin Member, Williams et al. 1990) whereas some larger volume deposits are less intensely welded (e.g. McMullen Creek Member; Chapter 2).

A phreatomagmatic origin?

A possibility which explains all the features seen in the Deadeye Member is phreatomagmatism. The presence of the pods of fine ash in section C of the Deadeye Member interpreted as representing ash falling as clumps have been reported from phreatomagmatic eruptions (e.g. Walker 1981b; Wilson 2001). The abundance of ash aggregates, both accretionary lapilli and coated pellets, in section B of the Deadeye Member is suggestive of an environment with abundant moisture. Ash aggregates are common, almost ubiquitous, in phreatomagmatic ignimbrites and tuffs (Self and Sparks 1978, Self 1983; McPhie 1986; Allen and Cas 1998; De Rita et al. 2002; Wilson 2001; Table 4.5). Although the Deadeye Member contains a higher proportion of aggregates than any other SR-type ignimbrite, this cannot be used alone as a discrimination between phreatomagmatic and magmatic deposits, as magmatic deposits are known to contain a variety of ash aggregates (e.g. Sakurajima, Gilbert and Lane 1994; Unzen, Watanabe et al. 1999; Montserrat, Bonadonna et al. 2002; Tenerife, Brown and Branney 2004). The deformation of these aggregates reflects cool emplacement conditions in contrast to the surrounding welded ignimbrites. This divergence in emplacement temperatures from similar magmatic temperatures (Fig. 4.16) is consistent with the magma interacting with

water as non-welded ignimbrites are common from phreatomagmatic eruptions (e.g. Self and Sparks 1978; Brand and White 2007).

The presence of the abundant hyaloclastite clasts both within the ignimbrite and the fall deposits is also consistent with an eruptive source that was sub-aqueous for some period at least. While other, intensely welded, ignimbrites contain these hyaloclastite chips (e.g. Branney et al. 2008; Chapters 2 and 3), other characteristics (such as their high emplacement temperature) argue against a phreatomagmatic origin for these units.

Silicic phreatomagmatism

Deposits of large and small volume may be readily defined as the products of phreatomagmatism (e.g. Sheridan and Updike 1975; Bond and Sparks 1976; De Rita et al. 2002). Smaller volume deposits commonly form tuff rings or tuff cones (morphological features) which are defined as being of either Surtseyan or Taalian eruptive style. The variety seen within the larger volume deposits of phreatomagmatism (e.g. Table 4.4) suggests that they are not simply scaled-up Surtseyan or Taalian style eruptions. The terms commonly used to describe phreatomagmatic eruptions are described below.

Surtseyan

Surtseyan eruptions result when external water gains access to the top of a vent (Kokelaar 1983), so that a slurry of tephra, hyaloclasts and water slumping into the top of the vent mixes with erupting magma and steam (Kokelaar 1983). As rising magma passes through this three phase slurry, mixing of the fluids occurs and some of the water flashes to steam on contact with the magma and rapidly expands resulting in continuous jets of tephra slurry rather than a single explosion (Kokelaar 1983). Fine comminution of the pyroclasts is thought to result from multiple involvements in eruptive events; such recycling of clasts has also been recognised in larger phreatomagmatic eruptions (Houghton and Smith 1993). Surtseyan eruptions are small-scale, with 1 km from the vent considered to be distal during the Caphelinhos eruptions of 1958 (Cole et al. 2001) and associated density current

deposits being small volume ($\ll 1 \text{ km}^3$). Surtseyan eruptions have only been reported from basaltic settings (Kokelaar 1983; Kokelaar and Durant 1983; Cole et al. 2001; Table 4.5).

Taalian

Taalian eruptions are produced by the explosive interaction of rising magma and water within the surrounding aquifer (Moore et al. 1966; Kokelaar 1986). As a result, fragmentation of the magma disrupts the aquifer, and the deposits contain a large proportion of lithic clasts. In contrast to Surtseyan eruptions, Taalian eruptions occur where water gains access to the volcanic conduit below the vent (Kokelaar 1986). The deposits of Taalian eruptions include fallout deposits and density current deposits (Sohn 1996). Taalian eruptions are most commonly basaltic (Table 4.5).

Phreatoplinian

In contrast to the terms Surtseyan and Taalian, phreatoplinian refers to a deposit rather than an eruptive style. Self and Sparks (1978) defined phreatoplinian as fallout deposits with a dispersal index (D) $> 500 \text{ km}^2$ and a high fragmentation index (F). Dispersal index is the area in km^2 enclosed by the 0.01 isopach of maximum thickness; and F is the weight percentage less than 1 mm collected where the 0.1 isopach of maximum thickness collected on the dispersal axis (Walker 1971; Self and Sparks 1978). Subsequently, the term phreatoplinian has been used to refer to density current deposits (e.g. Camus et al. 2000; De Rita et al. 2002) or a style of eruption (Allen and Cas 1998). The mechanism of how phreatoplinian deposits are formed is still unclear; it is thought to reflect large-scale fuel-coolant interaction yet how this occurs in high mass-flux, large volume eruptions has yet to be resolved. Fine-grained density current deposits, commonly bearing abundant ash aggregates have been reported in association with phreatoplinian ashfall layers (e.g. Wilson 2001; De Rita 2002). However welded deposits inferred to represent transitions to magmatic activity (Branney 1991) are also known.

Eruption style Characteristic	Surtseyan	Taalian	Phreatoplinian and associated deposits	Deadeye eruption
	Magma composition	usually basaltic	usually basaltic	andesitic to silicic
Volume (km ³)	<< 1	normally < 1	up to 100	1.3
Widespread fallout deposit	no	often	yes	Yes
Density current deposit thickness (m)	< 2	< 5	> 100 (NYT)	< 5
Massive facies	subordinate	present	dominant	40%
Cross-stratified facies	dominant	abundant	subordinate	60%
Accretionary lapilli	abundant	abundant	common to abundant	in upper reaches
Mud clumps	not reported	uncommon	sometimes	in upper reaches
Lithic proportion	high proportion of recycled tephra from cone margins	high	0.5-20%	< 5%
Glass chips in density current deposits	not reported	not common	may be present	common
Pumice in density current deposits	vesicular scoria may be present	ash dominated but may be present	common	rare to absent
Ballistics in proximal areas	yes, may be fluidal	common	yes	not exposed
Runout distance of density current (km)	1 or less	typically 5-10	>> 10	>20
Disruption of aquifer	no	characteristic	possible	unlikely

Table 4.4 Comparison of the characteristic deposits produced by some phreatomagmatic eruption styles and those recorded in the Deadeye Member. Necessarily the Surtseyan, Taalian and Phreatoplinian columns are generalisations.

Feature Reference	Tuff rings						Deadeye this work	
	Astroni Isala et al. (2004)	Averno Mastroiorenzo (1994)	Caldera del Rey Davila-Harris (2008)	Giaramera (Brown et al. 2007)	Sugarloaf Mtn. Sheridan and Updike (1975)	Santorini Bond and Sparks (1976)		Monte Guardia De Rosa et al. (2003)*
Area covered (km ²)	350	30	21	800	28	'wide areas'	c. 25	255
Volume (km ³)	1.02 (7 events)	0.29	0.105	0.2-0.5	< 0.3	not reported	0.25	1.3
Dune-bedded proximally	within 3 km of source	within 0.5 km of source	yes	yes	yes	very common	yes	not exposed
Ballistic blocks	abundant	50 cm within 1 km of source	abundant reaching 1 m in diameter	possibly	not reported	yes	yes	not recorded
Density current runoff (km)	< 8	5	< 3	up to 12	1.2	not reported	8	> 20
Pumice lapilli in density current deposits	yes	yes	yes	yes	yes	yes	yes	rare to absent
Welding intensity	non-welded	non-welded	non-welded	moderately welded and eutaxitic	non-welded	non-welded	non-welded	non-welded
Dominant facies in current deposits	massive to stratified	massive	stratified	massive to stratified	massive to cross-stratified	cross-stratified	cross-stratified to stratified	diffuse cross-stratified
Lithic proportion	< 10 %	abundant	proximally 10-15%	up to 20%	not reported	generally low	present up to 10%	< 2%
Ash aggregates	accretionary lapilli abundant throughout	abundant	abundant	rims pellets and accretionary lapilli common	not reported	not reported	abundant	accretionary lapilli and rims pellets both present
Composition	trachytic	trachyte	phonolite	dactitic	rhyolitic	rhyo-dactite	rhyolitic	rhyolitic
Tectonic setting	back arc rifting	back arc rifting	oceanic hotspot	subduction	continental hotspot?	subduction	subduction	continental hotspot

Table 4.5 Comparison of a number of phreatomagmatic deposits produced from magmas of more evolved compositions.

Feature Reference	Tuff rings			Phreatomagmatic			Deadeye this work
	Laacher See van den Bogaard and Schmincke (1985)	King's Tuff Moore and Kokelaar (1998)**	Puketarata Brooker et al. (1993)	Cana Creek McPhie (1986)	Neapolitan Yellow Tuff Scarpati et al. (1993)	Oruanui Wilson (2001)	
Area covered (km ²)	not reported	c. 147	320	1,400	>1,000	750,000	255
Volume (km ³)	1.7	< 1	0.014	100	79	750	1.3
Dune-bedded proximally	not reported	not reported	yes	not reported	yes	some	not exposed
Ballistic blocks	not reported	yes	10-40 cm blocks of poorly vesiculated juvenile rhyolite	not reported	not reported	not reported	not recorded
Density current runoff (km)	20	7	not reported	> 20	12	> 60	> 20
Pumice lapilli in density current deposits	yes	yes	yes	abundant	yes	yes	rare to absent
Welding intensity	non-welded	non-welded	non-welded	non-welded	rarely welded	non-welded	non-welded
Dominant facies in current deposits	not reported	stratified	cross-stratified	massive	massive to stratified	massive	diffuse cross-stratified
Lithic proportion	10-49%	present	variable	variable up to 5 mm	not reported lithics up to 65 cm	variably present	< 2%
Ash aggregates	abundant	abundant accretionary lapilli	not reported	abundant rimmed pellets	both accretionary lapilli and rimmed pellets present	accretionary lapilli dominant	accretionary lapilli and rimmed pellets both present
Composition	phonolite	rhyolitic	rhyolitic	rhyolitic	trachyte	rhyolitic	rhyolitic
Tectonic setting	hotspot?	extension	subduction	subduction	back arc rifting	subduction	continental hotspot

Table 4.5 Cont. *additional information from Colella and Hiscott (1997) and ** Kokelaar pers. comm.

Phreatomagmatic

Feature Reference	Tsumaya Aramaki (1984)	Pisolitic Tuffs De Rita et al. (2002)	Akdag-Zelve Schumacher and Mues-Schumacher (1997)	Whorneyside Branney (1991)	Kos Plateau Tuff Allen et al. (1999)	Deadeye this work
Area covered (km ²)	443	1600	1200	>> 100	>8,000	255
Volume (km ³)	13	> 37 4 eruptions	180	> 100	60	1.3
Dune-bedded proximally	not reported	not exposed	yes	minor	some	not exposed
Ballistic blocks	not reported	not recorded	no	yes	not reported	not recorded
Density current runoff (km)	> 15 km	c. 30	30	> 20	60	> 20
Pumice lapilli in density current deposits	yes	rare	yes	yes	yes	rare to absent
Welding intensity	non-welded	non-welded	non-welded	welded	non-welded	non-welded
Dominant facies in current deposits	massive to cross-stratified	massive to stratified	massive	massive	massive	diffuse cross-stratified
Lithic proportion	present to abundant	up to 5%	up to 9 wt. %	c 5% in ignimbrite	abundant	< 2%
Ash aggregates	accretionary lapilli present	abundant accretionary lapilli	accretionary lapilli abundant	abundant mostly rimmed pellets	accretionary lapilli present	accretionary lapilli and rimmed pellets both present
Composition	dacitic	mafic	rhyolitic	andesitic	rhyolitic	rhyolitic
Tectonic setting	subduction	extensional	subduction	subduction	subduction	continental hotspot

Table 4.5 Cont.

Eruptive style of the Deadeye Member

Section A of the Deadeye Member contains a series of fallout deposits which are similar to other ashfall deposits of the central Snake River Plain (Branney et al. 2008) and beds of pumice which were produced by magmatic activity prior to the onset of phreatomagmatic activity. This switch between magmatic and phreatomagmatic eruptive behaviour has been recorded in numerous other phreatomagmatic eruptions, e.g. Santorini (Bond and Sparks 1976), Neapolitan Yellow Tuff (Scarpati et al. 1993), Kos Plateau Tuff (Allen and Cas 1998; Allen et al. 1999) and Oruanui (Wilson 2001).

Section B of the Deadeye Member represents the onset of phreatomagmatism, producing variably massive, diffuse cross-stratified and ash aggregate-bearing diffuse cross-stratified tuff facies. Silicic phreatomagmatic deposits commonly exhibit massive (e.g. Cana Creek, McPhie 1986; Astroni, Isaia et al. 2004; Oruanui, Wilson 2001), cross-stratified (e.g. Pisolithic tuffs, De Rita et al. 2002; Caldera del Rey, Davila-Harris 2008) and ash aggregate-bearing facies (e.g. Whorneyside, Branney 1991; Neapolitan Yellow Tuff, Scarpati et al. 1993; Glaramara, Brown et al. 2007), with massive deposits dominating in ignimbrites associated with phreatoplinian deposits (e.g. Table 4.5). The pod-bearing fallout deposits overlying the density current deposits of section B are similar to those described from large-scale phreatomagmatic eruptions (e.g. Askja C, Sparks et al. 1981; Oruanui, Wilson 2001).

The Deadeye Member contains facies with similarities to both tuff ring-forming deposits and those from larger phreatomagmatic events. This reflects a gradation in processes between eruptions which form tuff-rings and those associated with phreatoplinian deposits, as suggested by Brown et al. (2007); this intergradation is further emphasised by the volume and runout distance of density currents of the Deadeye Member which are intermediate between the two end members (Table 4.4). In terms of an eruptive style, neither Surtseyan nor Taalian are suitable for the Deadeye Member and the term phreatoplinian represents a deposit produced by a poorly-understood, un-named style of

eruption. The Deadeye Member represents an eruption intermediate in scale between the small-volume tuff-ring forming eruptions and larger phreatoplinian-forming eruptions.

Other phreatomagmatic units in the Snake River Plain

The Deadeye Member represents the first recognised example of silicic phreatomagmatism in the central Snake River Plain. Other units from the province show facies which are suggestive of phreatomagmatism, discussed in order of decreasing evidence for phreatomagmatism.

Unnamed unit in Big Cottonwood Canyon

At the mouth of Big Cottonwood Canyon (Fig. 4.1), a series of ashfall deposits are overlain by a non-welded density current deposit. The fallout deposits are parallel-bedded, well-sorted and composed of medium to coarse ash, identical to the //bT facies of the Deadeye Member. The overlying ignimbrite is fine-grained and contains abundant accretionary lapilli. The ignimbrite in this unnamed unit does not exhibit any of the facies seen by the Deadeye Member as it is massive whilst containing accretionary lapilli (Fig. 4.17). The Deadeye Member is exposed further south west in Cottonwood Canyon, at a higher stratigraphic interval and the fallout stratigraphies of the two deposits differ. The unnamed unit has yet to be recognised elsewhere in the central Snake River Plain.

Jackpot 6

The Jackpot 6 unit of Andrews et al. (2008) is exposed south of the town of Jackpot in the Rogerson Graben where it is cross-stratified, non to partially welded and contains abundant clasts of non-vesicular black glass which reach up to 3 cm diameter (Fig. 4.17 C). These clasts of non-vesicular glass may act as the core of accretionary lapilli (Fig. 4.17 D) which reach a few centimetres in size and are common in this unit. Jackpot 6 is deposited directly atop a thick, intensely welded ignimbrite (Jackpot 1-5, Andrews et al. 2008; Chapter 3). The Jackpot 6 unit is widespread, extending east to the Cassia Mountains (Chapter 2).



Figure 4.17 Log of the unnamed unit at the mouth of Big Cottonwood canyon. This unit is stratigraphically lower than the Deadeye Member. **A.** The ignimbrite at the top of the log is a massive deposit containing accretionary lapilli, in contrast to the Deadeye Member which is commonly diffuse cross-stratified where it contains aggregates. The large glass clast in the centre of the photograph has a crystal content higher than any of the glass clasts in the Deadeye Member. **B.** The fallout deposits of the unnamed unit are similar to the //bT facies of the Deadeye Member, but with a different stratigraphy to the Deadeye Member.

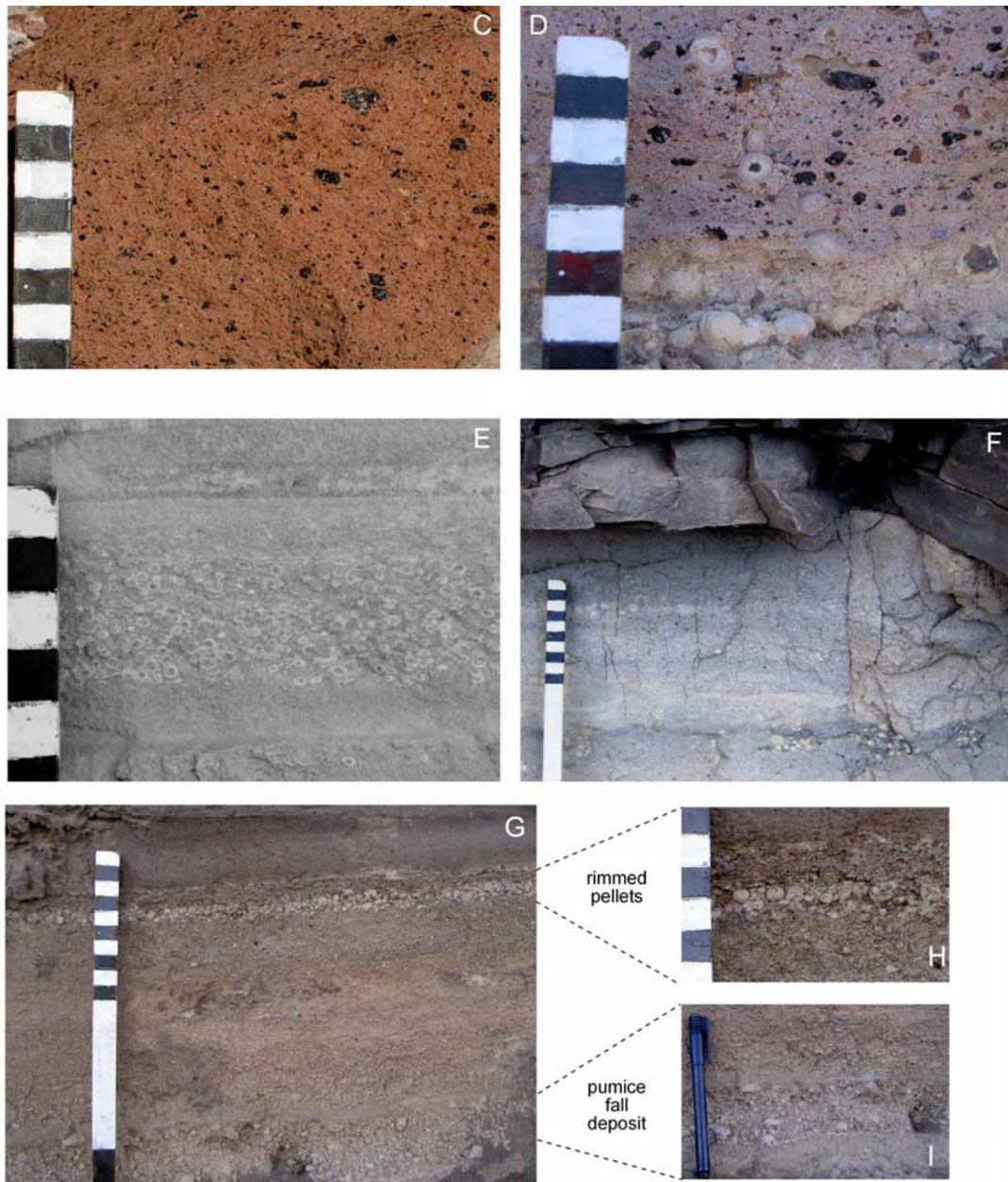


Figure 4.17 cont. **C.** Abundant clasts of non-vesicular glassy rhyolite in Jackpot 6. The matrix is partially welded by heat from the underlying lava-like and rheomorphic Jackpot 1-5 (Andrews et al. 2008). **D.** Accretionary lapilli in Jackpot 6, with some containing clasts of non-vesicular dense glass for their core. **E.** Rimmed pellets with a single fine-grained white rim surrounding a core of medium ash above the welded ignimbrite. At the top of the pellet-bearing layer, a series of flattened pellets can be seen. **F.** Non-welded tuff beneath the Rabbit Springs ignimbrite showing the presence of accretionary lapilli in a fine ash matrix. **G.** Base of Cougar Point Tuff 15 at Murphy Hot Springs, the non-welded ignimbrite seen at the top of the photograph, beneath are the layer of rimmed pellets and pumice lapilli. **H.** Close-up of the rimmed pellet layer, showing the clast-supported nature of the pellets. **I.** Massive pumice lapilli bed, a rare facies in the central Snake River Plain.

Wooden Shoe Butte Member

The Wooden Shoe Butte Member contains two ignimbrite cooling units, which vary in welding intensity from lava-like to moderately welded. The base of the unit is a thick succession of fallout and variably reworked deposits which in Rock Creek are fused to glass by the heat conducted downwards from the ignimbrite. Within these ashfall deposits are layers of coated pellets which are fused in Rock Creek but are non-welded and show impact marks in Trapper Creek to the east. In Trapper Creek, the succession of non-welded material above the ignimbrite also contains abundant coated pellets, more than 9 separate layers. The coated pellets seen in the Wooden Shoe Butte Member are much smaller (< 1 cm) than those seen in the Deadeye Member, and may reflect moisture in the atmosphere rather than phreatomagmatic activity. Despite the welded nature of the Wooden Shoe Butte Member, the presence of multiple beds of coated pellets (Fig. 4.17 E) are suggestive of some interaction with water.

Rabbit Springs Member

The Rabbit Springs Member was erupted c. 10.44 ± 0.13 Ma (Bonnichsen et al. 2008) and is located in the Rogerson Graben where it is moderately welded with basal and upper vitrophyre and a eutaxitic fabric (Andrews et al. 2008). Beneath the welded ignimbrite of the Rabbit Springs Member is a non-welded, cross-stratified tuff containing abundant accretionary lapilli (Fig. 4.17 F). The accretionary lapilli have multiple rims and reach a centimetre in diameter within a well-sorted ash deposit. This non-welded cross-stratified tuff may represent a precursory phreatomagmatic phase to the Rabbit Springs eruption, prior to the main part of the eruption which deposited the welded ignimbrite.

Cougar Point Tuff 15

At Murphy Hot Springs, Cougar Point Tuff 15 is well exposed and the basal fallout deposits contain framework supported pumice lapilli (rare for Snake River-type volcanism) shown in Figure 4.17 G and I. The fallout succession also contains a distinct bed of coated pellets which are composed of a core of medium ash with a single fine-grained rim (Fig.

4.17 H). Above the fallout deposits the ignimbrite varies from non-welded to intensely welded. Similarly to the Deadeye Member, at Murphy Hot Springs, Cougar Point Tuff 15 has pumice lapilli within its fallout deposit, it contains ash aggregates and has a non-welded ignimbrite. However, when traced laterally, the ignimbrite of Cougar Point Tuff 15 becomes an intensely welded sheet of glass, a feature not seen in the Deadeye Member.

Conclusions

Detailed fieldwork in the Cassia Mountains of southern Idaho has discovered the presence of an entirely non-welded eruption unit within a sequence previously mapped as reworked sediments. The Deadeye Member represents the first entirely non-welded eruption unit described from the central Snake River Plain and it has similar geochemical characteristics to the surrounding intensely welded ignimbrites. This suggests that the difference in depositional facies were the result of differing eruption processes. The Deadeye eruption began in magmatic style producing Plinian pumice fallout deposits before a transition to phreatomagmatism.

The presence of ash clumps; abundant accretionary lapilli; low emplacement temperature and non-welded nature of the density current deposit; and the presence of abundant hyaloclastite are interpreted as the result of interaction between a rising, hot rhyolitic magma and shallow or surficial water.

Given that the non-welded, slope-forming units in the central Snake River Plain are poorly exposed and have received little attention, it is possible that phreatomagmatism is an underestimated component of volcanism from the central Snake River Plain. Following the recognition of the Deadeye Member as a phreatomagmatic deposit, other units which have some similar characteristics have been proposed as representing variable degrees of phreatomagmatism. The presence of a lake in the current Yellowstone caldera makes phreatomagmatic activity similar to that inferred for the Deadeye Member a possible future scenario at Yellowstone.

Chapter 5: Pre-eruptive volatile contents and eruptive behaviour of Snake River-type ignimbrites and lavas

Abstract

The pre-eruptive water, fluorine and chlorine contents of Snake River-type magmas have been determined from analyses of plagioclase-hosted melt inclusions in six rhyolitic units. The chosen units comprise three experiments each containing a lava and an ignimbrite which were erupted over the same geographic area, closely spaced in time and of similar geochemical characteristics. The water contents of the inclusions are relatively low and are in agreement with both previous estimates and the observed anhydrous mineral assemblage. Chloride contents are lower than those reported from other rhyolites and fluorine contents are similar. No systematic difference in pre-eruptive volatile contents was observed between magmas that formed ignimbrites or lavas suggesting the divergence in eruptive style must be controlled by another factor. The uniformly low chloride contents with varied water contents are inferred to reflect a magmatic system that entrapped inclusions during degassing. The low chloride content of the inclusions may reflect the presence of another magmatic volatile, such as carbon dioxide, acting to reduce the solubility of chloride. The central Snake River Plain is inferred to have a gas-saturated magmatic system, similar to recent models proposed for the current Yellowstone magmatic system. The low halogen contents determined from the inclusions and groundmass suggest that low emplacement viscosities in these units, and more broadly within Snake River-type ignimbrites, is a function of the combination of high emplacement temperatures and high mass fluxes rather than due to the retention of magmatic volatiles.

Introduction

Silicic volcanism in the Yellowstone-Snake River mega-province has been shown to be broadly time-transgressive along the Yellowstone hotspot track (Pierce and Morgan 1992; Smith and Braille 1994) decreasing in age towards Yellowstone in the east. Along the hotspot track in southern Idaho and northern Nevada (Fig. 5.1), an enigmatic and catastrophic style of volcanism defined from 13-8 My-aged deposits has been recognised and termed ‘Snake River (SR)-type’ volcanism (Branney et al. 2008).

SR-type volcanism brings together eighteen volcanic facies that are unusual in their association, such as (1) well-sorted ignimbrites lacking pumice and lithic lapilli; (2) ashfall deposits, in place of the pumice lapilli fall deposits that typify Plinian deposits; (3) a predominance of large volume, highly rheomorphic, intensely welded ignimbrites (Bonnichsen and Citron 1982; Cathey and Nash 2004; Andrews et al. 2008); and (4) large volume rhyolitic lavas, reaching 200 km³ (Bonnichsen 1982; Manley 1996), many times larger than typical silicic lavas that have outcrops in the range of 5 km² (e.g. Fink and Bridges, 1985).

Rationale

The highly rheomorphic nature of SR-type ignimbrites and areal extent of the ignimbrites and lavas, suggest a low viscosity upon emplacement, which could be controlled by numerous factors including volatile content and/or temperature. High magmatic temperatures of both ignimbrites and lavas have been inferred in a number of previous studies (Honjo et al. 1992; Cathey and Nash 2004; Andrews et al. 2008; Chapter 2), yet the pre-eruptive volatile contents of SR-type magmas have not been constrained. The main objectives of this study are:

- 1) to determine and quantify the main volatile species present and lost during SR-type eruptions and
- 2) to examine whether there is a difference between pre-eruptive volatile contents in lavas and ignimbrites in SR-type eruptions. Determination of the main volatile species present in

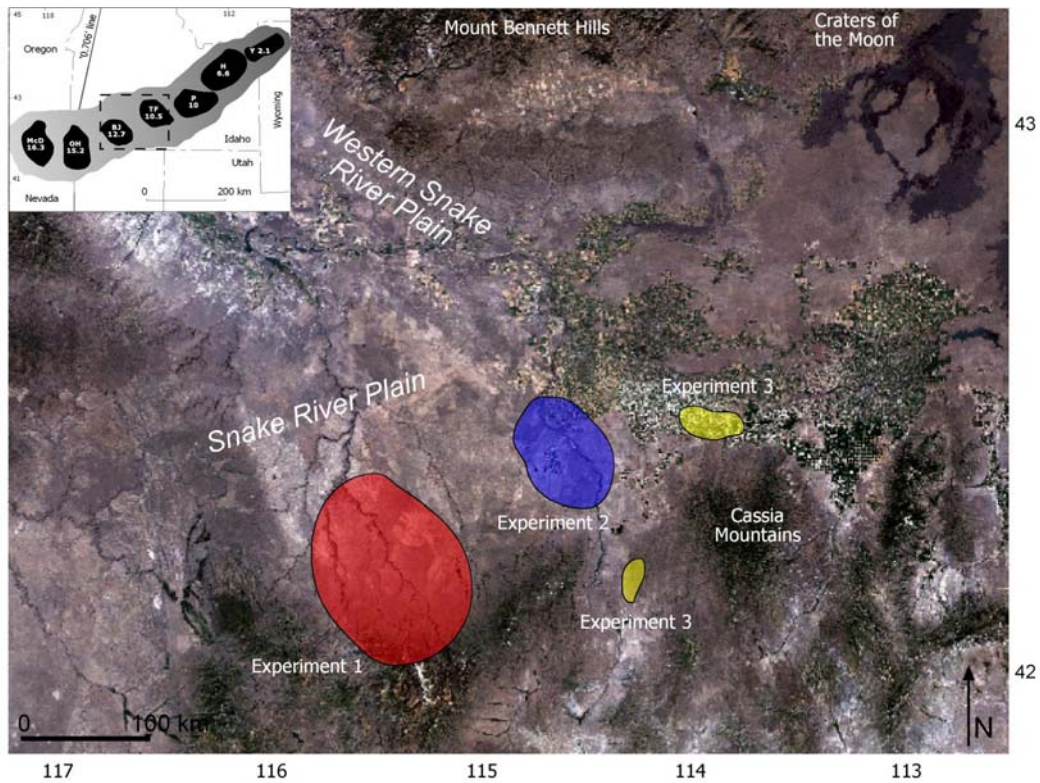


Figure 5.1 Composite satellite image showing the location of the units comprising the experiments in this study. Inset shows the location of the samples in the central Snake River Plain with the dotted rectangle representing the area shown. The abbreviations represent the eruptive centres and the numbers refer to the age of onset of activity at that centre (Pierce and Morgan 1992). McD - McDermitt, OH - Owyhee-Humboldt, BJ - Bruneau-Jarbidge, TF - Twin Falls, P - Picabo, H - Heise and Y - Yellowstone.

the SR-type magmas is of interest because these high temperature rhyolitic magmas have an anhydrous crystal assemblage indicative of relatively low water contents at the time of crystallisation, yet the majority still erupt in a highly explosive manner.

Previous studies

Lava versus ignimbrite discrimination criteria

Distinguishing lava-like ignimbrites (*sensu* Branney and Kokelaar 1992) from true lavas in the field has long been considered problematic (Henry et al. 1988; Henry and Wolff 1992; Green and Fitz 1993). Criteria for distinguishing between a strongly rheomorphic

ignimbrite and a lava were proposed by Henry and Wolff (1992); lavas can be defined by the presence of a basal autobreccia (although rheomorphic ignimbrites may locally have basal autobreccias e.g. Sumner and Branney 2002) and steep terminations. Ignimbrites may be definitively recognised where they grade into non-welded facies. The relationship of the deposit with topography is the most reliable indicator of eruptive style, with ignimbrites feathering out as they onlap fault scarps whereas lavas are restricted to palaeovalleys. Snake River-type lavas are rarely less than 20 m thick, whereas numerous ignimbrites are known to be metre-thick sheets of glass (e.g. Grey's Landing, Sand Springs and Cougar Point Tuff 15). The characteristics of a typical SR-type lava and ignimbrite are shown in Figure 5.2. In many locations in the Snake River Plain, the lack of basal exposure prevents unequivocal interpretation of the mode of deposition of thick rhyolites, due to the dense welding and lava-like appearance of the ignimbrites. Units chosen for this study were selected on the basis of unambiguous field evidence.

Melt inclusions

Studies of melt inclusions within silicic ignimbrites have typically found pre-eruptive water contents from 2-7 wt.% e.g. Katmai (Lowenstern 1993), Bishop Tuff (Anderson et al. 1989), Mt. St. Helens (Rutherford et al. 1985) and Taupo volcanic zone (Dunbar et al. 1989), see Table 5.1. Carbon dioxide contents are normally 1000 ppm or less (Anderson et al. 1989; Skirius et al. 1990; Lowenstern 1993). Chlorine contents are often higher than CO₂ with typical values of 0.1-0.2 wt. % (Newman and Chesner 1989; Stix et al. 1993; Lowenstern 1994). Fluorine contents are typically 400-1500 ppm although they can be much larger in continental settings, up to 6000 ppm in the Taylor Creek rhyolite (Webster and Duffield 1991; Lowenstern 1995). Sulphur is present typically in small concentrations up to 200 ppm (e.g. Dunbar et al. 1989).

The only previous study of melt inclusions from rhyolites in the Snake River Plain was that of the Badlands lava from the Owyhee-Humboldt eruptive centre (Manley 1996b; Fig. 5.1 inset) which reported water contents ranging from 0.73 to 4.55 wt.%. Despite its proximity to the type area of Snake River-type volcanism, the rhyolites from Owyhee-Humboldt

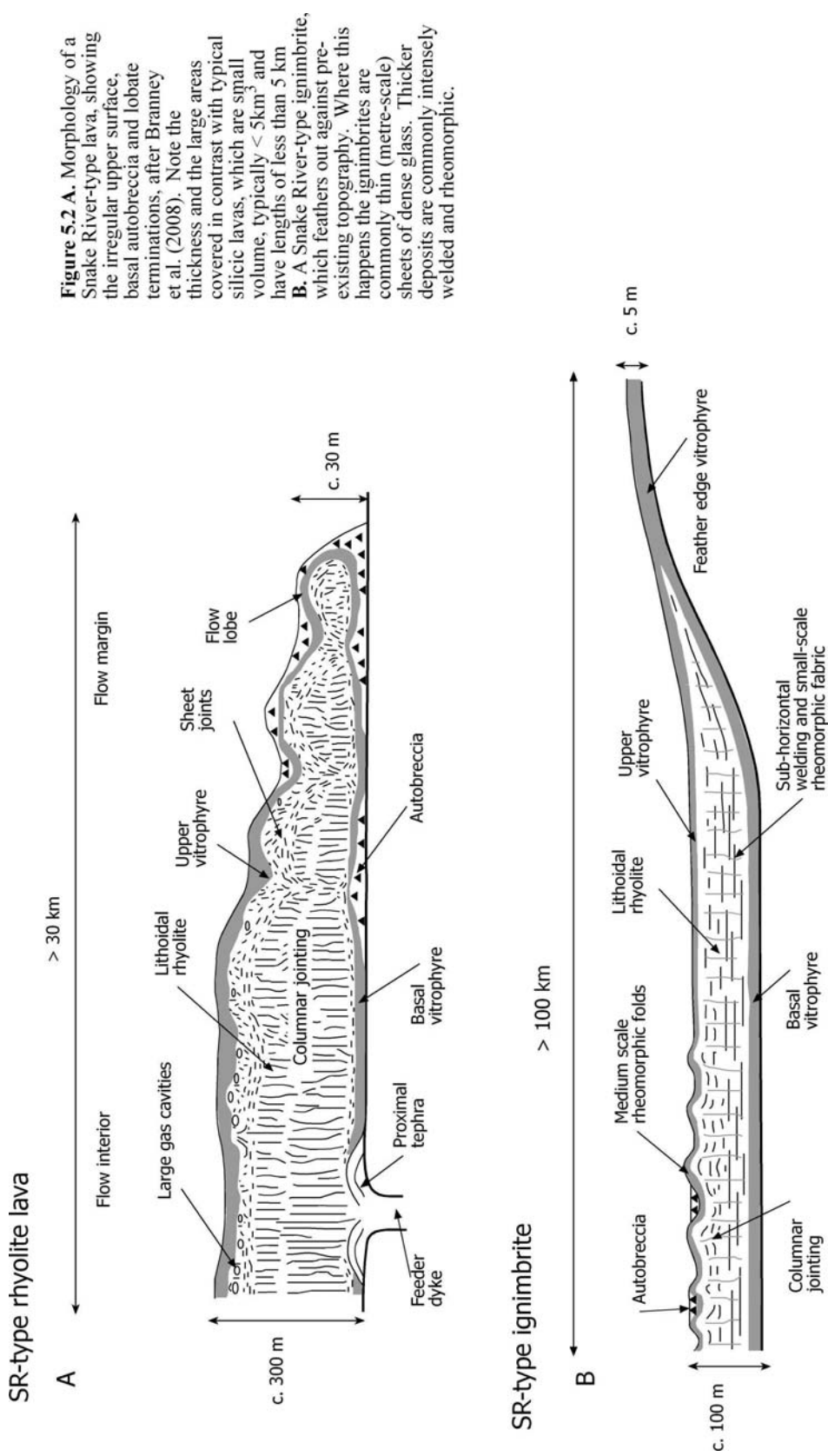


Figure 5.2 A. Morphology of a Snake River-type lava, showing the irregular upper surface, basal autobreccia and lobate terminations, after Branney et al. (2008). Note the thickness and the large areas covered in contrast with typical silicic lavas, which are small volume, typically < 5 km³, and have lengths of less than 5 km **B.** A Snake River-type ignimbrite, which feathers out against pre-existing topography. Where this happens the ignimbrites are commonly thin (metre-scale) sheets of dense glass. Thicker deposits are commonly intensely welded and rheomorphic.

Volatile species	Typical concentrations	Additional comments
H ₂ O	Rarely <3% or more than 7 wt%	Lower concentrations are common in leaked melt inclusions
CO ₂	Up to 1000 ppm though some systems contain very little c. 25 ppm	Concentration highly dependent on pre-entrapment degassing
Cl	600 to 2000 ppm	Peralkaline and mafic inclusions may contain >3000 ppm
F	400 to 1500 ppm	Continental systems may reach > 1 wt% (10,000 ppm)
S	Usually <200 ppm; often < 60 ppm	Concentrations are higher in basalts and andesites

Table 5.1 Typical volatile concentrations in melt inclusions within high silica rhyolites after Lowenstern (1995)

differ in a number of respects. Eruptions from the Owyhee-Humboldt eruptive centre were exclusively effusive, with no ignimbrites yet defined (Manley and McIntosh 2002) and the analysed rhyolites were chemically more evolved, than those studied here, up to 78 wt.% SiO₂ with magmatic temperatures (~850°C) lower than those which characterise SR-type volcanism (Manley 1996; Manley and McIntosh 2002).

Melt inclusion compositions may be modified if the phenocryst host is ruptured (Danyushevsky et al. 2002; Wallace 2005). Decompression may cause rupture of phenocrysts and although broken phenocrysts are common in other ignimbrites (Best and Christiansen 1997), they are relatively rare in SR-type ignimbrites. If a melt inclusion contracts more than the surrounding crystal, it may produce a vapour (or shrinkage) bubble. The formation of such a bubble may leave the melt inclusion depleted in volatile components such as CO₂ (Anderson and Brown 1993; Wallace 2005). The presence or

absence of vapour bubbles appears to have little effect on the water content of an inclusion (e.g. Blundy and Cashman 2005).

Criteria for unit selection

To enable conclusions to be drawn relating to eruptive style, it is necessary to compare units which are as similar as possible. Samples were split into three experiments, with each experiment containing an ignimbrite and a lava from a geographically similar area. Where possible, the units within an experiment were in stratigraphic contact with each other, making comparison of the units easier. Bonnicksen et al. (2008) showed that during certain time periods, distinct chemical compositions (as determined by whole rock analyses) dominated the erupted products, with FeO and TiO₂ values best differentiating the units into composition and time (CAT) groups. To ensure that samples selected for comparison in this study were from similar magma batches, each pair of samples was taken from within single CAT groups of Bonnicksen et al. (2008). Whole rock chemistry (see analytical techniques section later for details) of the units within the three experiments is shown in Figure 5.3.

Units within a single experiment have similar pyroxene compositions (see analytical techniques section for technical details) in terms of MgO and FeO wt.% in both pigeonites and augites (Fig 5.4). The Balanced Rock and Castleford Crossing units of experiment 2 are distinct from the other units in having abundant orthopyroxene and rare pigeonite, whereas co-existing augite and pigeonite is a much more common phenocryst assemblage for Snake River rhyolites (e.g. Honjo et al. 1992; Cathey and Nash 2004; Chapter 2).

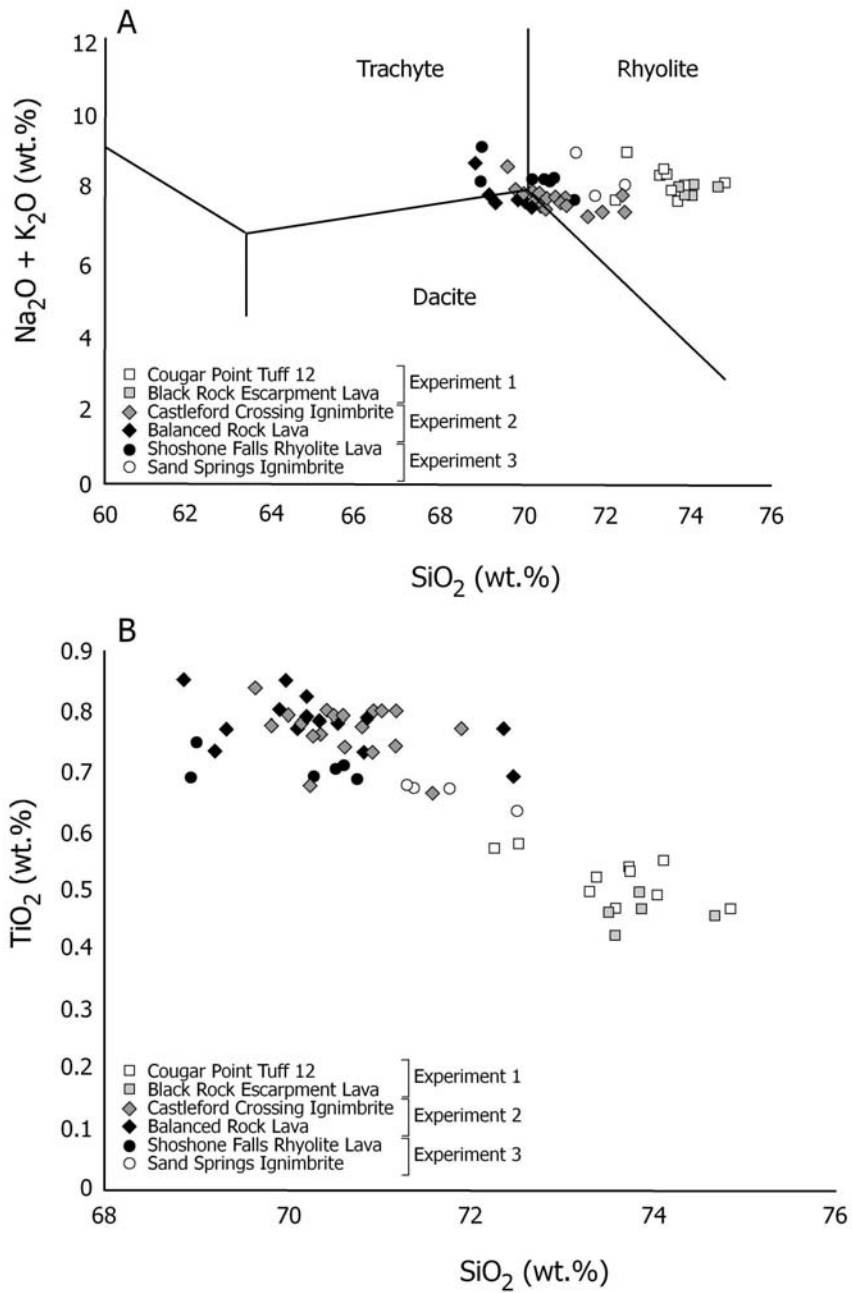


Figure 5.3 Whole rock geochemistry from this study and data from Bonnicksen et al. (2008) **A.** Enlarged section of a TAS diagram **B.** Difference in SiO_2 and TiO_2 contents between the experiments is pronounced between experiment 1 and experiment 2.

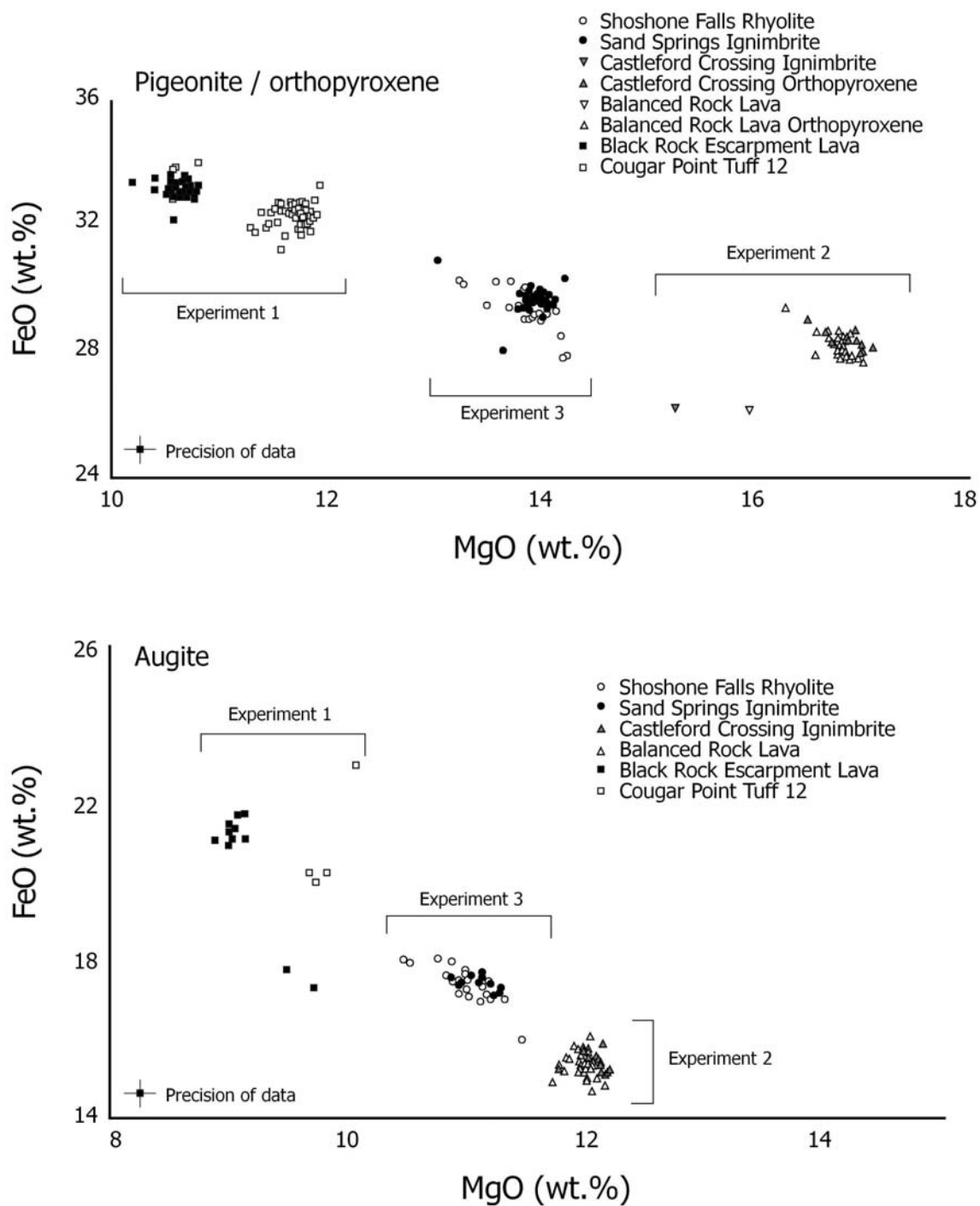
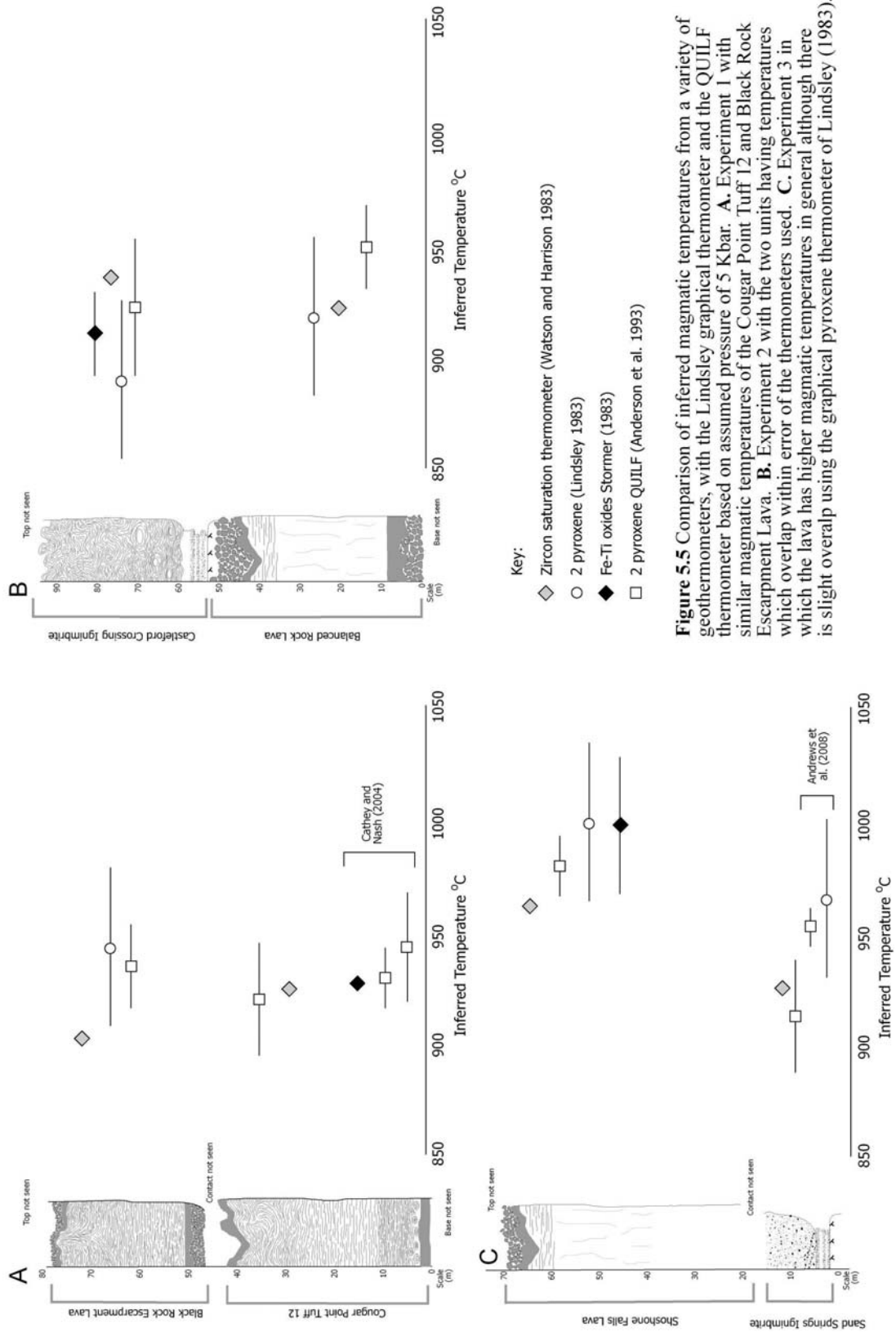


Figure 5.4. Pyroxene compositions of the units in the experiments, reflecting the overall similarities in magmas within an experiment. The units in experiment 2, Balanced Rock Lava and Castleford Crossing Ignimbrite contain more orthopyroxene than pigeonite.

A variety of geothermometers (techniques as in Chapter 2) were employed to test whether the samples within each experiment had similar magmatic temperatures. As in Chapter 2, the use of mineral thermometers assumes that the rim of the mineral has equilibrated with the liquid even if the core may not have. In experiment 1, both the ignimbrite and the lava had magmatic temperatures which overlapped within error of the thermometers around 930 °C (Fig. 5.5). These results for Cougar Point Tuff 12 and Black Rock Escarpment Lava agree with previously published work (Cathey and Nash 2004). The Balanced Rock Lava and the Castleford Crossing Ignimbrite also have magmatic temperatures which overlap within error, although the lava appears to have had a slightly higher pre-eruptive temperature (Fig. 5.5). In experiment 3, the Shoshone Falls Rhyolite Lava consistently suggests a higher magmatic temperature than the Sand Springs Ignimbrite. The magmatic temperatures determined for the Sand Springs Ignimbrite in this study are slightly lower than those determined by Andrews et al. (2008), illustrated in Figure 5.5.

In order for units to be included in this study, samples required a suitable phenocryst assemblage that contained melt inclusions. The melt inclusions in this study were between 20 and 80 µm and hosted in plagioclase phenocrysts (Fig. 5.6). Where possible individual phenocrysts were examined under a binocular microscope to select inclusions that contained neither microlites nor vapour bubbles. Typical melt inclusions similar to those used in this study are shown in Figure 5.6. Inclusions hosted in feldspar have been considered to be less reliable than those hosted in quartz (Lowenstern 1995), because the feldspar is more likely to fracture along its cleavage and possibly lose water from the inclusion. However, recent work has shown that plagioclase can be used successfully (e.g. Blundy and Cashman 2001; 2005).



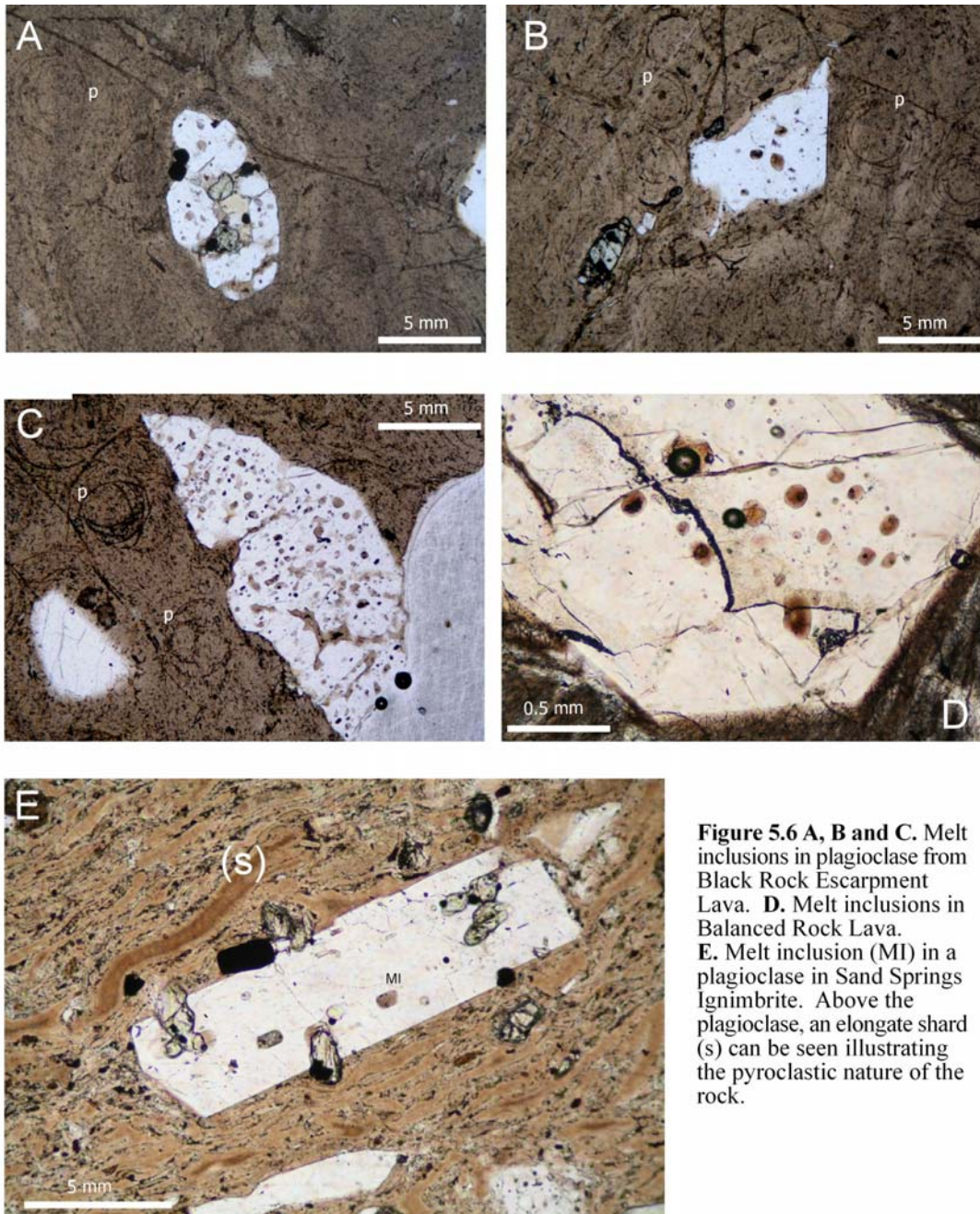


Figure 5.6 A, B and C. Melt inclusions in plagioclase from Black Rock Escarpment Lava. **D.** Melt inclusions in Balanced Rock Lava. **E.** Melt inclusion (MI) in a plagioclase in Sand Springs Ignimbrite. Above the plagioclase, an elongate shard (s) can be seen illustrating the pyroclastic nature of the rock.

Analytical techniques

Whole Rock Chemistry

Samples were analysed by X-ray fluorescence at the University of Leicester and Washington State University (Bonnichsen et al. 2008). Sample preparation for X-ray

fluorescence analysis is detailed in Chapter 2. The results of X-ray fluorescence analysis are shown in Figure 5.3.

Electron microprobe

Samples were analysed with a JEOL JXA-8600S electron microprobe at the Department of Geology at the University of Leicester, using the methodology as described in Chapter 2. Some melt inclusions have insufficient exposed area to allow two analyses with a beam diameter of > 40 microns. In these cases it was necessary to use a focussed beam, so multiple spots of a groundmass glass sample were analysed using the two-run method and compared to multiple analyses of groundmass glass using a focussed beam, and correction factors were applied where necessary to correct the results from the focussed beam experiments to those of the two-run experiments. Phenocrysts were analysed using standard operating conditions of a 10 micron beam and an operating current of 30 nanoamps.

Ion microprobe

Samples were analysed using the NERC Scientific Services CAMECA IMS-4f ion microprobe at the University of Edinburgh. Inclusions and their enclosing phenocrysts were hand-picked and set in resin before being sectioned; with additional samples coming from thin sections. One inch round sections were polished initially using diamond paste, followed by a final thirty second polish with Al₂O₃, cleaned using methanol then gold coated. The primary beam was O⁻ ions with an accelerating voltage of 15 keV. The beam was initially rastered over a 50 mm² area for two minutes to remove any surface contamination from the sample. The sample was then analysed using a 15 µm diameter spot. Spots were analysed for a total of twenty cycles; a total of 1000 seconds for all elements. The first eight cycles are not considered in the determination of elemental abundance to further reduce the chance of surface contamination, giving a total counting time of 600 seconds. Secondary ions produced were accelerated to 4500 V, and an offset of 75 keV was used to reduce the chances of analysing molecular ions. The following

isotopes were analysed ^1H , ^7Li , ^{12}C , ^{19}F , ^{25}Mg , ^{26}Mg , ^{35}Cl , ^{42}Ca , ^{47}Ti and ^{54}Fe with the major elements ratioed to ^{30}Si as determined by electron microprobe analyses. The ion yield of H/Si mirrors the change in Si content so that as the silica content increases, the ionisation of H relative to Si also increases. Thus the ratio of H/Si can be used as a constant (basalt or rhyolite would both work); this was determined from known standard compositions and gave a constant to apply to the measured H/Si ratio of the unknown. Carbon also shows the same ionisation behaviour and can be measured in the same way.

Backgrounds

Backgrounds were estimated by analysis of standards such as BOG quartz, and tested by analysing plagioclase phenocrysts for H and C. Using the BOG quartz standard, backgrounds were: H, 0.02 wt.%; C, 81.5 ppm; F ~2 ppm; and Cl, 12 ppm.

Analytical errors

Errors determined by ionprobe are based on counting statistics for the elements of interest; these are typically small (e.g. 0.0009 wt.% on an abundance of 4.01 wt.% water for the Siss51 standard). This gives an error of 0.017% and represents the smallest possible error on that analysis. A more realistic method of expressing error is to use the standard deviation of multiple replicates of a standard homogeneous material to assess the precision of the ionprobe. Using the Siss51 glass as a standard, as its water content most closely matches the water contents of the samples (as inferred from electron microprobe totals), the standard deviation of 7 replicate analyses was 0.22 wt.%. This value represents 4.8 % of the average water content determined for that glass, and this percentage can be used as the error on the unknowns. For F the relative standard deviation (using NIST610) was 7.01% and for Cl, 3.33%. For C, Rb 497 gives a relative standard deviation of 3.4 %, with Siss51 giving a relative standard deviation of 9.03 %.

Accuracy

Abundances of water determined from the standards were somewhat higher than the certified values. For example, the NIST610 standard glass has a certified water contents of 0.013 wt.% whereas the average abundance determined during this study was 0.029 wt.%. The Siss51 standard glass has a nominal water content of 4.00 wt.% (Mangan and Sisson 2000), however multiple replicates during this work average at 4.30 wt.%, again an over-estimate. The smaller over-estimate of Siss51 glass as opposed to the NIST610 standard supports use of the former as primary standard. Chlorine contents were also slightly higher than expected; Siss51 glass (Mangan and Sisson 2000) nominally contains 600 ppm Cl, whereas values obtained here ranged from 740-960 ppm. Over-estimation of F in the NIST610 glass was significant with the average determined at 854 ppm, rather than the quoted range of 295-611 ppm (<http://georem.mpch-mainz.gwdg.de/>). The difference between the certified values of the standards and the values returned by analysis, suggests that the results here may be slightly higher than the actual values, and may be considered an upper limit on the true values. The apparent over-estimation may be a function of the efficiency of detector in use at the time of analysis (Hinton *pers. comm.*).

Experiment 1

Field description

Cougar Point Tuff XII

Located within the Cougar Point Tuff succession of Bonnicksen and Citron (1982), Cougar Point Tuff 12 is a 30 m thick, intensely welded ignimbrite with an estimated volume between 10-100 km³ (Boroughs et al. 2005). The base of the unit contains a dense vitrophyre with an overlying zone of lithophysae and spherulites (Fig. 5.7). It is strongly sheet jointed in places, with some medium scale open folds above the sheet jointed facies. The age of Cougar Point Tuff 12 is estimated as 11.1 Ma (Cathey and Nash 2004; Bonnicksen et al. 2008), as it is interbedded between units which are well constrained in terms of age by ⁴⁰Ar/³⁹Ar geochronology, Cougar Point Tuff 11, aged 11.29 ± 0.07 Ma and Cougar Point Tuff 13, aged 10.86 ± 0.06 Ma (Bonnicksen et al. 2008; Chapter 3).

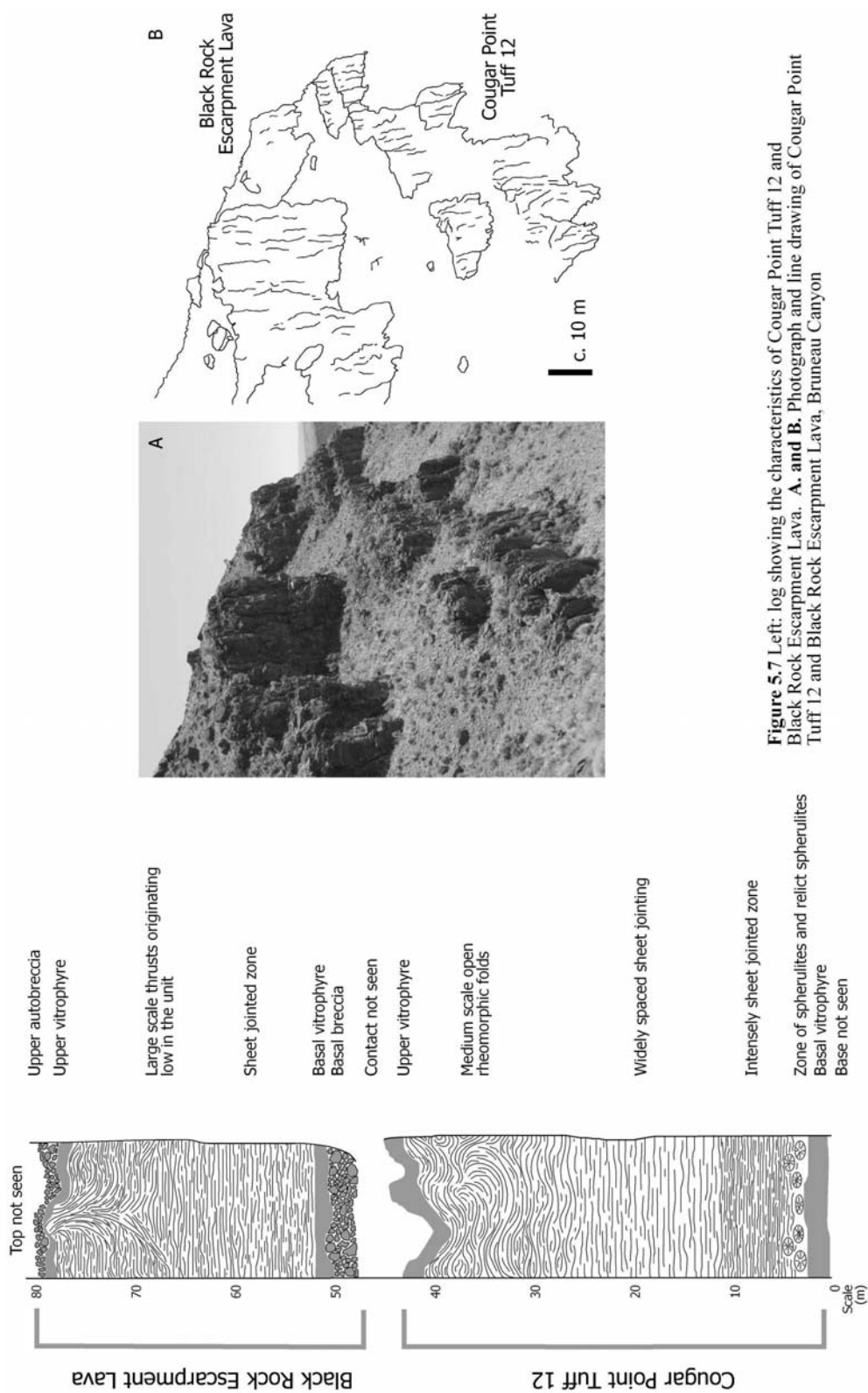


Figure 5.7 Left: log showing the characteristics of Cougar Point Tuff 12 and Black Rock Escarpment Lava. **A. and B.** Photograph and line drawing of Cougar Point Tuff 12 and Black Rock Escarpment Lava, Bruneau Canyon

Black Rock Escarpment Lava

First described as the unnamed lava within the Cougar Point Tuff succession (Bonnichsen 1982), the Black Rock Escarpment Lava ranges in thickness from 20 to 60 m. It has a blunt termination and large scale thrusts that extend from the base of the unit to the upper surface. The Black Rock Escarpment Lava outcrops in the Bruneau River canyon but is absent in the Jarbidge River canyon.

Electron microprobe*Inclusions*

Melt inclusions in both Cougar Point Tuff 12 and Black Rock Escarpment Lava are rhyolitic, with the ignimbrite containing 72.9-78.9 wt.% SiO₂ and the lava 74.5-77.9 wt.% SiO₂ (Fig. 5.8 A). While the melt inclusions in the lava and ignimbrite overlap in abundances of all major elements, the melt inclusions from the lava have a smaller geochemical variation and a slightly higher abundance of TiO₂. The average F content of the melt inclusions is low, 0.11 wt.% (1100 ppm) in the lava and 0.04 wt.% (400 ppm) in the ignimbrite (Table 5.2). Chlorine contents are low in both the lava and the ignimbrite, around 300 ppm in the ignimbrite and 100 ppm in the lava. Although the lava has considerably more F than Cl, in the ignimbrite the abundances are similar (Table 5.2). However the abundances of halogens as determined by electron microprobe should be regarded with some caution (see later). The melt inclusions have electron probe totals which are high, the average for Cougar Point Tuff 12 is 98.8% and for the Black Rock Escarpment Lava it is 97.1%. These totals suggest that the total initial volatile content of the lava was higher than that of the ignimbrite.

Groundmass

Cougar Point Tuff 12 and Black Rock Escarpment Lava have similar groundmass glass chemistries, although the ignimbrite shows a greater range of FeO and CaO than the lava (Fig. 5.8). Cathey and Nash (2004) show that the fallout deposit associated with Cougar

	Experiment 1			Experiment 2			Experiment 3			Typical Absolute Error 2 sigma			
	Lava	Ignimbrite		Lava	Ignimbrite		Lava	Ignimbrite					
	BREL inclusions	BREL groundmass	CPT12 inclusions	CPT12 groundmass	BRL inclusions	BRL groundmass	CFCI inclusions	CFCI groundmass	SFRL inclusions	SFRL groundmass	SSI inclusions	SSI groundmass	n
SiO ₂	n = 18 76.43	n = 76 76.47	n = 13 76.05	n = 52 77.04	n = 45 76.68	n = 58 77.43	n = 16 75.96	n = 56 77.70	n = 30 77.56	n = 58 76.25	n = 27 75.65	n = 55 76.40	0.26
TiO ₂	0.32	0.29	0.25	0.28	0.40	0.32	0.29	0.30	0.39	0.29	0.32	0.36	0.05
Al ₂ O ₃	11.17	11.71	12.11	12.04	11.86	11.71	11.61	11.97	10.90	12.28	12.23	12.09	0.09
Cr ₂ O ₃	0.01	0.01	0.01	0.01	0.01	0.01	0.01	0.01	0.01	0.01	0.01	0.01	0.04
FeO	2.07	1.85	1.69	1.71	1.62	1.51	0.95	1.16	1.71	1.64	1.46	1.55	0.08
MnO	0.04	0.03	0.04	0.03	0.03	0.03	0.02	0.02	0.03	0.03	0.02	0.03	0.03
MgO	0.07	0.08	0.08	0.07	0.18	0.11	0.05	0.05	0.11	0.06	0.09	0.11	0.02
CaO	1.07	0.75	1.17	0.73	1.21	0.61	0.70	0.46	0.70	0.53	1.04	0.84	0.04
Na ₂ O	1.87	2.45	1.87	2.33	2.52	2.67	2.67	2.86	2.48	2.84	3.02	2.41	0.10
K ₂ O	6.65	6.30	6.62	5.67	5.82	5.50	6.59	5.39	5.96	5.97	5.96	6.06	0.08
NI0	0.01	0.01	0.01	0.01	0.01	0.01	0.00	0.01	0.01	0.01	0.01	0.01	0.01
F	0.11	0.07	0.04	0.10	0.08	0.11	0.08	0.09	0.07	0.07	0.08	0.12	0.18
Cl	0.02	0.01	0.03	0.02	0.03	0.01	0.02	0.02	0.04	0.02	0.03	0.04	0.03
SO ₃	0.01	0.01	0.01	0.01	0.01	0.01	0.01	0.01	0.01	0.01	0.01	0.03	0.04
Total	100	100	100	100	100	100	100	100	100	100	100	100	

Table 5.2 Electron microprobe analyses (recalculated to 100%) of the groundmass glass and inclusions of the units in this study. The values given are averages, with the number of analyses at the top of the column. The right hand column gives representative errors on a single analysis. Abbreviations for the units are as follows, BREL - Black Rock Escarpment Lava, CPT 12 - Cougar Point Tuff 12, BRL - Balanced Rock Lava, CFCI - Castleford Crossing Ignimbrite, SFRL - Shoshone Falls Rhyolite Lava, SSI - Sand Springs Ignimbrite

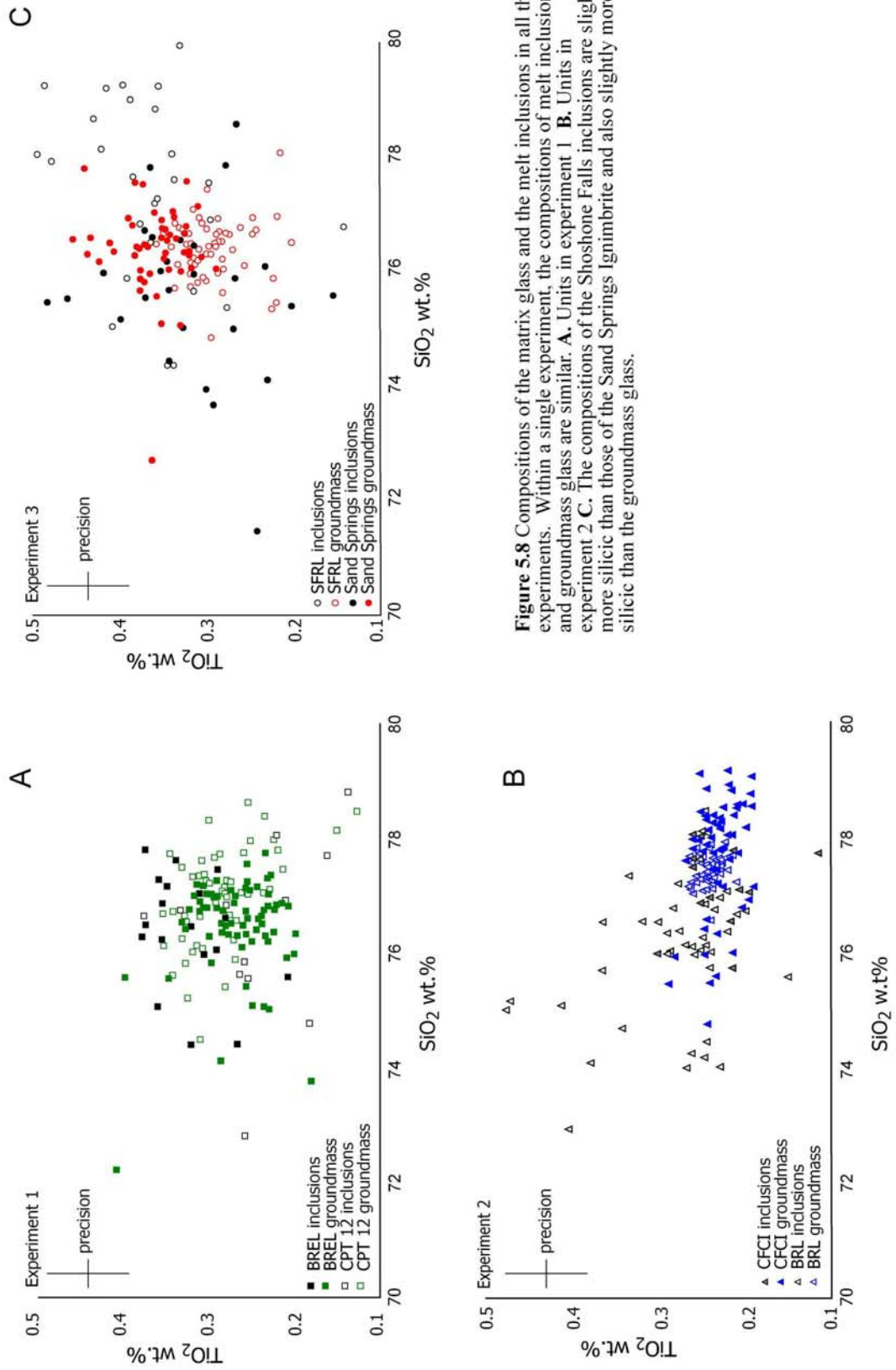


Figure 5.8 Compositions of the matrix glass and the melt inclusions in all the experiments. Within a single experiment, the compositions of melt inclusions and groundmass glass are similar. **A**, Units in experiment 1 **B**, Units in experiment 2 **C**. The compositions of the Shoshone Falls inclusions are slightly more silicic than those of the Sand Springs Igimbrite and also slightly more silicic than the groundmass glass.

Point Tuff 12 has a number of compositional modes of different chemistry in terms of SiO₂ and FeO. If such modes were homogenised within the welded ignimbrite this may explain the greater variability in glass compositions. The average F and Cl contents of both the lava and the ignimbrite are similar, for F (1000 ppm for the ignimbrite and 700 ppm in the lava) and for Cl was 200 ppm for the ignimbrite and 100 ppm in the lava. The average groundmass glass totals are 96.8 and 96.5 for Cougar Point Tuff 12 and Black Rock Escarpment Lava respectively, reflecting hydration of the glass post-emplacment.

Experiment 2

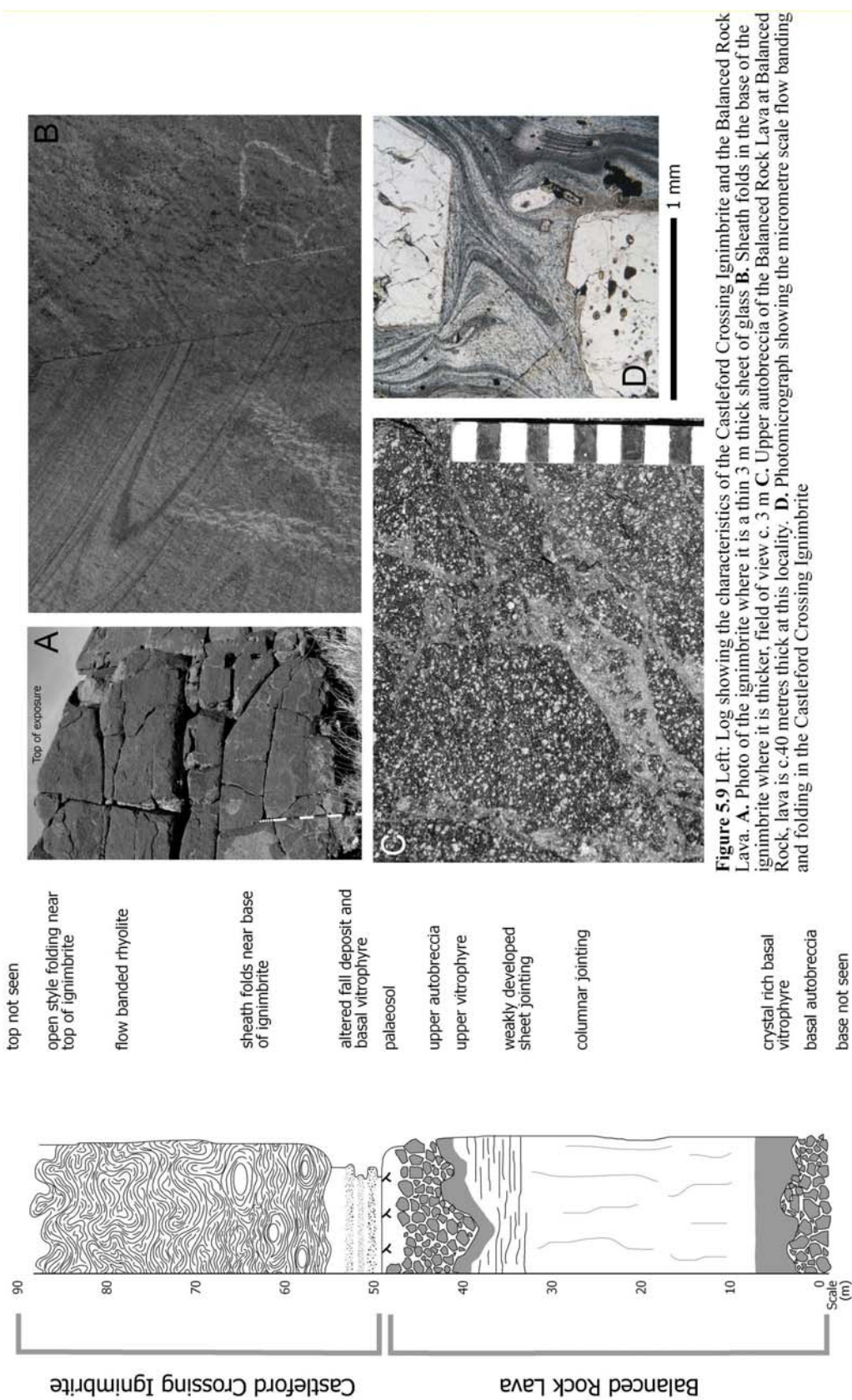
Field description

Balanced Rock Lava

The thickness of the Balanced Rock Lava ranges between 30-50 m with autobreccias at the top and bottom of the unit (Fig. 5.9 C). Both breccias are glassy with the devitrified centre of the lava being roughly columnar (Fig. 5.9). This unit covers at least 400 km², and has a minimum estimated volume of 16 km³.

Castleford Crossing Ignimbrite

This unit overlies a palaeosol above the irregular upper autobreccia of the Balanced Rock Lava. Directly above the soil lies a series of well-sorted parallel-bedded cm-scale fall deposits dominated by fine to coarse ash. Such ashfall deposits are typical of SR-type eruptions (Branney et al. 2008). Above the fall deposits is a m-thick vitrophyre which passes up into lava-like ignimbrite reaching 50 m in thickness. The Castleford Crossing Ignimbrite is highly rheomorphic showing flow banding and flow folds (Fig. 5.9 D) including beautifully preserved sheath folds. Sheath folds predominate in the lower parts of the ignimbrite (Fig. 5.9 B) and larger scale open folds are seen in the upper reaches of the ignimbrite; a similar style of folding to that seen in other SR-type ignimbrites e.g. Greys Landing ignimbrite (Andrews et al. 2008). The Castleford Crossing Ignimbrite is unusual with respect to SR-type ignimbrites in that flow banding picks out the majority of the rheomorphic features and sheet jointing is rare. This suggests that rheomorphism may well



have finished by the time that the ignimbrite had cooled sufficiently to behave in a brittle manner. Where the ignimbrite thins against palaeotopography it becomes entirely vitrophyric (Fig. 5.9 A). The Castleford Crossing ignimbrite has normal magnetic polarity, unlike the underlying Balanced Rock Lava, and has a $^{40}\text{Ar}/^{39}\text{Ar}$ age of 8.13 ± 0.29 Ma (Bonnichsen et al. 2008).

Electron microprobe

Inclusions

Inclusions in both the ignimbrite and the lava are rhyolitic with similar average compositions (e.g. Table 5.2, Fig. 5.8). The melt inclusions in the lava have higher abundances of TiO_2 and slightly lower values of SiO_2 , similar to the whole rock chemistry which shows the lava to be slightly more mafic than the ignimbrite (Fig. 5.3). The compositional range in melt inclusions is larger in the lava than in the ignimbrite, with SiO_2 varying by 5.5 wt.% in the lava and 3.8 wt.% in the ignimbrite, although this may be a function of the greater number of analyses in the lava (45 for the lava, 16 for the ignimbrite). Fluorine and chlorine contents of the inclusions are similar albeit with large errors (see later). Average microprobe totals are around 95% for the lava and around 98.5% for the ignimbrite.

Groundmass

The groundmass glass compositions of the Balanced Rock Lava and Castleford Crossing Ignimbrite overlap in terms of major elements (Table 5.2). Both the groundmass compositions are rhyolitic, with the ignimbrite 74.7 to 79.2 wt.% SiO_2 and the lava 76.6 to 78.8 wt.% SiO_2 . The range of most major elements is larger in the ignimbrite than the lava (e.g. SiO_2 , Al_2O_3 , CaO , FeO and MgO). Fluorine and chlorine contents in the groundmass have an almost identical range of values in the lava and ignimbrite (1100 ppm lava and 900 ppm ignimbrite for F and 100 ppm lava and 200 ppm ignimbrite for Cl). In contrast to the inclusions, the groundmass electron probe totals are almost identical (Table 5.2).

Experiment 3

Field description

Sand Springs Ignimbrite

The Sand Springs Ignimbrite is a small volume unit ($< 10 \text{ km}^3$) that outcrops in the north of the Rogerson Graben (Andrews et al. 2008; Fig. 5.1). It has thin ($< 5 \text{ cm}$) fall deposits overlain by a non-welded ignimbrite which contains abundant small angular chips of dense, black, volcanic glass (Fig. 5.10). The base of the ignimbrite is cross-stratified and passes upwards into a massive lapilli-tuff. The unit is progressively more fused until it becomes partially welded at the uppermost exposed section. The ignimbrite is exceptionally well-sorted ($\sigma\phi$ 0.82 compared to $\sigma\phi$ 2-5 for typical ignimbrites; Branney and Kokelaar 2002) and the fall deposits which it overlies are medium ash. The Sand Springs Ignimbrite is of unknown age, but is within the CAT group of estimated age 5.5-7.5 Ma (Bonnichsen et al. 2008).

Shoshone Falls Rhyolite Lava

Well exposed in the Snake River canyon, the Shoshone Falls Rhyolite Lava has a highly irregular upper surface with a characteristic breccia composed of poorly sorted black clasts of dense black vitrophyric rhyolite in a red, hydrothermally altered ash matrix. The lava is at least 60 m thick near the Perrine Bridge, however drilling has shown that the true thickness is around 200 m (Street and DeTar 1987). The age of the lava is approximately $6.4 \pm 0.3 \text{ Ma}$ (average of K-Ar determinations of Armstrong et al. 1975, 1980; Bonnichsen et al. 2008). Unfortunately, the Shoshone Falls Rhyolite Lava and the Sand Springs Ignimbrite are not seen in stratigraphic contact so their relative ages are unclear.

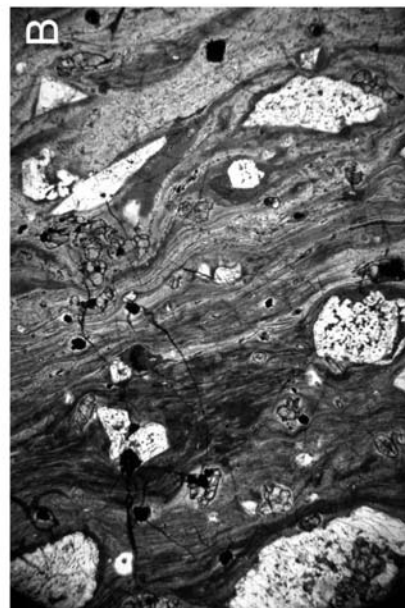
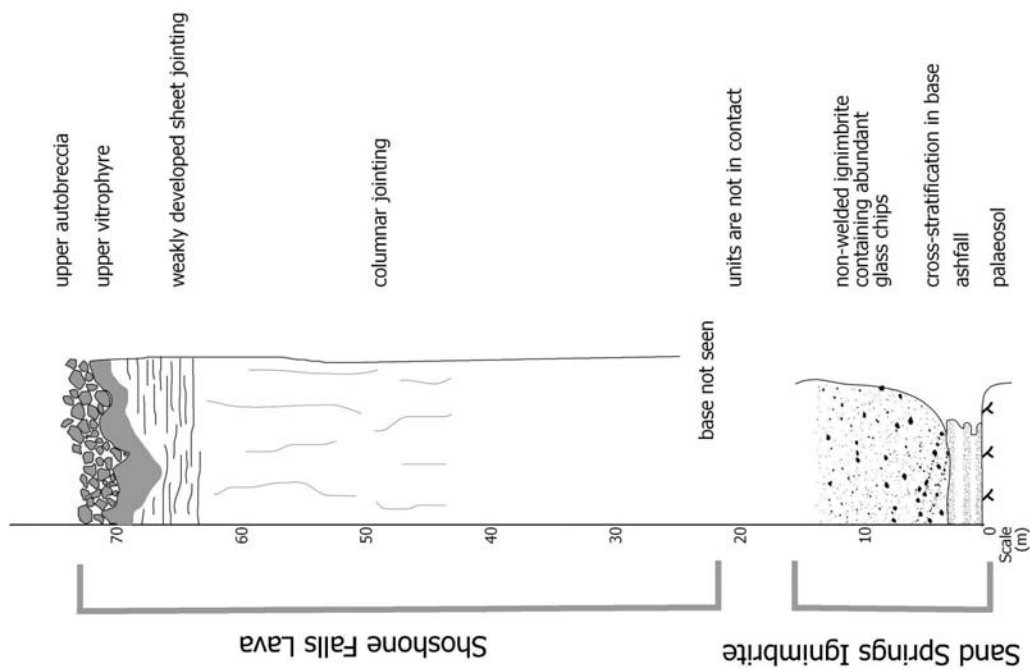


Figure 5.10 Left: Log showing the characteristics of the Shoshone Falls Rhyolite Lava and the Sand Springs Ignimbrite. The relative stratigraphic position of these two units is uncertain. A. Non-welded facies of the Sand Springs Ignimbrite with abundant glass chips. B. Flow banding in Shoshone Falls Rhyolite Lava.

Electron Microprobe

Inclusions

Melt inclusions in the Sand Springs Ignimbrite are more mafic than those in the Shoshone Falls Rhyolite Lava (Table 5.2; Fig. 5.8). The inclusions from the lava have a more restricted compositional range than those of the ignimbrite; in terms of SiO₂ the range in the lava is 4.8 wt.% whereas it is 7.1 wt.% in the ignimbrite. The halogen abundances in the ignimbrite and lava of experiment 3 are almost identical, with Cl present at 400 ppm in the lava and 300 ppm in the ignimbrite, and the F contents of 700 ppm in the lava and 800 ppm in the ignimbrite.

Groundmass

The average groundmass compositions of the Sand Springs Ignimbrite and the Shoshone Falls Rhyolite Lava are similar (Fig. 5.8). The ignimbrite contains slightly higher abundances of TiO₂ (0.36 to 0.29 wt.%) and CaO (0.84 to 0.48 wt.%) than the lava (Fig. 5.8). The compositional range of the groundmass in the ignimbrite is larger for all elemental oxides except Al₂O₃ than the lava. The average F contents are 1100 ppm in the lava and 1200 ppm in the ignimbrite; the average Cl content of the lava is 200 ppm and 400 ppm in the ignimbrite. Electron probe totals of the ignimbrite and the lava are similar, with the lava 96.6 and the ignimbrite 97%.

Ionprobe Results

H₂O

Experiment 1

The abundance of water in the melt inclusions of Cougar Point Tuff 12 ranges from 2.07 to 2.86 wt.%, with an average of 2.55 wt.% (Fig. 5.11) while the overlying Black Rock Escarpment Lava has higher water contents (2.20 to 3.96 wt.%, average 3.12 wt.%). In this experiment the electron probe totals are consistent with the water contents as determined by

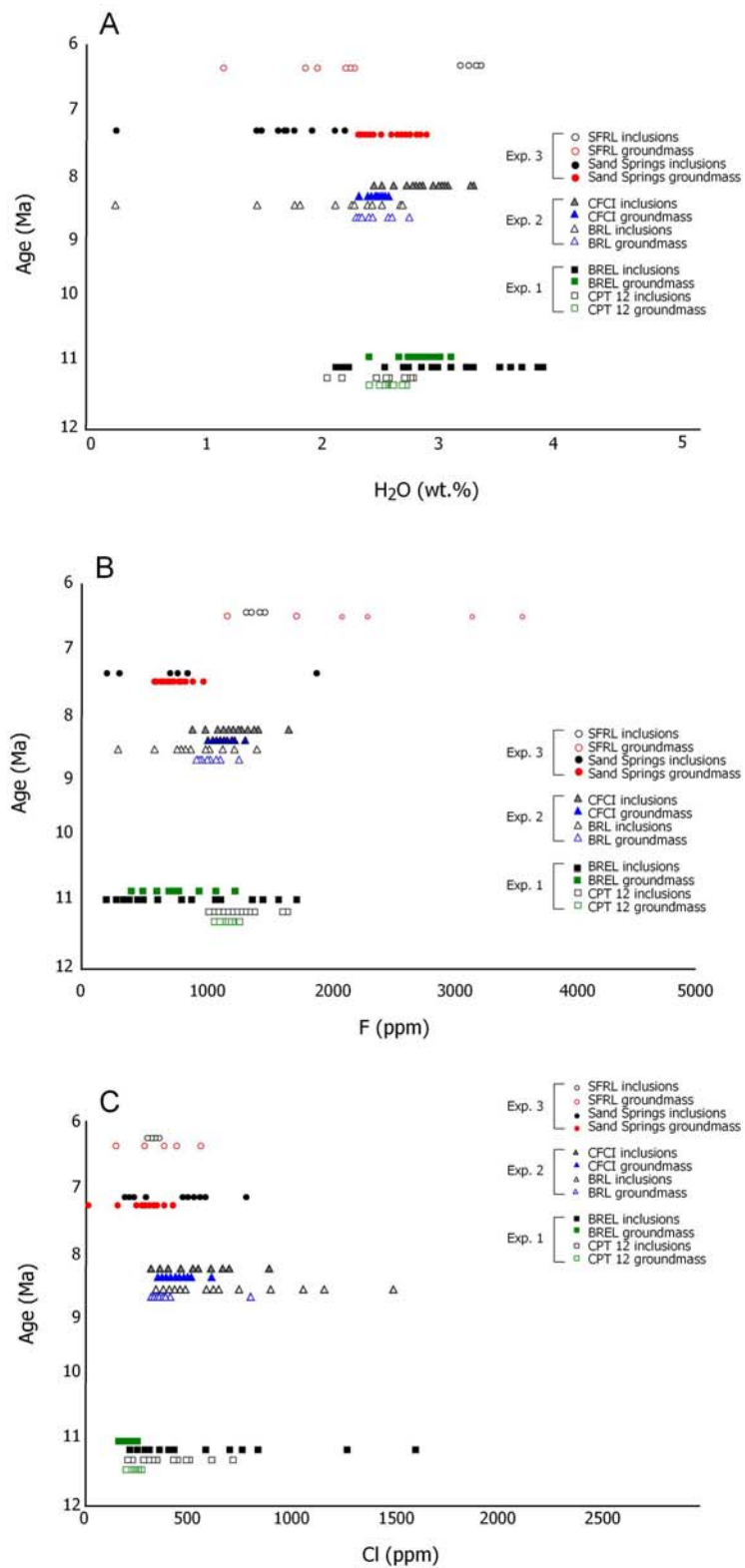


Figure 5.11 Volatile contents of melt inclusions and groundmass glass for all the units studied determined by ion microprobe (IMP). Examples of inclusions that have leaked in Balanced Rock Lava and Sand Springs Ignimbrite show very low water contents, lower than both the matrix and the rest of the unruptured inclusions.

the ionprobe. The groundmass water contents of the glasses are similar in both the lava and the ignimbrite (Table 5.3; Fig. 5.11) around 2.5 wt. %.

Experiment 2

The Balanced Rock Lava has a range of water contents from 1.49-2.71 wt.% (Fig. 5.11) with an average of 2.11 wt.%. The Castleford Crossing Ignimbrite has water contents ranging from 2.41-3.27 wt.% with an average of 2.84 wt.%. Within the analyses of the Balanced Rock Lava, one analysis provided an anomalously low water content of 0.4 wt.% which is discussed at the end of the section. The groundmass glass in both the lava and ignimbrite contains around 2.5 wt. % water.

Experiment 3

On the basis of inclusion data, the Shoshone Falls Rhyolite Lava has a higher pre-eruptive water content (3.21 to 3.33 wt.%; average 3.27 wt.%) than the Sand Springs Ignimbrite (1.48 to 2.25 wt.%; average 1.82 wt.%). In the case of the Shoshone Falls Rhyolite Lava, the water contents of the inclusions are distinct from the water contents of the groundmass glass (1.13 to 2.26 wt.%; average 1.93 wt.%; Fig. 5.11). The differences between the water contents derived from inclusions and groundmass glasses support the notion that the inclusions represent the magmatic water contents.

Leaked inclusions

A few inclusions analysed in this study produced significantly lower water contents than the majority of inclusions analysed from that unit, e.g. one inclusion from Balanced Rock Lava contained 0.4 wt.% H₂O as opposed to the average of 2.11 wt.% and an inclusion in Sand Springs Ignimbrite an inclusion contained 0.3 wt.% H₂O compared to the average of 1.82 wt.% (Fig. 5.11). That these low water contents overlap with neither the majority of the melt inclusions, nor the groundmass glass suggests that these analyses represent inclusions which have leaked.

Experiment 1

	CPT12 inc.	CPT12 gm.	BREL inc.	BREL gm.
H ₂ O	2.55	2.65	3.11	2.85
Li	17	25	17	12
F	1258	1148	828	763
Mg	1086	417	1012	1407
Cl	443	224	704	216
Ca	4677	3400	8593	4455
Ti	1666	1530	2007	1564
Fe	15392	11625	23897	17336

Experiment 2

	BRL inc.	BRL gm.	CFCI inc.	CFCI gm.
H ₂ O	2.11	2.40	2.84	2.45
Li	17	17	26	24
F	1229	1076	1714	1201
Mg	997	658	1771	838
Cl	660	419	645	421
Ca	8597	3549	4668	4082
Ti	1866	1692	2042	1564
Fe	13484	9659	8146	12492

Experiment 3

	SSI inc.	SSI gm.	SFRL inc.	SFRL gm.
H ₂ O	1.82	2.56	3.27	1.93
Li	22	25	36	25
F	4257	821	1413	2393
Mg	2545	891	559	613
Cl	1853	270	327	369
Ca	26799	5583	3662	3659
Ti	1721	1797	1667	1548
Fe	15621	14542	13466	10780

Table 5.3 Average ionprobe results for the melt inclusions and groundmass glass of all units. H is reported as wt.% H₂O and all other elements are reported as ppm.

Rehydration of groundmass

For groundmass glass at surficial pressure, < 0.2 wt.% water is soluble in rhyolite using experimental data (Blank et al. 1993; Newman and Lowenstern 2002). The high water contents of the groundmass glasses suggest that this water is not magmatic, but reflects post-emplacment alteration of the glass. Abundant perlitic cracks in the glass matrix support this suggestion (Fig. 5.12), as has been seen in other locations (e.g. New Mexico; Duffield and Dalrymple 1990) whereas non-hydrated volcanic glass (e.g. Crater Lake) typically contains close to 0 wt.% H₂O (Bacon et al. 1992).

Summary

The water contents of the melt inclusions in this study show no relationship with eruptive style; in experiments 1 and 3 the water contents of the lava-forming magmas was higher than the ignimbrite forming equivalents, whereas in experiment 2 the ignimbrite has a greater abundance of water. This suggests that the pre-eruptive water content is not the primary controlling factor in terms of eruptive style.

Fluorine

Fluorine contents in Snake River-type magmas range from 175 to ~3700 ppm, similar to those determined for other high silica rhyolites which range from 300 ppm (Bacon et al. 1992) to > 1 wt.% (Webster and Duffield 1994), with higher values expected in continental systems (Lowenstern 1995).

Experiment 1

The inclusions in the lava and ignimbrite overlap in F contents with the lava having a wider range of F contents than the ignimbrite. The groundmass F contents are similar to or slightly less than the abundances in the melt inclusions (Fig. 5.11). The similarity in F contents between the groundmass and the inclusions suggests that little fluorine is lost

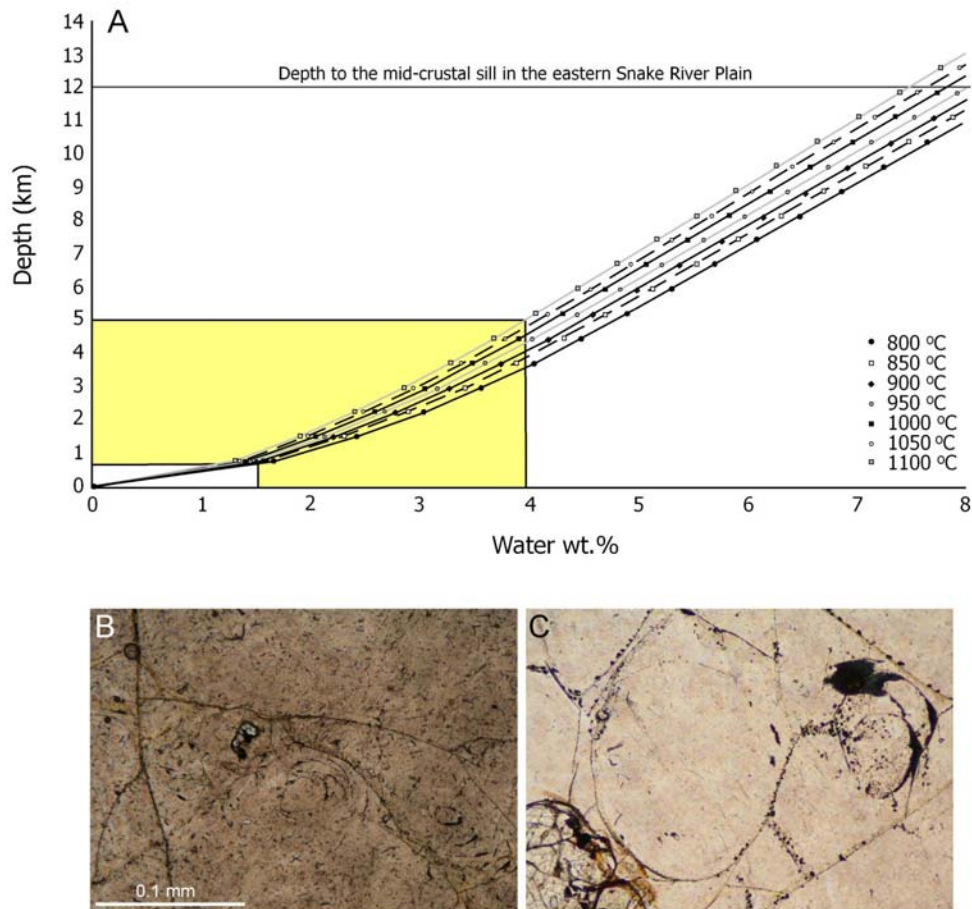


Figure 5.12 **A.** Solubility of water in rhyolitic magma at relevant temperatures, with solubility curves after Newman and Lowenstern (2002). Yellow filled area represents the water contents as determined from the melt inclusions analysed here, and the depths that these water contents would correspond to in a saturated system. If the system is not water-saturated then these depths are a minimum. **B.** Photomicrograph of the perlitic cracking in the groundmass of the Black Rock Escarpment Lava in experiment 1. **C.** Perlitic texture in the Balanced Rock Lava, indicating hydration of the groundmass.

during the course of the eruption. In terms of average compositions, the Black Rock Escarpment Lava and Cougar Point Tuff 12 lose similar amounts of their pre-eruptive fluorine, with the lava losing 7.8% and the ignimbrite 8.8%.

Experiment 2

The melt inclusions in the Castleford Crossing Ignimbrite have larger abundances of F than the lava (ignimbrite average 1741 ppm, lava average 1229 ppm) although there is a large amount of overlap between the two units. The F contents of the groundmass of the Balanced Rock Lava and Castleford Crossing Ignimbrite are very similar (Fig. 5.11). In experiment 2, the lava lost 12.4% of its pre-eruptive F content whereas the ignimbrite lost 29.9% of its F during eruption.

Experiment 3

The inclusions in the Sand Springs Ignimbrite and the Shoshone Falls Rhyolite Lava overlap in terms of F content (Fig. 5.11), with the ignimbrite having a wider range of values, reaching up to 784 ppm. The groundmass compositions are similar in both the ignimbrite and the lava with the lava reaching 565 ppm. An interesting feature of the results is that the Shoshone Falls Rhyolite Lava has higher values of F in its groundmass than in its inclusions (albeit only four inclusions were analysed) whereas most of the units lose F during an eruption as would be expected. The Sand Springs Ignimbrite in contrast, loses 80.7% of its F during the period between entrapment of melt inclusions and emplacement as ignimbrite.

Summary

Fluorine contents of the lavas and ignimbrites overlap in all the experiments although the ranges of F contents may vary between the ignimbrite and lava of a single experiment. Given that the abundances of F overlap, the variation in F is not the cause of the divergence in eruptive style.

Chlorine

Chlorine contents within SR-type magmas are typically in the range of 200-800 ppm, lower than those reported from other areas (e.g. 1700 ppm Taupo Volcanic Zone, Dunbar et al.

1989; ~1700 ppm Katmai, Westrich et al. 1991; 900-2500 ppm Galeras, Stix et al. 1993; Figure 5.14 B).

Experiment 1

The average chloride contents of the inclusions in experiment one are very similar, with the range of chloride abundances larger in the Black Rock Escarpment Lava (Fig. 5.11). Chloride contents in the groundmass of the Black Rock Escarpment Lava and Cougar Point Tuff 12 have a very restricted range and are similar between the units with the ignimbrite having slightly higher values. Both the units in experiment 1 have much lower Cl contents in their groundmass than their inclusions, Black Rock Escarpment Lava loses 69% of its Cl between entrapment and deposition while Cougar Point Tuff 12 loses 49%.

Experiment 2

Melt inclusions from the Castleford Crossing Ignimbrite and the Balanced Rock Lava have similar chloride contents with the lava having a larger range of values which stretch to larger abundances of Cl (up to 1441 ppm). The groundmass values of Cl in experiment 2, as in experiment 1, are constant and have a smaller range than the abundances in the melt inclusion. The relative loss of Cl between inclusions and groundmass of both the ignimbrite and lava in experiment 2 is around 35%.

Experiment 3

The inclusions in the Sand Springs Ignimbrite and the Shoshone Falls Rhyolite Lava have similar abundances of Cl to those from the units in experiments 1 and 2. The inclusions in the ignimbrite have some higher values than the lava in this experiment. The groundmass glass abundances of chloride in the Shoshone Falls Rhyolite Lava span the range seen in the inclusions, similar to the results for F. Sand Springs Ignimbrite loses 85% of its pre-eruptive Cl while Shoshone Falls Rhyolite Lava gains 12% more Cl than was present in the inclusions.

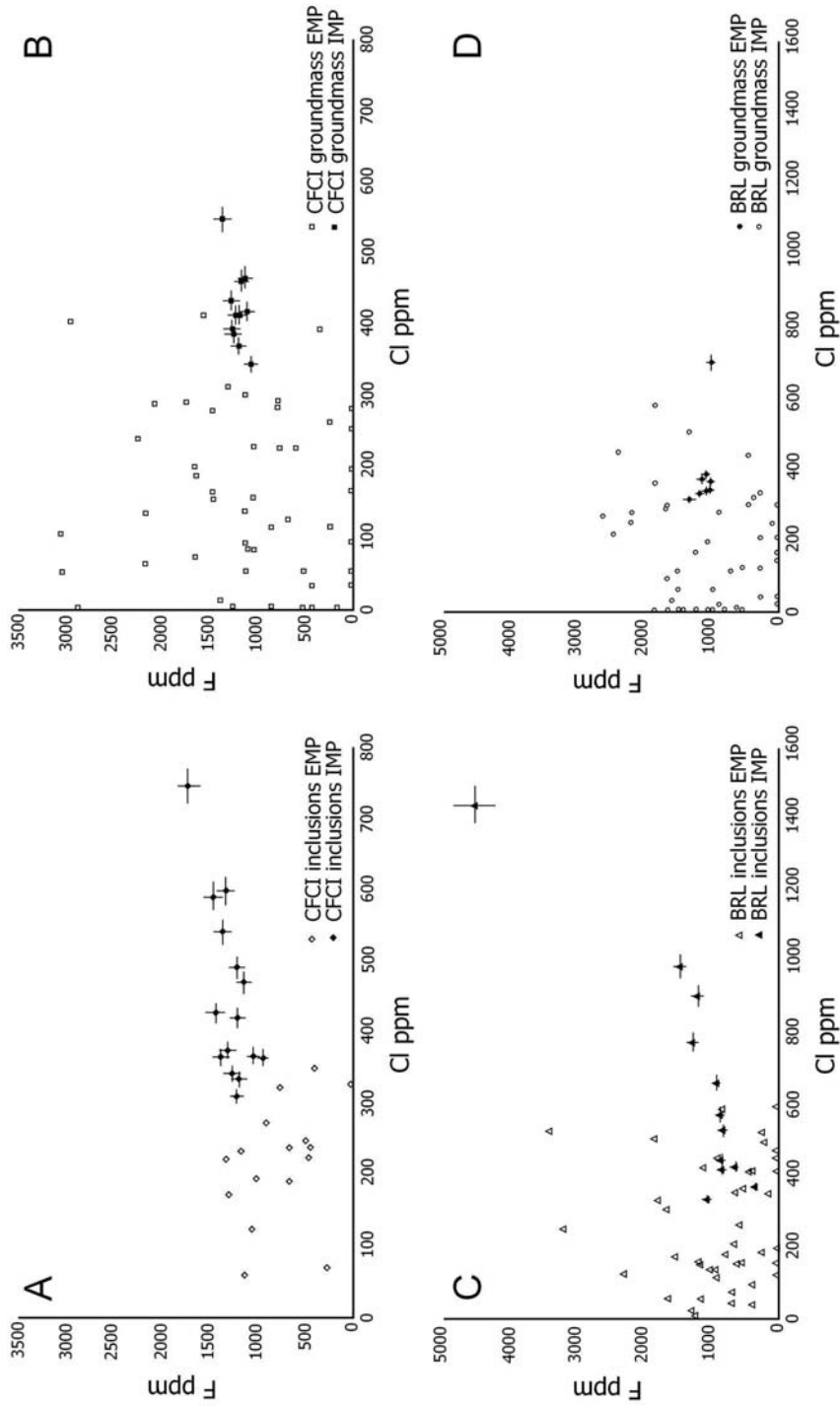


Figure 5.13 A. F plotted against Cl for Castleford Crossing inclusions; B. F plotted against Cl for Castleford Crossing groundmass; C. F plotted against Cl for Balanced Rock Lava inclusions; D. F plotted against Cl for Balanced Rock Lava groundmass. Errors on microprobe data are large at such low abundances of F and Cl, errors on CI are 387% and on F 32.4%. The ionprobe (IMP) data seems to give slightly higher values for Cl than the electron microprobe (EMP), however given the precision on the EMP data these two methods are within error.

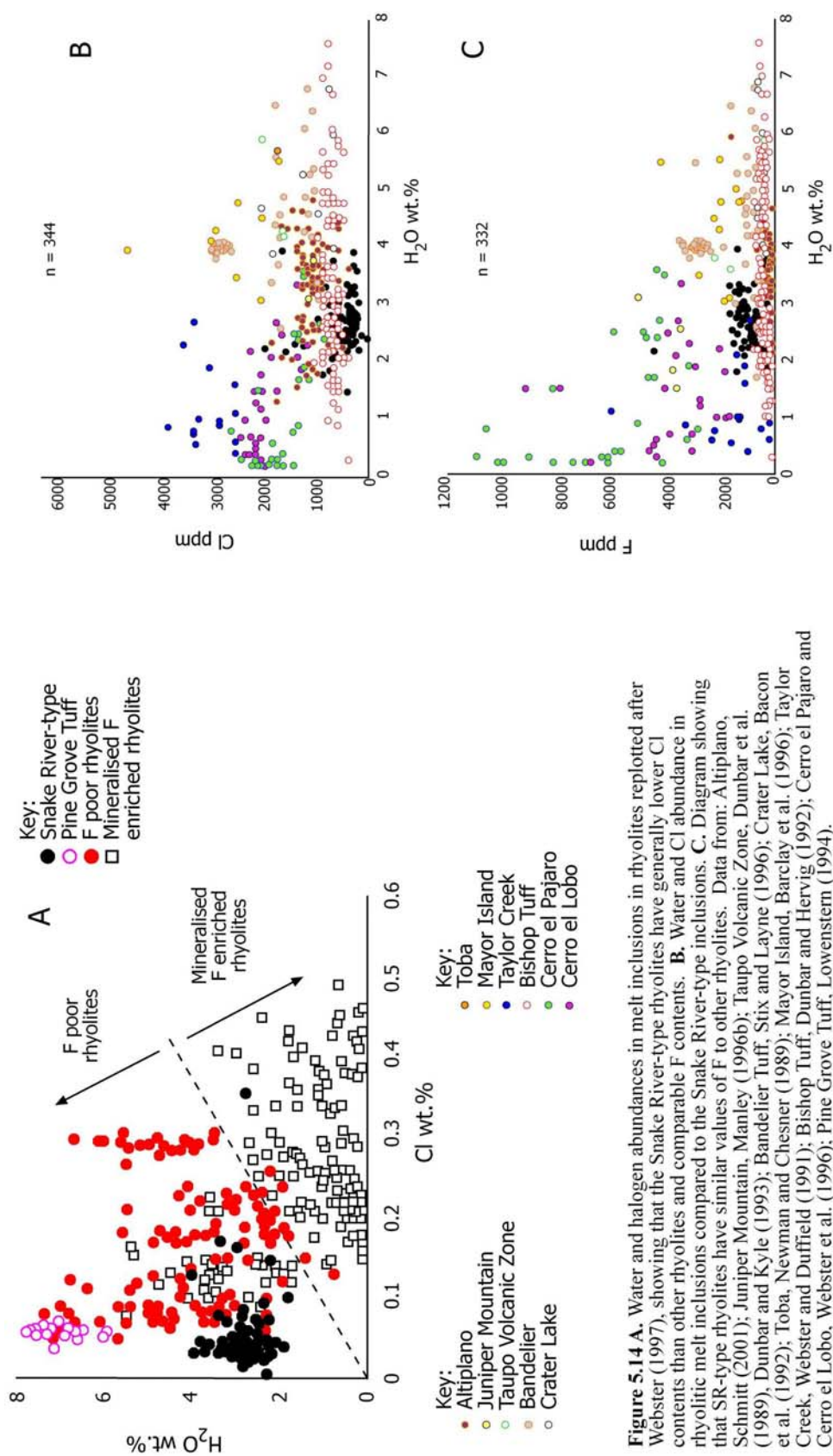


Figure 5.14 A. Water and halogen abundances in melt inclusions in rhyolites replotted after Webster (1997), showing that the Snake River-type rhyolites have generally lower Cl contents than other rhyolites and comparable F contents. **B.** Water and Cl abundance in rhyolitic melt inclusions compared to the Snake River-type inclusions. **C.** Diagram showing that SR-type rhyolites have similar values of F to other rhyolites. Data from: Altiplano, Schmitt (2001); Juniper Mountain, Manley (1996b); Taupo Volcanic Zone, Dunbar et al. (1989), Dunbar and Kyle (1993); Bandalier Tuff, Stix and Layne (1996); Crater Lake, Bacon et al. (1992); Toba, Newman and Chesner (1989); Mayor Island, Barclay et al. (1996); Taylor Creek, Webster and Duffield (1991); Bishop Tuff, Dunbar and Hervig (1992); Cerro el Pajaro and Cerro el Lobo, Webster et al. (1996); Pine Grove Tuff, Lowenstern (1994).

Summary

The Cl contents of the inclusions are uniformly low in all the experiments (Fig 5.11 C). Not only do the lavas and ignimbrites within a single experiment have overlapping Cl abundances, but all the units in this study overlap. This shows that Cl contents have no bearing on the subsequent eruptive style.

A note regarding F and Cl results

The agreement in the fluorine and chlorine as measured by electron microprobe and ion microprobe is shown in Figure 5.13. The results show that the electron microprobe tends to give lower values of Cl than the ionprobe, while the values of F are similar. All the ionprobe values are within the error (at 2σ) of the electron microprobe analyses, which is unsurprising given the large errors by electron microprobe ($> 300\%$) on the low abundances of these elements.

CO₂

The carbon analyses gave highly variable results, for both melt inclusions and groundmass. While values of CO₂ in melt inclusions from other rhyolites are commonly up to 1000 ppm (see Table 5.1), abundances measured in this study for CO₂ in groundmass glass range from zero to $> 10,000$ ppm or 1 wt.% (Fig. 5.15). Carbon is dissolved in rhyolites as molecular CO₂ (Fogel and Rutherford 1990) and is increasingly soluble with increasing pressure, but decreasingly soluble with increasing temperature, with the effect of temperature much less significant than pressure (Fogel and Rutherford 1990; Lowenstern 1995). The high abundance of C in the groundmass glass of the Snake River-type rhyolites was unexpected. There are some possibilities to explain this:

- 1) The values represent the actual abundance of C dissolved in the rhyolitic glass. This scenario is highly unlikely because experimental work on high silica rhyolites has shown that at a pressure of < 1 bar the solubility of CO₂ in rhyolite is virtually zero, irrespective of temperature (Blank et al. 1993; Newman and Lowenstern 2002). Even using the temperatures most relevant to this study (e.g. 950 °C) pressures greatly exceeding 10,000

bars would be required to dissolve > 10,000 ppm in rhyolitic glass; equivalent to a depth of 37 kilometres, which cannot be the case for groundmass glass.

2) Rare samples may have bubbles of CO₂ within them which are giving elevated C abundances. This scenario is also unlikely, for a number of reasons; firstly, there is no reason why CO₂ should remain in bubbles in the groundmass rather than be released during the eruption. Secondly, the pattern of release of C during the numerous cycles of analysis from which one result is determined are not what would be expected if ablation of the sample was exposing a bubble of CO₂ (Fig. 5.15). If a bubble were exposed during ablation of the sample, a sudden rise in the counts per second of C would be recorded, which would then drop off during the next analysis cycle. Also shown in Figure 5.15 are data from a plagioclase which was run at the same time as the groundmass, which shows that the high C counts are not related to a high background of C.

3) Another possibility is that the samples are contaminated with carbon. The samples were prepared using diamond paste in the polishing and some were subsequently carbon coated for use in the electron microprobe. Samples were cleaned twice using methanol in an attempt to remove all traces of carbon and given a final polish with Al₂O₃ but it is possible that some remained. This situation would be especially prevalent if the sections had any topography on them, even on a micro-scale, which would allow carbon to collect in the valleys. This might explain the variable results seen in these samples, a reflection of the variable amounts of contamination in each locality. However, given the process of analysis of two minute rastering, then 8 cycles of counting on the spot which are not included before analysis begins, any contaminating material would be expected to have been ablated by the time of analysis. Despite this misgiving, the contamination of samples with C appears the most credible explanation for the data (Fig. 5.16). Given that the C analyses in these experiments may be unreliable, they are not considered in the discussion below.

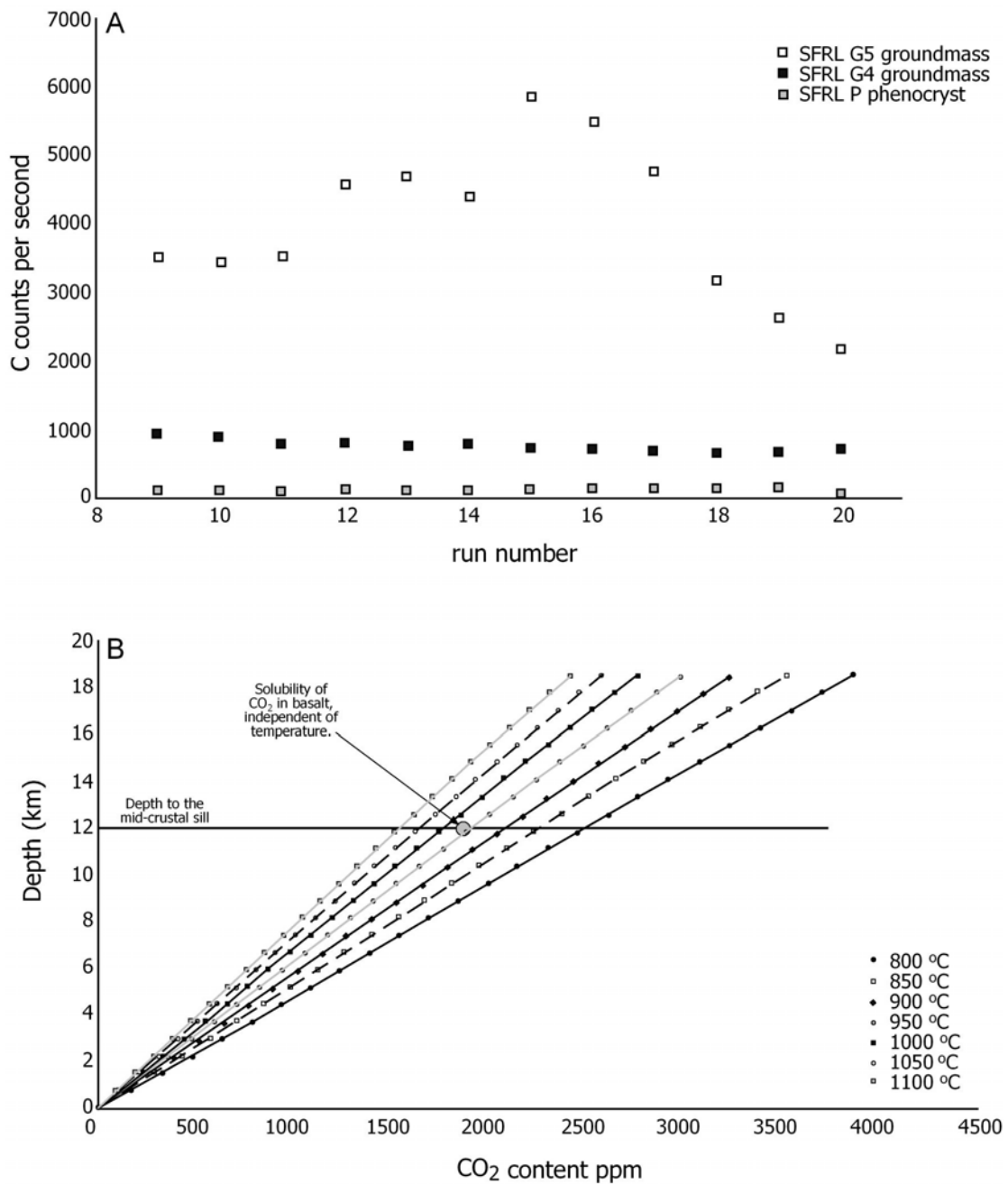


Figure 5.15 **A.** C counts per second for two samples of Shoshone Falls Rhyolite Lava groundmass (SFRL G4 and G5) and a feldspar phenocryst SFRL P which can be treated as background showing the variation in C counts between samples and within a single run **B.** Solubility of CO₂ with depth at a variety of temperatures showing the very low solubilities of CO₂ at surficial pressures, plotted using the VolatileCalc program of Newman and Lowenstern (2002). This suggests that the high values shown by groundmass sample SFRL G5 which relate to c. 1.6 wt.% CO₂ represent contamination.

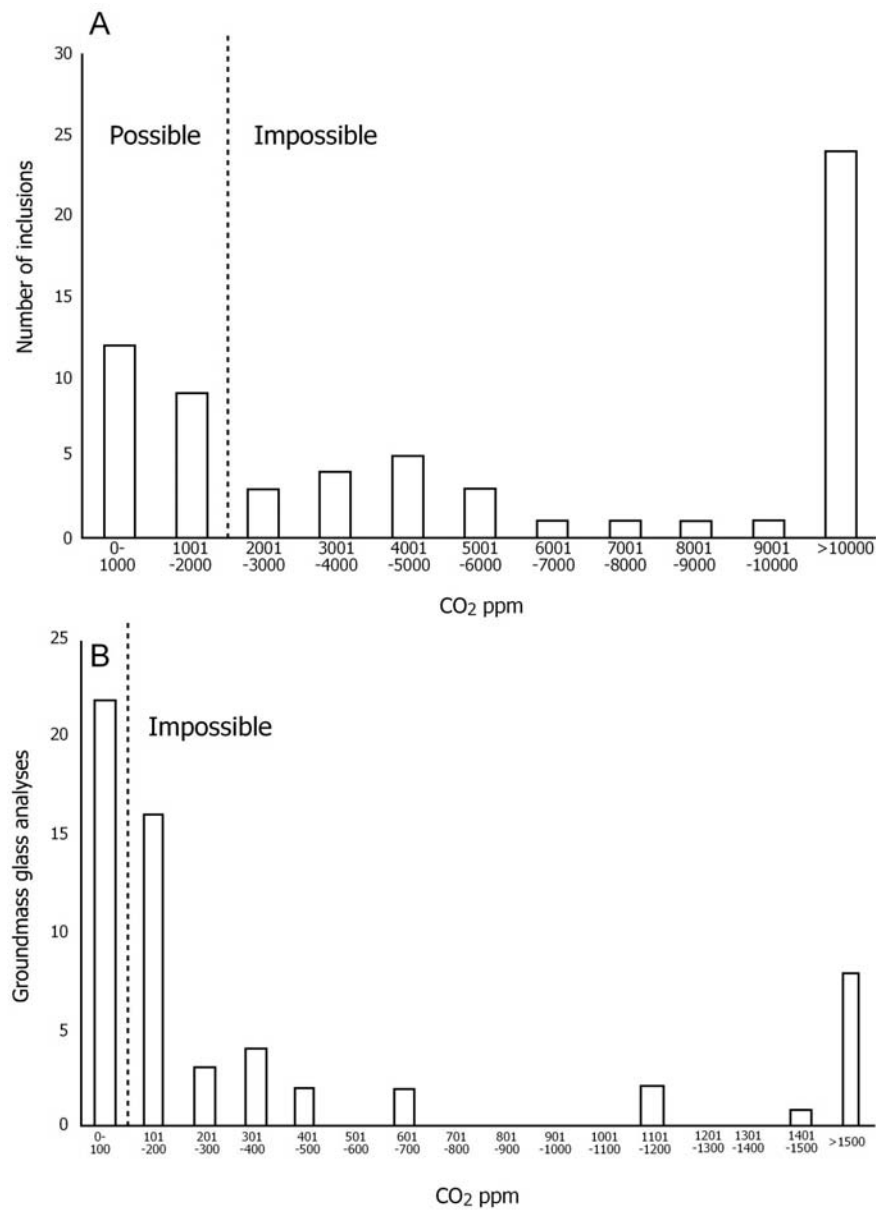


Figure 5.16 Abundance of C as determined by SIMS for **A**. Inclusions and **B**. Groundmass. In the inclusions, at relevant magmatic temperatures for SR-type rhyolites (~ 1000 °C) the solubility of C in rhyolite at 12 km depth (the depth of the mid-crustal sill reported from the eastern Snake River Plain) would be c. 1700 ppm; the majority of the inclusions show significantly more C than this. The graphs are split into areas whereby the CO₂ abundances within the glass are possible or impossible based on solubility curves for CO₂ in rhyolite (Newman and Lowenstern 2002). In the case of the groundmass whereby at atmospheric pressure, almost no CO₂ is soluble in rhyolite, most of the results cannot be considered reliable.

Discussion

Snake River-type rhyolites

The SR-type rhyolites as defined from the Snake River Plain have an anhydrous phenocryst assemblage dominated by quartz, sanidine, plagioclase, pyroxenes, ilmenite, titanomagnetite and accessory minerals such as zircon and apatite (Bonnichsen and Citron 1982; Cathey and Nash 2004; Chapter 2), leading to them being termed hot and dry magmas (Honjo et al. 1992; Christiansen and McCurry 2008), volatile under-saturated (Ekren et al. 1984) and water under-saturated (Bonnichsen et al. 2008). Snake River-type volcanism has been described from other volcanic provinces; how these units compare to the Snake River rhyolites in terms of temperature and pre-eruptive magmatic temperature is discussed below and summarised in Table 5.4.

The Gawler volcanic province

In the Mesoproterozoic Gawler volcanic range in southern Australia the Yardea dacite is reported as being a 3,000 km³ lava. It has an anhydrous mineral assemblage and an estimated magmatic temperature between 900 -1000 °C (Creaser and White 1991). Pre-eruptive water contents for the Yardea dacite are estimated as being < 2 wt.% (Creaser and White 1991; Garner and McPhie 1999). The 675 km³ Eucarro rhyolite from the same province, interpreted as a lava by Allen and McPhie (2002), is silicic (71 to >74 wt.% SiO₂) with pyroxene as the main ferromagnesian phase although amphibole is present in some places. However, not all of the units within the Gawler province are entirely of Snake River-type, for example the Bittali rhyolite comprises lava domes and ignimbrites with abundant pumice and fiammé (Parker and Flint 2005).

Trans Pecos, Texas

The Oligocene-Eocene Trans Pecos province in Texas contains a number of units interpreted as intensely welded ignimbrites and lavas, formed in a subduction-related system dominated by major caldera volcanism (Henry et al. 1990). The Bracks rhyolite, a

low silica rhyolite, containing alkali feldspar, clinopyroxene, fayalite and magnetite has an estimated magmatic temperature of around 900°C (Henry et al. 1990), based on similar rhyolites which have co-existing ilmenite and magnetite pairs. With the lack of hydrous mineral phases, the total volatile contents are inferred to be low, less than 2 wt.% (Henry et al. 1990, Henry et al. 1994).

Etendeka-Paraná

The Mesozoic rhyolitic units of the Etendeka-Paraná province were formed in response to a combination of continental rifting and mantle upwelling associated with the Tristan da Cunha hotspot (O'Connor and Duncan 1990; Ewart et al. 1998). These quartz latite units have an anhydrous phenocryst assemblage dominated by plagioclase, pyroxene, titanomagnetite and ilmenite (Milner et al. 1992; Ewart et al. 1998). Magmatic temperatures, as estimated by pyroxene thermometry are >1,000 °C and the magmas that produced the quartz latites are interpreted as having been water-undersaturated (Ewart et al. 1998).

Middle Proterozoic Keewenawan volcanics, Minnesota

The Keewenawan volcanics were produced in a mid-continental setting where rhyolites formed by crustal melting were related to a mantle plume (Green and Fitz 1993). Both rheomorphic ignimbrites and large-volume lavas are present with anhydrous mineralogies. The phenocryst assemblage and high iron contents are thought to reflect low water contents which are associated with high magmatic temperatures inferred to be in the range of 970-1100°C (Green and Fitz 1993).

The majority of these global examples of Snake River-type volcanism have evidence for high magmatic temperatures and estimations of low water contents, consistent with the data produced in this study. Units from intra-continental settings that have low water contents and exhibit only limited characteristics of Snake River-type volcanism are described below.

Province	Etendeka-Parana (Ewart et al. 1998)	Trans-Pecos Texas (Henry et al. 1988; 1990; 1994)	Keweenawan (Green and Fitz 1993)	Snake River Plain (Cathy and Nash 2004; Bonnichsen et al. 2008)	Gawler (Creaser and White 1991; Allen and McPhie 2002)	Alid, Eritrea (Lowenstern et al. 1997)
Wt.% SiO ₂ Whole Rock	66-68	68-72	67-75	70-75	71-72	73
Phenocryst Assemblage	Plagioclase, augite, pigeonite, quartz, titanomagnetite, apatite.	Sanidine, clinopyroxene, fayalite, magnetite	Sanidine, quartz, plagioclase, olivine, augite, pigeonite, zircon, apatite	Sanidine, quartz, plagioclase, clinopyroxene, ilmenite, titanomagnetite, apatite, zircon	Plagioclase, sanidine, olivine, pyroxene, amphibole, quartz, apatite, zircon	Alkali feldspar, clinopyroxene, magnetite, zircon, apatite
Volume km ³ single unit	Up to 2,300	1,000	> 500	> 1,000	> 675	-
Magmatic Temperature °C	> 1000	900	970-1100	850-1000	900-1000	870
Thermometer	2 pyroxene Lindsley (1983)	2 oxide	Estimate	2 pyroxene, Zr sat. Ti in quartz, 2 oxide	2 pyroxene, 2 feldspar, apatite	Zr Saturation
H ₂ O content wt.%	'water-undersaturated'	< 2	Low	1.8-3.2	< 2	2.6
Method	Inference	Estimate	Estimate	SIMS	Estimate	FTIR
Notes	Unknown origin. Units closely spaced in time	Well developed autobreccias at the top and base and steep flow front terminations	Some pyroclastic material, mostly lavas.	Type are of Snake River-type volcanism (Branney et al. 2008)	Eucarro contains large blocks of granite, compositionally zoned. Possibly an ignimbrite?	From pumice block within ignimbrite. Eritrea shows some SR-type characteristics.

Table 5.4 Comparison of other provinces which are thought to have some aspects of Snake River-type volcanism with the Snake River Plain.

Eritrea

The Alid volcanic centre formed near a triple junction due to the same rifting currently forming the Red Sea (Barberi and Varet 1977). Rhyolites from this centre exhibit some Snake River-type characteristics such as an anhydrous mineralogy (although amphibole is present in some of the older deposits). The main phenocryst phases are alkali feldspar, clinopyroxene and magnetite with accessory minerals such as apatite and zircon (Lowenstern et al. 1997). Non SR-type features include the presence of blocks of granophyric intrusives which contain biotite. Analysis of melt inclusions in the 'pf' ignimbrite give water contents ranging from 1.99 to 3.40 wt.% and the magmatic temperature was estimated at 870 °C based on zircon thermometry (Lowenstern et al. 1997).

Pantelleria

Pantelleria represents the sub-aerial portion of a submerged rift (Villari 1974). It has produced numerous pantelleritic ignimbrites and lavas with anhydrous mineral assemblages commonly containing quartz, sanidine, clinopyroxene, rare olivine and ilmenite (Wolff and Wright 1981). The presence of well-developed Plinian pumice lapilli fallout deposits and peralkaline composition are not features of Snake River-type volcanism. Melt inclusions hosted in quartz phenocrysts were analysed by Lowenstern and Mahood (1991) with water contents ranging from 1.4 to 2.1 wt.%.

'Typical' rhyolites

Rhyolites formed in subduction zones commonly have lower magmatic temperatures and higher volatile contents than Snake River-type rhyolites (Table 5.1; Fig. 5.17). For example, water contents from Taupo Volcanic Zone range from 4.3-5.9 wt.%, those from Toba range from 3.8-5.3 wt.% (Newman and Chesner 1989) and Crater Lake 5.1-6.8 wt.% (Bacon et al. 1992).

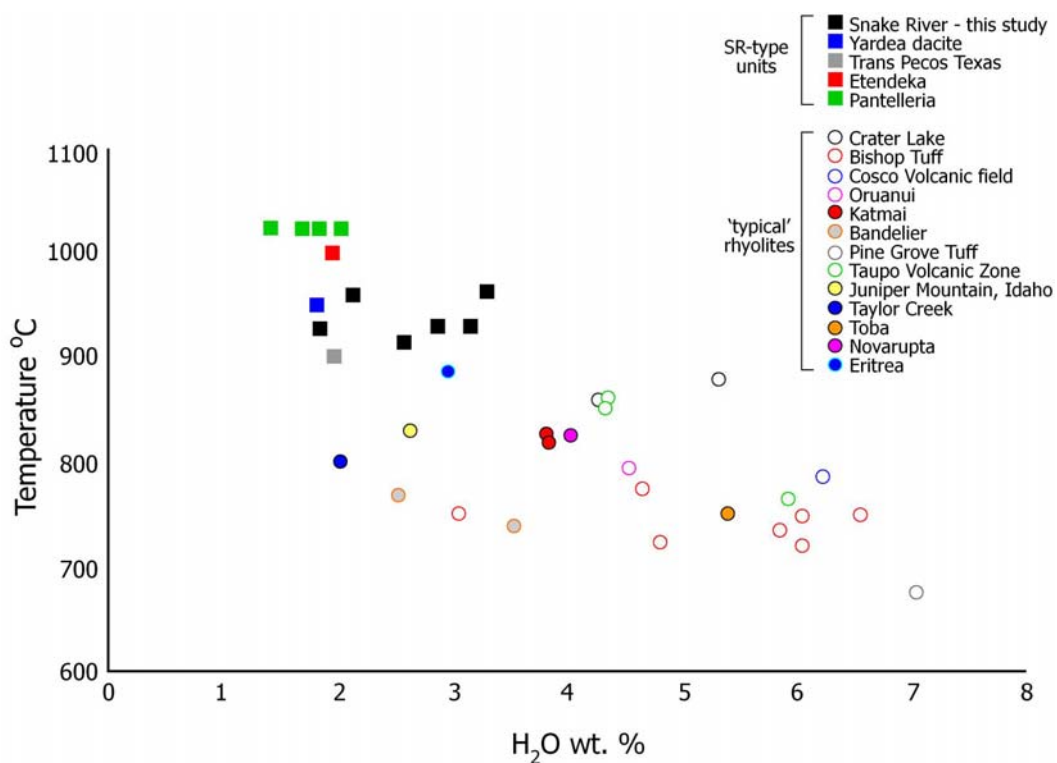


Figure 5.17 Water content of the Snake River-type rhyolites as compared to other rhyolites. Units with similarities to Snake River-type volcanism are plotted as squares. (*) denotes volatile estimates rather than measured data. Yardea dacite (Creaser and White 1991)(*), Etendeka (Ewart et al. 1998) (*), Trans Pecos Texas (Henry et al. 1989)(*), Pantelleria (Lowenstern and Mahood 1991). ‘Typical’ rhyolites are plotted as circles; Crater Lake (Druitt and Bacon 1989; Bacon et al. 1992; Nekada et al. 1983), Bishop Tuff (Hildreth 1979; Anderson et al. 1989; Skirius et al. 1990; Dunbar and Hervig 1992), Cosco volcanic field (Manley and Bacon 2000), Oruanui (Wilson et al. 2006), Katmai (Westrich et al. 1991; Lowenstern 1993), Bandelier Tuff (Dunbar and Hervig 1992; Warshaw and Smith 1988), Pine Grove Tuff (Lowenstern 1994), Taupo Volcanic Zone (Dunbar et al. 1989; Smith et al. 2005), Juniper Mountain (Manley 1994), Taylor Creek (Webster and Duffield 1994), Toba (Newman and Chesner 1989), Novarupta (Coombs and Gardner 2001) and Eritrea (Lowenstern et al. 1997).

This work quantitatively shows that Snake River-type rhyolites have low pre-eruptive water contents as predicted by Ekren et al. (1984), Honjo et al. (1992) and Bonnicksen et al. (2008). However, as shown in Figure 5.17, the H₂O contents of some of the Snake River-type rhyolites overlap with those from other provinces (e.g. Eritrea, Taylor Creek, Bandelier), albeit at different magmatic temperatures. This overlap in water contents is consistent with the idea of Snake River-type volcanism being an association of numerous

facies (see Branney et al. 2008), which may be variably present, giving a greater or lesser degree of Snake River-type behaviour.

Eruptive style

It has been suggested that magmatic water content is responsible for controlling eruptive style from a number of studies of variable magma compositions; andesite at Mt. St. Helens (Blundy and Cashman 2005), phonolite at Vesuvius (Webster et al. 2003) dacite in the Andes (Schmitt 2001) and the rhyolitic Bishop Tuff (Anderson et al. 1989). In contrast, other work has suggested that there is no link between magma volatile content and the subsequent eruptive style e.g. Crater Lake (Bacon et al. 1992), Mayor Island, New Zealand (Barclay et al. 1996), Pantelleria (Lowenstern and Mahood 1991) and Taupo Volcanic Zone (Dunbar and Kyle 1993). Other factors considered to control eruption style include: rates of magma ascent and supply (Barclay et al. 1996) and degassing prior to eruption (Lowenstern and Mahood 1991).

Given that pre-eruptive H₂O, F and Cl contents in these magmas show no variation between lavas and ignimbrites, it is proposed that this is not the controlling factor in terms of subsequent eruptive style in the Snake River Plain. Therefore other factors must be responsible for the differences of eruption style. Possibilities are discussed below:

CO₂ content

Variable input of CO₂ into a magmatic system could be a control on eruptive style. The addition of heat and CO₂ to a silicic system from basalt below, so called 'gas sparging' (Bachmann and Bergantz 2003), has been proposed as the trigger mechanism for the explosive eruptions of the Fish Canyon Tuff (Bachmann and Bergantz 2003) and the Bishop Tuff (Wark et al. 2007). Abundant CO₂ is emitted by the hydrothermal system at Yellowstone, suggesting both the hydrothermal system and the deeper magmatic system are gas saturated, with the overall source being underlying basalt (Lowenstern and Hurwitz 2008). Although the deposits of Yellowstone and the central Snake River Plain are

significantly different, the Yellowstone volcanic field remains the best analogue for the central Snake River Plain. However this would only be the cause of the divergence in style if the input were episodic rather than continuous, or if the degassing of the rhyolite was variable.

Variation in ascent rate

Variation in ascent rate has been suggested as the cause of variation between explosive and effusive eruptions (e.g. Barclay et al. 1996), with higher ascent rates relating to explosive eruptions (e.g. Dingwell 1996; Gonnermann and Manga 2007). The ascent rate is a complex function of a number of inter-related factors including chamber overpressure, conduit geometry, rheology of the rising magma, outgassing, viscous heating and crystal growth (Gonnerman and Manga 2007). Castro and Gardner (2008) experimentally recreated microlite textures seen in Inyo volcanic chain sub-Plinian and effusive rhyolites in decompression experiments suggesting that there was no significant difference in magma ascent rate between the explosive and effusive deposits. They explain this observation by a downward propagating fragmentation front, similar to that proposed for Vulcanian style eruptions (Alidibirov and Dingwell 1996). An implication of this model is that the magma chamber was zoned in terms of bubble content (as this prevents the run-away of the fragmentation front). It is not clear how these small, sub-Plinian scale eruptions may be scaled to the size of the large Snake River-type eruptions.

Degassing

Using melt inclusion data to infer the water content of a magma at the time of eruption is based on the assumption that no degassing occurs between entrapment of the inclusion and subsequent eruption. Degassing may have caused variable loss of volatiles from the magma and allowed the eruptive styles to be controlled by volatile content at the time of eruption. In this case it is assumed that the magmas erupted as lavas degassed to a greater degree than those which erupted as ignimbrites. Mechanisms to explain this anticipated loss of volatiles include the production of a permeable foam which subsequently collapses

following degassing (Eichelberger et al. 1986) or brecciation of conduit walls and country rock (Gonnermann and Manga 2003; Rust et al. 2004). Degassing has been suggested as the cause of different eruptive styles from studies whereby no evidence of a difference in volatile contents was recorded in melt inclusions (Barclay et al. 1996; Lowenstern and Mahood 1991).

Magma chamber conditions

The melt inclusion data allow speculation about the conditions within the magmatic plumbing systems which gave rise to the SR-type rhyolites. Firstly, the relationship of water and chloride in melt inclusions can be used to infer conditions in the magma. Chloride saturation is dependent upon the composition of the magma in question, for example chloride solubility increases with increasing ANCM/S (molar (Al + Na + Ca + Mg)/ Si) in a linear manner (Webster 1997). Samples from the Snake River Plain have low ANCM/S (Fig. 5.18), ranging from 0.22 to 0.31, reflecting a low chloride solubility. When considering Cl solubility, the abundance of F must also be considered, as high levels of fluorine act to increase Cl solubility considerably (Webster et al. 1999). The abundance of fluorine required to have an effect on chloride solubility is ≥ 1.2 wt. % (Webster 1997), considerably more than that found in Snake River rhyolites (0.02 to 0.82 wt. %).

The relationships between Cl and water from a variety of rhyolitic magmas are shown in Figure 5.19. Magmas which show trends of increasing H₂O with increasing Cl that would intersect the origin (Fig. 5.19 A and B) are interpreted as being produced in systems undergoing fractional crystallisation in the absence of a magmatic volatile phase (Webster 1997). The slope of the line will partially relate to the crystallising phases, but the trend will remain the same. If the slope of the trend line is negative i.e. decreasing Cl with increasing water contents (Fig. 5.19 B), then the trend is following the experimentally derived solubility curves for chloride in vapour-saturated magmatic systems (Webster 1997; Webster et al. 1999).

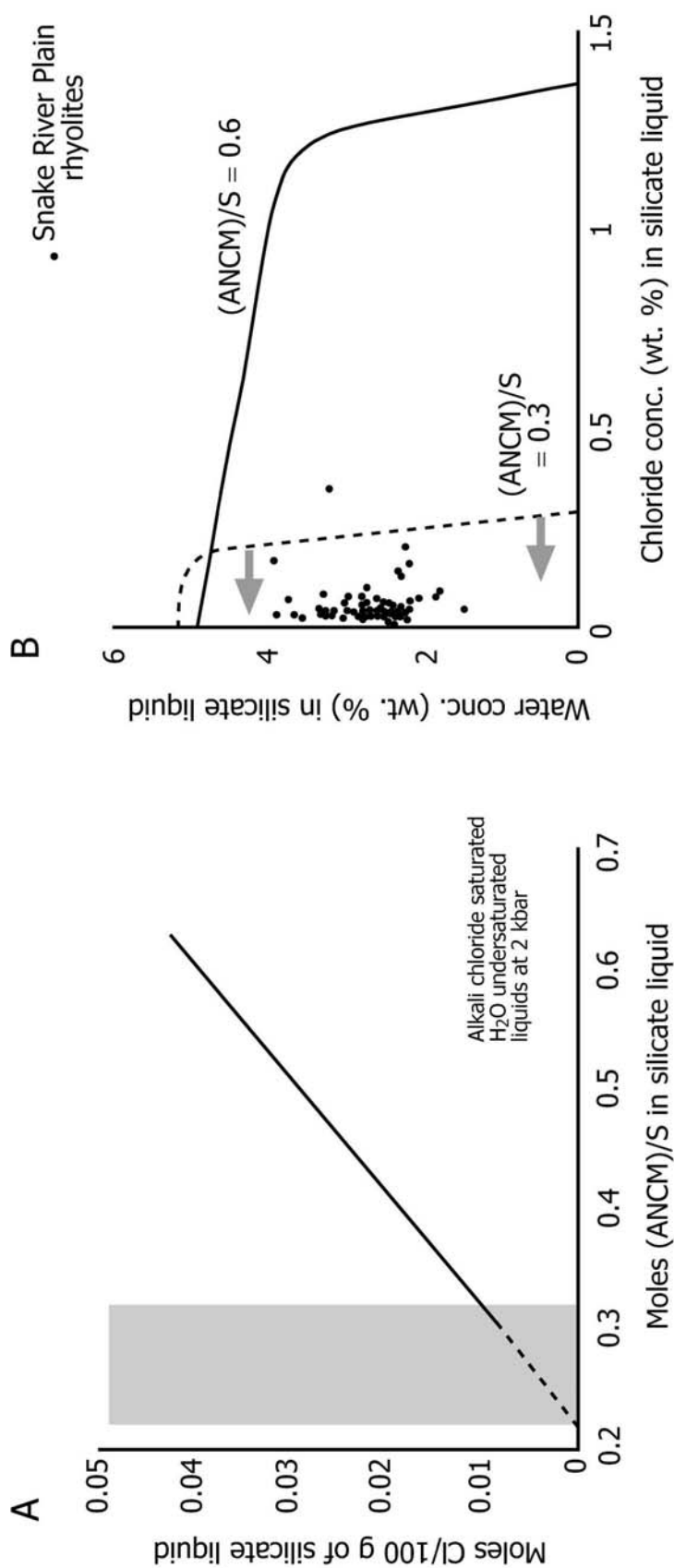


Figure 5.18 A. Relationship between composition of the silicate liquid and the solubility of Cl, redrawn after Webster (1997). ANCM/S represents the molar abundances of (Al+Na+Ca+Mg)/Si. As can be seen, the solubility of Cl increases with increasing ANCM/S. The grey shaded area represents the ANCM/S values for the units in this study based on whole rock data (glass data from the electron microprobe gives lower values). **B.** Solubility curves for H₂O and Cl based on experiments on haplogranite and latite at 2 kbar and temperatures ranging from 825-1170 °C after Webster (1997). The black circles represent the results from this study and the grey arrows show how lowering the ANCM/S to values relevant for Snake River rhyolites affects the solubility curve.

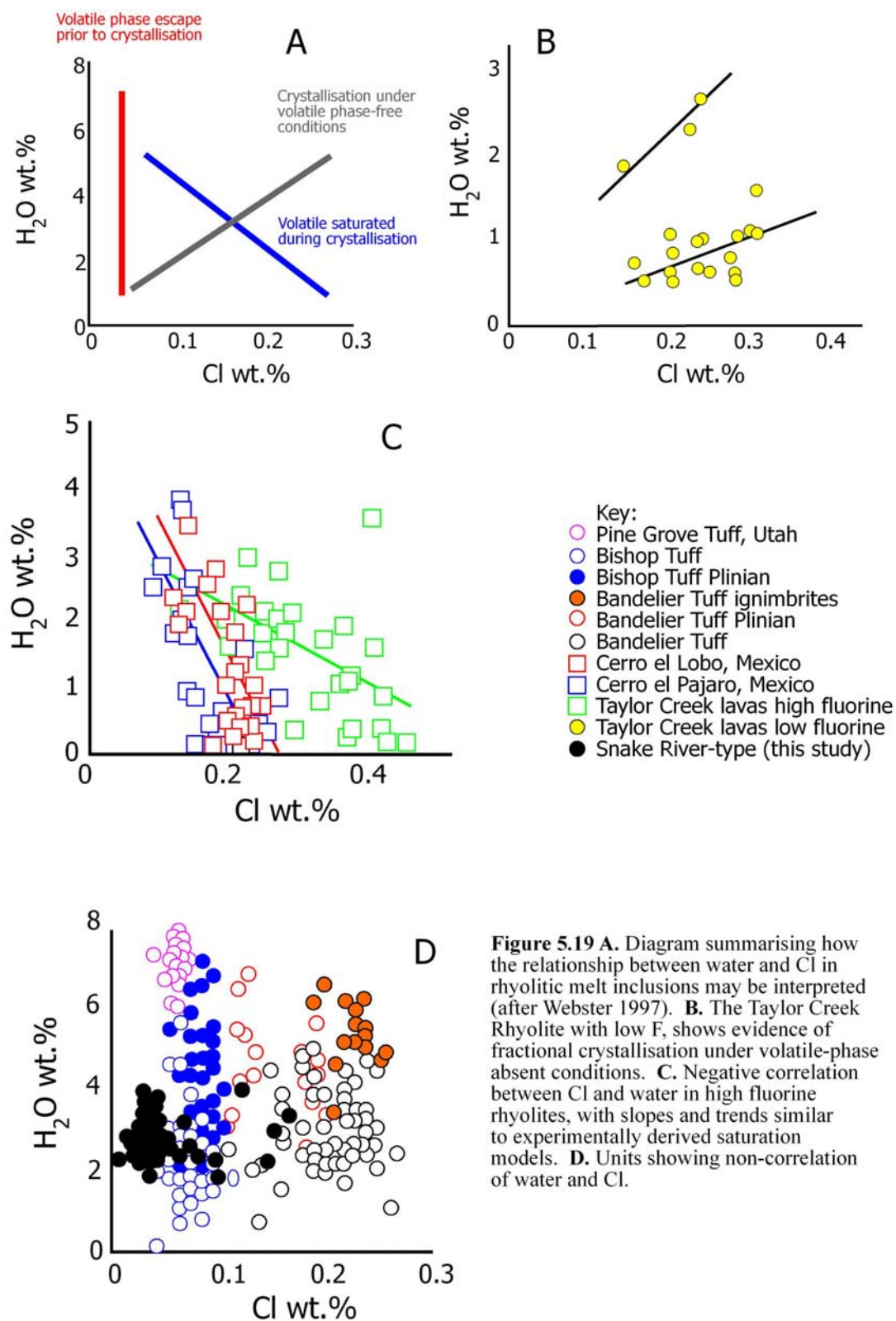


Figure 5.19 A. Diagram summarising how the relationship between water and Cl in rhyolitic melt inclusions may be interpreted (after Webster 1997). **B.** The Taylor Creek Rhyolite with low F, shows evidence of fractional crystallisation under volatile-phase absent conditions. **C.** Negative correlation between Cl and water in high fluorine rhyolites, with slopes and trends similar to experimentally derived saturation models. **D.** Units showing non-correlation of water and Cl.

A third trend, of varying water contents with low, non-varying chloride contents has been reported from inclusions in the Bandelier Tuff (Dunbar and Hervig 1992; Stix and Layne 1996), the Bishop Tuff (Dunbar and Hervig 1992) and the Pine Grove Tuff (Lowenstern, 1994). Such a trend has been interpreted as resulting from entrapment of inclusions from magmas which had already degassed to some degree (Dunbar and Hervig 1992; Stix and Layne 1996). The trends in terms of Cl and water are shown (Fig. 5.19 D) with the Snake River rhyolites most closely resembling the third trend of low, stable chloride contents and variable water (Fig. 5.14), suggest that degassing may have been occurring while the inclusions were entrapped (Fig. 5.19).

Source of the volatiles

The magma chamber currently situated underneath Yellowstone is estimated to be 15,000 km³ in volume (Lowenstern et al. 2006) and is degassing a minimum of 45,000 tonnes of CO₂ per day (Werner and Brantley 2003). Using C and He isotopes, 30-50 % of the CO₂ emitted by Yellowstone is attributed to pre-Tertiary basement rocks, with the remainder inferred to be produced by degassing of the magma (Werner and Brantley 2003). Melt inclusions from post-caldera rhyolites contain 0 to 400 ppm CO₂ (Lowenstern and Hurwitz 2008), so using 500 ppm as the CO₂ content of the magma chamber, if the measured flux of CO₂ had the rhyolitic magma as its only source, the entire magma chamber would be degassed in terms of CO₂ in around 1000 years (Lowenstern and Hurwitz 2008). The gas emitted from Yellowstone has abundances of CO₂ orders of magnitude larger than halogens (whereas rhyolitic melt inclusions have the reverse e.g. Table 5.1), suggesting a basaltic source (Lowenstern and Hurwitz 2008). Therefore it is likely that the rhyolitic magma is not the main source of the volatiles which are currently being emitted from Yellowstone, rather the basaltic magma likely to underlie the rhyolitic magma. In the central Snake River Plain, the hotspot was three times more productive than at present (Cathey and Nash 2004). Given that the majority of the CO₂ at Yellowstone comes from basaltic magma, it seems a reasonable assumption that with a higher influx of basalt, the CSRP magma chambers were also saturated with CO₂. A mid-crustal sill (Rodgers et al. 2002; Shervais et al. 2006), inferred to be approximately 10 km thick and lie at 12 km depth has been located

under the eastern Snake River Plain and a similar feature may have been present under the central plain. At 12 km depth, the solubility of CO₃ in basalt is 1700 ppm, irrespective of temperature (Newman and Lowenstern 2002), and the solubility in rhyolite is slightly higher depending upon the temperature.

Rheomorphism

Many of the ignimbrites in the central Snake River Plain are intensely welded and show abundant rheomorphic features (e.g. Branney et al. 2004; Branney et al. 2008). The Castleford Crossing Ignimbrite in experiment 2 shows numerous rheomorphic features e.g. folding on a variety of scale (including sheath folds) and flow banding. Rheomorphism is primarily controlled by emplacement temperature, chemistry, dissolved volatile content and mass flux (e.g. Mahood 1984; Branney et al. 2004) with the solid and vesicle contents of lesser importance. The intense degree of rheomorphism in the Snake River Plain has been attributed to a combination of high emplacement temperatures and the retention of halogens (e.g. Branney et al. 2008). The controls on rheomorphism in the Snake River Plain are assessed below.

Solid and bubble content

Increasing the solid content of a magma has been shown to increase the viscosity (Pinkerton and Stevenson 1992) with the magnitude of the increase in viscosity increasing with larger axial ratio. Snake River-type ignimbrites commonly contain 10% phenocrysts (e.g. Cathey and Nash 2004; Andrews et al. 2008) whereas non-welded ignimbrites from other provinces may have lower phenocryst contents e.g. Granadilla ignimbrite on Tenerife contains < 5% phenocrysts (Bryan et al. 2002). Increasing the bubble content of a magma has been shown to slightly decrease its viscosity (Manga et al. 1998). Although the Snake River-type ignimbrites contain abundant lineations, interpreted as reflecting the shearing of bubbles in the ignimbrite (e.g. Branney et al. 2004; Andrews et al. 2008), the low volume fraction of these vesicles (<< 1%) and the small change in viscosity that results from such bubble contents is unlikely to be the cause of the rheomorphism.

Water Content

The addition of water to a magma reduces viscosity (Giordano et al. 2004). The non-linear curve (Fig. 5.20), means that adding 2 wt.% water to a dry rhyolite will decrease its viscosity by approximately 6 log units. The addition of a further 2 wt.% (from 2 to 4 wt.%) will only cause the viscosity to decrease by one additional order of magnitude. Although Snake River-type ignimbrites have magmatic water contents distinct from 'typical' rhyolites, this is unlikely to have any bearing on rheomorphism. Firstly SR-type rhyolites tend to have lower magmatic water contents than the majority of rhyolites (a factor which would act to increase the viscosity of the rhyolite Fig. 5.20 B and C). Secondly, rheomorphism is a post-fragmentation, syn-depositional process. Little if any water will be remaining in the ignimbrite at this stage, as shown by solubility models of water contents in rhyolite (e.g. Zhang 1999; Newman and Lowenstern 2002) and from analyses of pristine rhyolitic glass (e.g. Bacon et al. 1992; Manley 1996). On this basis water cannot be the cause of the rheomorphism.

Halogens

Increasing halogen content decreases melt viscosity, depolymerising the melt by breaking the Al_2O_3 framework (Dingwell et al. 1985), with fluorine having a larger effect than chlorine. Fluorine contents in melt inclusions from the Snake River Plain rhyolites are similar to those seen from rhyolites in other provinces (Fig. 5.14C) while chlorine abundances are slightly lower than other rhyolites. Fluorine and chlorine are variably lost during the processes of eruption, with typically only 7-30 % of the fluorine lost during the eruptions (with the exception of the Sand Springs Ignimbrite which lost 81 % of its F) and 35-85 % of the chlorine. Fluorine is commonly retained to a greater degree than chlorine in rhyolitic eruptions (Bacon et al. 1992; Barclay et al. 1996). The Plinian fallout preceding the Bandelier Tuff and a fallout deposit underlying the Cerro Toledo rhyolite (Fig. 5.14C) contain fluorine abundances three times larger than the Snake River Plain rhyolites and both are associated with non-welded pyroclastic deposits.

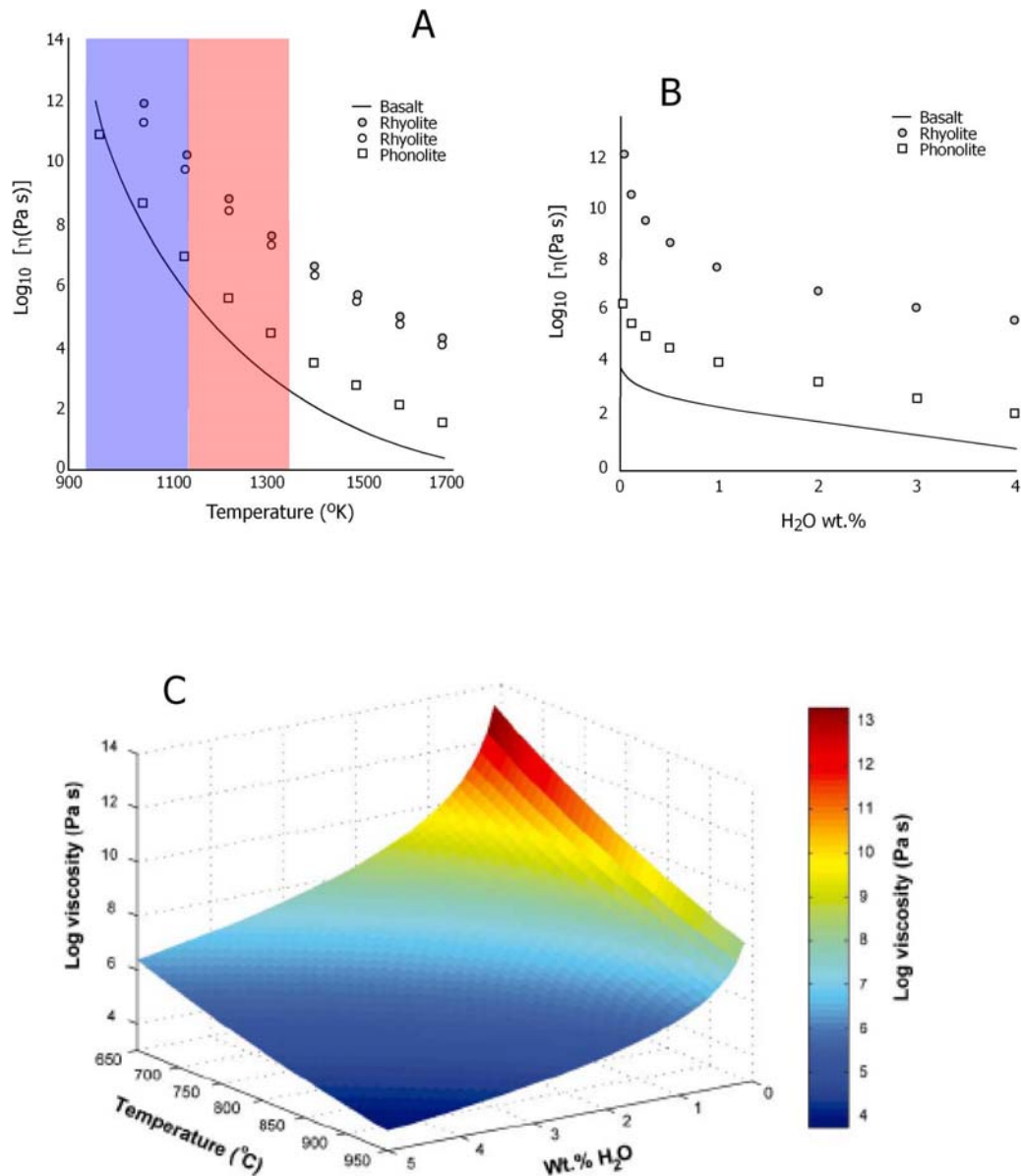


Figure 5.20 Viscosity of a magma as a function of water content and temperature. **A.** Illustrating the importance of temperature on the viscosity of rhyolite, redrawn from Giordano et al. (2004). The red shaded area represents the inferred magmatic temperatures for Snake River-type ignimbrites, the blue shaded area represents the range of inferred magmatic temperature from 'typical' Plinian rhyolitic eruptions (Branney et al. 2008). As can be seen the viscosity of a rhyolite at a temperature of the mid point of the Snake River temperature range is at least 4 log units lower than that at the mid point of the Plinian style rhyolites. **B.** Diagram showing the influence of water on viscosity, the basalt is from Mount Etna, the phonolite is from Vesuvius and the rhyolite is from Hess and Dingwell (1996). Redrawn after Giordano et al. (2004). **C.** Cumulative effect of temperature and water content on the viscosity of a leucogranite based on the calculations of Hess and Dingwell (1996), from Manga and Gonnerman (2007).

Temperature

The temperature of a rhyolitic magma is the first order control on its viscosity (Murase and McBirney 1973). For basaltic compositions viscosity may change by a factor of 10^{13} as the magma cools through a temperature interval of 200 °C (Pinkerton and Stevenson 1992). Evaluating the influence of temperature on rheomorphism is problematic as although the magmatic temperatures may be inferred with a reasonable amount of certainty, the depositional temperatures are unknown.

Mass flux of the eruption likely plays a significant role as a control on rheomorphism yet the significance of this role cannot be evaluated. To examine the controls on viscosity, groundmass glass compositions from numerous rhyolites were input into the viscosity model of Giordano et al. (2008) to determine the emplacement viscosities. Two assumptions were made in doing so: i) the water contents of the glasses upon emplacement were 0.1 wt.% (see above) and ii) deposit emplacement temperatures were equal to their magmatic temperatures. Using these two assumptions, the relative effects of fluorine content and temperature on viscosity and therefore rheomorphism can be evaluated (Fig. 5.21). As previously shown (Fig. 5.14C) Snake River rhyolites are not particularly enriched in halogens, and there is no relationship between the viscosity at emplacement and the fluorine content of the ignimbrite (Fig. 5.21A). However, in terms of temperature, there is a relationship between increasing emplacement temperature and decreasing viscosity (Fig. 5.21B). This suggests that the intense rheomorphism seen in the Snake River Plain is a result of the combination of high emplacement temperatures and high mass flux rates.

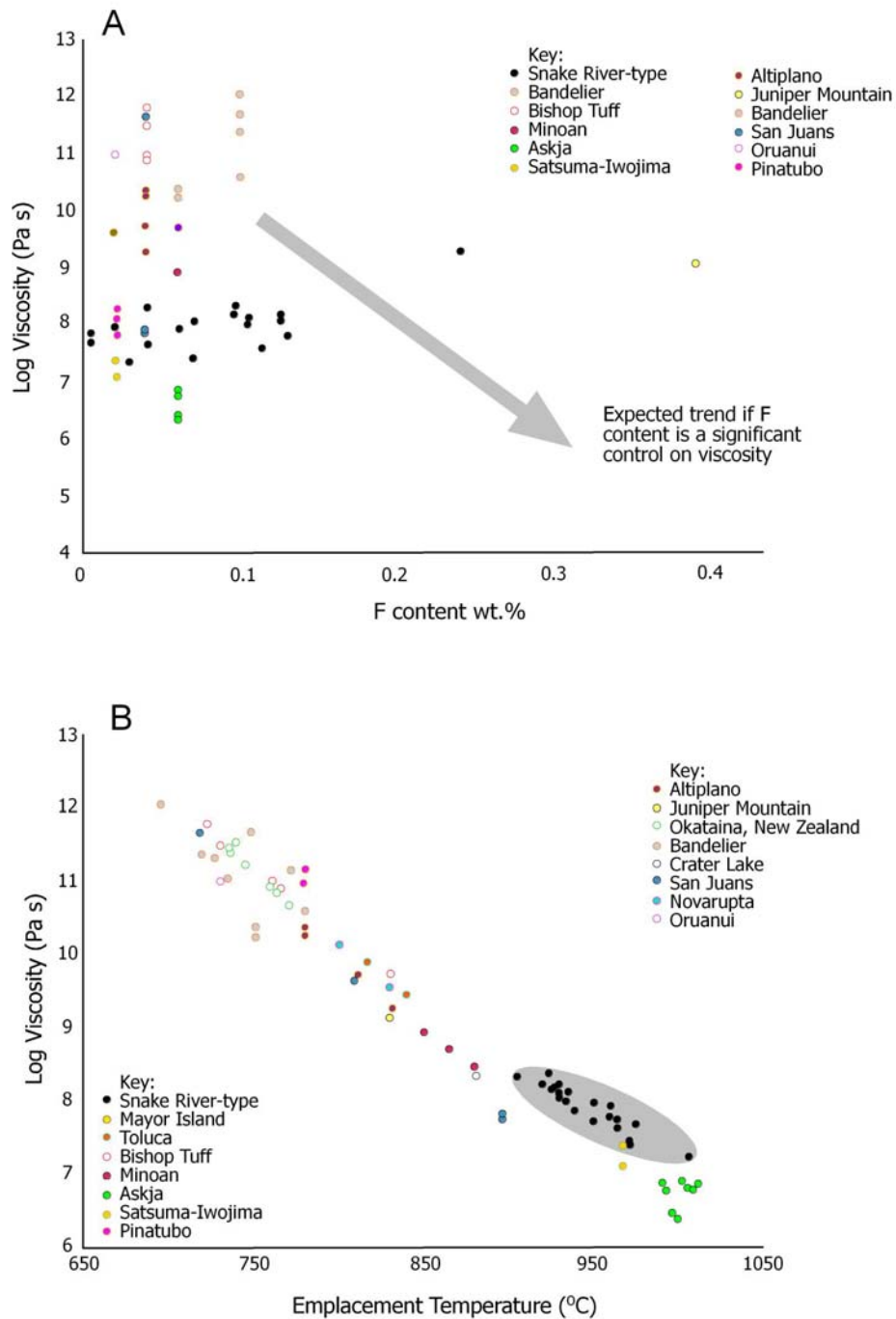


Figure 5.21 **A.** Relationship between F content and emplacement viscosity, grey arrow shows the expected trend to lower viscosity with higher F contents expected if F is a control on deposit viscosity. **B.** Relationship between emplacement temperature and viscosity. References for data are the same as in previous figures with the addition of: Okataina (Smith et al. 2006), Askja (Sigurdsson and Sparks 1981), Novarupta (Coombs and Gardner 2001), San Juans (Whitney and Stormer 1985), Satsuma-Iwojima (Saito et al. 2001), Minoan (Michaud et al. 2000), Pinatubo (Hammer et al. 1999), Toluca (Arce et al. 2005).

Conclusions

1. Water contents of SR-type magmas are lower than those reported from other volcanic provinces. The pre-eruptive water contents of the SR-type lavas and ignimbrites are in agreement with estimations of pre-eruptive volatile content from other SR-type provinces (e.g. Etendeka, Keewenawan, and Gawler).
2. The volatile content (H₂O, Cl and F) of SR-type lavas and ignimbrites does not appear to be the controlling factor in terms of eruptive style. Therefore the porosity of the conduit or the ascent rate of the magma is more likely to be the cause of the divergence in eruptive style.
3. The intense rheomorphism present in Snake River-type ignimbrites is a function of their high inferred magmatic and emplacement temperatures. Fluorine contents of melt inclusions are similar to those of other rhyolites and chlorine contents are slightly lower. In accordance with other studies, the majority of fluorine and chlorine is retained in the ignimbrite after emplacement. This suggests that retention of dissolved volatiles did not play a significant role in promotion of rheomorphism in Snake River-type rhyolites; rather it was due to high emplacement temperature.

Chapter 6 Conclusions and Further Work

This thesis documents the first detailed volcanological study of a little-understood, new category of silicic volcanism, Snake River-type volcanism, as defined by Branney et al. (2008). The main conclusions of this work are:

Ignimbrite stratigraphy and geochemistry of the Cassia Mountains

This work has documented the stratigraphy of the Snake River Plain between ~11.3 and 9 Ma as recorded in the Cassia Mountains of southern Idaho, thought to contain ignimbrites from the proposed Twin Falls eruptive centre. In ascending order they are; the Magpie Basin, Big Bluff, Steer Basin, Deadeye (newly discovered unit), Wooden Shoe Butte and McMullen Creek members.

- The ignimbrites are of broadly similar rhyolitic composition, but show a trend towards less evolved compositions up section, in terms of whole rock composition (e.g. decreasing SiO₂ and increasing TiO₂ wt.%), pigeonite, augite phenocryst compositions (decreasing FeO and increasing MgO wt.%) and plagioclase phenocryst compositions (increasing anorthite content). This trend is consistent with that proposed for the entire central Snake River Plain by Bonnicksen et al. (2008) on the basis of whole rock data.
- The ignimbrites in the Cassia Mountains contain anhydrous phenocryst assemblages and have high inferred magmatic temperatures as determined from the two-feldspar, two-pyroxene, two oxide, zircon saturation and titanium in quartz thermometers. The inferred temperatures remain relatively stable through the succession (875-940°C). Significantly higher than the typical 750-850°C for rhyolites.
- There is little vertical zonation within individual ignimbrites, Some of them (e.g. the Steer Basin, Wooden Shoe Butte and McMullen Creek members) contain multiple compositional populations of pigeonite and augite. The pigeonites and augites within a unit are consistent with being in equilibrium with each other (i.e. the iron

rich pigeonite is found with the iron rich augite) and the variability of composition is not due to zoning within the crystals. Glomerocrysts within these ignimbrites contain only one population of both pigeonite and augite, and these populations are also consistent with being in equilibrium.

- Following a period of quiescence in the Cassia Mountains of ~ 1 Ma, the McMullen Creek Member was erupted, with geochemical compositions more evolved than the preceding rhyolites. The Neodymium isotopic signature of the McMullen Creek Member is more crustal than the other Cassia Mountain ignimbrites and it may represent a break in the system, possibly reflecting a shift of activity to a new eruptive centre.
- The clinopyroxene compositions and the restricted compositions of the glomerocrysts are interpreted as representing a magmatic system in which two or more similar magmas are crystallising in parallel before being simultaneously erupted and mixing to give the heterogeneous compositions recorded in an ignimbrite.

New correlations and eruption volume calculations

The first approximation of the stratigraphy of the central Snake River Plain was the CAT groups of Bonnicksen et al. (2008) which split the whole province into broad groups based on age, whole rock chemical composition (particularly FeO and TiO₂ wt.% contents), magnetic polarity and relative position. The present project has demonstrated that combining detailed geochemical analyses of pigeonite and augite phenocrysts with a variety of other techniques, including whole rock and glass chemistry, magnetic polarity, oxygen isotopes and ⁴⁰Ar/³⁹Ar geochronology, can be used to correlate individual ignimbrite eruption-units in adjacent massifs surrounding the central Snake River Plain.

- Three new correlations have been defined by use of the combination of techniques described above. This has allowed the correlation of Cougar Point Tuff 11 and Browns Bench Unit 5; the Big Bluff Member, Jackpot 1-6 and Browns Bench 7; and the Steer Basin Member, Jackpot 8 and Browns Bench 8.

- The correlations allow new eruption volume estimates of the Steer Basin Tuff (640 km³), Cougar Point Tuff 11 (927 km³) and the Big Bluff Tuff (1,200 km³). The intense welding of these deposits means that their bulk volume is very similar to the dense rock equivalent. The magnitudes of these deposits are 8.15, 8.36 and 8.47 respectively. This study presents the first reasonably constrained eruption volume estimates from the central Snake River Plain. The larger eruptions were super-eruptions of comparable volume to those from the Yellowstone plateau.
- Other proposed correlations between Browns Bench 3, Cougar Point Tuff 7 and the Buckhorn Ignimbrite; and between Upper Grasmere Escarpment Ignimbrite, Cougar Point Tuff 11 and Windy Gap have been refuted on the basis of clinopyroxene compositions, oxygen isotope characteristics, glass chemistry and ⁴⁰Ar/³⁹Ar geochronology.

A Snake River-type phreatomagmatic explosive eruption

A non-welded rhyolitic deposit (previously mapped as ‘reworked volcanoclastics’) has been discovered within the Cassia Mountains succession. It is unusual because most SR-type pyroclastic units are intensely welded.

- The Deadeye Member (new name) is a soil-bound eruption unit which is the first entirely non-welded pyroclastic deposit known from the central Snake River Plain. It is composed of three main sections; a basal parallel-bedded fallout succession, a pyroclastic density current deposit, and an upper series of fallout deposits.
- The basal fallout deposits of the Deadeye Member contain a distinctive bed of pumice lapilli that traces around the Cassia Mountains and thickens to the north suggesting either a source within the central Snake River Plain or a dispersal axis to the north. The bed is of Plinian dimensions and contains four distinct morphologies of glass, white pumice, black pumice, macroscopic shards and non-vesicular black glass clasts which all have rhyolitic chemistry.
- The Deadeye ignimbrite is fine-grained (lacks pumice lapilli) and entirely non-welded in contrast to the intensely welded rhyolitic ignimbrites of the central Snake

River Plain. It passes upwards from massive lapilli-tuff to diffuse cross-stratified tuff, the upper parts of which contain ash pellets, coated pellets and accretionary lapilli. Some of these ash aggregates show soft-state deformation indicating that they were cool, moist and unlithified upon deposition. Fallout deposits above the ignimbrite contain flattened pods of finer ash, inferred to record aggregation of ash due to the presence of moisture in the atmosphere.

- The Deadeye Member has similar geochemical and oxygen isotope characteristics to the surrounding welded ignimbrites and was erupted from a magma which had a high (c. 925 °C) inferred magmatic temperature. Therefore the difference in its appearance is inferred to be a function of a phreatomagmatic eruptive style. The Deadeye eruption is the first rhyolitic phreatomagmatic explosive eruption to be recorded at the Yellowstone hotspot.

Pre-eruptive volatile contents of Snake River-type magmas

Snake River-type eruption centres produce both lavas and ignimbrites, sometimes closely spaced in time, and of almost identical chemical characteristics. When the ignimbrites are extremely high-grade (lava-like) it can be difficult to distinguish between lavas and ignimbrites without good continuity of exposure. In an experiment to test whether the pre-eruptive water content of the magma was the control on eruptive style, three pairs of lava and ignimbrite were chosen where their mode of eruption was unambiguous.

- Pre-eruptive water contents of Snake River-type lavas and ignimbrites are low (1.5 to 3.3 wt.%) compared to other rhyolites which contain up to 7 wt.% H₂O. These results are consistent with the estimated high magmatic temperatures for these magmas and the anhydrous phenocryst assemblages. Water contents from the plagioclase-hosted melt inclusions appear reliable, as rare leaked inclusions have values separate from both the groundmass (which has been rehydrated) and the majority of other inclusions.
- There is no significant difference in the water content of magmas from closely spaced lavas and ignimbrites. Ignimbrites did not have higher pre-eruptive volatile contents than lavas. Therefore another mechanism must account for this divergence

in behaviour, suggestions include post-entrapment degassing of the lavas whereby the inclusions are trapped prior to degassing and so at the time of eruption lavas have a lower volatile content. This degassing could be through fractures in the magma, in the wallrock or through a vesicle network. Variations in ascent rate may also play a part in determining eruptive style.

- The fluorine and chlorine contents of (1000-2000 ppm) and (200-600 ppm) respectively are similar to melt inclusions in other rhyolite magmas. The fluorine contents remaining in groundmass glass were similar to those from other rhyolites indicating that the intense rehomorphism characteristic of SR-type ignimbrites is not caused by retention of halogens as previously thought, but is due to the high emplacement temperatures.

Future work

Much is still to be learned about the volcanic deposits and processes of Snake River-type volcanism. During this research numerous questions have arisen which merit further investigation; these include:

1. How do the McMullen Creek ignimbrites relate to the rest of the Cassia stratigraphy? They have distinct Nd isotopic compositions in comparison with the older ignimbrites in the Cassia Mountains, as they have more evolved phenocryst compositions. Does the apparent long (~ 1 Ma) time gap between eruptions suggest that they derive from a separate 'eruptive centre'? Also, is the time gap currently estimated a true gap in the volcanic record, or are the deposits of this age preserved elsewhere?
2. How are the large volumes of very low $\delta^{18}\text{O}$ rhyolite generated? Snake River-type rhyolites have a distinct depletion in $\delta^{18}\text{O}$ and the volumes of the SR-type ignimbrites are of the order of 1,000 km³. The Boroughs et al. (2005) model requires a significant amount of Idaho batholith to be hydrothermally altered to the lowest values as yet recorded from the batholith. An alternative model of Bindeman et al. (2007) involves 'crustal

cannibalisation' whereby the magma assimilates a down-dropped hydrothermally altered caldera block from a previous eruption. This model however struggles to explain the volumes of rhyolite generated in a single eruption; the 1,200 km³ of the Big Bluff Tuff at $\delta^{18}\text{O} \sim 3$ would require the hydrothermally altered caldera block to be far below 0 in terms of $\delta^{18}\text{O}$. Neither model currently satisfies the available evidence, to understand the generation of this rhyolite, the volumes of individual eruptions need to be well-constrained. The model of Branney et al. (2008) invoking flooded calderas could help to explain the oxygen isotopic characteristics of the rhyolites if lacustrine water was assimilated along with intracaldera deposits.

3. What are the true volumes of individual Snake River-type eruptions? The Big Bluff Tuff and Steer Basin Tuff have phenocryst compositions, whole rock chemistry and polarity similar to units from the Cougar Point Tuff succession further west. Further geochronology on these samples is required to test for correlations, ideally analysing samples in the same laboratory. Moreover, how many of the units in the margins of the Snake River Plain have correlatives either along the margin or across the plain. To resolve this would require significant effort but given the success of this study using multitude of techniques, and with the possibility of developing additional correlation techniques, developing a province-wide rhyolitic stratigraphy is an achievable goal.

4. What role did silicic phreatomagmatism play in the central Snake River Plain? Non-welded deposits are poorly exposed in the central Snake River Plain, and only painstaking work revealed the presence and nature of the Deadeye Member. During this study several other non-welded units with characteristics similar to the Deadeye Member were discovered (e.g. the presence of accretionary lapilli, coated pellets and non-welded fine-grained ignimbrites), and given that the non-welded intervals in all the massifs surrounding the CSRP have not been studied, there is the possibility that many more phreatomagmatic deposits exist. Unfortunately, many of these non-welded intervals are poorly exposed. Understanding the role of phreatomagmatism in the history of the hotspot would add an important dimension to current understanding.

5. What is the role of CO₂ in these eruptions? The present-day Yellowstone magmatic and hydrothermal system emits abundant CO₂, however the erupted products of the Yellowstone calderas more closely resemble deposits produced by Plinian-style eruptions. Given the low water contents of SR-type ignimbrites, was CO₂ at least partially responsible for driving these eruptions?

References

- Alidibirov M, Dingwell DB (1996) Magma fragmentation by rapid decompression. *Nature* 380: 146-148
- Allen SR, Cas RAF (1998) Rhyolitic fallout and pyroclastic density current deposits from a phreatoplinian eruption in the eastern Aegean Sea, Greece. *J Volcanol Geotherm Res* 86: 219-251
- Allen SR, McPhie J (2002) The Eucarro Rhyolite, Gawler Range Volcanics, South Australia: A >675 km³, compositionally zoned lava of Mesoproterozoic age. *Geol Soc Am Bull* 114 12:1592-1609
- Allen SR, Stadlbaur E, Keller J (1999) Stratigraphy of the Kos Plateau Tuff: product of a major Quaternary explosive rhyolitic eruption in the eastern Aegean, Greece. *Int Journ Earth Sci* 88:132-156
- Anders MH, Sleep NH (1992) Magmatism and Extension: the thermal and mechanical effects of the Yellowstone hotspot. *J Geophys Res* 9 B11:15279-15393
- Andersen DJ, Lindsley DH, Davidson PM (1993) QUILF: a Pascal program to assess equilibria among Fe-Mg-Mn-Ti oxides, pyroxenes, olivine, and quartz. *Comp Geosci* 19:1333-1350
- Anderson AT, Jr., Newman S, Williams SN, Druitt, TH, Skirius C, Stolper E (1989) H₂O, CO₂, Cl, and gas in Plinian and ashflow Bishop rhyolite. *Geology* 17:221-225
- Anderson RS, Bunas KL (1993) Grain size segregation and stratigraphy in Aeolian ripples modelled with a cellular automaton. *Nature* 365:740-743
- Anderson AT, Brown GG (1993) CO₂ contents and formation pressures of some Kilauean melt inclusions. *Am Mineral* 78:794-803
- Andrews GDM, Branney MJ, Bonnicksen B, McCurry M (2008) Rhyolitic ignimbrites in the Rogerson Graben, southern Snake River Plain volcanic province: volcanic stratigraphy, eruption history and basin evolution. *Bull Volcanol* 70 3:269-291
- Annen C, Sparks RSJ (2002) Effects of repetitive emplacement of basaltic intrusions on thermal evolution and melt generation in the crust. *Earth Plan Sci Lett* 203 3-4:937-955
- Aramaki S (1984) Formation of the Aira Caldera, Southern Kyushu, ~22,000 years ago. *Journ Geophys Res* 89 B10:8485-8501
- Aramaki S, Lipman P (1965) Possible leaching of Na₂O during hydration of volcanic glasses. *Proc Japan Acad* 41 6:467-470
- Arce JL, Cervantes KE, Macias JL, Mora JC (2005) The 12.1 ka Middle Toluca Pumice: a dacitic Plinian-subplinian eruption of Nevado de Toluca in central Mexico. *J Volcanol Geotherm Res* 147 1-2:125-143
- Armstrong RL, Harakal JE, Neill WM (1980) K-Ar dating of Snake River Plain (Idaho) volcanic rocks-new results. *Isochron West* 27:5-10
- Armstrong RL, Leeman WP, Malde HE (1975) K-Ar dating of Quaternary and Neogene volcanic rocks of the Snake River Plain, Idaho. *Am J Sci* 275:225-251
- Bachmann O, Bergantz GW (2003) Rejuvenation of the Fish Canyon magma body: a window into the evolution of large-volume silicic magma systems. *Geology* 31:789-792
- Bacon CR, Adami LH, Lanphere MA (1989) Direct evidence for the origin of low-d¹⁸O silicic magmas: Quenched samples of a magma chamber's partially fused granitoid walls, Crater Lake, Oregon. *Earth Plan Sci Lett* 96:199-208

- Bacon CR, Druitt TH (1988) Compositional evolution of the zoned, calc-alkaline magma chamber of Mount Mazama, Crater Lake, Oregon. *Contrib Mineral Petrol* 76:53–59
- Bacon CR, Hirschman MM (1988) Mg/Mn partitioning as a test for equilibrium between co-existing Fe-Ti oxides. *Am Mineral* 73:57-61
- Bacon CR, Newman S, Stolper E (1992) Water, CO₂, Cl, and F in melt inclusions in phenocrysts from three Holocene explosive eruptions, Crater Lake, Oregon. *Am Mineral* 77:1021-1030
- Baksi AK (1993) A geomagnetic polarity time scale for the period 0-17 Ma, based on Ar-40/Ar-39 plateau ages for selected field reversals. *Geophys Res Lett* 20 15:1607-1610
- Barberi F, Cioni R, Rosi M, Santacroce R, Sbrana A, Vecci R (1989) Magmatic and phreatomagmatic phases in explosive eruptions of Vesuvius as deduced by grain size and component analysis of the pyroclastic deposits. *J Volcanol Geotherm Res* 38: 287-307
- Barberi F, Varet J (1977) Volcanism of Afar: small-scale plate tectonics implications. *Geol Soc Am Bull* 88:1251-1266
- Barclay J, Carroll MR, Houghton BF, Wilson CNJ (1996) Pre-eruptive volatile content and degassing history of an evolving peralkaline volcano. *J Volcanol Geotherm Res* 74:1-2 75-87
- Bennett VC, De Paolo DJ (1987) Proterozoic crustal history of the western United States as determined by neodymium isotopic mapping. *Geol Soc Am Bull* 99:674-685
- Best MG, Christiansen EH (1997) Origin of broken phenocrysts in ash flow tuffs. *Geol Soc Am Bull* 109 1:63-73
- Bindeman IN, Valley JW (2000) Formation of low $\delta^{18}\text{O}$ rhyolites after caldera collapse at Yellowstone, Wyoming. *Geology* 28 8:719-722
- Bindeman IN, Valley J (2001) Low- $\delta^{18}\text{O}$ rhyolites from Yellowstone: Magmatic evolution based on analyses of zircons and individual phenocrysts. *J Petrol* 42:1491-1517
- Bindeman IN, Valley J (2003) Rapid generation of both high- and low- $\delta^{18}\text{O}$, large-volume silicic magmas at the Timber Mountain/Oasis Valley caldera complex, Nevada. *Geol Soc Am Bull* 115 5:581-599
- Bindeman IN, Watts KE, Schmitt AK, Morgan LA, Shanks PWC (2007) Voluminous low $\delta^{18}\text{O}$ magmas in the late Miocene Heise Volcanic Field, Idaho: implications for the fate of Yellowstone hotspot calderas. *Geology* 35 11:1019-1022
- Blank JG, Stolper EM, Carroll MR (1993) Solubilities of carbon dioxide and water in rhyolitic melt at 850 C and 750 bars. *Earth Plan Sci Lett* 119 1-2:27-36
- Blundy J, Cashman K (2001) Ascent-driven crystallisation of dacite magmas at Mount Saint Helens 1980-1986. *Contrib Mineral Petrol* 140 6:631-650
- Blundy J, Cashman K (2005) Rapid decompression-driven crystallisation recorded by melt inclusions from Mount St. Helens volcano. *Geology* 33 10:793-796
- Bonadonna C, Mayberry GC, Calder ES, Sparks RSJ, Choux C, Jackson P, Lejeune AM, Loughlin SC, Norton GE, Rose WI, Ryan G, Young SR (2002) Tephra fallout in the eruption of Soufriere Hills Volcano, Montserrat. *Geol Soc London Memoirs* v 21:483-516
- Bond A, Sparks RSJ (1976) The Minoan eruption of Santorini, Greece. *J Geol Soc* 132:1 1-16
- Bonnichsen B (1982) The Bruneau-Jarbridge Eruptive Center, Southwestern Idaho. In: Bonnichsen B, Breckenridge RM (eds) *Cenozoic Geology of Idaho*. Idaho Bur Min Geol Bull 26:237-254

- Bonnichsen B (1982b) Rhyolite lava flows in the Bruneau–Jarbidge Eruptive Center, southwestern Idaho. In: Bonnichsen B, Breckinridge RM (eds) *Cenozoic Geology of Idaho*. Idaho Bur Min Geol Bull 26:283–320
- Bonnichsen B, Citron GP (1982) The Cougar Point Tuff, southwestern Idaho. In: Bonnichsen B, Breckenridge RM (eds) *Cenozoic Geology of Idaho*. Idaho Bur Mines Geol Bull 26:255–281
- Bonnichsen B, Godchaux MM (2002) Late Miocene, Pliocene, and Pleistocene geology of southwestern Idaho with emphasis on basalts in the Bruneau–Jarbidge, Twin Falls, and Western Snake River Plain regions. In: Bonnichsen B, White CM, McCurry M (eds.) *Tectonic and Magmatic Evolution of the Snake River Plain Volcanic Province*. Idaho Geol Surv Bull 30:233–312
- Bonnichsen B, Kauffman DF (1987) Physical features of rhyolite lava flows in the Snake River Plain volcanic province, Southwestern Idaho. *Geol Soc Am Spec Pap* 212:119-145
- Bonnichsen B, Leeman WP, Honjo, N, McIntosh WC, Godchaux MM (2008) Miocene silicic volcanism in southwestern Idaho: geochronology, geochemistry, and evolution of the central Snake River Plain. *Bull Volcanol* 70:3 315-342
- Boroughs S, Wolff J, Bonnichsen B, Godchaux M, Larson P (2005) Large-volume, low- $\delta^{18}\text{O}$ rhyolites of the central Snake River Plain, Idaho, USA. *Geology* 33:10 821-824 DOI 10.1130/G21723.1
- Bouma A (1962) *Sedimentology of some Flysch deposits; a graphic approach to facies interpretation*. Elsevier 168 pp
- Brand BD, White CM (2007) Origin and stratigraphy of phreatomagmatic deposits at the Pleistocene Sinker Butte Volcano, Western Snake River Plain, Idaho. *J Volcanol Geotherm Res* 160(3-4):319-339
- Branney MJ (1991) Eruption and depositional facies of the Whorneyside Tuff: an exceptionally large-magnitude phreatoplinian eruption. *Geol Soc Am Bull* 203:886-897
- Branney MJ, Barry TL, Godchaux M (2004). Sheathfolds in rheomorphic ignimbrites. *Bull Volcanol* 66 6: 485-491
- Branney MJ, Bonnichsen B, Andrews GDM, Ellis B, Barry TL, McCurry M (2008) ‘Snake River (SR) –type’ volcanism at the Yellowstone hotspot track: distinctive products from unusual, high-temperature silicic super-eruptions. *Bull Volcanol* 70 3:293-314
- Branney MJ, Kokelaar BP (1992) A reappraisal of ignimbrite emplacement: progressive aggradation and changes from particulate to non-particulate flow during emplacement of high-grade ignimbrite. *Bull Volcanol* 54 6:504-520
- Branney MJ, Kokelaar BP (1997) Giant bed from a sustained catastrophic density current flowing over topography; Acatlan ignimbrite, Mexico. *Geology* 25:2 115-118
- Branney MJ, Kokelaar BP (2002) Pyroclastic density currents and the sedimentation of ignimbrites. *Geol Soc London, Memoirs* 27:1-152
- Branney MJ, Kokelaar BP, McConnell BJ (1992) The Bad Step Tuff: a lava-like ignimbrite in a calc-alkaline piecemeal caldera, English Lake District. *Bull Volcanol* 54: 187-199
- Breddam K, Kurz MD, Storey M (2000) Mapping out the conduit of the Iceland mantle plume with helium isotopes. *Earth Plan Sci Lett* 176:45-55
- Brooker MR, Houghton BF, Wilson CJN, Gamble JA (1993) Pyroclastic phases of a rhyolitic dome-building eruption: Puketarata tuff ring, Taupo Volcanic Zone, New Zealand. *Bull Volcanol* 55:395-406

- Brown GM, Vincent EA (1963) Pyroxenes from the late stages of fractionation of the Skaergaard intrusion, East Greenland. *J Petrol* 4 2:175-197
- Brown RJ, Barry TL, Branney MJ, Pringle MS, Bryan SE (2003) The Quaternary pyroclastic succession of southeast Tenerife, Canary Islands: explosive eruptions, related caldera subsidence, and sector collapse. *Geol Mag* 140 3:265-288
- Brown RJ, Branney MJ (2004) Event stratigraphy of a caldera-forming ignimbrite eruption on Tenerife: the 273 ka Poris Formation. *Bull Volcanol* 66:392-416
- Brown R, Branney MJ, Davila-Harris P, Maher C (2008) New origin of accretionary lapilli: growth in pyroclastic density currents. IAVCEI general assembly Reykjavik
- Brown RJ, Kokelaar BP, Branney MJ (2007) Widespread transport of pyroclastic density currents from a large silicic tuff ring: the Glaramara tuff, Scafell caldera, English Lake District, UK. *Sedimentology* 54:5 1163-1190 DOI 10.1111/j.1365-3091.2007.00877.x
- Bryan SE, Cas RAF, Marti J (2002) The 0.57 Ma Plinian eruption of the Granadilla Member, Tenerife (Canary Islands): an example of complexity in eruption dynamics and evolution. *J Volcanol Geotherm Res* 103 1-4:209-238
- Buchanan DL (1978) A combined transmission electron microscope and electron microprobe study of Bushveld pyroxenes from the Bethal area. *J Petrol* 20 2:327-354
- Camp VE, Ross ME (2004) Mantle dynamics and genesis of mafic magmatism in the intermontane Pacific Northwest. *J Geophys Res* 109 B08204 DOI 10.1029/2003JB002838
- Camp VE, Ross ME, Hanson WE (2003) Genesis of flood basalts and Basin and Range volcanic rocks from Steens Mountain to Malheur River Gorge, Oregon. *Geol Soc Am Bull* 115 1:105-128
- Camus G, Gourgaud A, Mossand-Berthommier P-C, Vincent P-M (2000) Merapi (Central Java, Indonesia): An outline of the structural and magmatological evolution, with a special emphasis to the major pyroclastic events. *J Volcanol Geotherm Res* 100 1-4:139-163
- Cande SC, Kent DV (1995) Revised calibration of the geomagnetic polarity time scale for the Late Cretaceous and Cenozoic. *Jour Geophys Res* 100:6093-6095
- Carey S, Sigurdsson H (1986) The 1982 eruptions of El Chichon volcano, Mexico (2): Observations and numerical modelling of tephra-fall distribution. *Bull Volcanol* 48 2-3:127-141
- Carrasco-Nunez G, Branney MJ (2005) Progressive assembly of a massive layer of ignimbrite with a normal-to-reverse compositional zoning: the Zaragoza ignimbrite of central Mexico. *Bull Volcanol* 68 1:3-20
- Cas RAF, Wright JV (1987) Volcanic successions: modern and ancient. Alan & Unwin London pp. 1-528
- Castro JM, Gardner JE (2008) Did magma ascent rate control the explosive-effusive transition at the Inyo volcanic chain, California. *Geology* 36 4:279-282
- Cathey HE, Nash BP (2004) The Cougar Point Tuff: implications for thermochemical zonation and longevity of high-temperature, large volume silicic magmas of the Miocene Yellowstone hotspot. *J Petrol* 45:27-58
- Christiansen EH, McCurry M (2008) Contrasting origins of Cenozoic silicic volcanic rocks from the western Cordillera of the United States. *Bull Volcanol* 70 3:251-267

- Christiansen RL (1984) Yellowstone magmatic evolution: Its bearing on understanding large-volume explosive volcanism. In: Explosive volcanism: Inception, evolution, and hazards: Washington, D.C., National Academy of Sciences, p. 84–95
- Christiansen RL (2001) The Quaternary and Pliocene Yellowstone Plateau Volcanic Field of Wyoming, Idaho, and Montana. US Geol Surv Prof Paper 729-G. Reston Virginia.
- Christiansen RL, Lageson DR (2003) Structural control and plate-tectonic origin of the Yellowstone melting anomaly. In: The hotspot handbook, proceedings of the Penrose Conference Plume IV: beyond the plume hypothesis, Hveragerdi, Iceland (abst)
- Christiansen RL, Foulger GR, Evans JR (2002) Upper mantle origin of the Yellowstone hotspot. *Geol Soc Am Bull* 114 10:1245-1256
- Clemens DM, Wood SH (1993) Late Cenozoic stratigraphy and geochronology of the Mount Bennett Hills, central Snake River Plain, Idaho. *Isochron West* 60:3-14
- Coble MA, Mahood GA (2008) New geologic evidence for additional 16.5-15.5 Ma silicic calderas in northwest Nevada related to initial impingement of the Yellowstone hot spot. *IOP Conf Series: Earth and Env Sci* 3:012002
- Cole PD, Guest JE, Duncan AM, Pacheco J-M (2001) Caphelinhos 1957-1958, Faial, Azores: deposits formed by an emergent Surtseyan eruption. *Bull Volcanol* 63:204-220
- Cole PD, Scarpati C (1993) A facies interpretation of the eruption and emplacement mechanisms of the upper part of the Neapolitan Yellow Tuff, Campi Flegrei, southern Italy. *Bull Volcanol* 55 5:311-326
- Colgan JP, Dumitru TA, McWilliams M, Miller EL (2006) Timing of Cenozoic volcanism and Basin and Range extension in northwestern Nevada: New constraints from the northern Pine Forest Range. *Geol Soc Am Bull* 118 1/2:126-139
- Colgan JP, Dumitru TA, Miller EL (2004) Diachroneity of Basin and Range extension and Yellowstone hotspot volcanism in northwestern Nevada. *Geology* 32 2:121-124
- Collela A, Hiscott RN (1997) Pyroclastic surges of the Pleistocene Monte Guardia sequence (Lipari island, Italy): depositional processes. *Sedimentology* 44:47-66
- Coombs ML, Gardner JE (2001) Shallow storage conditions for the rhyolite of the 1912 eruption at Novarupta, Alaska. *Geology* 29:9 775-778 DOI 10.1130/0091-7613(2001)029.
- Cox KG (1989) The role of mantle plumes in the development of continental drainage patterns. *Nature* 342:873-877
- Creaser RA, White AJR (1991) Yardea Dacite; large volume; high-temperature felsic volcanism from the middle Proterozoic of South Australia. *Geology* 19 1:48-51
- Danyushevsky LV, McNeill A, Sobolev AV (2002) Experimental and petrological studies of melt inclusions in phenocrysts from mantle-derived magmas: an overview of techniques, advantages and complications. *Chem Geol* 183:1-4 5-24
- Dávila Harris P (2008) Explosive ocean-island volcanism: the 1.8–0.7 Ma explosive eruption history of Cañadas volcano recorded by the pyroclastic successions around Adeje and Abona, southern Tenerife, Canary Islands. Unpub. PhD thesis, University of Leicester
- De Paolo DJ, Perry FV, Baldrige WS (1992) Crustal versus mantle sources of granitic magmas; a two-parameter model based on Nd isotopic studies, in Brown PE, Chappell BW (eds.), *The Second Hutton*

- Symposium on the Origin of Granites and Related Rocks; Proceedings, Special Paper, vol. 272, Geol Soc Am, Boulder, CO, pp 439-446
- De Rita D, Giordano G, Esposito A, Fabbri M, Rodani S (2002) Large volume phreatomagmatic ignimbrites from the Colli Albani Volcano (Middle Pleistocene, Italy). *J Volcanol Geotherm Res* 118(1-2): 77-98
- De Rosa R, Donato P, Gioncada A, Masetti M, Santacroce R (2003) The Monte Guardia eruption (Lipari, Aeolian Islands): an example of a reversely zoned magma mixing sequence. *Bull Volcanol* 65 7:530-543
- De Rosen-Spence AF, Provost G, Dimroth E, Gochnaver K, Owen V (1980) Archean subaqueous felsic flows, Rouyn-Noranda, Quebec, Canada and their Quaternary equivalents. *Precamb Res* 12: 43-77
- De Silva SL (1989) Altiplano-Puna volcanic complex of the central Andes. *Geology* 17:1102-1106
- De Silva SL, Francis PW (1991) *Volcanoes of the Central Andes*. Springer, Berlin Heidelberg New York 216pp
- Di Vito MA, Isaia R, Orsi G, Southon J, De Vita S, D'Antonio M, Pappalardo L, Píocchi M (1999) Volcanism and deformation since 12,000 years at the Campi Flegrei caldera (Italy). *J Volcanol Geotherm Res* 91 2-4:221-246
- Dingwell DB (1996) Volcanic dilemma - flow or blow? *Science* 273 5278:1054-1055
- Dingwell DB, Scarfe CM, Cronin DJ (1985) The effect of fluorine on viscosities in the system $\text{Na}_2\text{O}-\text{Al}_2\text{O}_3-\text{SiO}_2$; implications for phonolites, trachytes and rhyolites. *Am Mineral* 70 1-2:80-87
- Dodson A, Kennedy BM, De Paolo DJ (1997) Helium and neon isotopes in the Imnaha basalt, Columbia River Basalt Group: Evidence for a Yellowstone plume source. *Earth Plan Sci Lett* 150:443-451
- Draper DS (1991) Late Cenozoic bimodal magmatism in the northern Basin and Range Province of southeastern Oregon. *J Volcanol Geotherm Res* 47 3-4:299-328
- Druitt TH, Bacon CR (1986) Lithic breccia and ignimbrite erupted during the collapse of Crater Lake Caldera, Oregon. *J Volcanol Geotherm Res* 29 (1-4):1-32
- Druitt TH, Sparks RSJ (1982) A proximal ignimbrite breccia facies on Santorini, Greece. *J Volcanol Geotherm Res* 13 1-2:147-171
- Duffield WA, Dalrymple GB (1990) The Taylor Creek Rhyolite of New Mexico: a rapidly emplaced field of domes and flows. *Bull Volcanol* 52 6:475-487
- Dunbar NW, Hervig RL (1992) Volatile and trace element composition of melt inclusions from the lower Bandelier Tuff, implications for magma chamber processes and eruptive style. *J Geophys Res* 97 B11:15,129-15,150
- Dunbar NW, Hervig RL, Kyle PK (1989) Determination of pre-eruptive H_2O , F and Cl contents of silicic magmas using melt inclusions: Examples from Taupo volcanic center, New Zealand. *Bull Volcanol* 51 3:177-184
- Dunbar NW, Kyle PR (1993) Lack of volatile gradient in the Taupo Plinian-ignimbrite transition: Evidence from melt inclusion analysis. *Am Mineral* 78:612-618
- Eby GN (1990). The A-type granitoids: a review of their occurrence and chemical characteristics and speculations on their petrogenesis. *Lithos* 26 115-134

- Edgar CJ, Wolff JA, Olin PH, Nichols HJ, Pittari A, Cas RAF, Reiners PW, Spell TL, Martí J (2007) The late Quaternary Diego Hernandez Formation, Tenerife: Volcanology of a complex cycle of voluminous explosive phonolitic eruptions. *J Volcanol Geotherm Res* 160:59-85
- Eichelberger JC, Carrigan CR, Westrich HR, Price RH (1986) Non-explosive silicic volcanism. *Nature* 323:598-602
- Ekren EB, McIntyre DH, Bennett EH (1984) High-temperature, large volume, lavalike ash-flow tuffs without calderas in southwestern Idaho. *US Geol Surv Prof Pap* 1272.
- Elston WE, Seager WR, Clemons RE (1975) Emory cauldron, Black Range, New Mexico, source of the Kneeling Nun Tuff. *Field Conf Guide NM Geol Soc* 26:283–292
- Ewart A, Milner SC, Armstrong RA, Duncan AR (1998) Etendeka volcanism of the Gobobseb Mountains and Messum Igneous Complex, Namibia, Parts I and II. *J Petrol* 39:191–253
- Farmer GL, Broxton DE, Warren RG, Pickthorn W (1991) Nd, Sr, and O isotopic variations in metaluminous ash-flow tuffs and related volcanic rocks at the Timber Mountains/Oasis Valley caldera complex, SW Nevada: implications for the origin and evolution of large-volume silicic magma bodies. *Contrib Mineral Petrol* 109:53–68
- Ferns ML (1989) Geology and mineral resources map of the Graveyard Point quadrangle, Malheur County, Oregon, and Owyhee County, Idaho. *Oregon Dept Geol Mineral Ind GeolMap Series 1:24000* 54:1-45
- Ferriz H, Mahood G (1987) Strong compositional zonation in a silicic magmatic system: Los Humeros, Mexican Neovolcanic Belt. *J Petrol* 28:171–209
- Fierstein J, Hildreth W (1992) The Plinian eruptions of 1912 at Novarupta, Katmai national park, Alaska. *Bull Volcanol* 54 8:646-684
- Fierstein J, Wilson CJN (2005) Assembling an ignimbrite: compositionally-defined flow packages in the 1912 Valley of Ten Thousand Smokes ignimbrite, Alaska. *Geol Soc Am Bull* 117:1094-1107
- Fink JH, Bridges NT (1995) Effects of eruption history and cooling rate on lava dome growth. *Bull Volcanol* 57 4:229-239
- Fisher JA, Krapf CBE, Lang SC, Nichols GJ, Payenberg THD (2008) Sedimentology and architecture of the Douglas Creek terminal splay, Lake Eyre, central Australia. *Sedimentology* 55:1915-1930
- Fisher RV (1984) Submarine pyroclastic rocks. *Geol Soc London Spec Pub* 16:5-27
- Fleck RJ (1990) Neodymium, strontium, and trace-element evidence of crustal anatexis and magma mixing in the Idaho Batholith. In: Anderson J L (ed.) *The Nature and Origin of Cordilleran Magmatism*. *Geol Soc Am, Memoir* 174:359-373
- Fogel RA, Rutherford MJ (1990) The solubility of carbon dioxide in rhyolitic melts: A quantitative FTIR study. *Am Mineral* 75:1311-1326
- Francis PW, Sparks RSJ, Hawkesworth CJ, Thorpe RS, Pyle DM, Tait SR, Mantovani M, McDermott F (1989) Petrology and geochemistry of volcanic rocks of the Cerro Galan caldera, northwest Argentina. *Geol Mag* 126:515–547
- Fuhrman ML, Lindsley DL (1988) Ternary-feldspar modelling and thermometry. *Am Mineral* 73:201–215
- Furnes H, Fridleifsson IB, Atkins FB (1980) Subglacial volcanics: on the formation of acid hyaloclastites. *J Volcanol Geotherm Res* 8:95–110

- Garner A, McPhie J (1999) Partially melted lithic megablocks in the Yardea Dacite, Gawler Range Volcanics, Australia: implications for eruption and emplacement mechanisms. *Bull Volcanol* 61 6:396-410
- Geshi N, Shimano T, Chiba T, Nakada S (2002) Caldera collapse during the 2000 eruption of Miyakejima Volcano, Japan. *Bull Volcanol* 64:1 55-68 DOI 10.1007/s00445-001-0184-z
- Ghiorso MS (1984) Activity/composition relations in the ternary feldspars. *Contrib Mineral Petrol* 87:282–296
- Gilbert JS, Lane SJ (1994) The origin of accretionary lapilli. *Bull Volcanol* 56 5:398-411
- Giordano D, Romano C, Papale P, Dingwell DB (2004) The viscosity of trachytes, and comparison with basalts, phonolites, and rhyolites. *Chem Geol* 213 1-3:49-61
- Giordano D, Russel JK, Dingwell DB (2008) Viscosity of magmatic liquids: a model. *Earth Plan. Sci Lett* 271 1-4:123-134
- Giordano G, De Rita D, Fabbri M, Rodani S (2002) Facies associations of rain-generated versus crater lake-withdrawal lahar deposits from Quaternary volcanoes, central Italy. *J Volcanol Geotherm Res* 118 1-2:145-159
- Giorgis S, Tikoff B, McClelland W (2005) Missing Idaho arc: transpressional modification of the $^{87}\text{Sr}/^{86}\text{Sr}$ transition on the western edge of the Idaho batholith. *Geology* 33 6:469-472
- Godchaux MM, Bonnicksen B (2002) Syneruptive magma-water and posteruptive lava-water interactions in the Western Snake River Plain, Idaho, during the past 12 million years. In: Bonnicksen B, White CM, McCurry M (eds) *Tectonic and magmatic evolution of the Snake River Plain Volcanic Province*. Idaho Geol Surv Bull 30:387-434
- Gonnermann HM, Manga M (2003) Explosive volcanism may not be an inevitable consequence of magma fragmentation. *Nature* 426:432-435
- Gonnermann HM, Manga M (2007) The Fluid Mechanics Inside a Volcano. *Annu Rev Fluid Mech* 39:321–356
- Greeley R (1982) The Snake River Plain, Idaho: representative of a new category of volcanism. *J Geophys Res* 2705-2712
- Green JC (1989) Physical volcanology of mid-Proterozoic plateau lavas: the Keweenawan North Shore Volcanic Group, Minnesota. *Geol Soc Amer Bull* 101:486–500
- Green JC, Fitz TZ (1993) Extensive felsic lavas and rheognimbrites in the Keweenawan Midcontinent Rift plateau volcanics, Minnesota: petrographic and field recognition. *J Volcanol Geotherm Res* 54 3-4:177-196
- Grunder AL, Mahood GA (1988) Physical and chemical models of zoned silicic magmas: the Loma Seca Tuff and Calabozos caldera caldera, southern Andes. *J Petrol* 29 4:831-867
- Hammer JE, Cashman KV, Hoblitt RP, Newman S (1999) Degassing and microlite crystallization during pre-climactic events of the 1991 eruption of Mt. Pinatubo, Philippines. *Bull Volcanol* 60 5:355-380
- Heiken GH, Wohletz K (1985) *Volcanic Ash*. University of California Press. 246pp
- Henry CD, Castor SB, McIntosh WC, Heizler MT, Cuney M, Chemillac R (2006) Timing of oldest Steens basalt magmatism from precise dating of silicic volcanic rocks, McDermitt caldera and northwest Nevada Volcanic Field. *Eos Trans AGU*, 87(52), Fall Meet Suppl, Abstract V44C-08
- Henry CD, Kunk MJ, McIntosh WC (1994) $^{40}\text{Ar}/^{39}\text{Ar}$ chronology and volcanology of silicic volcanism in the Davis Mountains, Trans-Pecos Texas. *Geol Soc Am Bull* 106 11:1359-1376

- Henry CD, Price JG (1984) Variations in caldera development in the Tertiary volcanic field of trans-Pecos Texas. *J Geophys Res* 89:8765–8786
- Henry CD, Price JG, Rubin JN, Laubach SE (1990) Case study of an extensive silicic lava: the Bracks Rhyolite, Trans-Pecos Texas. *J Volcanol Geotherm Res* 43:113–132
- Henry CD, Price JG, Rubin JN, Parker DF, Wolff JA, Self S, Franklin R, Barker DS (1988) Widespread, lava-like silicic volcanic rocks of Trans-Pecos Texas. *Geology* 16: 509-512.
- Henry CD, Wolff JA (1992) Distinguishing strongly rheomorphic tuffs from extensive silicic lavas. *Bull Volcanol* 54:171-186
- Hess KU, Dingwell DB (1996) Viscosities of hydrous leucogranitic melts: a non-Arrhenian model. *Am Mineral* 81:1297–300
- Hildebrand RT, Newman KR (1985) Miocene sedimentation in the Goose Creek basin, south-central Idaho, northeastern Nevada and northwestern Utah, *in* Flores, RM, et al. eds., *Cenozoic paleogeography of the western U.S.: Rocky Mountain Section, Society of Economic Paleontologists and Mineralogists* p. 55–70
- Hildreth W (1979) The Bishop Tuff: evidence for the origin of compositional zonation in silicic magma chambers. In: Chapin CE, Elston WE (eds) *Ash-flow tuffs*. Geological Society of America, Special Paper (1979) 180:43–75.
- Hildreth W (1983) The compositionally zoned eruption of 1912 in the Valley of Ten Thousand Smokes, Katmai National Park, Alaska. *J Volcanol Geotherm Res* 18 1-4:1-56.
- Hildreth W, Wilson CJN (2007) Compositional zoning of the Bishop Tuff. *J Petrol* 48 5:951-999
- Honjo N, Bonnicksen B, Leeman WP, Stormer JJC (1992). Mineralogy and geothermometry of high-temperature rhyolites from the central and western Snake River Plain. *Bull Volcanol* 54, 220-237
- Honjo N, McElwee KR, Duncan RA, Leeman WP (1986) K-Ar ages of volcanic rocks from the Magic Reservoir eruptive center, Snake River Plain, Idaho. *Isochron West* 46: 9-14
- Honjo N, Leeman WP (1987) Origin of hybrid ferrolatite lavas from the Magic Reservoir Eruptive center, Snake River Plain Idaho. *Contrib Mineral Petrol* 96 2:163-177
- Hooper PR, Binger BG, Lees KR (2002) Age of the Steens and Columbia River flood basalts and their relationship to extension-related calc-alkaline volcanism in eastern Oregon. *Geol Soc Am Bull* 114 1:43-50
- Hooper PR, Camp VE, Reidel SP, Ross ME (2007) The origin of the Columbia River Flood Basalt province: plume versus non-plume models. In: *Plates, plumes and planetary processes*. Foulger and Jurdy (eds.) *Geol Soc Am spec pap* 430: 635-668
- Houghton BF, Smith RT (1993) Recycling of magmatic clasts during explosive eruptions: estimating the true juvenile content of phreatomagmatic volcanic deposits. *Bull Volcanol* 55:6 414-420 DOI 10.1007/BF00302001
- Huff WD, Kolata DR, Bergstrom SM, Zhang Y-S (1996) Large magnitude Middle Ordovician volcanic ash falls in North America and Europe: dimensions, emplacement and post-emplacement characteristics. *J Volcanol Geotherm Res* 73:285–301
- Humphreys ED, Dueker KG, Schutt DL, Smith RB (2000) Beneath Yellowstone: Evaluating plume and nonplume models using teleseismic images of the upper mantle: *GSA Today*. 10:1-7

- Isaia R, D'Antonio M, Dell'Erba F, Di Vito M, Orsi G (2004) The Astroni volcano: the only example of closely spaced eruptions in the same vent area during the recent history of the Campi Flegrei caldera (Italy). *J Volcanol Geotherm Res* 133:171-192
- Jerram DA (2002) Volcanology and facies architecture of flood basalts. *Geol Soc Am Spec Paper* 362:119-132
- Jordan BT, Grunder AL, Duncan RA, Deino AL (2004) Geochronology of age-progressive volcanism of the Oregon High Plains: implications for the plume interpretation of Yellowstone. *J Geophys Res* 109 B10202-B10221
- Kataoka K, Nakajo T (2002) Volcaniclastic resedimentation in distal fluvial basins induced by large-volume explosive volcanism: the Ebisutoge-Fukuda tephra, Plio-Pleistocene boundary, central Japan. *Sedimentology* 49:319-334
- Kellogg KS, Harlan SS, Mehnert HH, Snee LW, Pierce, KL, Hackett WR, Rogers DW (1994) Major 10.2 Ma rhyolitic volcanism in the eastern Snake River Plain, Idaho—Isotopic age and stratigraphic setting of the Arbon Valley Tuff member of the Starlight Formation: U.S. Geol Surv Bull 2091 18pp
- Kimura JI, Yoshida T (1999) Magma plumbing system beneath Ontake Volcano, central Japan. *Island Arc* 8 1:1-29
- Kneller BC, Branney MJ (1995) Sustained high-density turbidity currents and the deposition of thick massive sands. *Sedimentology* 42 4:607-616
- Kokelaar BP (1983) The mechanism of Surtseyan volcanism. *J Geol Soc* 140:6 939-944 DOI 10.1144/gsjgs.140.6.0939
- Kokelaar BP (1986) Magma-water interactions in subaqueous and emergent basaltic volcanism. *Bull Volcanol* 48:5 275-289 DOI 10.1007/BF01081756
- Kokelaar BP, Durant GP (1983) The submarine eruption and erosion of Surtla (Surtsey), Iceland. *J Volcanol Geotherm Res* 19 3-4:239-246
- Kokelaar P, Moore I (2006) *Classical Areas of British Geology: Glencoe Caldera Volcano, Scotland*. British Geological Survey, Keyworth.
- Kokelaar P, Raine P, Branney MJ (2007) Incursion of a large-volume, spatter-bearing pyroclastic density current into a caldera lake: Pavey Ark ignimbrite, Scafell caldera, England. *Bull Volcanol* 70:23-54
- Lanphere MA, Champion DE, Christiansen RL, Izett GA, Obradovich JD (2002) Revised ages for tuffs of the Yellowstone plateau volcanic field: Assignment of the Huckleberry Ridge Tuff to a new geomagnetic polarity event. *Geol Soc Am Bull* 114 5:559-568
- Lavigne F, Suwa H (2004) Contrasts between debris flows, hyperconcentrated flows and stream flows at a channel of Mount Semeru, East Java, Indonesia. *Geomorphology* 61:41-58
- Lee M-Y, Chen C-H, Wei K-Y, Iizuka Y, Carey S (2004) First Toba super-eruption revival. *Geology* 32:61–64
- Leeder M (1999) *Sedimentology and Sedimentary Basins from Turbulence to Tectonics*. Blackwell Science, Oxford 592 pp.
- Leeman WP (1982) Tectonic and magmatic significance of strontium isotope variations in Cenozoic volcanic rocks from the western United States. *Geol Soc Am Bull* 93 6:487-503
- Leeman WP (2004) Evolution of Snake River Plain (SRP) silicic magmas—the Magic Reservoir eruptive center. *Geol Soc Am Abst with Prog* 36: 24

- Leeman WP, Annen C, Dufek J (2008) Snake River Plain – Yellowstone silicic volcanism: implications for magma genesis and magma fluxes. In: Annen C, Zellmer GF (eds.) Dynamics of Crustal Magma Transfer, Storage and Differentiation. Geol Soc London Spec Pub 304:235-259
- Leeman WP, Menzies MA, Matty DJ, Embree GF (1985) Strontium, neodymium and lead isotopic compositions of deep crustal xenoliths from the Snake River Plain; evidence for Archean basement. Earth Plan Sci Lett 75:354-368
- Leeman WP, Oldow JS, Hart WK (1992). Lithosphere-scale thrusting in the western US Cordillera as constrained by Sr and Nd isotopic transitions in Neogene volcanic rocks. Geology 20:63-66
- Lindsay JM, de Silva SL, Trumbull RB, Emmermann R, Wemmer K (2001a) La Pacana caldera, N. Chile: a re-evaluation of the stratigraphy of one of the world's largest resurgent calderas. J Volcanol Geotherm Res 106:145–173
- Lindsley DH (1983) Pyroxene thermometry. Am Mineral 68:477–493
- Lipman PW (1975) Evolution of the Platoro caldera complex and related volcanic rocks, southeastern San Juan Mountains, Colorado. US Geol Surv Prof Pap 852:1–128
- Lipman PW (1997) Subsidence of ash-flow calderas: relation to caldera size and magma chamber geometry. Bull Volcanol 59:198–218
- Lipman PW, Friedman I (1975) Interaction of meteoric water with magma: an oxygen-isotope study of ash-flow sheets from southern Nevada. Geol Soc Am Bull 86 5:695–702
- Lipman PW, Prostka HJ, Christiansen RL (1971) Evolving Subduction Zones in the Western United States, as Interpreted from Igneous Rocks. Science 174 4011:821-825.
- Lipman PW, Prostka HJ, Christiansen RL (1972) Cenozoic volcanism and plate tectonic evolution of the Western United States . Early and Middle Cenozoic. Phil Trans Roy Soc London A 271:217-248
- Lipman PW, Steven TA, Luedke RG, Burbank WS (1973) Revised volcanic history of the San Juan, Uncompahgre, Silverton, and Lake City calderas in the western San Juan Mountains, Colorado. J Res, US Geol Surv 1:627–642
- Liu X, Zhao Z, Zhao Y, Chen J, Liu X (2003) Pyroxene exsolution in mafic granulites from the Grove Mountains, East Antarctica: constraints on Pan-African metamorphic conditions. Eur Jour Mineral 15 1:55-65
- Lowenstern JB (1993) Evidence for a copper-bearing fluid in magma erupted at the Valley of ten thousand smokes, Alaska. Contrib Mineral Petrol 114 3:409-421
- Lowenstern JB (1994) Dissolved volatile concentrations in an ore-forming magma. Geology 22 10:893-896
- Lowenstern, JB (1995) Applications of silicate melt inclusions to the study of magmatic volatiles. In: Thompson, J.F.H. (ed.) Magmas, Fluid and Ore Deposits. Mineralogical Association of Canada Short Course 23, 71-99
- Lowenstern JB (2000) A review of the contrasting behavior of two magmatic volatiles: chlorine and carbon dioxide. J Geochem Explor 69-70:287-290
- Lowenstern JB, Smith RB, Hill DP (2006) Monitoring super-volcanoes: geophysical and geochemical signals at Yellowstone and other large caldera systems. Phil Trans Roy Soc A 364 1845:2055-2072
- Lowenstern JB, Clynne MA, Bullen TB (1997) Comagmatic A-type granophyre and rhyolite from the Alid volcanic center, Eritrea, northeast Africa. J Petrol 38:1707-1721

- Lowenstern JB, Hurwitz S (2008) Monitoring a Supervolcano in Repose: Heat and Volatile Flux at the Yellowstone Caldera. *Elements* 4 1: 35-40
- Lowenstern JB, Mahood GA (1991) New data on magmatic H₂O contents of patellerites, with implications for petrogenesis and eruptive dynamics at Pantelleria. *Bull Volcanol* 54:78-83
- Ludwig KR (2003) Isoplot 3.00. Berkeley Geochronology Center, Spec Pub 4, 70 pp.
- Maeno F, Taniguchi H (2006) Silicic lava dome growth in the 1934–1935 Showa Iwo-jima eruption, Kikai caldera, south of Kyushu, Japan. *Bull Volcanol* 68 7-8:673-688
- Mahood GA (1984) Pyroclastic rocks and calderas associated with strongly peralkaline magmatism. *J Geophys Res* 89:8540-8552
- Malde HE, Powers HA (1962) Upper Cenozoic stratigraphy of western Snake River Plain, Idaho. *Geol Soc Am Bull* 73:1197-1220
- Manga M, Castro J, Cashman K, Loewenberg M (1998) Rheology of bubble-bearing magmas. *J Volcanol Geotherm Res* 87 1-4:15-28
- Mangan M, Cashman KV (1996) The structure of basaltic scoria and reticulate and inferences for vesiculation, foam formation and fragmentation in lava fountains. *J Volcanol Geotherm Res* 73:1-18
- Mangan M, Sisson T (2000) Delayed, disequilibrium degassing in rhyolitic magma: decompression experiments and implications for explosive volcanism. *Earth Plan Sci Lett* 183 3-4:441-455
- Manley CR (1996) Physical volcanology of a voluminous rhyolite lava flow: The Badlands lava, Owyhee plateau, southwestern Idaho. *J Volcanol Geotherm Res* 71 2-4:129-153
- Manley CR (1996b) Morphology and maturation of melt inclusions in quartz phenocrysts from the Badlands rhyolite lava flow, southwestern Idaho. *Am Mineral* 81:158-168
- Manley CR, Bacon CR (2000) Rhyolite Thermobarometry and the Shallowing of the Magma Reservoir, Coso Volcanic Field, California. *J Petrol* 41 1:149-174
- Manley CR, McIntosh WP (2002) The Juniper Mountain Volcanic Center, Owyhee County, Southwestern Idaho: Age Relations and Physical Volcanology. In: Bonnicksen B, White CM, McCurry M (eds) *Tectonic and Magmatic Evolution of the Snake River Plain Volcanic Province*. Idaho Geol Surv Bull 30:205-227
- Manville V, Wilson CJN (2004) Vertical density currents: a review of their potential role in the deposition and interpretation of deep-sea ash layers. *J Geol Soc London* 161:947-958
- Markl G, White C (1999) Complex zoning between super-calcic pigeonite and augite from the Graveyard Point sill, Oregon: a record of the interplay between bulk and interstitial liquid fractionation. *Contrib Mineral Petrol* 137 1-2:170-183
- Mason BG, Pyle DM, Oppenheimer C (2004) The size and frequency of the largest explosive eruptions on Earth. *Bull Volcanol* 66:735-768
- Masson G (1996) Catastrophic collapse of the volcanic island of Hierro 15 ka ago and the history of landslides in the Canary Islands. *Geology* 24 3:231-234
- Mastrolorenzo G (1994) Averno tuff ring in Campi Flegrei (south Italy). *Bull Volcanol* 56 6-7: 561-572
- Maughan LL, Christiansen EH, Best MG, Gromm CS, Deino AL, Tingey DG (2002) The Oligocene Lund Tuff, Great Basin, USA: a very large volume monotonous intermediate. *J Volcanol Geotherm Res* 113:129–157

- McCurry M, Hayden KP, Morse LH, Mertzman S (2008) Genesis of post-hotspot, A-type rhyolite of the Eastern Snake River Plain volcanic field by extreme fractional crystallisation of olivine. *Bull Volcanol* 70 3:361-383
- McCurry M, Watkins AM, Parker JL, Wright K, Hughes SS (1996) Preliminary volcanological constraints for sources of high-grade, rheomorphic ignimbrites of the Cassia Mountains, Idaho: implications for the evolution of the Twin Falls Volcanic Centre. *Northwest Geol* 26:81-91
- McDougall I, Roksandic Z (1974) Total fusion $^{40}\text{Ar}/^{39}\text{Ar}$ ages using Hifar reactor. *Aust J Earth Sci* 21 1:81-89
- McPhie J (1986) Primary and redeposited facies from a large magnitude, rhyolitic, phreatomagmatic eruption: Cana Creek Tuff, late Carboniferous, Australia. *J Volcanol Geotherm Res* 28: 319-350
- Michaud V, Clocchiatti R, Sbrana S (2000) The Minoan and post-Minoan eruptions, Santorini (Greece) in the light of melt inclusions: chlorine and sulphur behaviour. *J Volcanol Geotherm Res* 99 1-4:195-214
- Milner SC, Duncan AR, Ewart A (1992) Quartz latite rheoignimbrite flows of the Etendeka Formation, north-western Namibia. *Bull Volcanol* 54:200-219
- Moore I, Kokelaar P (1998) Tectonically-controlled piecemeal caldera collapse: a case study of Glencoe volcano, Scotland. *Geol Soc Am Bull* 110 11:1448-1466
- Moore JG, Nakamura K, Alcarez A (1966) The 1965 eruption of Taal volcano. *Science* 25 151 3713:955-960
- Morgan LA, Doherty DJ, Leeman WP (1984) Ignimbrites of the Eastern Snake River Plain: evidence for major caldera-forming eruptions. *J Geophys Res* 89:8665-8678
- Morgan LA, McIntosh WC (2005) Timing and development of the Heise volcanic field, Snake River Plain, Idaho, western USA. *Geol Soc Am Bull* 117: 288-306
- Mulder T, Alexander J (2001) The physical character of subaqueous sediment density flows and their deposits. *Sedimentology* 48 2:269-299
- Murase T, McBirney AR (1973) Properties of Some Common Igneous Rocks and Their Melts at High Temperatures. *Geol Soc Am Bull* 84 11:3563-3592
- Mytton JW, Williams PL, Morgan WA (1990) Geologic map of the Stricker 4 quadrangle, Cassia, Twin Falls, and Jerome Counties, Idaho. *US Geol Surv Misc Invest Series Map I-2052*, scale 1:48 000
- Nakagawa M, Wada K, Thordarson T, Wood CP, Gamble JA (1998) Petrologic investigations of the 1995 and 1996 eruptions of Ruapehu volcano, New Zealand: formation of discrete and small magma pockets and their intermittent discharge. *Bull Volcanol* 61 1-2:15-31
- Nash BP, Perkins ME, Christiansen JN, Lee DC, Halliday AN (2006) The Yellowstone hotspot in space and time: Nd and Hf isotopes in silicic magmas. *Earth Plan Sci Lett* 247:143-156
- Newhall CG, Self S (1982) The volcanic explosivity index (VEI); an estimate of explosive magnitude for historical volcanism. *J Geophys Res* 87:1231-1238
- Newman S, Lowenstern JB (2002) Volatile Calc: a silicate melt-H₂O-CO₂ solution model written in Visual Basic for excel. *Comp Geosci* 28 5:597-604.
- Newman S, Chesner C (1989) Volatile compositions of glass inclusions from the 75Ka Toba Tuff Sumatra. *Geol Soc Am Abstracts with Programs*, 21, A27 1
- Noble DC, McKee EH, Smith JG, Korrington MK (1970) Stratigraphy and geochronology of Miocene volcanic rocks in northwestern Nevada: U.S.Geol Surv Prof Paper 700D:23-32

- O'Connor JM, Duncan RA (1990) Evolution of the Walvis Ridge-Rio Grande Rise hot spot system: implications for African and South American plate motions over plumes. *J Geophys Res* 95:17475–17502
- Oakley WL, Link PK (2006) Geologic map of the Davis Mountain Quadrangle, Gooding and Camas Counties, Idaho. Idaho Geological Survey technical report T-06-6.
- Ort MH (1993) Eruptive processes and caldera formation in a nested downsag collapse caldera: Cerro Panizos, central Andes Mountains. *J Volcanol Geotherm Res* 56:221–252
- Pabst S, Wörner G, Civetta L, Tesoro R (2007) Magma chamber evolution prior to the Campanian Ignimbrite and Neapolitan Yellow Tuff eruptions (Campi Flegrei, Italy). *Bull Volcanol* 70 8:961-976
- Palladino DM, Taddeucci J (1998) The basal ash deposit of the Sovana Eruption (Vulsini Volcanoes, central Italy): the product of a dilute pyroclastic density current. *J Volcanol Geotherm Res* 87 1-4:233-254
- Parker AJ, Flint RB (2005) Yardea, South Australia. 1:250,000 Sheet S153-3 International Index. Government of South Australia, Primary Industries and Resources, South Australia
- Parker DF, McDowell FW (1979) K-Ar geochronology of Oligocene volcanic rocks, David and Barrilla Mountains, Texas. *Geol Soc Am Bull* 90:1100–1110
- Parker JL, Hughes SS, McCurry M (1996) Physical and chemical constraints on the emplacement of the tuff of Wooden Shoe Butte, Cassia Mountains, Idaho. In: Hughes SS, Thomas RC (eds) *Geology of the crook in the Snake River Plain, Twin Falls and vicinity, Idaho*. *Northwest Geol* 26: 92-106
- Patino Douce AE (1997) Generation of metaluminous A-type granites by low-pressure melting of calc-alkaline granitoids. *Geology* 25:743-746
- Pearce J, Harris NBW, Tindle AG (1984) Trace element discrimination diagrams for the tectonic interpretation of granitic rocks. *J Petrol* 25 4:956-983
- Peng X, Humphreys ED (1998) Crustal velocity structure across the eastern Snake River Plain and the Yellowstone swell. *J Geophys Res* 103 B4:7171
- Perkins ME, Nash WP (2002) Explosive silicic volcanism of the Yellowstone hotspot: The ash fall tuff record. *Geol Soc Am Bull* 114: 367-381.
- Perkins ME, Nash WP, Brown FH, Fleck RJ (1995) Fallout tuffs of Trapper Creek Idaho – a record of Miocene explosive volcanism in the Snake River Plains volcanic province. *Geol Soc Am Bull* 107:1484-1506
- Perkins ME, Williams SK, Brown FH, Nash WP, McIntosh W (1998) Sequence, age, and source of silicic fallout tuffs in middle to late Miocene basins of the northern Basin and Range Province. *Geol Soc Am Bull* 110: 344-360
- Pfeiffer T (2001) Vent development during the Minoan eruption (1640 BC) of Santorini as suggested by ballistic blocks. *J Volcanol Geotherm Res* 106 3-4:229-242
- Pierce KL, Morgan LA (1992) The track of the Yellowstone hotspot: volcanism, faulting, and uplift. In: Link PK, Kuntz MA, Platt LB (eds) *Regional Geology of Eastern Idaho and Western Wyoming*. *Geol Soc Am Mem* 179:1-53
- Pinkerton H, Stevenson RV (1992) Methods of determining the rheological properties of magmas at sub-liquidus temperatures. *J Volcanol Geotherm Res* 53 1-3:47-66

- Pittari A, Cas RAF, Edgar CJ, Nichols HJ, Wolff JA, Marti J (2006) The influence of palaeotopography on facies architecture and pyroclastic flow processes of a lithic-rich ignimbrite in a high gradient setting: The Abrigo Ignimbrite, Tenerife, Canary Islands. *J Volcanol Geotherm Res* 152 3-4:273-315
- Ratte JC, Marvin RF, Naeser CW (1984) Calderas and ash flow tuffs of the Mogollan Mountains, southwestern New Mexico. *J Geophys Res* 89:8713–8732
- Renne PR, Swisher CC, Deino AL, Karner DB, Owens TL, De Paolo DJ (1998) Intercalibration of standards, absolute ages and uncertainties in $^{40}\text{Ar}/^{39}\text{Ar}$ dating. *Chem Geol* 145 1-2:117-152
- Reubi O, Nicholls IA (2005) Structure and dynamics of a silicic magmatic system associated with caldera-forming eruptions at Batur Volcanic Field, Bali, Indonesia. *J Petrol* 46 7:1367-1391
- Rodgers DW, Ore HT, Bobo RT, McQuarrie N, Zentner N (2002) Extension and subsidence of the eastern Snake River Plain, Idaho. In: Bonnicksen B, McCurry M, White CM (eds) Tectonic and magmatic evolution of the Snake River Plain Volcanic Province. *Idaho Geol Surv Bull* 30:121-155
- Rose WI, Chesner CA (1987) Dispersal of ash in the great Toba eruption, 75 ka. *Geology* 15:913–917
- Rose WI, Riley CM, Darteville S (2003) Sizes and shapes of 10 Ma distal fall pyroclasts in the Ogallala Group, Nebraska. *J Geol* 111: 115-124
- Rosi M, Vezzoli L, Aleotti P, De Censi M (1996) Interaction between caldera collapse and eruptive dynamics during the Campanian Ignimbrite eruption, Phlegrean Fields, Italy. *Bull Volcanol* 57 7:541-554
- Rowley PD, MacLeod NS, Kuntz MA, Kaplan AM (1985) Proximal bedding deposits related to pyroclastic flows of May 18, 1980, Mount St. Helens, Washington. *Geol Soc Am Bull* 96:11 1373-1383
- Rust AC, Cashman KV (2007) Multiple origins of obsidian pyroclasts and implications for changes in the dynamics of the 1300 B.P. eruption of Newberry Volcano, USA. *Bull Volcanol* 69:8 825-845 DOI 10.1007/s00445-006-0111-4
- Rust A, Cashman KV, Wallace PJ (2004) Magma degassing buffered by vapor flow through brecciated conduit margins. *Geology* 32 4:349-352
- Rutherford MJ, Sigurdsson H, Carey S, Davis A (1985) The May 18, 1980, eruption of Mount St. Helens I - Melt composition and experimental phase equilibria. *J Geophys Res* 90 10:2929-2947
- Saito G, Kazahaya K, Shinohara H, Stimac J, Kawanabe Y (2001) Variation of volatile concentration in a magmatic system of Satsuma-Iwojima volcano deduced from melt inclusions. *J Volcanol Geotherm Res* 108 1-4:11-31
- Sanford RF (2005) Geology and stratigraphy of the Challis Volcanic Group and related rocks, Little Wood River Area, south-central Idaho. *US Geol Surv Bull* 2064-II
- Scarpati C, Cole PD, Perrotta A (1993) The Neapolitan Yellow Tuff — A large volume multiphase eruption from Campi Flegrei, Southern Italy. *Bull Volcanol* 55 5:343-356
- Schermer ER, Busby C (1994) Jurassic magmatism in the central Mojave desert: implications for arc palaeogeography and preservation of continental volcanic sequences. *Geol Soc Am Bull* 106 6:767-790
- Schmitt AK (2001) Gas-saturated crystallization and degassing in large-volume, crystal-rich dacitic magmas from the Altiplano-Puna, northern Chile. *J Geophys Res* 106 12 2:30561-30578
- Schneider JL, Le Ruyet A, Chanier F, Buret C, Ferriere J, Proust JN, Rosseel JB (2001) Primary or secondary distal volcanoclastic turbidites: how to make the distinction? An example from the Miocene of New Zealand (Mahia Peninsula, North Island). *Sed Geol* 145:1-22

- Schumacher R, Mues-Schumacher U (1997) The pre-ignimbrite (phreato) plinian and phreatomagmatic phases of the Akdag-Zelve ignimbrite eruption in Central Anatolia, Turkey. *J Volcanol Geotherm Res* 78:139-153
- Self S (1983) Large-scale phreatomagmatic silicic volcanism: a case study from New Zealand. *J Volcanol Geotherm Res* 17: 433-469
- Self S, Sparks RSJ (1978) Characteristics of widespread pyroclastic deposits formed by the interaction of silicic magma and water. *Bull Volcanol* 41-3:196-212
- Sheridan MF, Updike RG (1975) Sugarloaf Mountain Tephra – A Pleistocene Rhyolitic Deposit of Base Surge Origin in Northern Arizona. *Geol Soc Am Bull* 86:571-581
- Shervais JW, Hanan BB (2008) Lithospheric topography, tilted plumes, and the track of the Snake River-Yellowstone hot spot. *Tectonics* 27 TC5004
- Shervais JW, Vetter SK, Hanan BB (2006) Layered mafic sill complex beneath the eastern Snake River Plain: Evidence from cyclical geochemical variations in basalt. *Geology* 34 5:365-368 doi: 10.1130/G22226.1
- Shimizu N, Hart SH (1982) Applications of the ion microprobe to geochemistry and cosmochemistry. *Ann Rev Earth Plan Sci* 10:483-526
- Sigurdsson H, Sparks RSJ (1981) Petrology of Rhyolitic and Mixed Magma Ejecta from the 1875 Eruption of Askja. *J Petrol* 22 1:41-84
- Sisson TW, Grove TL (1993). Experimental investigations of the role of H₂O in calc-alkaline differentiation and subduction zone magmatism. *Contrib. Mineral. Petrol.* 113:143–166
- Skirius CM, Peterson JW, Anderson AT, Jr (1990) Homogenising rhyolitic glass inclusions from the Bishop Tuff. *Am Mineral* 75:1381-1398
- Smith GA (1986) Coarse-grained nonmarine volcanoclastic sediment: Terminology and depositional processes. *Geol Soc Am Bull* 97:1-10
- Smith RB, Braile LW (1994) The Yellowstone hotspot. *J Volcanol Geotherm Res* 61:121-187.
- Smith RB, Siegel L (2000) *Windows into the Earth: The Geologic Story of Yellowstone and Grand Teton National Parks*, Oxford University Press, New York.
- Smith RL (1960) Ash flows. *Geol Soc Am Bull* 71:795-842
- Smith RT, Houghton BF (1995) Vent migration and changing eruptive style during the 1800a Taupo eruption: new evidence from the Hatepe and Rotongaio phreatoplinian ashes. *Bull Volcanol* 57:6 432-439
- Smith VC, Shane P, Nairn IA (2005) Trends in rhyolite geochemistry, mineralogy, and magma storage during the last 50 kyr at Okataina and Taupo volcanic centres, Taupo Volcanic Zone, New Zealand. *J Volcanol Geotherm Res* 148 3-4:372-406
- Smith VC, Shane P, Nairn IA, Williams CM (2006) Geochemistry and magmatic properties of eruption episodes from Haroharo linear vent zone, Okataina Volcanic Centre, New Zealand during the last 10 kyr. *Bull Volcanol* 69 1:57-88
- Sohn YK (1996) Hydrovolcanic processes forming basaltic tuff rings and cones on Cheju island, Korea. *Geol Soc Am Bull* 108 10:1199-1211
- Sohn YK, Chough SK (1989) Depositional processes of the Suwolbong tuff ring, Cheju Island (Korea). *Sedimentology* 36 5:837-855

- Sohn YK, Park HK, Yoon SK (2008) Primary versus secondary and subaerial versus submarine hydrovolcanic deposits in the subsurface of Jeju Island, Korea. *Sedimentology* 55:899-924
- Sparks RSJ, Francis PW, Hamer RD, Pankhurst RJ, O'Callaghan LO, Thorpe RS, Page R (1985) Ignimbrites of the Cerro Galan caldera, NW Argentina. *J Volcanol Geotherm Res* 24:205-248
- Sparks, R.S.J. Self S. and working group (2005). Super-eruptions: global effects and future threats. Rep Geol Soc London Working Group 2nd ed pp 24. Geol. Soc. London.
- Sparks RSJ, Wilson L, Sigurdsson H (1981) The pyroclastic deposits of the 1875 eruption of Askja, Iceland. *Phil Trans Roy Soc London* 299 1447:241-273
- Spell TL, McDougall I, Dougeris AP (1996) Cerro Toledo Rhyolite, Jemez Volcanic Field, New Mexico: $^{40}\text{Ar}/^{39}\text{Ar}$ geochronology of eruptions between two caldera-forming events. *Bull Geol Soc Am* 108 12:1549-1566
- Steven TA, Lipman PW(1976) Calderas of the San Juan Volcanic Field, Southern Colorado: Eighteen Major Ash-flow Tuff Sheets. *US Geol Surv Prof Pap* 958:1-35
- Stix J, Layne G (1996) Gas saturation and evolution of volatile and light lithophile elements in the Bandelier magma chamber between two caldera-forming eruptions. *J Geophys Res* 101(B11):25181-25196
- Stix J, Zapata JA, Calvache M, Cortes GP, Fischer TP, Gomez D, Ordonez M, Ortega A, Torres R, Williams S (1993) A model of degassing at Galeras Volcano, Columbia, 1988-1993. *Geology* 21:11 963-967
- Stormer JC, Jr (1983) The effects of recalculation on estimates of temperature and oxygen fugacity from analyses of multi-component iron-titanium oxides. *Am Mineral* 68:586-594
- Streck M and Ferns M (2004) The Rattlesnake Tuff and other Miocene silicic volcanism in Eastern Oregon. In. Haller KM and Wood SH (eds.) *Geological field trips in southern Idaho, eastern Oregon and northern Nevada*. USGS Open File Report 2004-1222
- Streck MJ, Grunder AL (1997) Compositional gaps and gradients in high-silica rhyolites of the Rattlesnake Tuff, Oregon. *J Petrol* 38 1:133-163
- Street LV, DeTar RE (1987) Geothermal resource analysis in Twin Falls County, Idaho: Idaho Department of Water Resources Water Information Bulletin 30 Part 15
- Sumner JM, Branney MJ (2002) The emplacement of a remarkable heterogeneous, chemically zoned and locally lava-like rheomorphic ignimbrite: 'TL' on Gran Canaria. *J Volcanol Geotherm Res* 115:109-138
- Svensden J, Stollhofen H, Krapf CBE, Stanistreet IG (2003) Mass and hyperconcentrated flow deposits record dune damming and catastrophic breakthrough of ephemeral rivers, Skeleton Coast Erg, Namibia. *Sed Geol* 160 1-3:7-31
- Swanson DA, Wright TL, Hooper PR, Bentley RD (1979) Revisions in stratigraphic nomenclature of the Columbia River Basalt Group. *US Geol Surv Bull* 1457-G
- Takahashi E, Nakajima K, Wright TL (1998) Origin of the Columbia River basalts: melting model of a heterogeneous plume head. *Earth Plan Sci Lett* 162:63-80
- Talbot JP, Self S, Wilson CJN (1994) Dilute gravity current and rain-flushed ash deposits in the 1.8 ka Hatepe Plinian deposit, Taupo, New Zealand. *Bull Volcanol* 56:6-7 538-551
- Taylor, HP (1968) The oxygen isotope geochemistry of igneous rocks. *Contrib Mineral Petrol* 19: 1-71
- Trofimovs J, Amy L, Boudon G, Delpus C, Doyle E, Fournier N, Hart MB, Komorowski JC, Le Friant A, Lock EJ, Pudsey C, Ryan G, Sparks RSJ, Talling PJ (2006) Submarine pyroclastic deposits formed at the

- Soufrière Hills volcano, Montserrat (1995–2003): What happens when pyroclastic flows enter the ocean? *Geology* 34 7:549-552
- Troll VR, Donaldson CH, Emeleus CH (2004) Pre-eruptive magma mixing in ash-flow deposits of the Tertiary Rum igneous centre, Scotland. *Contrib Mineral Petrol* 147 6:722-739
- Ukstins Peate IA, Baker JA, Kent AJR, Al-Kadasi M, Al-Subbary A, Ayalew D, Menzies M (2003) Correlation of Indian Ocean tephra to individual Oligocene silicic eruptions from Afro-Arabian flood volcanism. *Earth Planet Sci Lett* 211:311–327
- Valentine GA, Giannetti B (1995) Single pyroclastic beds deposited by simultaneous fallout and surge processes: Roccamonfina volcano, Italy. *J Volcanol Geotherm Res* 64 1-2:129-137
- Van den Bogaard P, Schmincke H-U (1985) Laacher See Tephra: a widespread isochronous late Quaternary tephra layer in Central and Northern Europe. *Geol Soc Am Bull* 96 12:1554-1571
- Villari L (1974) The island of Pantelleria. *Bull Volcanol* 38:680-724
- Waite GP, Smith RB, Allen RM (2006) Vp and Vs structure of the Yellowstone hotspot from teleseismic tomography: evidence for an upper mantle plume. *J Geophys Res* 111 B04303
- Walker GPL (1971) Grain-size characteristics of pyroclastic deposits. *J Geol* 79: 696-714
- Walker GPL (1981) Plinian eruptions and their products. *Bull Volcanol* 44 3:223-240
- Walker GPL (1981b) Characteristics of two phreatoplinian ashes, and their water-flushed origin. *J Volcanol Geotherm Res* 9:395-407
- Walker GW (1974) Some implications of late Cenozoic volcanism to geothermal potential in the High Lavas Plains of south-central Oregon. *Ore Bin* 36:109-119
- Wallace PJ (2005) Volatiles in subduction zone magmas: concentrations and fluxes based on melt inclusion and volcanic gas data. *J Volcanol Geotherm Res* 140 1-3:217-240
- Wark DA, Hildreth W, Spear FS, Cherniak DJ, Watson EB (2007) Pre-eruption recharge of the Bishop magma system. *Geology* 35 3:235-238 DOI 10.1130/G23316A
- Wark DA, Watson EB (2006) TitaniQ: A titanium-in-quartz geothermometer. *Contrib Mineral Petrol* 152:743-754 DOI 10.1007/s00410-006-0132-3081
- Warshaw CM, Smith RL (1988) Pyroxenes and fayalites in the Bandelier Tuff, New Mexico: Temperatures and comparison with other rhyolites. *Am Mineral* 73:1025-1037
- Watanabe K, Ono K, Sakaguchi K, Takada K, Hoshizumi H (1999) Co-ignimbrite ashfall deposits of the 1991 eruptions of Fugen-dake, Unzen Volcano, Japan. *J Volcanol Geotherm Res* 89:1-4 95-112
- Watkins AM, McCurry M, Hughes SS (1996) Preliminary report on the stratigraphy and geochemistry of the tuff of Steer Basin, Cassia Mountains, Idaho. *Northwest Geol* 26 107-120
- Watson EB, Harrison TM (1983) Zircon saturation revisited: temperature and composition effects in a variety of crustal magma types. *Earth Plan Sci Lett* 64:295-304
- Webster JD (1997) Chloride solubility in felsic melts and the role of chloride in magmatic degassing. *J Petrol* 38 12:1793-1807
- Webster JD, Burt DM, Aguillon RA (1996) Volatile and lithophile trace-element geochemistry of Mexican tin rhyolite magmas deduced from melt inclusions. *Geochem Cosmochem Acta* 60 17:3267-3283
- Webster JD, De Vivo B, Tappen C (2003) Volatiles, magmatic degassing and eruptions of Mt. Somma-Vesuvius: Constraints from silicate melt inclusions, Cl and H₂O solubility experiments and modelling.

- In: De Vivo B, Bodnar RJ (eds) Melt inclusions in volcanic systems: methods, applications and problems. Elsevier
- Webster JD, Duffield WA (1991) Volatiles and lithophile elements in Taylor Creek Rhyolite: constraints from glass inclusion analysis. *Am Mineral* 76:1628-1645
- Webster JD, Duffield WA (1994) Extreme halogen abundances in tin-rich magma of the Taylor Creek Rhyolite, New Mexico. *Econ Geol* 89 4:840-850
- Webster JD, Kinzler RJ, Mathez EA (1999) Chloride and water solubility in basalt and andesite melts and implications for magmatic degassing. *Geochim Cosmochim Acta* 63 5:729-738
- Wells MK, Bowles JFW (1981) The textures and genesis of metamorphic pyroxene in the Freetown Intrusion. *Min Mag* 44 344:245-255
- Wen S, Nekvasil H (1994) SOLVCALC: an interactive graphics program package for calculating the ternary feldspar solvus and for two-feldspar geothermometry. *Comp Geosci* 20:1025–1040
- Werner C, Brantley S (2003) CO₂ emissions from the Yellowstone Volcanic System. *Geochem Geophys Geosys* 4 7:1061
- Westrich HR, Eichelberger JC, Hervig RL (1991) Degassing of the 1912 Katmai magma. *Geophys Res Lett* 18 8:1561-1564
- White JDL, Houghton BF (2006) Primary volcanoclastic rocks. *Geology* 34:8 677-680 DOI 10.1130/G22346.1
- Whitney JA, Stormer JC Jr. (1985) Mineralogy, Petrology and Magmatic Conditions from the Fish Canyon Tuff, Central San Juan Volcanic Field, Colorado. *J Petrol* 26 3:726-762
- Williams PL, Covington HR, Mytton JW (1991) Geologic map of the Stricker 2 quadrangle, Twin Falls and Cassia Counties, Idaho. US Geol Surv Misc Invert Ser Map I-2146
- Williams PL, Mytton JW, Morgan WA (1990) Geologic Map of the Stricker 3 Quadrangle, Twin Falls and Cassia Counties, Idaho. Geologic Investigations Series I-2633. USGS
- Wilson CJN (2001) The 26.5ka Oruanui eruption, New Zealand: an introduction and overview. *J Volcanol Geotherm Res* 112:133-174
- Wilson CJN, Blake S, Charlier BLA, Sutton AN (2006) The 26.5 ka Oruanui Eruption, Taupo Volcano, New Zealand: Development, Characteristics and Evacuation of a Large Rhyolitic Magma Body. *J Petrol* 47(1) 35-69 DOI 10.1093/petrology/egi066
- Wohletz KH (1999) MAGMA: Calculates IUGS Volcanic Rock Classification, Densities, and Viscosities. Los Alamos National Laboratory computer code LA-CC 99-28, Los Alamos New Mexico
- Wohletz KH, Orsi G, de Vita S (1995) Eruptive mechanisms of the Neapolitan Yellow Tuff interpreted from stratigraphy, chemistry, and granulometry. *J Volcanol Geotherm Res* 67:263-290
- Wolf DE, Leeman WP, Vervoort JD (2005) U-Pb zircon geochronology of crustal xenoliths confirms presence of Archean basement beneath the central and eastern Snake River Plain. *Geol. Soc. Am. Abs. with Programs* v. 37 7:60
- Wolff JA, Balsley SD, Gregory RT (2002) Oxygen isotope disequilibrium between quartz and sanidine from the Bandelier Tuff, New Mexico, consistent with a short residence time of phenocrysts in rhyolitic magma. *J Volcanol Geotherm Res* 116 1-2:119-135.
- Wolff JA, Wright JW (1981) Rheomorphism of welded tuffs. *J Volcanol Geotherm Res* 10:13-34

-
- Wood SH, Gardner JN (1984) Silicic volcanic rocks of the Miocene Idavada Group, Bennett Mountain, southwestern Idaho. Final contract report to the Los Alamos National Laboratory from Boise State University, July 42p
- Wright KE, McCurry M, Hughes SS (2002) Petrology and geochemistry of the Miocene tuff of McMullen Creek, central Snake River Plain. In: Bonnicksen B, McCurry M, White CM (eds.) Tectonic and Magmatic Evolution of the Snake River Plain Province. Idaho Geol Surv Bull 30:177-194
- Yuan H, Decker K (2005) Upper Mantle Tomographic V_p and V_s Images of the Rocky Mountains in Wyoming, Colorado and New Mexico: Evidence for a Thick Heterogeneous Chemical Lithosphere. In: Karlstrom K, Keller GR (eds.) The Rocky Mountain region – an evolving lithosphere: tectonics, geochemistry and geophysics . Geophysical Monograph Series 154, Am Geophys Union
- Zhang Y (1999) H_2O in rhyolitic glasses and melt: Measurement, speciation, solubility and diffusion. Rev Geophys 37:493-516

Appendix A: Sample locations

Sample name	Member description	UTM 11T unless stated	XRF	Probe	Ar/Ar	Location description
MAGFA2	Magpie Basin ashfall	725823, 4681014	*			Just after turn to third fork, cross bridge 1.5 km upstream
MAGPIE	Magpie Basin ignimbrite	725823, 4681014	*	*		Just after turn to third fork, cross bridge 1.5 km upstream
TBB	Big Bluff basal vit.	725606, 4681240	*	*	*	Base of the unit above the Magpie Basin unit
BVSB	Steer Basin basal vit.	724541, 4689825	*	*	*	Located next to small diatomite quarry NE of road
SBSR1UV	Steer Basin upper vit.	713096, 4672717	*			On Shoshone Road, rheomorphic unit with thin upper vitrophyre
SBUV	Steer Basin upper vit.	724504, 4690151	*	*		Near cowgrid, north of diatomite quarry
PIII	Deadeye ignimbrite	725831, 4684191	*			Directly above Steer Basin campsite
TCPU7	Deadeye ignimbrite	12T 255142, 4673687	*	*		Past Trapper Creek reservoir and 2 roadside crosses, low outcrop near road
PIJFC11	Deadeye ashfall	726899, 4682495	*			W side of Rock CK, cross at 3 rd fork and walk back north
TCPU8 PJC	Deadeye ignimbrite	12T 255142, 4673687	*	*		Past Trapper Creek reservoir and 2 roadside crosses, low outcrop near road
HARWS 5	Wooden Shoe Butte ashfall	727191, 4686607	*			2 km along track from Harrington fork picnic ground outcrop on N side
HARWS 2	Wooden Shoe Butte ashfall	727191, 4686607	*			2 km along track from Harrington fork picnic ground outcrop on N side
HARWS 1	Wooden Shoe Butte ashfall	727191, 4686607	*			2 km along track from Harrington fork picnic ground outcrop on N side
HARWSB BV	Wooden Shoe basal vit.	727191, 4686607	*			2 km along track from Harrington fork picnic ground outcrop on N side
BVTWSB GOAT	Wooden Shoe basal vit.	706641, 4685303	*			3 km S of Nat Soo Pah, north side of Goat Springs canyon
TWSBBV CAS2	Wooden Shoe basal vit.	724102, 4690674	*			E side Rock Creek where Little Creek joins Rock Creek
TWSBBV	Wooden Shoe basal vit.	722097, 4696787	*	*		Mouth of Rock Creek, outcrop low on LHS of road as driving south
TWSB GOOSE	Wooden Shoe basal vit.	12T 257675, 4662153	*			Thick welded unit in Goose Creek, high on cliff SW side of track
TWSBBV CAS1	Wooden Shoe basal vit.	724504, 4690151	*			Near cowgrid, above a prominent non-welded outcrop
WSBBV3 DRY	Wooden Shoe basal vit.	732114, 4696603	*			Location at the mouth of Dry Creek, drive to the main farm and then turn left to the welded unit low down
TWSBBV BCC2	Wooden Shoe basal vit.	744731, 4685768	*			Walk along track c. 3 km from gate on NW side of stream, 100 m or so above track
TWSBMV4 BCC2	Wooden Shoe medial vit.	744731, 4685768	*			Walk along track c. 3 km from gate on NW side of stream, 100 m or so above track
WSBMV 2	Wooden Shoe medial vit.	723011, 4691584	*			Near turn into Rock Ck, above well exposed fall at road level
HARWSB UV	Wooden Shoe upper vit.	727191, 4686607	*			2 km along track from Harrington fork picnic ground outcrop on N side
WSB UV1	Wooden Shoe upper vit.	723011, 4691584	*			Near turn into Rock Ck, above well exposed fall at road level
MCMJO	McMullen Creek basal vit.	723070, 4691752	*			Near Chuck's farm, on weakly developed palaeosol above WSBM
BBU3	Browns Bench 3 basal vit.	682167, 466052		*	*	At Corral Creek section along a track, then past a NA game hide, up a scree slope and next to a fence
BBU5	Browns Bench 5 upper vit.	682167, 466052	*	*	*	At Corral Creek, above BB3 below slope-forming BB6
BBU7	Browns Bench 7 basal vit.	682167, 466052	*	*	*	At Corral Ck. BB7 has multiple weathering horizons, see CH3 appendix
BBU8	Browns Bench 8 basal vit.	682167, 466052	*	*	*	BB8 is above BB7, see appendix for photo location
J5	Jackpot 5 upper vit.	692670, 4649181	*	*	*	I93 roadcut about 3 km S of the town of Jackpot, next to a llama farm
J52	Jackpot 5 devit interior	691715, 4645853	*			Rest-area 5 km S of Jackpot, track leads to Browns Bench from rest area
J7	Jackpot 7 basal vit.	692210, 4646948	*	*	*	W of the main rest area south of Jackpot on path that leads to Browns Bench
UGEI	Upper Grasmere Escarpment basal vit.	582759, 4681823	*	*	*	Poorly exposed in roadcut, vesicular top of ignimbrite
BUCK	Buckhorn upper vit.	BB	*	*	*	Sample provided by Dr. Bill Bonnicksen
WINDY	Windy Gap	BB	*	*	*	Sample provided by Dr. Bill Bonnicksen
FRENCH	Frenchman Springs	WS	*	*	*	Sample provided by Will Starker, WSU
CPT12V	Cougar Point 12 basal vit.	631366, 4649317	*	*		2 km into NV, between 'Freighter defeat' and Buck Creek
CPT XII	Cougar point 12 basal vit.	BB	*			Sample provided by Dr. Bill Bonnicksen
BREL	Black Rock Escarpment lava	BB	*	*		Sample provided by Dr. Bill Bonnicksen
CFC2 FALL	Castleford Crossing ashfall	668072, 4712124	*			Fallout above BRL breccia between pumping station and Balanced Rock
CFC1	Castleford Crossing basal vit.	668072, 4712124	*			Massive rheomorphic ignimbrite from roadcut above fallout
CFCIV	Castleford Crossing basal vit.	667796, 4712379	*	*		c.15 m above Bal. Rock. Ignimbrite is 3 m thick sheet of glass
CFC2	Castleford Cross. Basal vit.	667796, 4712379	*			c.15 m above Bal. Rock. Ignimbrite is 3 m thick sheet of glass
BRL	Balanced Rock Lava base	667796, 4712379	*	*		50 m above pumping station down service track
BRL2 HYDRO	Balanced Rock Lava base	673216, 4717105	*			West of Buhl, towards Lucerne apartments close to hydro plant
SSI	Sand Springs partially welded	692087, 4661329	*	*		Roadcut on I93
SFRL	Shoshone Falls lava upper vit.	707780, 4719316	*			Past Centenary park, S side of Snake River, at the end of a golf course
SFRLV	Shoshone Falls lava upper vit.	713517, 4719290	*	*		N side of Snake River, in a housing estate which contains outcrops of the upper vitrophyre

Appendix B: Electron Microprobe

Electron beam

The electron microprobe has four main stages, the first of which is the heating of a tungsten filament which eventually produces electrons. These electrons are accelerated down a column at high voltage (15 keV) which focuses them into a beam. The beam is then passed through a series of lenses to remove any interferences and to further focus the beam. This allows a beam of electrons to be fired at the sample with a spot size on the order of a few microns. For most of the work in this thesis 10 microns was the smallest spot sized used.

X-ray generation

When the beam of electrons impacts the polished surface of the sample, they impact into the sample to a degree, referred to as the interaction volume, and produce X-rays. The X-rays of each element have characteristic energies allowing them to be counted. The X-rays pass through a crystal and then on to a detector whereby comparison of the X-rays of the sample with a known standard allows identification of that element.

Standards

The standards used during electron microprobe analyses were the following:

Name	Standard for	Colour	Composition	Notes
MgO	Mg	Pink / green	Mg - 60.31 O - 39.69	Synthetic (A. Peckett, Geol. Dept. Durham 1973)
Al ₂ O ₃	Al	Yellow / white	Al - 51.9 Cr - 1.3 O - 46.8	Synthetic (A. Mills, Geol. Dept. University of Leicester, 1976)
JAD	Na, Al	Yellow / pink	Si - 27.8 Al - 13.30 Fe - 0.1 Na - 11.20 O - 47.50	Natural jadeite (R. Symes, Natural History Museum, 1973)
WOLL	Ca, Si	Yellow / red	Si - 24.0 Ca - 34.5 O - 41.5	Natural wollastonite (P. Suddaby, Imperial College, 1973)
CH14	K	Yellow / black	Si - 30.24 Al - 9.73 Na - 0.14 K - 13.76 Ba - 0.10 O - 45.98	Natural microcline (I. Steele, University of Chicago, 1974)
RUT	Ti	Orange / brown	Ti - 59.69 Fe - 0.33 O - 39.98	Natural rutile (R.J. King, Geology Department, University of Leicester 1973)

CR	Cr	Green / orange	Cr – 100.00	Pure (Koch-Light < 1969)
RHOD	Mn	Orange / green	Si – 21.83 Al – 0.09 Fe – 2.80 Mn – 31.58 Mg – 0.34 Ca – 5.59 O – 37.46	Natural rhodonite, (R.J. King, Geology Department, University of Leicester, 1973)
Fe	Fe	Blue / green	Fe – 100.00	Pure (>3N) Johnson Matthey < 1969
Co	Co	Blue / red	Co – 100.00	Pure (>4N) Johnson Matthey < 1969
Ni	Ni	Blue / pink	Ni – 100.00	Pure (>4N) Johnson Matthey < 1969
FRISCH	Secondary	Brown / red	SiO ₂ – 50.1 TiO ₂ – 0.82 Al ₂ O ₃ – 8.1 FeO – 5.8 MnO – 0.1 MgO – 15.8 CaO – 18.0 Na ₂ O – 1.3	Natural augite (P. Suddaby, Imperial College, 1973).
NaCl	Na, Cl		Na – 39.34 Cl – 60.66	Synthetic, Geology Department, University of Leicester
Fe ₃ O ₄	Fe	Pink / black	Fe – 72.66 O - 27.64	Synthetic (I. Steele, University of Chicago, 1975)
SrF ₂	Sr, F	Yellow / blue	Sr – 69.75 F – 30.25	Synthetic (Opran < 1969)
SCAP	Cl	Brown / yellow	Si – 23.45 Al – 13.24 Ca – 7.43 Na – 4.6 K – 3.2 C – 0.69 S – 0.30 Cl – 1.15 Fe – 0.24 O – 46.08	Natural scapolite (R.J. King, Geology Department, University of Leicester, 1974)
BAR	Ba, S	Brown / blue	Ba – 58.84 S – 13.74 O – 27.42	Natural barite (R.J. King, Geology Department, University of Leicester, 1974)
CH5	Ca, Mg	Black / orange	Ca – 14.29 Mg – 8.66 Si – 42.83 O – 34.22	Natural diopside (I. Steele, University of Chicago, 1974)
CH15	Ti	Black / pink	Ti - 29.73 Fe – 36.87 Mn – 0.66 Mg – 0.66 O – 31.04	Natural ilmenite (I. Steele, University of Chicago, 1974)
CH20	Ca, P	Brown / black	Ca – 39.10 P – 18.06 Mg – 0.07	Natural apatite, (I. Steele, University of Chicago, 1974)

			Cl – 0.08 Fe – 0.05 Sr – 0.07 O – 39.05	
AMAB	Na	Orange / red	Si – 31.87 Al – 10.38 Fe – 0.06 Ca – 0.06 K – 0.23 Na -8.6 O – 48.62	Amelia albite (Amelia Co.) Unknown < 1969, Analysis from DHZ, vol. 4

Generation of results

To generate final results from the counts of the various elements there are three corrections that are required, referred to as the ZAF correction.

Atomic number correction (Z)

The atomic number correction has two aspects, the first is the degree to which the incident beam of electrons is stopped by the sample, and the second is the degree to which X-rays produced are scattered. This scattering may be either large angle or by a progression of small angle deflections. This scattering decreases the X-ray signal recorded at the detector, and the degree of scattering increases with increasing atomic number, therefore a correction is required to address this. The effects of scattering and stopping act in opposing directions and are often of approximately equal intensity.

Absorption correction (A)

Where X-rays are generated beneath the surface of the sample, they suffer from absorption within the sample before passing out to the detector. This correction is a function of the take-off angle used in analysis (in this work, 45° was used as a take-off angle), sample composition, distribution of elements and wavelength of X-rays produced. The surface of the sample may also be important, with an irregular surface causing variation in path length for X-rays, thus explaining the necessity of well-polished sections.

Fluorescence correction (F)

Any element has an excitation threshold above which it will generate X-rays, this threshold may be exceeded not only by the electron beam from the source, but also by X-rays produced from elements which have a higher excitation threshold.

Appendix C: Ion Microprobe and Secondary Ion Mass Spectroscopy

Secondary ion mass spectroscopy (SIMS) requires a system which has the following components:

- A primary ion source
- A polished sample with a flat surface that is stable under vacuum.
- A collector for the secondary ions
- A mass analyser to discriminate the ion of interest from other ions and molecular species produced.
- An ion detector to measure the secondary ion signal.

Ion beam:

The ion beam in CAMECA 4f instrument is produced by a duoplasmatron. This creates numerous ions which are selected using the primary beam mass filter. The beam used in this study as an O^+ beam which pass down a primary beam column, used to focus the beam and remove any impurities from it. The top of the primary column has a mass filter which, when using the duoplasmatron source removes OH, N, Fe and Ni. This filter only allows oxygen ions to bombard the surface of the sample. Upon passing down the column, the beam is focussed through numerous electrostatic lenses and deflector plates which allow the size and shape of the beam to be controlled.

Sputtering

Having been focussed, the ion beam impacts the surface of the sample and ejects material. This sputtering actually occurs by a collision between molecules within the sample, rather than collision between the primary ion beam and the sample (Shimizu and Hart 1982). When the ions hit the sample at high energy, they produce multiple collisions termed a collision cascade. Some of these collisions result in the production of an atom with a vector directed back to the sample surface, and a small proportion of these result in a surficial atom being ejected. Post sputtering the molecules which were removed from the sample are then ionised, although how this specifically happens is still not fully understood. Shimizu and Hart (1982) suggest that the ionisation occurs when a sputtered ion interacts with the sample surface rather than with a cloud of neutral atoms.

Secondary ion extraction

The sample is held at high voltage 4,500 V and the first lens of the extraction lens is held at ground potential, this variation in voltage causes the ions produced by sputtering to be

accelerated away from the sample. The ions are passed through a series of lenses, which act to improve the spatial resolution of the analysis, but decrease the ion yield.

Mass spectrometer

The secondary ions then pass into the mass spectrometer, where the first sector is the electromagnetic sector. This sector has a number of slits to focus the ion beam and acts to discriminate between the ions at higher and lower energies. After passing through numerous slits and lenses, the magnetic sector then deflects the ion beam based on mass:charge ratio, removing atomic species before they reach the detector.

Detector

The detector in an ion microprobe may be either an electron multiplier or a Faraday Cup. In this work an electron multiplier detector was used. This consists of a series of electrodes called dynodes with the first at ground potential and the last somewhere between +1500 and +3500V. When an electron (or any particle) strikes the first dynode it causes a number of secondary electrons to be emitted. These electrons are then accelerated to the next dynode in the series, creating a cascade which then passes through a pulse discriminator before passing to the counting system.

For a detailed introduction to how the ion microprobe works, the reader is directed to:

<http://www.geos.ed.ac.uk/facilities/ionprobe/SIMS4.pdf>

Appendix D: X-ray fluorescence spectroscopy

All samples were analysed at the Geology Department at the University of Leicester with sample preparation described in Chapter 2. Standard data is provided below:

Major elements

		SiO ₂	TiO ₂	Al ₂ O ₃	Fe ₂ O ₃	MnO	MgO	CaO	Na ₂ O	K ₂ O	P ₂ O ₅	Total
RHF1102	Whin sill	50.92	2.55	13.35	13.55	0.184	5.17	8.58	3.22	1.266	0.309	99.10
RHF1103	Whin sill	51.28	2.46	13.35	13.64	0.179	5.05	8.54	3.26	1.248	0.303	99.31
RHF1113	Whin sill	51.16	2.49	13.41	13.59	0.179	5.36	8.74	3.05	1.397	0.312	99.69
RHF1142	Whin sill	51.07	2.59	13.54	13.71	0.18	5.33	8.82	3.13	1.42	0.309	100.10
RHF1145	Whin sill	51.12	2.61	13.56	13.68	0.173	5.31	8.88	3.12	1.411	0.311	100.18
RHF1146	Whin sill	51.07	2.59	13.54	13.71	0.18	5.33	8.82	3.13	1.42	0.309	100.10
RHF1148	Whin sill	50.64	2.52	13.48	13.74	0.167	5.24	8.93	3.22	1.348	0.313	99.60
RHF1150	Whin sill	50.95	2.56	13.33	13.64	0.168	5.12	8.84	3	1.335	0.314	99.26
Mean		51.03	2.55	13.45	13.66	0.18	5.24	8.77	3.14	1.36	0.31	99.67
Std. Dev.		0.142	0.042	0.085	0.053	0.005	0.094	0.112	0.069	0.056	0.003	0.350
RHF1102	Bardon microgranite	68.05	0.37	14.02	5.83	0.126	2.52	3.31	4.28	0.801	0.062	99.37
RHF1103	Bardon microgranite	68.21	0.37	13.9	5.87	0.129	2.48	3.19	4.19	0.803	0.058	99.2
RHF1113	Bardon microgranite	67.95	0.42	13.96	5.81	0.13	2.58	3.39	3.82	0.896	0.064	99.02
RHF1142	Bardon microgranite	67.95	0.38	13.93	5.87	0.136	2.65	3.25	3.92	0.805	0.067	98.96
RHF1145	Bardon microgranite	68.01	0.38	14.02	5.86	0.137	2.63	3.29	3.94	0.808	0.069	99.14
RHF1146	Bardon microgranite	68.29	0.38	14	5.9	0.137	2.66	3.27	3.94	0.809	0.067	99.45
RHF1148	Bardon microgranite	68.47	0.38	13.85	5.89	0.132	2.67	3.18	4.09	0.791	0.074	99.53
RHF1150	Bardon microgranite	68.32	0.39	13.82	5.91	0.127	2.61	3.24	3.96	0.798	0.072	99.25
Mean		68.16	0.38	13.94	5.87	0.13	2.60	3.27	4.02	0.81	0.07	99.24
Std.Dev.		0.194	0.016	0.076	0.034	0.004	0.069	0.068	0.155	0.034	0.005	0.201
BCS375	Feldspar powder	66.83	0.44	20.11	0.13	0.001	-0.17	0.87	10.36	0.799	0.017	99.39
BCS375	Feldspar powder	66.84	0.44	20.18	0.13	0.002	-0.16	0.87	10.34	0.798	0.017	99.46
BCS375	Feldspar powder	66.84	0.44	20.18	0.13	0.002	-0.16	0.87	10.34	0.798	0.017	99.46
BCS375	Feldspar powder	66.99	0.44	20.2	0.13	0.001	-0.16	0.86	10.4	0.794	0.016	99.67
BCS375	Feldspar powder	67.03	0.44	20.23	0.13	0.001	-0.17	0.87	10.44	0.798	0.016	99.79
BCS375	Feldspar powder	66.87	0.43	20.11	0.13	0.002	-0.16	0.87	10.44	0.802	0.016	99.51
Mean		66.90	0.44	20.17	0.13	0.00	-0.16	0.87	10.39	0.80	0.02	99.54
Std. Dev.		0.09	0.00	0.05	0.00	0.00	0.01	0.00	0.05	0.00	0.00	0.15

Trace elements

		As	Ba	Co	Cr	Cu	Ga	Mo	Nb	Ni	Pb	Rb	Sc	Sr	Th	U	V	Y	Zn	Zr
:NIM-G	Granite, RSA	14.8	99.1	2.2	13.6	1.0	27.2	1.9	53.9	2.8	35.1	311.6	7.9	11.2	52.5	13.8	-3.6	139.4	43.8	290.4
:NIM-G	Granite, RSA	13.1	111.8	2.1	16.7	4.8	28.3	1.9	57.7	1.7	37.7	318.9	1.5	11.3	50.8	14.9	2.3	142.5	45.9	292.7
:NIM-G	Granite, RSA	15.2	112.4	1.4	16.8	2.3	27.0	2.6	54.1	3.6	34.8	314.2	2.2	11.7	49.6	13.7	2.6	144.1	45.0	288.4
:NIM-G	Granite, RSA	15.0	99.4	2.0	15.8	-0.6	26.9	2.1	55.0	0.8	32.0	314.7	2.2	9.7	50.2	13.8	-1.1	142.4	44.6	282.1
:NIM-G	Granite, RSA	13.5	107.3	2.3	17.3	0.9	26.3	1.6	54.1	1.8	36	317.3	1.2	4.7	50.2	15.3	-0.5	139	44.3	278.8
Mean		14.3	106.0	2.0	16.0	1.7	27.1	2.0	55.0	2.1	35.1	315.3	3.0	9.7	50.7	14.3	-0.1	141.5	44.7	286.5
St. dev.		1.0	6.5	0.4	1.5	2.0	0.7	0.4	1.6	1.1	2.1	2.8	2.8	2.9	1.1	0.7	2.6	2.2	0.8	5.8
:G-2	Granite (USGS)	1.1	1856.0	5.5	-3.2	11.8	22.3	1.1	12.4	5.5	28.0	167.2	2.8	477.4	21.6	1.1	38.4	8.6	82.9	322.7
:G-2	Granite (USGS)	1.0	1878.0	5.8	3.8	10.1	21.9	0.6	12.0	2.8	26.6	167.6	4.9	473.5	23.6	0.4	34.3	8.2	84.9	319.8
:G-2	Granite (USGS)	-0.1	1886.7	5.0	8.3	9.2	22.5	0.5	11.4	4.5	32.5	166.8	4.5	476.8	25.1	1.6	37.9	8.6	84.4	322.0
:G-2	Granite (USGS)	2.7	1851.6	5.3	5.5	10.3	21.9	1.8	13.6	2.9	26.4	170.9	-1.5	477.2	25.1	1.7	32.8	7.6	86.1	324.2
:G-2	Granite (USGS)	-0.2	1873.7	4.2	10.1	9.1	22.2	-0.7	13	3.9	27.2	168.9	5.1	477.6	25	4.3	37.7	7.2	85	326
Mean		0.9	1869.2	5.1	4.9	10.1	22.1	0.7	12.5	3.9	28.1	168.3	3.2	476.5	24.1	1.8	36.2	8.0	84.6	322.9
St. dev.		1.2	14.9	0.6	5.1	1.1	0.3	0.9	0.9	1.1	2.5	1.7	2.7	1.7	1.5	1.5	2.5	0.6	1.2	2.3
:JR-1	Rhyolite, (JGS)	17.4	52.1	-1.3	5.4	0.1	16.2	2.8	16.2	-0.1	15.6	245.9	3.5	28.3	29.5	8.2	3.5	46.1	29.1	105.1
:JR-1	Rhyolite, (JGS)	16.0	51.6	-0.5	-0.9	-1.2	16.1	1.9	14.8	0.1	17.3	246.3	4.0	27.8	27.8	7.6	6.2	43.1	31.0	99.9
:JR-1	Rhyolite, (JGS)	16.6	50.5	-1.3	2.8	-0.3	17.1	1.8	15.3	1.7	17.1	244.6	4.7	27.0	28.4	8.1	6.7	43.9	29.0	101.6
:JR-1	Rhyolite, (JGS)	15.0	50.9	0.0	-3.0	-0.4	16.5	3.3	15.1	3.1	17.2	247.6	6.5	26.2	25.3	7.0	0.5	43.4	28.7	100.8
:JR-1	Rhyolite, (JGS)	15.2	48.8	0.5	1.1	0.5	15.4	2.9	14.8	2.2	19.7	247.1	5.2	27.7	27.5	10.2	6.8	45.3	29.1	99.4
Mean		16.0	50.8	-0.5	1.1	-0.3	16.3	2.5	15.2	1.4	17.4	246.3	4.8	27.4	27.7	8.2	4.7	44.4	29.4	101.4
St. dev.		1.0	1.3	0.8	3.2	0.6	0.6	0.7	0.6	1.4	1.5	1.2	1.2	0.8	1.5	1.2	2.7	1.3	0.9	2.3
:JR-2	Rhyolite, (JGS)	20.0	34.1	-0.7	0.8	-1.2	17.2	2.6	19.9	-2.5	20.1	294.9	3.5	8.6	31.9	10.3	-6.3	49.5	26.0	97.2
:JR-2	Rhyolite, (JGS)	20.2	31.5	-0.6	2.7	-1.9	16.4	1.9	17.4	-2.0	20.1	297.2	3.9	6.0	34.2	11.0	2.4	49.1	27.0	89.7
:JR-2	Rhyolite, (JGS)	19.4	28.9	-1.8	-3.5	-1.6	16.5	2.6	20.1	-1.2	21.4	295.1	4.7	9.6	33.3	11.8	1.3	51.3	26.0	96.6
:JR-2	Rhyolite, (JGS)	17.3	23.6	0.4	-0.8	-2.0	17.0	3.2	18.2	-2.6	23.6	297.8	4.3	9.7	33.2	11.8	-4.2	50.7	25.9	93.0
:JR-2	Rhyolite, (JGS)	17.6	37	-0.2	-1.4	-0.6	16.8	2.4	18.4	0	23.7	293.7	4.9	6.3	31.7	10.9	0.3	49.8	25.4	95
Mean		18.9	31.0	-0.6	-0.4	-1.5	16.8	2.5	18.8	-1.7	21.8	295.8	4.3	8.0	32.9	11.2	-1.3	50.1	26.0	94.3
St. dev.		1.3	5.1	0.8	2.3	0.6	0.4	0.4	1.2	1.1	1.8	1.7	0.6	1.8	1.1	0.6	3.8	0.9	0.6	3.0